The Transcriptional Regulation of Acclimation to High Light in *Arabidopsis thaliana*

Ellie Jane Stallard

A thesis submitted for the Degree of Doctor of Philosophy

School of Life Sciences

University of Essex

June 2022

23

Acknowledgements

I would like to thank everyone who has helped my research efforts come to fruition. I foremostly want to thank Prof. Philip M. Mullineaux for taking me in, inspiring me and providing me with the opportunity to flourish. I want to thank those previously of the Mullineaux group who have assisted me throughout their time at Essex. I want to thank those from Lab 5.36 and Lab 6.23 who have been invaluable not just for their knowledge and assistance but for the kind and welcoming atmosphere they've created. I would finally like to thank my partner, my parents and my grandparents, who have always encouraged and supported me.

Abstract

Plants undergo the process of HL acclimation in response to new higher light conditions. Over 5 to 9 days of higher light exposure, plants enhance their photosynthetic capacity to take advantage of the new environment. HL acclimation is mediated through light-responsive photoreceptors such as CRY1, which drive changes in transcription. Transcriptional regulators are crucial in bringing about cellular alterations required for HL acclimation through changing the expression of genes. A previous study created a network of HL acclimation transcription factors centred around the transcriptional regulator *BBX32* and the transcription factor *HY5*. *BBX32* and *HY5 Arabidopsis thaliana* mutants were experimentally shown to have perturbed HL acclimation phenotypes. I aimed to investigate HL acclimation through further testing of the HL TF network and analysis of transcriptional data. *Arabidopsis thaliana* mutants of HL TF network genes were experimentally tested for HL acclimation perturbations. Analysis was conducted on an RNA-seq data set of *BBX32* over-expressor and *hy5-2* mutants exposed to a HL treatment. Novel HL acclimation genes have been experimentally validated by using mutants of genes from the HL TF network. A *BBX32* allelic series of mutants created utilising a CRISPR/CAS9 gene editing system has provided further evidence of the role of *BBX32* within HL acclimation. New links have been discovered between phytohormone signalling, systemic acquired resistance and HL acclimation. Together these results give further insight into HL acclimation and its potential uses for improving plant productivity.

Abbreviations

ABA	Abscisic acid
ANOVA	Analysis of variance
BH	Benjamini-Hochberg post-hoc correction
BR	Brassinosteroids
BSA	Bovine serum albumin
CFU	Colony-forming units
CRISPR	Clustered of regularly interspaced short palindromic repeats
DEG	Differentially expressed gene
DNA	Deoxyribonucleic acid
FDR	False discovery rate
GA	Gibberellins
GEO	Gene expression omnibus
GH	Games-Howell post-hoc statistical analysis
GO	Gene ontology
gRNA	Guide RNA
HL	Higher light intensities
HPC	High-performance cluster
JA	Jasmonates/ Jasmonic acid
JTT model	Jones-Taylor-Thornton model
LB	Luria Broth
LHC	Light-harvesting complex
LL	Low light/ Growth light conditions
MS	Murashige and Skoog media

NPQ	Non-photochemical quenching
OD	Optical density
OX	Over-expressor
PAM	Protospacer adjacent motifs
PCR	Polymerase chain reaction
PPFD	Actinic photosynthetic photon flux density (measured in µmol m^{-2} s^{-1})
PQ	Photochemical quenching
PSII	Photosystem II
Q_A	Quinone acceptor
RNA	Ribonucleic acid
RNA-seq	RNA sequencing
ROS	Reactive oxygen species
RT	Reverse transcriptase
RT-qPCR	Reverse transcriptase – quantitative polymerase chain reaction
SA	Salicylic acid
SAR	Systemic acquired resistance
SD	Standard deviation
SE	Standard error
TF	Transcription factor
Tukey HSD	Tukey honest significant difference
UV	Ultraviolet light
VBSSM	Variation Bayesian state-space model
VP	Valine-Proline residues
WT	Wild-type

Contents

Chapter 1: Introduction

Plants must adapt when exposed to increased light intensity. In the natural world, plants often encounter new conditions due to, for example, growth into space with higher light intensities (hereafter termed HL) and seasonal changes. Local light environment changes require a response from the plant as HL can cause irreversible photooxidative damage to the photosynthetic reaction centres (Foyer *et al*., 1994; Muñoz and Munné-Bosch, 2018). Plants can defend themselves against HL-induced stress. However, HL can also be beneficial to a plant by boosting photosynthesis. Enhancing photosynthetic capacity to HL also has the doubled effect of defending the plant against photooxidative damage and increasing the rate of photosynthesis (Triantaphylidès *et al*., 2008; Ruban and Belgio, 2014). HL acclimation is the process that enables a plant to enhance its photosynthetic capacity to both utilise and combat any adverse effects of HL conditions.

1.1: Defining acclimation to light

Plants utilise their local light environment through the process of photosynthesis. They use light to fixate atmospheric carbon and increase their biomass. Plants adapt to their environment through the process of acclimation, which results in a change in their composition. This optimisation can occur from the scale of entire organs down to the concentrations of metabolites and proteins (Dyson *et al*., 2015). New light environments initiate light acclimation, enhancing photosynthetic capacity (Oguchi *et al*., 2003; Athanasiou *et al*., 2010; Albanese *et al*., 2016; Alvarez-Fernandez *et al*., 2021). Understanding how plants acclimate to optimise photosynthesis to a changing light environment is crucial to maximising crop yield.

Previous research categorised plants as enhancing their photosynthetic capacity through alterations in morphology or chloroplast physiology (Walters and Horton, 1994; Adams *et al*., 2014; Hoshino *et al*., 2019; Walters, 2005). Morphological changes include alterations to leaf thickness, dry mass per area, and vasculature (Weston *et al*., 2000; Oguchi *et al*., 2003; Stewart *et al*., 2017). Chloroplast physiological alterations describe changes in chloroplast density (i.e., the number per cell), the composition, and stoichiometry of photosynthetic reaction centres and chlorophyll concentrations, which reflect changes in both photosystems' antennae (Walters *et al*., 1999; Weston *et al*., 2000; Bailey *et* al., 2004; Albanese *et al*., 2016; Miller *et al*., 2017; Stewart *et al*., 2017; Albanese *et al*., 2020; Flannery *et al*., 2021).

Previous studies created separate terms to delineate acclimation to new light conditions at different leaf maturities. Developmental acclimation describes changes that immature leaves or newly growing plants undergo to enhance their photosynthetic capacity to their light environment. Developmental acclimation induces changes in shoot morphology and chloroplast physiological enhancements of photosynthesis (Walters *et al*., 1999; Flannery *et al*., 2021).

An early study on the growth of *Alocasia macrorrhiza* plants under LL and HL conditions (17 and 400 µmol m^{-2} s^{-1} photosynthetically active photon flux density (PPFD), respectively) showed a significant increase under HL conditions for morphological characteristics such as leaf thickness, cell size (palisade and spongy mesophyll), and cell number (Sims and Pearcy, 1992). These morphological changes accompanied a 66% increase in maximum photosynthetic capacity for the

HL-grown leaves. Developmental acclimation is a long-term strategy for plants to take advantage of their light environment.

Dynamic acclimation involves mature, fully expanded leaves grown in a LL environment exposed to new HL conditions where they must adapt. Chloroplast physiological alterations of dynamic acclimation are often more significant than morphological changes plants undergo during developmental acclimation (Oguchi *et al*., 2003). For example, the mature leaves of *Chenopodium album* underwent morphological enhancements when transferred from LL to HL growth conditions (70 and 700 µmol m^{-2} s^{-1}, respectively; Oguchi *et al*., 2003). These included increasing leaf thickness and leaf mass per area compared to the LL control. However, these increases were not as significant as the difference between the plants grown solely under either LL or HL conditions. Photosynthetic capacity was also significantly enhanced upon transfer from LL to HL growth conditions but was not as significant as the difference between LL and HL-grown plants (Oguchi *et al*., 2003). Dynamic acclimation, the increase of photosynthetic capacity in mature leaves in response to new HL conditions, has been observed in several plant species (Oguchi *et al*., 2003; Athanasiou *et al*., 2010; Gerganova *et al*., 2016).

Some ecotypes of *Arabidopsis thaliana* did not undergo dynamic acclimation under certain light conditions; 100 µmol m^{-2} s^{-1} growth and 400 µmol m^{-2} s^{-1} HL conditions (Athanasiou *et al*., 2010). Under these conditions, the *Arabidopsis* ecotype Wassilewskija-2 (Ws-2) was capable of enhancing photosynthetic capacity to a comparable level of the HL-grown plants (Figure 1.1.1 [Page 19]). The relative increase in PPFD between LL and HL conditions was far lower than in previous

developmental acclimation experiments; 4 times (100 and 400 µmol m^{-2} s^{-1}) compared to 10 and 23.5 times (Sims and Percey, 1992; Oguchi *et al*., 2003). The relative differences in growth and new HL conditions may play a role in dynamic acclimation. A developmental acclimation study found only 20 of 22 plant species enhanced photosynthetic capacity (P_{max}/area) when grown under HL conditions compared to low light (LL) conditions (LL, 50 µmol m^{-2} s^{-1}; HL, 300 µmol m^{-2} s^{-1}; Murchie and Horton, 1997). Talhouët *et al*. (2020) found a reduction in photosynthetic rate (ΦPSII or Fq'/Fm' and A_{max}) of the alpine species *Soldanella alpina* upon transfer to from shaded conditions (800 µmol m^{-2} s^{-1}) to sun conditions (2000 µmol m^{-2} s^{-1}) compared to plants maintained in shade conditions. These results may be related to the relative differences between the growth and HL conditions or possibly photoinhibition (discussed further in section 1.2 [Page 20]).

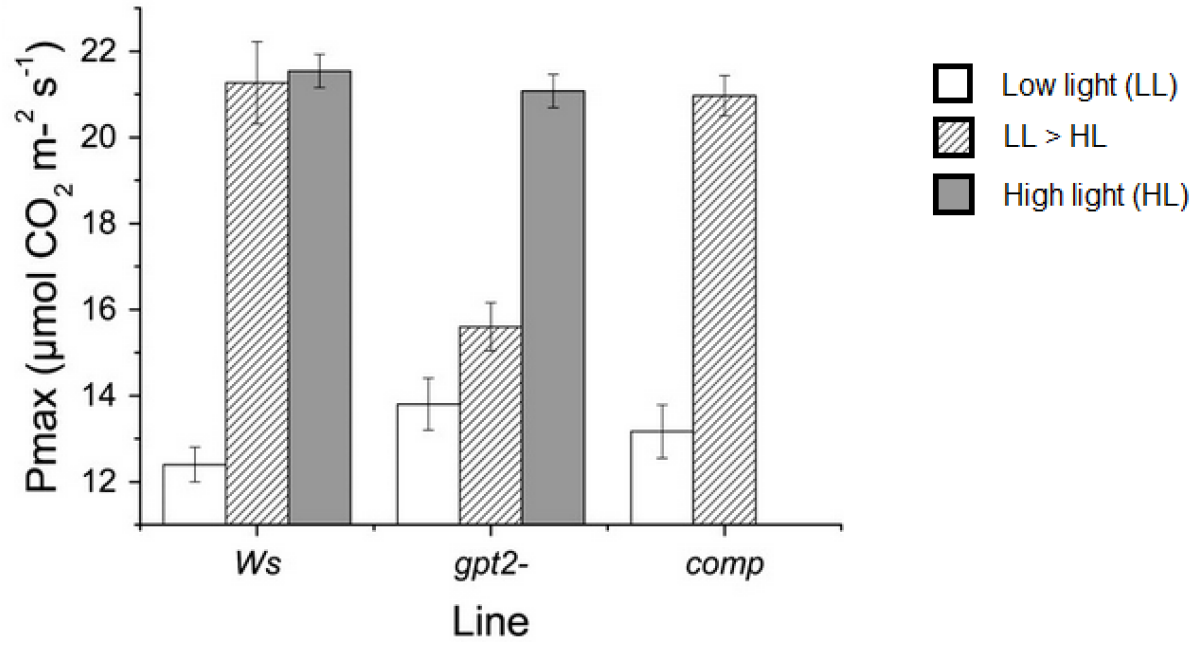

Figure 1.1.1: Dynamic acclimation of Wassilewskija-2 (Ws-2), *gpt2-*, and the *gpt2-* mutant complimented with a transgenic form of the *GPT2* gene (*comp*). Eight-week-old plants were grown at 100 µmol m^{-2} s^{-1} (LL; white) or grown at 100 µmol m^{-2} s^{-1}, and transferred to 400 µmol m^{-2} s^{-1} nine days before experimentation (LL > HL;

hatched), and grown at 400 µmol m^{-2} s^{-1} (dark; HL). Modified from Athanasiou *et al*. (2010).

I focused on mature leaves of *Arabidopsis thaliana* and uses the term HL acclimation for the enhancement of photosynthesis they undergo in response to HL; 150 µmol m^{-2} s^{-1} growth and 1000 µmol m^{-2} s^{-1} HL (see methods 2.2.1 and 2.2.2). This selection is due to the wide variety of mutants of *Arabidopsis* available, and previous studies have shown that these conditions initiate HL acclimation (or dynamic acclimation) within the common ecotype Columbia-0 (Col-0; Alvarez-Fernandez *et al*., 2021). HL acclimation and dynamic acclimation are practically interchangeable (further discussed in Chapter 7 [Page 260]); however, in this study, the term HL acclimation was used as the description is clearer from its label; it references the increased light condition. On the other hand, dynamic acclimation references the maturity state of the leaf, differentiating the term from developmental acclimation; however, it does not refer to the increased light conditions it defines.

1.2: Photosynthesis and HL acclimation

An episodic and sustained exposure to HL brings about the physiological alterations required to enhance photosynthetic capacity (Athanasiou *et al*., 2010; Alvarez-Fernandez *et al*., 2021). Athanasiou *et al*. (2010) showed the *Arabidopsis* ecotype Ws-2 increased its rate of photosynthesis over 7-9 days (short days; 8/16 hour day) of sustained HL (400 µmol m^{-2} s^{-1}) exposure compared to LL (100 µmol m^{-2} s^{-1}) grown plants. Alvarez-Fernandez *et al*. (2021; growth, 150 µmol m^{-2} s^{-1}; HL, 1000 µmol m^{-2} s^{-1}) used the Col-0 ecotype with a greater HL PPFD was only sustained across the central 4 hours of the 8-hour day. These plants increased their

photosynthetic capacity across only five days. The Col-0 plants received less light over the five days compared to the Ws-2 plants over the nine days, indicating a relationship between light intensity and the rate of HL acclimation.

There are physiological limitations to the HL PPFD used for HL acclimation experiments. If the PPFD is too great for the photosynthetic reaction centres to process, non-photochemical quenching (NPQ) is relied on to protect the plant. Plants use NPQ to safely dissipate excess excitation energy imparted into the photosynthetic reaction centres by increased light intensity (Baker, 2008). When the light is in great excess, a plant's NPQ capacity becomes overwhelmed, and photooxidative stress occurs (Mullineaux and Baker, 2010; Ruban and Murchie, 2012; Muñoz and Munné-Bosch, 2018). Alvarez-Fernandez *et al*. (2021) noted a lack of photoinhibition or significant tissue damage associated with photooxidative stress to Col-0 plants during the 1000 µmol m^{-2} s^{-1} HL exposure.

HL acclimation is fundamentally different to the response to excess light, a PPFD that induces irreversible photoinhibition (Mühlenbock *et al*., 2008; Alvarez-Fernandez *et al*., 2021). Mühlenbock *et al*. (2008) identified that Col-0 grown at 100 µmol m^{-2} s^{-1} experienced light stress upon exposure to 2000 µmol m^{-2} s^{-1} of light. This excess light initiated a response resulting in programmed cell death (Mühlenbock *et al*., 2008). Reactive oxygen species (ROS) and salicylic acid (SA) signalling pathways trigger the cell death response (Karpiński *et al*., 2013). These are retrograde signalling pathways; initiated within the chloroplast to signal the nucleus (Karpiński *et al*., 2013). HL acclimation signalling currently known favours anterograde (nucleus to chloroplast) light signalling (see section 1.3 [Page 22]; Alvarez-Fernandez *et al*.,

2021). The difference in signalling direction supports the view that light stress response and HL acclimation pathways are distinct (Mühlenbock *et al*., 2008; Mullineaux and Baker, 2010; Alvarez-Fernandez *et al*., 2021). In this study, I focused on HL acclimation, where minimal photoinhibition occurs.

1.3: Signalling of HL acclimation

HL acclimation is under genetic and environmental control (Kleine *et al*., 2007; Athanasiou *et al*., 2010). A change in the light environment alters the gene expression in the nucleus (Athanasiou *et al*., 2010; Miller *et al*., 2017). The nucleus encodes many integral photosynthesis genes, termed photosynthesis-associated nuclear genes (PhANGs). PhANGs are integral to components of the photosynthetic reaction centres and vital for photosynthesis. Exposure to HL alters the expression of PhANGs, which changes the composition of photosynthetic reaction centres (Albanese *et al*., 2016). This change was most dramatic in the light-harvesting antenna proteins; growth under HL conditions increased the abundance of LHCB4.3 and decreased LHCB3 and LHCB6 compared to LL-grown plants (developmental acclimation; Albanese *et al*., 2016). Researchers have not yet linked alterations of the photosynthetic reaction centres to photosynthetic capacity. However, the ability to enhance photosynthetic capacity by altering these factors is a probable determinant of plant fitness (Athanasiou *et al*., 2010; discussed in section 3.1 [Page 63]).

Upon the induction of HL, a set of transcriptional changes occur to enhance photosynthetic capacity (Athanasiou *et al*., 2010). Alvarez-Fernandez *et al*. (2021) conducted a microarray time-series experiment on six-week Col-0 plants exposed to

HL (150 µmol m^{-2} s^{-1} growth; 1000 µmol m^{-2} s^{-1} HL). The study took time points every half an hour between 0 and 6 hours of continual HL exposure with a LL (growth light) control. Differentially expressed transcription factors and co-factors, proteins that bind to DNA to alter gene expression and their co-factors, were extracted from the data set. The study inputted this data into Variational Bayesian State-Space Model (VBSSM) to calculate hidden states between the variables (Beal *et al*., 2005). This model produced the HL TF network, a directional network of transcription (co-) factors that act as a visual set of hypotheses (Figure 1.3.1 [Page 24]).

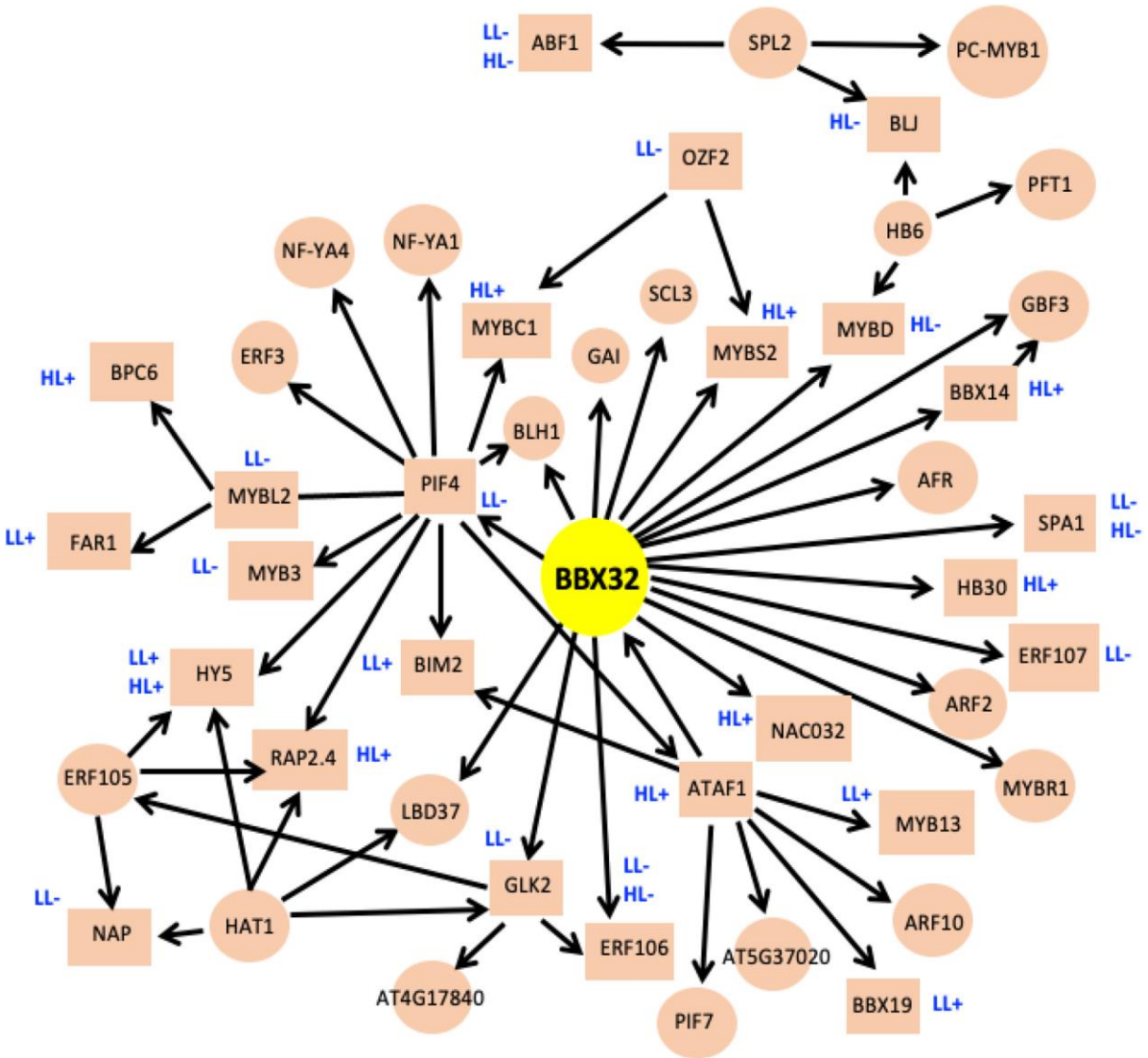

Figure 1.3.1: HL transcription factor network from Alvarez-Fernandez *et al*. (2021). Genes in rectangular nodes were perturbed by *BBX32* overexpression in HL or LL (blue) either positively or negatively (+/-).

The HL TF network centres around the transcription co-factor *B-BOX32* (*BBX32*). Plants that over-express *BBX32* had a perturbed HL acclimation phenotype (Alvarez-Fernandez *et al*., 2021; Figure 1.3.2 [Page 25]). The study measured PSII operational efficiency (Fq'/Fm' or ΦPSII), a factor indirectly related to photosynthetic capacity but can be measured without invasive methodologies (see section 2.2.3 [Page 36]). An *Arabidopsis* mutant is a HL acclimation mutant if the PSII operational efficiency significantly differs after five days of HL exposure across multiple measured PPFDs. For example, the *BBX32* over-expressor had a lower PSII operational efficiency after one day and five days of 4 hours of HL exposure (Alvarez-Fernandez *et al*., 2021).

Previous studies identified the impact of *BBX32* on seedling photomorphogenesis and plant fitness (Holtan *et al*., 2011; Preuss *et al*., 2012). Within *Glycine max*, *AtBBX32* over-expression increased seed yield by up to 8.7% in field trials furthering the connection between HL acclimation and plant fitness (Preuss *et al*., 2012). *BBX32* over-expressor seedlings display hyposensitivity to light, particularly blue light, through a mechanism involving *ELONGATED HYPOCOTYL5* (*HY5*; Holtan *et al*., 2011). Researchers identified that *HY5* increased in expression in response to HL compared to plants maintained under growth light after 24 and 72 hours (growth, 200 µmol m^{-2} s^{-1}; HL, 1000 µmol m^{-2} s^{-1}; Murchie *et al*., 2005). *HY5* is a member of the HL TF network (Figure 1.3.1 [Page 24]). The *HY5* mutants *hy5-2* and *hy5-215*

had perturbed HL acclimation phenotypes, similar to the BBX32-10 and BBX32-12 over-expressor mutants (Figure 1.3.2 [Page 25]).

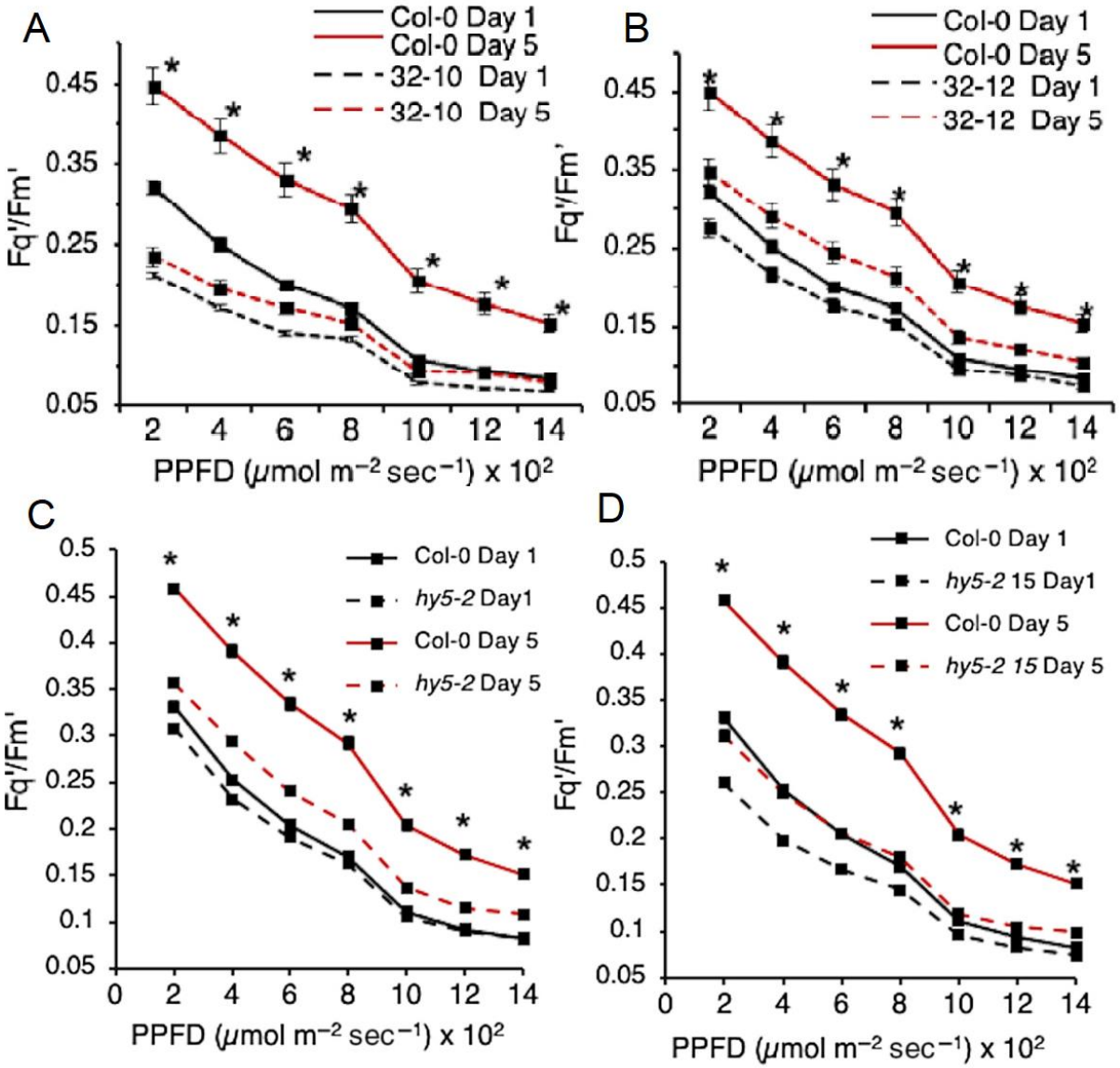

Figure 1.3.2: HL acclimation of BBX32-10 (32-10; A), BBX32-12 (32-12; B), *hy5-2* (C), *hy5-215* (D), and Col-0 plants. Fq'/Fm' was measured by chlorophyll fluorescence with a PPFD range of 200 µmol m^{-2} s^{-1} to 1400 µmol m^{-2} s^{-1} at 200 µmol m^{-2} s^{-1} increments. HL acclimation experiments used 4-6 week old plants with a minimum of 6 mature leaves each (mean ± SE). Arrows and asterisks denote a

significant difference between the day 1 and day 5 values respectively of the mutants and Col-0 (ANOVA, Tukey post-hoc; */↑ = $p < 0.05$; **/↑↑ = $p < 0.005$). Modified from Alvarez-Fernandez *et al*. (2021).

BBX32 impacts photomorphogenesis through a pathway involving HY5 (Holtan *et al*., 2011). BBX32 binds to the bridging protein BBX21, which can bind to HY5 (Holtan *et al*., 2011). However, plants lacking *BBX21* did not have a perturbed HL acclimation phenotype (Alvarez-Fernandez *et al*., 2021). It is unknown if *BBX32* and *HY5* influence HL acclimation through the same pathway despite their similar HL acclimation phenotypes.

1.4: Photoperception and HL acclimation

Plants perceive light through previously mentioned photosynthetic retrograde pathways (see section 1.2 [Page 20]; Karpiński *et al*., 2013). However, plants also contain other light signalling pathways independent of the chloroplast. Photoreceptors are proteins that initiate physiological alterations in response to specific wavelengths of light (Tilbrook *et al*., 2013). Different photoreceptors respond to different wavelengths of light (Kong and Okajima, 2016). Phytochromes respond to far-red (PHYTOCHROME A; phyA), red (phyB - phyE; Quail, 1991). CRYPTOCHROMES (CRY1 and CRY2; Ohgishi *et al*., 2004), PHOTOTROPINS (PHOT1 and PHOT2; Talbott *et al*., 2003) and ZEITLUPE (ZTL; Kim *et al*., 2007) respond to blue light. ULTRA-VIOLETB RESISTANCE8 (UVR8) responds to UV-B light (Kliebenstein *et al*., 2002). These proteins influence nuclear transcription, which alters anterograde, nuclear to chloroplast, signalling (Tilbrook *et al*., 2013).

Photoreceptors interpret the light environment and initiate changes in photosynthesis.

Walters *et al*. (1999) conducted an early study that determined the response of plants lacking specific photoreceptors genes to HL. I measured photosynthetic capacity (A_{max}), PSII operational efficiency (*Fq'/Fm'*) and other photosynthetic parameters of plants grown at different actinic PPFDs (developmental acclimation). WT plants grown at high PPFDs have an increased PSII operational efficiency. Mutant plants lacking the photoreceptors *CRY1* and *phyA* had an increased PSII operational efficiency measured at saturating PPFDs (approximately 1500 µmol m^{-2} s^{-1}) compared to the WT (Landsberg *erecta*) when grown under HL (400 µmol m^{-2} s^{-1}) conditions. The *phyB* mutant had Minimal differences in PSII operational efficiency. *hy5* mutants had a reduced difference between the PSII operational efficiencies of plants grown at LL and HL compared to the WT difference. Kleine *et al*. (2007) showed that *cry1* plants experience a more significant depression of maximum PSII quantum efficiency (*Fv/Fm*) after exposure to HL (100 µmol m^{-2} s^{-1}, growth;1000 µmol m^{-2} s^{-1}, HL) for 3, 6 and 9 hours compared to the WT control and *hy5* mutant. This decrease indicates a greater level of photoinhibition and light stress response. However, the study used plants that were only seven days old and had no mature leaves making these findings challenging to apply to HL acclimation. The findings of Walters *et al*. (1999) and Kleine *et al*. (2007) are notable for showing the impact of photoreceptors on photosynthesis and cellular signalling; however, their findings are not directly applicable to HL acclimation.

Weston *et al*. (2000) found morphological and physiological differences in photoreceptor mutants when transferred from growth conditions (150 µmol m^{-2} s^{-1}) and transferred to either LL or HL for six days (60 µmol m^{-2} s^{-1}, LL; 400 µmol m^{-2} s^{-1} for one day followed by 600 µmol m^{-2} s^{-1} for the remaining five days, HL). The double mutant *cry1cry2* and the mutant *phot1* had decreased chlorophyll a/b ratios compared to the corresponding WT when transferred to HL conditions. Researchers did not observe similar findings in the *cry1* or *cry2* single mutants. Plants exposed to lower light conditions tend to have more chlorophyll b, thereby lower chlorophyll a/b ratios due to the higher proportion of light-harvesting complex (LHC) proteins within the photosynthetic reaction centre, which disproportionally bind chlorophyll b (Anderson *et al*., 1995; Weston *et al*., 2000). HL-treated plants had a reduced quantity of LIGHT HARVESTING COMPLEXB1 (LHCB1) compared to the LL plants (Weston *et al*., 2000). *cry1cry2* plants had an increased quantity of LHCB1 following both LL and HL treatments which researchers did not observe in the *cry1* or *cry2* single mutants. Photoreceptors influence many factors related to photosynthesis during HL acclimation; however, Weston *et al*. (2000) did not measure photosynthetic capacity or photosynthetic operational efficiency. These experiments were also performed on young plants (14 days old) instead of on older plants with more mature leaves.

Alvarez-Fernandez *et al*. (2021) studied the ability of different photoreceptor mutants at six weeks old to acclimate to HL conditions (150 µmol m^{-2} s^{-1}, growth; 1000 µmol m^{-2} s^{-1} HL). Plants lacking *CRY1* had a reduced increase in PSII operational efficiency upon exposure to 5 days of 4 hours of HL compared to the WT control (Alvarez-Fernandez *et al*., 2021). The PSII operational efficiency after five days of

HL exposure of *cry2* plants was not significantly different from the WT. These paralogues were previously known to have distinctions in their mutant phenotypes; however, this novel separation is striking and shows that simply grouping the photoreceptor families is not always correct when studying the HL acclimation phenotype (Ponnu and Hoecker, 2022). Plants lacking *phyA* or *phyB,* two of the more prominent phytochromes, were also exposed to the same HL conditions as *cry1* for five days (Sharrock and Clack, 2002). Both *phyA* and *phyB* had a HL acclimation phenotype insignificantly different to the WT following five days of HL exposure (Alvarez-Fernandez *et al*., 2021).

Light perception influences HL acclimation and causes transcriptional changes to enhance photosynthetic capacity. Studies are yet to elucidate how these photoreceptors influence the HL TF network fully. However, other known pathways involving photoreceptors and these transcription factors, such as flowering time and photomorphogenesis, should be experimentally tested (Lau and Deng, 2012; Figure 1.5.1 [Page 32]). Distinguishing between these other pathways and HL acclimation would be beneficial information for altering HL acclimation and photosynthetic capacity without causing detrimental effects on plant productivity.

1.5: HL acclimation signal transduction

Light signals can cause a plant to change its transcriptome radically. The activation of photoreceptors alters the availability, quantity, and expression of transcription factors, thereby transducing a light signal (Boccalandro *et al*., 2004; Su *et al*., 2015). This light signal causes changes to the cellular environment. Specific photoreceptors such as phyA, phyB and CRY1 bind CONSTITUTIVELY

PHOTOMORPHOGENIC/DE-ETIOLATED1/FUSCA (COP/DET/FUS) complexes. These complexes act as E3 ubiquitin ligases, which ubiquitinate their target proteins to degrade them by the 26S proteosome (Deng *et al*., 1991; Ponnu and Hoecker, 2021). Many targets are TFs, such as the HL acclimation transcription factor HY5 (Lau *et al*., 2019; Alvarez-Fernandez *et al*., 2021). Pathways involving COP/DET/FUS transduce light signals from photoreceptors to influence many light-directed pathways such as flowering time, photomorphogenesis, and the circadian rhythm (Figure 1.5.1 [Page 32]; Ang *et al*., 1998; Lian *et al*., 2011; Lau and Deng, 2012; Xu, 2020)

CONSTITUTIVELY PHOTOMORPHOGENIC1 (COP1) is an integral part of many COP/DET/FUS complexes (Ma *et al*., 2003; Lau and Deng, 2012). Researchers named COP1 for its mutant photomorphogenic phenotype, short hypocotyls in the dark (Deng *et al*., 1991). Mutant *cop1* alleles can cause lethality in *Arabidopsis*. *cop1-5* is a lethal T-DNA insertion mutant, and researchers believe it represents a *cop1* null mutant (Ang and Deng, 1994; Stacey *et al*., 2000). Studies often use other *COP1* mutants in place of the null mutant, such as *cop1-4* and *cop1-6*, which only have C-terminal frame shift mutations (Q283STOP and five-residue-insertion at Q301, respectively; Stacey *et al*., 2000). Alvarez-Fernandez *et al*. (2021) experimentally tested the HL acclimation phenotype of the *cop1-4* mutant. After five days of 4 hours of HL exposure hours, *cop1-4* had a greater PSII operational efficiency than the WT control. However, *cop1-4* also had a greater PSII operational efficiency than the WT following only one day of 4 hours of HL exposure. This phenotype was labelled an accelerated acclimation phenotype. The reduced leaf and

567 petiole length of *cop1-4* make this mutant unviable for further study in other crop
568 species (Laubinger *et al*., 2004).
569
570 Another prominent COP/DET/FUS complex member is DE-ETIOLATED1 (DET1;
571 Chory *et al*., 1989; Pepper *et al*., 1994). The *det1-1* mutant has a short hypocotyl
572 phenotype in the dark, similar to the *cop1-4* mutant (Chory *et al*., 1989; Pepper *et al*.,
573 1994). The *det1-1* mutant did not have a significantly different PSII operational
574 efficiency from the WT following five days of 4 hours of HL exposure (Alvarez-
575 Fernandez *et al*., 2021). The lack of a HL acclimation phenotype of the *det1-1*
576 mutant divorced the HL acclimation phenotype from the photomorphogenic
577 phenotype.
578
579 Researchers have often linked the CRY1-COP1-HY5 pathway to
580 photomorphogenesis (Figure 1.5.1 [Page 32]; Ang *et al*., 1998; Lau and Deng,
581 2012). However, this may be because photomorphogenesis is easy to study as an
582 experimental system by determining the phenotype of hypocotyl length of
583 *Arabidopsis* seedlings under different light regimes. The new link presented by
584 Alvarez-Fernandez *et al.* (2021) showed photomorphogenic pathways could be
585 similar to other those of other functions (Figure 1.5.1 [Page 32]). This link may shed
586 light on the complexity of transcriptional regulation in HL acclimation and how distinct
587 functions can have overlapping evolutionary histories.
588

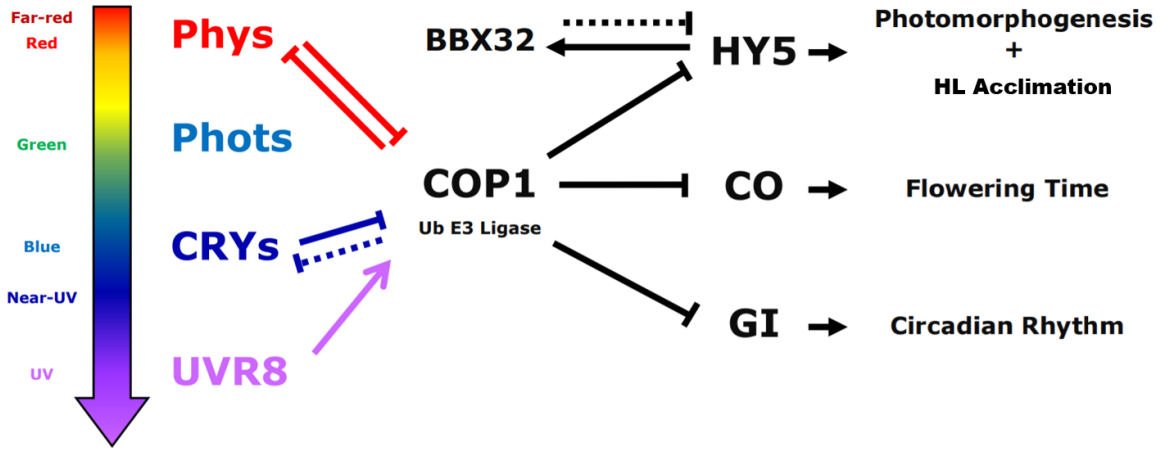

589

590 **Figure 1.5.1: Simplification of the light-governed pathways that initiate**
591 **transcriptional responses.** Common photoreceptors are given a shortened name
592 with a colour indicative of the wavelength they are sensitive to; Phys, Phytochromes;
593 Phots, Phototropins; CRYs, Cryptochromes; UVR8, UV-B RESISTANCE8. Dashed
594 lines represent indirect pathways of HY5 and BBX32 (Holtan *et al*., 2011) and CRY1
595 and COP1. CO, CONSTANS (BBX1); GI, GIGANTEA; Ub, Ubiquitin. Adapted from
596 Lau and Deng (2012).

597

598 1.6 Aims and objectives

599 HL acclimation is crucial for fully understanding how plants alter their photosynthetic
600 capacity to suit their light environment better. Improving plant productivity focuses on
601 increasing crop yields whilst reducing human environmental impact. A better
602 understanding of HL acclimation could improve yield in unnatural environments such
603 as crop fields and greenhouses where interspecies competition, predation and
604 disease are far less common. Through 20th-century breeding programs, researchers
605 consider light interception and biomass conversion to seed yield has reached a near

theoretical maximum (Long *et al*., 2006). However, the conversion of light energy to biomass can still be improved, which is the critical target of altering HL acclimation. Therefore, I intend to study HL acclimation through the following objectives;

- Determine if components of a BBX32-centric transcription factor network also influence HL acclimation, providing novel genes for further exploitation.
- Determine how *BBX32* impacts photosynthesis and productivity.
- Determine if novel *BBX32* alleles, created by gene editing, can be identified that maximise gains in photosynthetic capacity with minimum impact on other development processes such as flowering time, leaf senescence and photomorphogenesis.
- Determine how components of COP/DET/FUS complexes influence HL acclimation.
- Determine the impact of further photoreceptor mutants on HL acclimation.
- Determine the broader impact of *BBX32* and HL acclimation on systems such as stress-associated phytohormone signalling and pathogen defence.

Chapter 2: Materials and Methods

2.1: *Arabidopsis thaliana* Plant Material

2.1.1: Donated Plant Materials

The only *Arabidopsis thaliana* ecotype used within this study was Columbia-0 (Col-0). All plant lines used were from the Col-0 ecotype. The following plant lines have been previously described; BBX32-10, BBX32-12*, bbx32-1* (Holtan *et al*., 2011) and YHB (*phyB:phyB*^{Y276H}; Jones *et al*., 2015). *ataf1-4* and 35S:ATAF1 OX 17 were generously donated by Salma Balazadeh (University of Leiden; Garapati *et al*., 2015). *spa1-7 spa2-1 spa3-1* (*spa123*; Fittinghoff *et al*., 2006; Chen *et al*., 2016), *spa1-100* (SAIL; Sessions *et al*., 2002; Yang *et al*., 2005), *spa2-1* (GABI-KAT T-DNA; Rosso *et al*., 2003; Laubinger *et al*., 2004), *spa3-1* (Laubinger and Hoeker, 2003) and *spa4-1* (Laubinger and Hoeker, 2003) were generously donated from Ute Hoecker, University of Cologne.

2.1.2: Nottingham Arabidopsis Stock Centre

The following plant lines were obtained from the Nottingham Arabidopsis Stock Centre: some of which have not been characterised. References were given when a mutant line had been previously studied. *afr* (SALK_120395; Eroglu *et al*., 2016)*, arf2-8* (SALK_108995; Okushima *et al*., 2005), BBX14 (induced by 17β-estradiol; TRANSPLANTA collection; Coego *et al*., 2014; not characterised; TPT_1.68520.1H), *bbx19-2* (SALK_087493; Wang *et al*., 2015), *blh1-2* (GK-114D09; Pagnussat *et al*., 2007), *erf106* (SALK_097771; Walper *et al*., 2016), *erf107* (SALK_015182; Walper *et al*., 2016), *glk2-2* (SALK_117006; not characterised), *lbd37* (SALK_058867; Albinsky

et al., 2010), *mybd* (SALK_045905; Nguyen *et al*., 2015), *mybs2* (SAIL_1184_D04; Chen *et al*., 2017), *nac032* (SALK_087702; Maki *et al*., 2019), *pif7-1* (N68809; Leivar *et al*., 2008) and 35S:PIF7 (N72166; Leivar *et al*., 2008). *glk1* (N9805; Atglk1.1), *glk2* (N9806; Atglk2.1), *glk1glk2* (N9807; Atglk1.1; Atglk2.1), 35S:GLK1-GFP (N9805) and 35S:GLK2-GFP (N9806) were previously described in Fitter *et al*. (2002).

2.2: Arabidopsis Growth Conditions and Measurements

2.2.1: Standard Growth Conditions

Arabidopsis seeds were placed on a commercial compost mixture (Levington F2+S; The Scotts Company, Bramford, UK), watered, and stratified at 4 °C for 3 - 4 days. Plants were grown under short-day conditions (SD; 8-hour day, 16-hour night) unless otherwise specified. The climate was controlled at a temperature of 22°C ± one °C with a humidity of 59% ± 1% and a photosynthetically active photon flux density (PPFD) of 150 µmol m^{-2} s^{-1} ± 10 µmol m^{-2} s^{-1} (spectra: Figure S1 [Page 328]) was provided during the artificial day.

2.2.2: HL Acclimation Growth Conditions

Plants were grown under standard growth conditions (see 2.2.1) for 4 - 6 weeks. HL acclimation was initiated by transferring plants 2 hours after artificial dawn (ZT2) and placed under an Isolight3 (Technologica Ltd, Colchester, UK; spectra: Figure S1 [Page 328]). The plants were exposed to HL treatment of a photosynthetically active photon flux density (PPFD) of 1000 µmol m^{-2} s^{-1} ± 100 µmol m^{-2} s^{-1} for 4 hours. If necessary, chlorophyll fluorescence measurements (section 2.2.3 [Page 36]) would be performed at the end of the day's treatment. Elsewise, the plants would be transferred back to standard growth conditions for the remaining two hours of their

artificial day. This treatment would be repeated for a total of 5 days, after which the plants were considered HL acclimated, which would be determined by chlorophyll fluorescence (section 2.2.3 [Page 36]).

2.2.3: Chlorophyll Fluorescence

Chlorophyll fluorescence is the measurement of fluorescence emissions from chlorophyll molecules bound to reaction centres of PSII (Baker, 2008). The duration and intensity of PPFD can be used to manipulate the chlorophyll-PSII system to produce useful information from the fluorescence emissions. PSII is considered open or closed based on the redox state of the bound Q_A, the primary quinone acceptor of the electron transport chain where oxidised is open and reduced is closed. By providing a saturating light pulse, Q_A becomes maximally reduced, and the bound chlorophyll cannot transfer its excitation energy and therefore strongly fluoresces. Researchers can withhold light from the system, giving a maximally oxidised Q_A and weak chlorophyll fluorescence. The PSII-Q_A-chlorophyll system is, however, not binary and can be light-adapted to specific PPFDs. These methods of manipulating chlorophyll molecules provide the tools for non-destructively estimating the PSII operational efficiency.

The parameters used in chlorophyll fluorescence fall within two categories: light-adapted denoted as prime (*e.g.* Fm‘) or dark-adapted without a prime (*e.g.* Fm). I only used the light-adapted parameters: F_o’, F’, Fm’, Fv’ and Fq’. F_o’ is the low fluorescence a light-adapted system performs in the dark. F’ is the fluorescence a light-adapted system produces at the light-adapting PPFD. Fm’ is the maximal

emission of the system measured by providing the light-adapted system with a saturating pulse. Fv' is calculated as Fm' - F_o', and Fq' is calculated as Fm' - F'.

The most valuable measurements for this study were Fq' and Fm'. When Fq' is divided by Fm' (Fq'/Fm'), it forms a ratio between F' and Fm', as Fm' is used to calculate Fq'. Previous studies have defined Fq'/Fm' as the PSII operational efficiency (Baker *et al*., 2008). PSII uses light to reduce bound quinone, and researchers estimate this reaction's efficiency by using the parameter Fq'/Fm' at a given PPFD. F' increases relative to Fm' as the light-adapted PPFD increases, reducing Fq'/Fm', as Fq' is calculated from F' and Fm'. A low F' to Fm' ratio indicates a more efficient use of the given PPFD as there is a reduced remission of energy as chlorophyll fluorescence. Even though this is not a direct measurement of photosynthesis, it allows researchers to take measurements in a non-destructive manner allowing multiple days of measurements using the same plants.

I conducted chlorophyll fluorescence measurements between ZT6 and ZT10; immediately following HL exposure to 4 hours post-exposure. Plants were transferred from either growth conditions or HL treatment to the dark for at least 20 minutes, termed dark adapted. If the study required multiple sets of plants tested on the same day, plants remained in dark conditions until ready. Dark-adapted plants were placed in the Fluoroimager (Technologica Ltd, Colchester, UK), and the program was initiated. The program initially set the PPFD to 0 µmol m^{-2} s^{-1} to record dark-adapted parameters. The PPFD was subsequently increased to 200 µmol m^{-2} s^{-1} for the light-adapted cycles. A cycle consists of 5 minutes of PPFD exposure followed by a saturating pulse. A PPFD was held for 5 minutes during a cycle so the

plant could become light adapted to the specific PPFD; however, the first PPFD (200 µmol m^{-2} s^{-1}) was repeated for three cycles to ensure the transition from dark-adapted to light-adapted with only the measurements from the final cycle being used. Each cycle afterwards increased the PPFD by increments of 200 µmol m^{-2} s^{-1} with a final PPFD of 1400 µmol m^{-2} s^{-1}.

Chlorophyll fluorescence measurements would be typically taken after one day of HL treatment (day 1) or five days of HL treatment (day 5). Experiments that recorded more than two days of measurements took chlorophyll fluorescence measurements before any HL treatment (day 0) and after each day of HL treatment (day 1 - day 5).

Chlorophyll fluorescence measurements were analysed using the Fluoroimager program (https://www.technologica.co.uk/). The background was excluded using the colour cut tool. Each mature leaf was isolated from the rest of the plant (minimum 4) by deleting pixels between the leaves. Leaves were assigned a number using the isolate colonies tool. Each leaf was assigned a day and genotype, and the data was loaded into RStudio for statistical analysis. The P-value considered significant was reduced to account for the partial independence of each leaf.

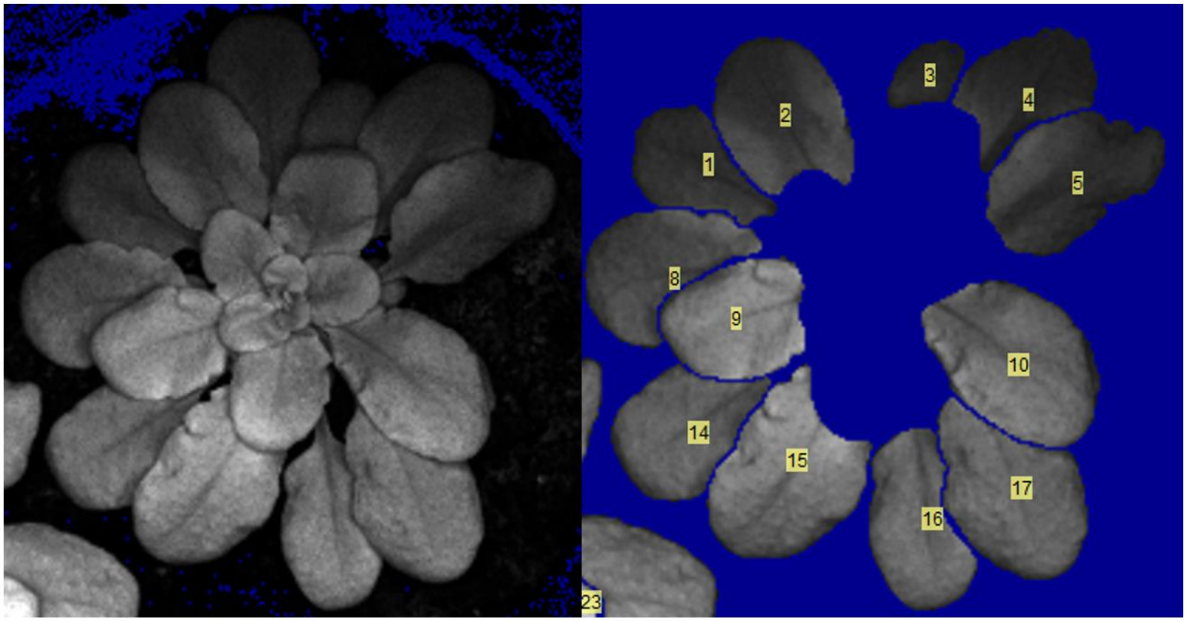

Figure 2.2.1: Chlorophyll fluorescence image of an eight-week-old *spa123* plant grown under standard growth conditions (section 2.2.1 [Page 35]) before and after processing.

2.2.4: Hypocotyl Growth Conditions

Seeds were surface sterilised (section 2.3.14 [Page 5046]) before being individually placed in rows by genotype on ½ strength MS agar plates (Murashige and Skoog, at pH 5.7; MilliporeSigma, Burlington, Massachusetts, United States). Multiple plates were used to randomise seed placement height on the plate. The plates were placed vertically to encourage the seedlings to grow up the agar. They were wrapped in aluminium foil and placed in the dark to stratify at 4 °C for 3 - 4 days. The seeds were exposed to 150 µmol m^{-2} s^{-1} of light for 16 hours to encourage uniform germination. The plates were wrapped again in aluminium foil twice to prevent light intrusion and humidity loss and placed in standard growth conditions to maintain temperature. After seven days of darkness, an image of each plate was taken using

a digital scanner to ensure a flat plane image and the lengths of the hypocotyls were measured using ImageJ (https://imagej.nih.gov/ij/).

2.2.5: Yield and Flowering Time measurements

Between 3 and 6 seeds were placed on 5 cm diameter pots to ensure a healthy plant on each pot. They were stratified and placed under standard growth conditions. Excess plants were culled after two weeks of growth. The placement of the plants in the growth cabinet was randomised twice a week to mitigate subtle differences in light and temperature within the growth cabinet. Flowering time was recorded when the first buds could be seen. The leaf number at flowering time was recorded at this time. The bolt was placed in a 25 mm clear florist cellophane tube to keep the plants separated. A bamboo cane was provided to maintain the stability of the tube. When 50 % of the siliques had matured, water was withdrawn, and the plants were allowed to dry. Once fully dry, the seeds were threshed from the plant and weighed.

2.2.6: Gas Exchange

Plants used for gas exchange were grown under standard growth conditions (section 2.2.1 [Page 35]) for eight weeks before experimentation due to the greater leaf size requirements. The plants were subjected to 5 days of daily 4-hour HL treatments (section 2.2.2 [Page 35]), and the gas exchange measurements were taken on the following day between artificial dawn and an hour before artificial dusk. A Li-Cor 6800 portable gas exchange system (Li-Cor, Lincoln, Nebraska, USA) was used for all gas exchange measurements. A fully expanded mature leaf was selected for experimentation and placed in the chamber. A leaf temperature of 23 °C, a constant cuvette condition of 400 µmol mol^{-1} of CO_2, a constant flow rate of 500 µmol s^{-1} and

774 a vapour pressure deficit of 1 .2 (±0.2) kPa were maintained throughout the
775 experiment. The ratio of leaf size to chamber size was obtained using photographs
776 and ImageJ (https://imagej.nih.gov/ij/).
777
778 AC_i curves were obtained by measuring the assimilation rate (A) as a function of the
779 intercellular CO_2 measured at a PPFD of 1500 µmol m^{-2} s^{-1}. Leaves were allowed to
780 stabilise at an ambient CO_2 of 400 µmol mol^{-1} within the chamber before the program
781 was begun. The CO_2 was decreased and then increased through a range of
782 concentrations (300, 200, 100, 80, 50, 550,700, 900, 1100, 1300, 1500 µmol mol^{-1}).
783 Measurements were taken when the A value was stable, allowing the program to
784 move on to the next value. Stabilisation typically took place between 30 - 90
785 seconds.
786
787 AQ curves measure the change in assimilation rate as a function of the PPFD. The
788 conditions were similar to AC_i curves; for each plant, the AQ measurements were
789 taken immediately following the AC_i measurements on the same leaf. Leaves were
790 stabilised at a PPFD of 1500 µmol m^{-2} s^{-1} before being decreased through 1300,
791 1100, 900, 700, 550, 400, 250, 150, 100, 50 and 0 µmol m^{-2} s^{-1}. Similarly to the AC_i
792 measurements, the measurements were taken once the A value was stable.
793 Stabilisation allowed the program to continue decrementing through the PPFD
794 decrements.

795 2.2.7: Spraying plants with SA

796 A solution of 10mM SA in 0.001 % Triton X-100 (MilliporeSigma, Burlington,
797 Massachusetts, United States) in water was used. Plants were sprayed each day

before HL treatment (section 2.2.2 [Page 35]) until covered in a film of the solution. Control plants were similarly treated with a solution of 0.001 % Triton X-100 (MilliporeSigma, Burlington, Massachusetts, United States) in water at the same time as the SA-treated plants.

2.3: Laboratory Methods

2.3.1: DNA extraction

Leaves or whole plants were extracted for a total wet mass of approximately 100 mg per sample. These were homogenised in 1.5 ml microcentrifuge tubes, and 400 µl of DNA extraction buffer (100 mM Tris-HCl, 100mM EDTA, 250 mM NaCl) was added. Samples were lysed with 40 µl of 20 % sodium dodecyl sulphate (w/v; SDS) followed by an incubation step at 65 °C for 1 hour with regular vortexing. Samples were centrifuged at 12225 xg for 15 minutes, and the supernatant was transferred to a new 1.5 ml microcentrifuge tube. 500 µl of chloroform was added, and the sample was vortexed and centrifuged at 12225 xg for 15 minutes. The supernatant was added to a fresh tube with 500 µl of ice-cold isopropanol, and the DNA was allowed to precipitate at -20 °C for an hour. The samples were centrifuged at 12225 xg for 15 minutes to pellet the DNA, and the supernatant was removed. The samples were washed with 70 % (v/v water) ice-cold ethanol followed by centrifugation at 12225 xg for 5 minutes and removal of the supernatant. The previous step was repeated with 100 % ice cold ethanol, and the samples were allowed to air dry for 30 minutes. DNA was resuspended in RO water, heated at 55 °C for 10 minutes and stored at -20 °C for use in experiments. The concentration of DNA was measured by spectrophotometry (section 2.3.7 [Page 45]).

2.3.2: RNA extraction

Leaves of approximately 100 mg of 6-week-old plants were frozen on liquid nitrogen and stored at -70 °C before extraction. Samples were homogenised while being cooled on dry ice and placed into 1.5 ml microcentrifuge tubes with 500 µl of TRIzol Reagent (Invitrogen, Waltham, Massachusetts, USA, 15596018). 200 µl of chloroform was added, and the samples were vortexed and allowed to incubate on ice for 5 minutes. Samples were centrifuged at 12225 xg and four °C for 15 minutes. The aqueous (upper) phase was transferred to a new 1.5 ml microcentrifuge tube containing 500 µl ice cold isopropanol and allowed to incubate on ice for 15 minutes. The samples were centrifuged at 12225 xg and 4 °C for 15 minutes, and the supernatant was removed. RNA was washed with 70 % (v/v) ice cold ethanol and centrifuged at 12225 xg and 4 °C for 5 minutes, and the supernatant was removed. The previous step was repeated with 100 % ice cold ethanol, and the samples were allowed to air dry. RNA was resuspended in diethyl pyrocarbonate (DPC) treated water and heated at 55 °C for 10 minutes. Samples were stored at -70 °C for use in experiments, and the RNA concentration was measured using spectrophotometry (section 2.3.7 [Page 45]).

2.3.3: Polymerase Chain Reaction (PCR)

PCR used an in-house Taq polymerase and a total reaction volume of either 20 µl or 50 µl depending on the quantity of PCR product required. The following describes a total reaction volume of 20 µl, which was scaled by 2.5 times for a total reaction volume of 50 µl. 20 µl reactions used; 2 µl of 10x DreamTaq buffer (Thermo Scientific, Waltham, Massachusetts, U.S.A), 0.5 µl of 10 µM of each both reaction-specific forward and reverse primers, 0.4 µl of 10 mM dNTPs, 50 - 500 ng of DNA

and 0.5 µl of Taq polymerase with the remaining volume being made up by milli-Q water. PCR was conducted on a thermal cycler, with the program being varied based on the specific primers and DNA used. A typical program consisted of; an initial denaturation step at 95 °C for 10 minutes, between 25 and 35 cycles of denaturation of 95 °C for 30 seconds, 55 - 60 °C annealing temperature (dependent on primer T_m) and extension of 72 °C for 30 seconds increasing by 60 seconds for every kilobase of replicated DNA. A final extension was performed at 72 °C for 10 minutes before the PCR product was cooled to 22 °C.

2.3.4: Primer design

Primers were designed using the Primer3Plus program with a target T_m of 60 °C using the target section of DNA (https://www.bioinformatics.nl/cgi-bin/primer3plus/primer3plus.cgi; Rozen and Skaletsky, 2000). Designed primer pairs were inputted into the NCBI Primer-BLAST (https://www.ncbi.nlm.nih.gov/tools/primer-blast/; Ye *et al*., 2012) program targeting the *Arabidopsis thaliana* genome. Primer pairs that computationally only target the desired DNA sequence were used.

2.3.5: cDNA Synthesis

The initial reaction used 1 µg of RNA, 1 µl of 100 µM random hexamer primer and water to make a total reaction volume of 12 µl. The reaction was incubated at 65 °C for 5 minutes and chilled on ice. The following reagents were added; 4 µl of 5x RT reaction buffer, 2 µl of 10 mM dNTPs, 1 µl of RevertAid reverse transcriptase (RT; 200 U /µl; Thermo Scientific, Waltham, Massachusetts, U.S.A) and 1 µl of water to make a total reaction volume of 20 µl. This was incubated in a thermal cycler at 25

°C for 10 minutes, followed by 42 °C for 60 minutes. The reaction was terminated by heating to 70 °C for 5 minutes. The cDNA was stored at -20 °C for experimentation.

2.3.6: qRT-PCR and Analysis

Quantitative RT-PCR was performed within a Biorad CFX96 thermal cycler (Biorad Laboratories Incorporated, USA) using the fluorescent DNA dye SYBR Green I. The reaction consisted of 10 µl of 2x Maxima SYBR Green qPCR Master Mix (Thermo Scientific, Waltham, Massachusetts, U.S.A, K0221), 1 µl of 10 µM of both reaction-specific forward and reverse primers and 100 ng of cDNA (calculated using the methodology outlined in section 2.3.7 [Page 45]) with water making up a total reaction volume of 20 µl. The thermal cycler was programmed for an initial denaturation at 95 °C for 5 minutes, followed by 40 cycles of denaturation at 95 °C for 15 seconds, annealing at 60 °C for 30 seconds and extension at 72 °C for 30 seconds with a fluorescence reading taken between each cycle. Following the qPCR, a melt curve was also conducted with increments of 0.2 °C to ensure qPCR product purity. The output data was processed into gene expression relative to a selected gene and manipulated using the $2^{-\Delta\Delta CT}$ methodology (Livak and Schmittgen, 2001).

2.3.7: Quantification of Nucleic Acids

The concentration of nucleic acids was measured using spectrophotometry. A NanoDrop ND-1000 UV-Vis spectrophotometer was used along with the NanoDrop V3.1 software (Labtech International Limited, UK). The optical density (OD) at specific wavelengths was used to determine purity and concentration. The Beer-Lambert law ($A = \varepsilon cl$) was used to calculate molar concentration (c) from the

absorbance (A), optical path length (l) and known molar absorptivity of DNA/RNA (ε). Purity could be determined by comparing the ratios of the ODs between 260 nm and 280 nm and 260 nm and 230 nm.

2.3.8: Measurement of the relative size of DNA Fragments using Gel Electrophoresis

Visualisation of the size of DNA fragments was determined using agarose gel electrophoresis. 2 % (w/v) agarose/ TAE (4.84g Tris-HCl, 1.14ml Ethanoic acid, 0.37g Disodium EDTA, pH 8.0 per litre) gels were used unless otherwise stated with higher percentage gels being preferred for smaller length DNA fragments. GelRed (Biotium, Fremont, California, USA) was added at 5 µl per 50 ml of gel to cause the DNA fragments to fluoresce under UV light. The size of the DNA fragments was measured against the DNA reference GeneRuler 100bp DNA ladder (Thermo Scientific, Waltham, Massachusetts, U.S.A, SM0241). Samples and DNA ladder were loaded into the gel wells with the supplied 6x TriTrack DNA loading buffer (Thermo Scientific, Waltham, Massachusetts, U.S.A, R1161). Gels were placed in a 1x TAE buffer, and 100 V were passed through the solution for 45 minutes. The gel was then imaged using the Gel Doc™ EZ System (Bio-Rad Laboratories Incorporated, Hercules, California, USA).

2.3.9: Bacterial Glycerol Stocks

E. coli (picked from a single colony) was inoculated into a 5 ml LB broth (1 % (w/v) Bacto Tryptone, 0.5 % Bacto Tryptone Yeast extract, 0.5 % (w/v) NaCl, 0.1 % (w/v) glucose, pH 7.0) containing an antibiotic the culture carries an immunity. These were grown in a 37 °C, 200 rpm shaker overnight. The culture was then centrifuged in a

1.5ml microcentrifuge tube at 4293 xg for 5 minutes, 1 ml at a time, with the supernatant being removed after each centrifugation. The pellet was resuspended in 80 % (v/v water) glycerol that was stored at -22 °C. The glycerol stock was stored at -70 °C for use in experiments.

2.3.10: Chemically Competent *E. coli* Cells

Glycerol stocks of *E. coli* cells were streaked onto antibiotic-selective LB plates and allowed to incubate overnight. A single colony was used to inoculate 5 ml of LB broth and was grown overnight in a 37 °C, 200 rpm shaker. 200 µl of this culture was inoculated into 10 ml of LB broth which was allowed to grow in a 37 °C, 200 rpm shaker until the OD at 600 nm reached 0.4. The cells were chilled on ice for 10 minutes and centrifuged at 1500 xg for 10 minutes, and the supernatant was discarded. The cells were washed with 10 ml of ice-cold 100 mM $CaCl_2$, gently resuspended, and allowed to sit on ice for 30 minutes. The cells were centrifuged at 1500 xg for 10 minutes, and the supernatant was removed. The previous washing steps were repeated twice more, and cells were resuspended in 80 % (v/v water) glycerol that was stored at -22 °C. Competent cells were aliquoted into single-use volumes (~50 µl) in microcentrifuge tubes and stored at -70 °C for use in experiments. Two strains of competent *E. coli* cells were made through this method; TOP10 (F- mcrA Δ(mrr-hsdRMS-mcrBC) φ80lacZΔM15 ΔlacX74 nupG recA1 araD139 Δ(ara-leu)7697 galE15 galK16 rpsL(StrR) endA1 λ-; Invitrogen) and DB3.1 (F-gyrA462 endA1 glnV44 Δ(sr1-recA) mcrB mrr hsdS20(rB-, mB-) ara14 galK2 lacY1 proA2 rpsL20(Smr) xyl5 Δleu mtl1) which contained the *ccdB* lethal gene.

2.3.11: Transformation and Growth of Chemically Competent *Escherichia coli*

An aliquot of competent *E. coli* cells in a microcentrifuge tube was thawed on ice for 30 minutes before 5 µl of a vector from a ligation reaction (see section 2.5.4 [Page 59]) was added. Cells were heat-shocked at 42 °C for 30 seconds and quickly transferred to ice for 10 minutes. 750 µl of room temperature LB broth was added, and the cells were allowed to grow in 37 °C, 200 rpm shaker for 1 hour. 100 µl of the cells were spread onto an LB agar plate containing an antibiotic to which the transformed cells were resistant. Plates were grown overnight at 37 °C and then checked for viable colonies.

2.3.12: Extraction of plasmid DNA

Overnight growth of *E. coli* containing the desired plasmid DNA in LB broth with a specific antibiotic was added to a 1.5 ml microcentrifuge tube, centrifuged at 12225 xg for 2 minutes, and the supernatant was discarded. This was repeated if more than 1 ml of culture was used (if a higher quantity of plasmid DNA was desirable). The pelleted bacterial cells were resuspended in 400 µl P1 buffer (50 mM Tris-HCl pH 8.0, 10 mM EDTA) and 4 µl of RNase A (100 µg/ml) was added. The solution was mixed through gentle inversion. 400 µl of lysis buffer (200 mM NaOH, 1 % SDS) was added, and the solution was mixed again by inversion. The solution was allowed to stand at room temperature for 5 minutes before 400 µl neutralisation buffer (4.2 M Guanidine Hydrochloride, 0.9 M Potassium acetate, pH 4.8) was added. The solution was mixed by inversion and centrifuged at 12225 xg for 2 minutes. 750 µl was added to a spin column and centrifuged at 6708 x g for 2 minutes. The flow-through was discarded, and the spin column was washed with 75 % ethanol and centrifuged at

6708 xg for 2 minutes. The previous step was repeated for a total of two washes, and the flow-through was once again discarded. The empty spin column was spun at 6708 x g for a further minute to remove any remaining ethanol. 50 µl of RNA-free water was added directly to the gel of the spin column and allowed to stand for 2 minutes. A new 1.5 ml microcentrifuge tube was added to the bottom of the spin column and spun for 6708 x g for 2 minutes. The eluted plasmid DNA was stored at -22 °C for future experiments.

2.3.13: Infection of Arabidopsis with Pseudomonas syringae

Pseudomonas syringae DC3000 cells were grown from a glycerol stock in a 28 °C, 200 rpm shaker for 48 hours in LB broth with rifampin (25 mg/ L) and kanamycin (50 mg/ L) antibiotics. 100 µl of the culture was spread onto an LB agar plate with rifampin and kanamycin and grown at 28 °C for 48 hours. A single colony was selected and grown at 28 °C, 200 rpm shaker for 48 hours in LB broth. 100 µl of this culture was inoculated into LB broth and allowed to grow until it reached an OD at 600 nm of 0.4. The culture was diluted down to an OD at 600 nm of 0.0002 with 10 mM $MgCl_2$ to create the pathogenic solution for the inoculation of *Arabidopsis*.

Six-week-old *Arabidopsis thaliana* plants grown under standard conditions were infected using the blunt-end syringe method. Experimentation was performed in the morning, an hour after the plants had been heavily watered. A blunt-end 10 ml syringe was loaded with the pathogenic solution and pressed against the abaxial (lower) leaf side. A seal was formed using a gloved finger gently pressed against the adaxial (top) side of the leaf opposite the syringe. The syringe was gently depressed, forcing the pathogenic solution into the intercellular space of the leaf. This was

repeated until the entire leaf had turned a darker colour from the ingress of the pathogenic solution. 6 fully expanded leaves of each plant (n = 5) were infiltrated with the pathogenic solution. Infiltrated leaves were marked on the petiole. Plants were returned to standard growth conditions and covered with a clear plastic propagation lid to increase humidity for the duration of the experiment.

Extractions from leaves were taken on day 0, day 2, and day 4. Day 0 extractions were taken immediately after infiltration. First, 4, 1 cm^2 leaf discs were punched out of infected leaves and ground in 500 µl of 10 mM $MgCl_2$. Next, 20 µl of the extract was added to 180 µl of 10mM $MgCl_2$. From this, a dilution series was prepared with a dilution factor of 10. The extract was diluted six times, creating a dilution series of 7 concentrations of extracts. 100 µl of each of the dilution series was grown on LB agar plates with rifampin and kanamycin at 28 °C for 48 hours, and the colonies were subsequently counted. The plates with between 50 and 500 colonies were used (where available) to calculate the colony-forming units per cm^2 (CFU per cm^2) of each genotype across the three days tested (0, 2, and 4 days).

2.3.14: Seed Surface Sterilisation

Between 500 and 10000 seeds were simultaneously sterilised in a 1.5 ml microcentrifuge tube within a flow hood. 500 µl of 0.1 % Tween 20 in 95 % ethanol (v/v/v). The microcentrifuge tubes were placed in a rotary wheel (FinePCR, Korea) for 3 minutes. The liquid was then removed by pipette, and the seeds were washed with 70 % ethanol. The tubes were placed in the rotary wheel for another 3 minutes, and the liquid was removed again. The wash-spin step with 70 % ethanol was repeated a total of 3 times before the seeds were allowed to dry in the flow hood on

sterilised filter paper. Sterilised seed could be safely used on MS media plates without fear of contamination.

2.4: Computational Methods

2.4.1: R programming language

The R programming language (https://www.r-project.org/, v4.1.1) was used throughout this study for data manipulation and figure generation. RStudio (https://www.rstudio.com/, v1.4.1717) was used to interface with the R language, install packages and build projects. Data manipulation was done with the support of dplyr (v1.0.7), tibble (v3.1.5), rstatix (v0.7.0), tidyr (v1.1.4) and stringr (v1.4.0). Figures were generated using in-built tools in the R language along with pheatmap (v1.0.12) and ggplot2 (v3.3.5).

2.4.2: High-performance cluster

The University of Essex high-performance cluster (HPC) was used to enable some of the computationally intensive data processing (https://repository.essex.ac.uk/). The Ceres cluster was built on the Rocks Clustering Solution with CentOS Linux and allowed intensive data processing such as RNA-seq to be performed faster.

2.4.3: Processing RNA-seq Data

The RNA-seq fastq files for the *BBX32-HY5* HL RNA-seq were obtained, of which the *BBX32* and Col-0 components were analysed by Alvarez-Fernandez *et al*. (2021; uploaded to GEO as GSE158898). The RNA-seq of the *hy5-2* mutant was performed simultaneously with *BBX32* and Col-0; however, analysis was not performed by Alvarez-Fernandez *et al*. (2021). The data was uploaded to the University of Essex

HPC, and the quality of the sequence reads was checked using Fastqc (v0.11.7). The reads were indexed using Hisat2 (v2.2.1) with the TAIR10 reference genome (http://www.arabidopsis.org). These read counts were associated with a specific gene using FeatureCounts (v2.0.2) with the TAIR10 GFF3 (http://www.arabidopsis.org). This data was downloaded from the Essex HPC and processed further in R. The data was processed with DesSeq2 (v1.34.0) in a complete pairwise analysis using Benjamini and Hochberg post-hoc correction. Analysis was conducted by extracting genes and comparing the $\log_2$ fold change between different genotypes and treatments.

2.4.4: Hypergeometric distribution

Hypergeometric distribution was calculated using the phyper function (R, v4.1.1). The calculation is performed where q is the number of positive genes, m is the number of genes that could be positive, and n is the total number of genes (the figure used was the size of the number of genes in the TAIR10 reference genome, 34218) subtracting m and k is the total number of genes in the comparison.

2.4.5: Gene Ontology Analysis

Gene ontology was performed using Panther (v17, Mi *et al*., 2021), analysing biological processes. Primary GO terms (terms with no parents) and their calculated false discovery rates (FDR) were downloaded and used for creating GO figures. The FDR was processed using the calculation $\log_{10}(1/FDR)$ to make the more significant terms positive and greater than the less significant GO terms.

2.4.6: Phytohormone ‘Response to’ Analysis

Genes were downloaded from the ‘Response to’ phytohormone groups on the TAIR10 database (http://www.arabidopsis.org; Table S1 [Page 337]). The pairwise log_2 fold changes for specific comparisons were extracted from the *BBX32-HY5* HL RNA-seq, and these were put into a boxplot using the R programming language and ggplot2 (section 2.4.1 [Page 51]). Statistics were performed using ANOVA between the log_2 fold changes of different pairwise comparisons.

2.4.7: Protein structure prediction

The primary sequence of different BBX32 homologues were submitted to Phyre 2.0 (Kelley *et al*., 2015). A screenshot of the generated protein was taken. The Alphafold structures were taken from the Alphafold database (https://alphafold.ebi.ac.uk/; Jumper *et al*., 2021).

2.4.8: Multiple sequence alignment

Multiple sequences were aligned within MEGA 11 (Tamura *et al*., 2021) using clustalW (Thompson *et al*., 1994). For display purposes, these sequences were sometimes manually adjusted to align individual domains. For phylogenetic analysis, sequences aligned by clustalW were used.

2.4.9: Phylogenetic analysis

Phylogenetic analyses were performed on aligned sequences using the maximum likelihood method. The JTT model was used with between 100, and 500 bootstrap replicates. Clades were named based on Khanna *et al*. (2009), and the clades formed within the phylogenetic analysis.

2.4.10: Gathering and Identifying BBX Sequences from Different Species

BBX genes of specific species were gathered through BLAST analysis (Altschul *et al*.,1990). A standardised B-box1 domain was created from each of the most common residues across all *Arabidopsis* BBX proteins. This was submitted to NCBI BLAST with the genome of the target species selected. A phylogenetic tree of the results and *Arabidopsis* BBX proteins was created, and duplicate and partial proteins were removed. The phylogenetic tree was repeated, and the proteins were assigned a number and clade based on their closeness to *Arabidopsis* BBX proteins. The molecular weights and theoretical isoelectric points were calculated from these protein sequences. The theoretical isoelectric point and molecular weight were determined using the Expasy pI/Mw tool (https://web.expasy.org/compute_pi/).

2.4.11: VP motif analysis

Potential VP motifs were discovered by searching the protein sequence for the VP in MEGA 11 (Tamura *et al*., 2021). These were analysed for anchor residues and similarities to other VP motifs from Lau *et al*. (2019).

2.4.12: Protein networking

The intra-BBX family binding partners were gathered from the BioGrid database (https://thebiogrid.org/, Oughtred *et al*., 2019). These connections were put into Cytoscape (v3.8.2; https://cytoscape.org/), and a diagram was built.

2.4.13: microRNA Prediction

The complete coding sequence of *BBX32* with the 5'UTR was submitted to miRbase (https://www.mirbase.org/; Kozomara *et al*., 2019). The E-value cut-off was 10, and only mature miRNAs were searched against.

2.5: Generation and Infiltration of a CAS9 vector

2.5.1: CRISPR/CAS9

The CRISPR/CAS9 is an immunological defence mechanism within some bacteria (Doudna and Charpentier, 2014). It acts as an RNA-guided endonuclease that can be programmed to cut a specific DNA sequence. The programmability of this system enables its use in gene editing. *CAS9* can be expressed *in planta* and targeted to a specific site within the plant's genome. The endonuclease action of CAS9 would create a break in the genomic DNA that is often incorrectly repaired by endogenous systems. An incorrect repair may create non-specific mutations in the plant genome near the gRNA target site.

The mature CAS9 protein is formed when the immature peptide binds with a guide RNA (gRNA). This provides the specificity of the endonuclease target site. Before plant transformation, the gRNAs can be swapped to target other sites or, as in this case, an empty vector lacking gRNAs can be used to speed up the generation of new complete and seamless vectors (Ordon *et al*., 2020). Multiple gRNAs can also be used to target CAS9 to multiple genomic sites with only a single vector. However, only a single gRNA can bind CAS9.

gRNAs provide the targeting specificity by binding the DNA target and the mature CAS9 protein (Doudna and Charpentier, 2014). However, the target selection of each gRNA is limited as CA\S9 requires a motif called a protospacer adjacent motifs (PAMs) sites in the target DNA sequence. The PAM sequence varies depending on the species of bacteria where the CAS9 gene originates. The endonuclease cut site is typically 3 to 4 bases upstream of the PAM site.

Other forms of the CAS9 protein have been developed that have slight variations in functionality. For example, $CAS9^{D10A}$ and $CAS9^{H840A}$ are known as nickases and, instead of forming double-strand breaks in the genomic DNA, only form single-strand breaks or 'nicks' (Jinek *et al*., 2012). In addition, by combining multiple nearby gRNA target sites, particular sections can be cleaved from the DNA. A homology-directed repair could be used to insert a non-endogenous section of DNA into the genome. However, I specifically aimed to create non-specific mutations, and therefore a WT CAS9 was used.

2.5.2: The pDGE277 and shuttle vectors

The *Arabidopsis*-specific vector containing the CAS9 construct, known as pDGE277, was described by Ordon *et al*. (2020). This construct was kindly provided by Johannes Stuttmann (University of Martin Luther) along with the required shuttle vectors and the cloning instructions. This system allows multiple shuttle vectors where each shuttle vector encodes a single gRNA. Either 1, 2, 4, or 8 shuttle vectors/ gRNAs can be used.

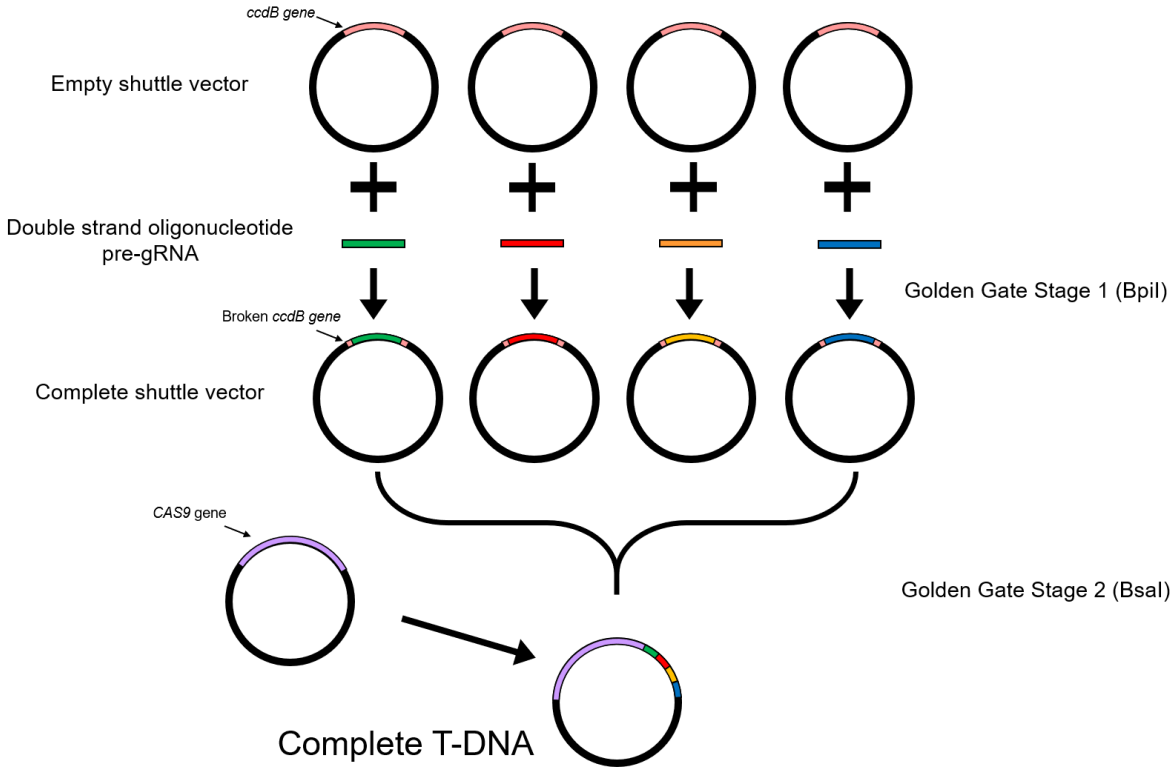

Figure 2.5.1: A schematic of the methodology for creating a completed *CAS9* T-DNA using the pDGE277 plasmid. Two stages of Golden Gate cloning and selection (section 2.5.4 [Page 59]) are required, which use two different restriction enzymes (BpiI and BsaI).

The empty vectors contain a *ccdB* cassette. This cassette contains the *ccdB* gene encoding a toxic protein which kills many *E. coli* cell lines. For long-term storage and propagation DB3.1 *E. coli* cells which contain the *ccdA* antidote to the *ccdB* cassette, were used (Lund *et al*., 2014). pDGE277 and the shuttle vectors were all transformed into DB3.1 cells and grown on LB agar plates with chloramphenicol (35 µg /ml). Single colonies were selected and propagated in LB broth (chloramphenicol, 35 µg /ml) and used to make glycerol stocks and extract more plasmid DNA.

The pDGE277 vector encodes the hygromycin resistance gene to allow for the selection of transformed *Arabidopsis* seeds grown on hygromycin (25 mg/L) containing ½ MS agar plates. pDGE277 also contains the FAST cassette, which produces RFP fluorescing seeds and enables quick negative seed selection.

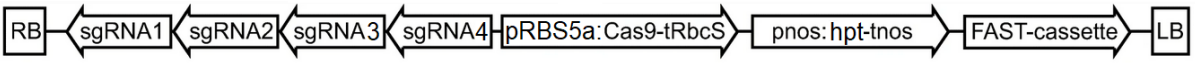

Figure 2.5.2: Schematic of the BBX32-CAS9 T-DNA construct designed by Ordon *et al*. (2020) with four sgRNAs. sgRNA 1-4 represent the selected gRNAs labelled A1 - A4. pRBS5a:CAS9-tRbcS is the CAS9 construct driven by the RBS5a promoter and terminated by trbs E9. pnos:hpt-tnos provides hygromycin resistance, and the FAST-cassette targets RFP tagged OLE1 to the seed coating for simplified selection (Shimada *et al*., 2010). Identical to Figure 6.4.4 [Page 234]. Modified from Ordon *et al*. (2020).

2.5.3: gRNA Selection

I selected four target sites within the *BBX32* gene (Figure 6.4.3 [Page 233]). The *BBX32* gene was inputted into several different CRISPR/CAS9 tool programs; Synthego (Robb, 2019), CRISPR-P 2.0 (Liu H *et al*., 2017), Deskgen (Hough *et al*., 2016), and Benchling (San Francisco, California). Prospective gRNAs were also inputted into the NCBI BLAST algorithm for matches against the *Arabidopsis* genome not to have off-site targets for CAS9 (Altschul *et al.*, 1990).

Four guide RNAs (gRNAs) were chosen from analysing all the outputs (Figure 6.4.3 [Page 233]). The positive and negative DNA oligonucleotides of the gRNA were required for cloning. They were both 20 bp long and altered to have overhanging

sticky ends. The positive oligonucleotide (sequence matching the gRNA sequence) had an ATTG prefix when the first nucleotide wasn't G and ATT where it was. The negative oligonucleotide had an AAAC prefix added. Each of these oligonucleotides was purchased as single-strand oligonucleotides (MilliporeSigma, Burlington, Massachusetts, United States) with a negative complement.

2.5.4: Golden Gate Cloning and Selection

Oligonucleotides were prepared by hybridising the complementing pairs. These were mixed by adding 5 µl of each to 40 µl of RNA-free water, heated to 98 °C for 5 minutes and allowed to slowly cool to room temperature. Next, 5 µl of the hybridised oligonucleotides was added to 995 µl of RNA-free water to create a 50 fmol/µl solution.

A golden gate reaction was performed within a thermal cycler. The reaction consisted of 1 µl of the 50 fmol/µl hybridised oligonucleotides, 60 ng of the empty shuttle vector, 1 µl 10x CutSmart buffer (New England BioLabs, USA), 0.5 µl BpiI (10000 U/ ml; New England BioLabs, USA), 0.5 µl T4 DNA ligase (30 U/ µL; Thermo Scientific, Waltham, Massachusetts, U.S.A), 1 µl BSA (10 mg/ ml) and made up to a total reaction volume of 10 µL with RNA-free water. The reaction was cycled at 37 °C for 2 minutes, followed by 5 minutes at 16 °C for 5 minutes for 30 cycles. The reaction was heated to 50 °C for 10 minutes, followed by a termination step at 80 °C for 10 minutes. 5 µL of this reaction was transformed into Top10 *E. coli* cells and plated onto LB agar with carbenicillin (100 µg/ mL) plates. Only cells transformed with a ligated plasmid would survive. Single colonies were selected and grown in LB

broth (carbenicillin, 100 µg/mL), plasmid DNA was extracted, and glycerol stocks were made.

A second golden gate reaction was performed using the pDGE277 and the full shuttle vectors. The reaction contained 220 ng of each of the full shuttle vectors, 40 ng of pDGE277, 2 µl 10 x CutSmart buffer (New England BioLabs, USA), 1 µl BsaI (1000 U/ ml; New England BioLabs, USA), 1 µl T4 DNA ligase (30 U/ µL; Thermo Scientific, Waltham, Massachusetts, U.S.A), 2 µl BSA (10 mg/ ml) and made up to a total reaction volume of 20 µL with RNA-free water. The reaction was cycled for 37 °C for 2 minutes, followed by 5 minutes at 16 °C for 5 minutes for 50 cycles. Then, the reaction was heated to 50 °C for 10 minutes, followed by a termination step at 80 °C for 10 minutes. 5 µL of this reaction was transformed into Top10 *E. coli* cells and plated onto LB agar with spectinomycin (100 µg/ mL) plates. Single colonies were selected and grown on LB broth (spectinomycin, 100 µg/mL). Plasmid DNA was extracted, and PCR was conducted with M13 primers. The PCR product was sent off for sequencing (Eurofins, Luxemburg) to confirm the correct insertion of the gRNA encoding oligonucleotides. Glycerol stocks were made of the completed T-DNA vector.

2.5.5: Transformation of *Agrobacterium* by Electroporation

In this study, the *Agrobacterium tumefaciens* strain LBA4404 was used. Cells were stored in 200 µl 10 % glycerol (water) at -70 °C until ready for use in 1.5 ml microcentrifuge tubes. When ready for use, cells were thawed on ice, and 150 ng of the *BBX32-CAS9* vector was added without mixing. These cells were transferred to an electroporation cuvette (Equibio, UK), and electroporation was performed using

an EasyJecT Prima Electroporator (Equibio, UK). A single electrical pulse of 1800 V was applied to the cuvette, and 500 µl of LB broth was added. The solution was transferred to a new 1.5 ml microcentrifuge tube and allowed to incubate at 28 °C for 3 hours. Next, 150 µl of cells were spread onto an LB agar plate containing rifampicin (50 µg/ml) and spectinomycin (100 µg/mL). Plates were incubated for 48 - 72 hours, and single colonies were added to LB broth containing rifampicin (50 µg/ml) and spectinomycin (100 µg/mL). From this culture, plasmid DNA was extracted, and glycerol stocks were made.

2.5.6: Floral inoculation transformation of *Arabidopsis thaliana* with *Agrobacterium*

The transformation methodology of *Arabidopsis thaliana* used in this study followed a similar methodology by Narusaka *et al*. (2010) but uses the standard growth conditions in section 2.2.1 [Page 35]. *Agrobacterium* cells inoculated with the *BBX32-CAS9* vector built in the previous section were grown in LB broth containing rifampicin (50 µg /ml) and spectinomycin (100 µg/ mL) for 48 hours. 1.5 ml of culture was centrifuged in a 2 ml centrifuged at 6708 xg for 5 minutes. The supernatant was removed, and the cells were resuspended in a 5 % sucrose solution (w/v; water). Immediately before inoculating *Arabidopsis* plants, 0.2 µl Silter L-77 was added to the cells and mixed well. Recently bolted plants were inoculated by placing 5 µl of the *Agrobacterium* cell solution onto each developing bud. Plants were covered with a clear plastic dome for two days and then allowed to grow and develop as described under standard growth conditions (section 2.2.1 [Page 35]). Once plants were dry, the T_0 seeds were harvested.

2.6: Selection of CAS9 mutated *Arabidopsis* lineages

2.6.1: Hygromycin-based selection of *BBX32-CAS9* T_1 plants

Seeds were surface sterilised (section 2.3.14 [Page 50]) and sown onto ½ MS media plates (pH 5.7) containing hygromycin (25 mg/L). These plates were covered and placed at 4 °C for 3 - 4 days. After stratification, the plates were placed flat in growth cabinets (8/16 hour, day/night; 150 µmol m^{-2} s^{-1}; 22 °C). After 14 days of growth, live seedlings were transferred to soil and were allowed to mature and set seed under standard growth conditions (section 2.2.1 [Page 35]).

2.6.2: Negative FAST selection of T_1 progeny

Seeds were fixated on small, welled plates using a thin layer of clear agarose. RFP was visualised under the white light, and EPI green LED lighting with a Y3 filter in a G: BOX lighting module (Syngene, UK). Images were compared to identify seeds visible under white light but without a corresponding RFP fluorescence. These seeds were grown under standard growth conditions as M_2 plants.

2.6.3: Sequencing *BBX32-CAS9* plants

DNA was isolated from M_2 and M_3 plants (section 2.3.1 [Page 42]) and used for PCR (section 2.3.3 [Page 43]). The PCR product was quantified by using a NanoDrop (section 2.3.7 [Page 45]) and by using gel electrophoresis (section 2.3.8 [Page 46]). The PCR product was diluted and had a further sequencing primer added before being sent to Eurofins (Luxemburg) for Sanger dideoxy sequencing.

Chapter 3: Transcriptional regulation of high light acclimation

3.1: Introduction

HL provides an opportunity and a threat to a plant. Higher light conditions can be favourable to a plant for use in photosynthesis. Plants can enhance their photosynthetic capacity to endure and exploit new higher light conditions. One means of alleviating the stress associated with excess excitation energy is to channel further light energy into photosynthesis. HL acclimation is the process that enables plants to enhance photosynthetic capacity to utilise and combat increased light intensities.

HL acclimation is under genetic and environmental control (Kleine *et al*., 2007; Athanasiou *et al*., 2010; Huang *et al*., 2019). Upon the induction of HL, a set of transcriptional changes occur to enhance photosynthetic capacity over five days (Alvarez-Fernandez *et al*., 2021). In mature leaves, an alteration of chloroplast physiology is primarily responsible for increases in light use efficiency (Athanasiou *et al*., 2010). In the meantime, plants must dissipate excess excitation energy from HL through non-photochemical/ photochemical quenching (NPQ/ PQ; Baker, 2008; Ruban and Belgio, 2014). NPQ is the mechanism where PsbS transfers excitation energy from HL excited chlorophylls to xanthophyll carotenoids resulting in thermal dissipation (Baker, 2008; Ruban and Belgio, 2014).

I called the physiological changes necessary to enhance photosynthetic capacity upon exposure to HL as HL acclimation initiation. Alvarez-Fernandez *et al*. (2021) conducted an *Arabidopsis* microarray time series to observe and model transcription factors crucial to this change. The transcription co-factor B-BOX32 (BBX32) is at the centre of a dynamic statistical modelling HL transcription factor network (Figure 1.3.1 [Page 24]; Alvarez-Fernandez *et al*., 2021). Plants overexpressing BBX32 (BBX32-10) have a reduced ability to enhance photosynthetic efficiency and capacity and a lower initial PSII operational efficiency under their initial growth conditions (Alvarez-Fernandez *et al*., 2021).

BBX32-10 seedlings have a photomorphogenic hyposensitivity to light, mainly blue light, through a mechanism involving ELONGATED HYPOCOTYL5 (HY5), another gene found within the HL TF network (Holtan *et al*., 2011; Alvarez-Fernandez *et al*., 2021BBX32 impacts photomorphogenesis through a tripartite protein complex involving a B-box family member, BBX21, and HY5 (Holtan *et al*., 2011). This evidence led to a HY5 mutant, *hy5-2*, being discovered to have a very similar acclimation phenotype to BBX32-10 (Alvarez-Fernandez *et al*., 2021; Figure 3.1.1 [Page 65]). Therefore, Alvarez-Fernandez *et al*. (2021) concluded that *HY5* and *BBX32* are positive and negative regulators of HL acclimation, respectively.

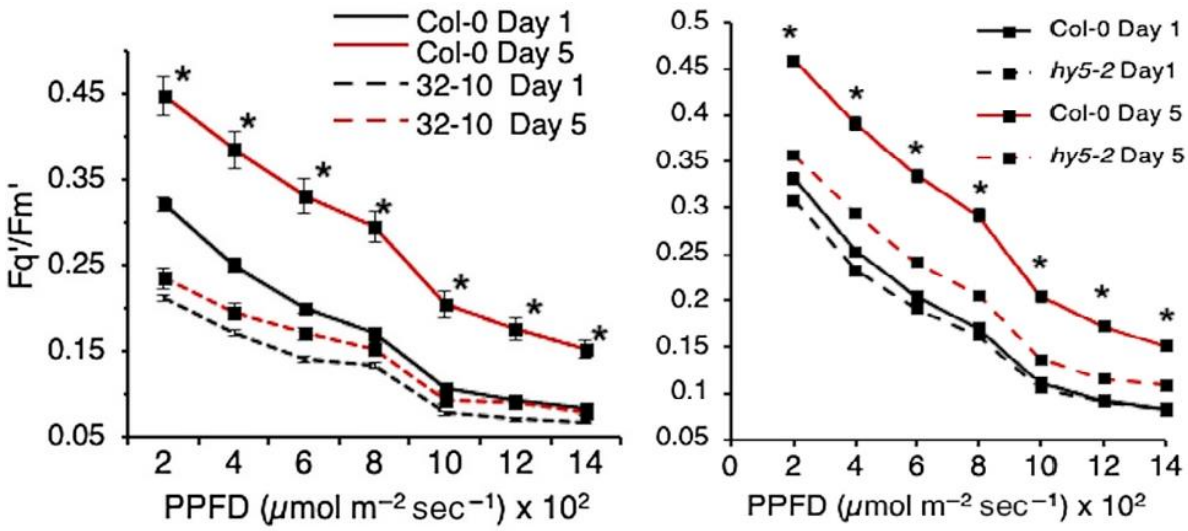

Figure 3.1.1: HL acclimation phenotype of BBX32-10 (32-10), *hy5-2* and Col-0 plants. Fq'/Fm' was determined by chlorophyll fluorescence with an actinic PPFD range of 200 µmol m^{-2} s^{-1} to 1400 µmol m^{-2} s^{-1} at 200 µmol m^{-2} s^{-1} increments. Modified from Alvarez-Fernandez *et al*. (2021).

An early study showed significant alterations in chloroplast physiology and photosynthetic capacity within mutants of light-sensing genes (photoreceptors) grown at PPFDs of 100 and 400 µmol m^{-2} s^{-1} (Walters *et al*., 1999). Walters *et al*. (1999) provided an initial link between light perception genes and HL acclimation, hinting that the process was not wholly plastid controlled. Plants lacking CRYPTOCHROME1 (CRY1), a blue light photoreceptor localised to the nucleus, have a reduced ability to enhance photosynthetic capacity in response to HL (Alvarez-Fernandez *et al*., 2021). In a classical photomorphogenic pathway. CRY1 and HY5 are linked through the CONSTITUTIVELY PHOTOMORPHOGENIC/DE-ETIOLATED1/FUSCA (COP/DET/FUS) module when no activated CRY1 protein is present (Figure 3.1.2 [Page 67]). Alvarez-Fernandez *et al*. (2021) performed a HL acclimation experiment on members of the COP/DET/FUS module to identify mutant phenotypes. A *CONSTITUTIVELY PHOTOMORPHOGENIC1* (*COP1*) mutant, *cop1-*

4, had an enhanced HL acclimation phenotype despite displaying a dwarf shoot morphology. *DE-ETIOLATED1* (*DET1*) mutants display a HL acclimation ability similar to the WT while having a typical dwarfed shoot morphology associated with impaired photomorphogenesis (Alvarez-Fernandez *et al*., 2021). COP1 forms complexes with other proteins as part of its role as an E3 ligase to induce signal transduction through protein degradation (Chen *et al*., 2006).

EARLY LIGHT INDUCED PROTEIN1 (*ELIP1*) *and ELIP2* are HL response genes whose proteins bind free chlorophylls and alter chlorophyll biogenesis. *cry1* mutants cannot increase the expression of *ELIP1* and *ELIP2* when exposed to high-intensity blue light (Kleine *et al*., 2007). HY5 binds to the promoters of the *ELIP* genes, and plants lacking *HY5* (*hy5*) cannot increase the expression of *ELIP1* in response to HL in seedlings (Lee *et al*., 2007; Hayami *et al*., 2015; Harari-Steinberg *et al*., 2001). The *COP1* knockdown, *cop1-4*, similarly cannot increase the expression of *ELIP1* in response to HL (Takeuchi *et al*., 2014). Studies use *ELIP1* and *ELIP2* as HL marker genes to identify HL expression manipulations caused by the CRY1-COP1-HY5 light signalling pathway *in vivo* (Kleine *et al*., 2007).

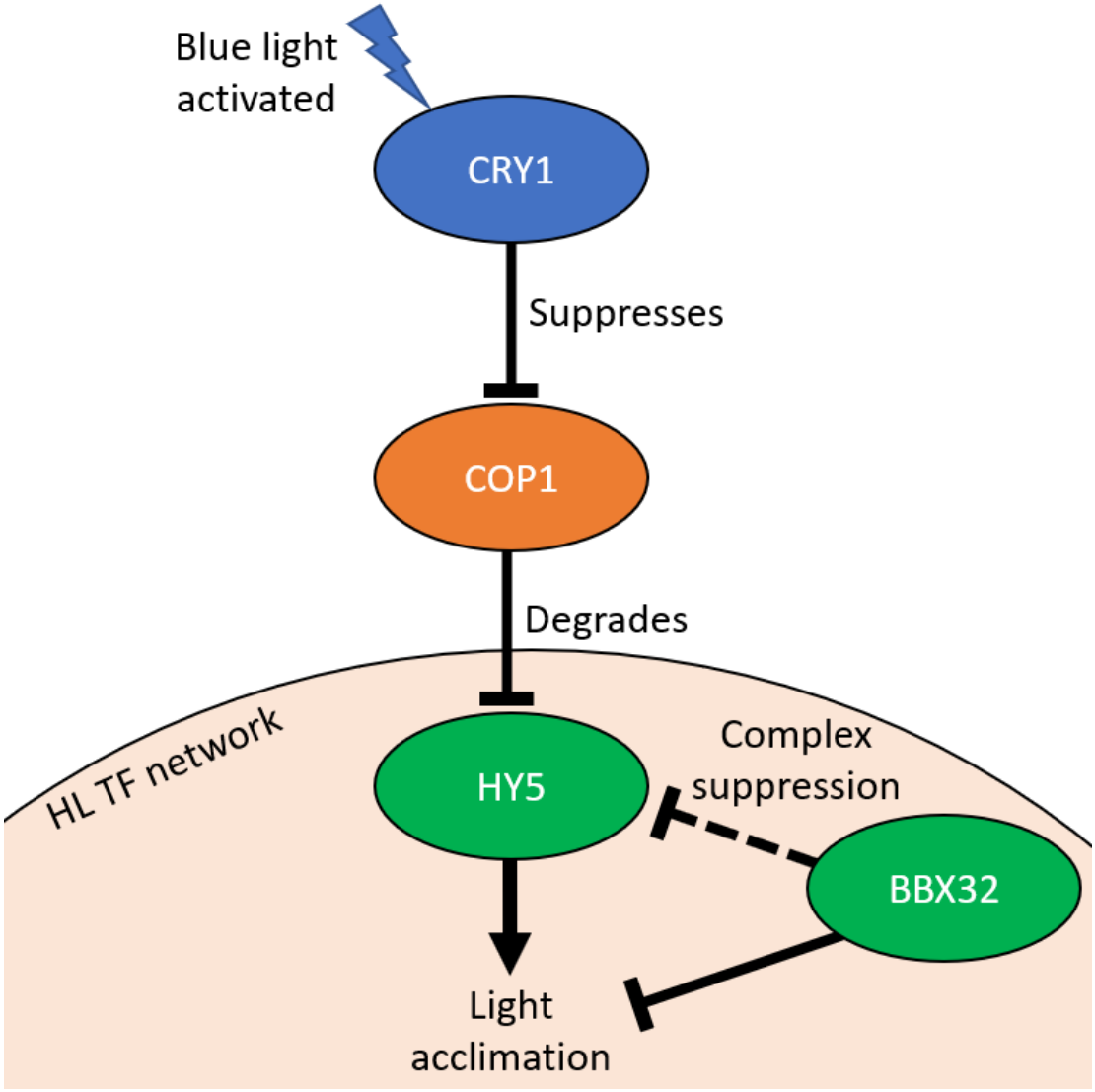

Figure 3.1.2: A model of known HL acclimation genes and their interactions. *HY5* and *BBX32* are a part of the HL TF network. Complex suppression indicates the suppression of HY5 by BBX32 in complex with BBX21 (Holtan *et al*., 2011).

This chapter aims to further the understanding of the transcriptional regulation required to initiate HL acclimation. These aims involve analysing the HL TF network and microarray time series from Alvarez-Fernandez et al. (2021). The connection between HL acclimation and HL response genes like *ELIP1* is essential in understanding how quick the initiation of HL acclimation occurs. Furthermore,

exploring these genes may reveal further HL acclimation genes that future studies could manipulate to increase plant productivity.

3.2: Methods

3.2.1: The analysis of *BBX32-HY5* HL RNA-seq data

All results chapters (Chapters 3 - 6) presented in this study used the *BBX32* HL RNA-seq data set from Alvarez-Fernandez *et al*. (2021; GSE158898) with the addition of the concurrently performed *HY5* data (section 2.4.3 [Page 51]). Section 3.4 [Page 73] explores this data in depth with a set of tasks in section 3.4.1 [Page 75]. The R programming language was used to perform tasks involving identifying overlapping gene lists and transcription factors (section 2.4.1 [Page 51]). A complete list of transcription factor genes was collated and can be found in Table S2 [Page 337]. Finally, GO analysis was performed on up and downregulated gene lists following the protocol in section 2.4.5 [Page 52].

3.2.2: Selection of HL TF network genes

I selected genes from the HL TF network for further study (section 3.5 [Page 91]; Figure 3.5.2 [Page 94]). Genes were selected with a direct connection or a close homologue with a direct connection. *SPA1* and the *SPA* gene family were studied further in Chapter 4 [Page 125]. Mutant plants were generously donated or obtained from the Nottingham Arabidopsis Resource Centre (section 2.1.1 [Page 34]; section 2.1.2 [Page 34]). Plants were subjected to HL acclimation experimental conditions (section 2.2.2 [Page 35]) and chlorophyll fluorescence parameters were recorded (section 2.2.3 [Page36]).

3.3 Light response and HL acclimation

This section aims to identify changes of expression caused by exposure to HL and induced in HL acclimation mutants. Alvarez-Fernandez *et al*. (2021) analysed a HL time-series microarray experiment and HL RNA-seq involving BBX32-10 and *hy5-2* HL acclimation mutants (Alvarez-Fernandez *et al*., 2021). This section uses these data sets (GSE78251, microarray; GSE158898, RNA-seq) to explore the linkage between responses to HL and the initiation of markers of HL acclimation.

3.3.1 HL-induced expression changes of HL acclimation genes

I looked at the expression of two HL acclimation genes to determine if limited HL response can impact the regulation of HL acclimation. *LHCB4.3* is a crucial component of HL acclimated PSII reaction centres and is the only gene encoding a light-harvesting protein with an abundance positively correlated with growth light irradiance (Albanese *et al*., 2016; Albanese *et al*., 2020). Plants lacking *GPT2* (*gpt2-*), a plastid glucose-6-phosphate/ inorganic-phosphate antiporter encoding gene, have decreased photosynthetic enhancement to HL, potentially due to alterations in primary metabolism (Athanasiou *et al*., 2010; Dyson *et al*., 2015; Miller *et al*., 2017). Alvarez-Fernandez *et al*. (2021) showed that HL-induced photosynthesis enhancement takes several days; therefore, an immediate change in expression of these genes is theoretically not necessary to bring about HL acclimation.

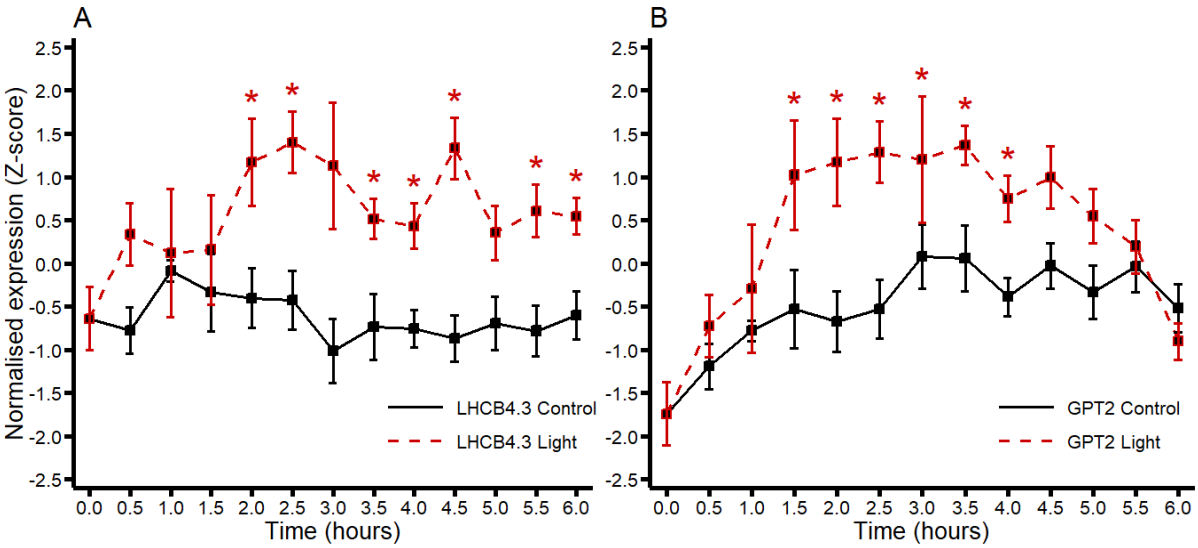

Figure 3.3.1: The expression *LHCB4.3* (A) and *GPT2* (B) from the Alvarez-Fernandez *et al*. (2021) time series acclimation microarray experiment. Asterisks and bars show time points significantly changed in expression between the control and light groups (n = 4; $p < 0.05$; ANOVA).

HL causes a significantly increased expression of *GPT2* and *LHCB4.3* compared to the control. The increase was not immediate, and the genes were only affected at 1.5 hours and 2 hours after the initial HL exposure. *LHCB4.3* RNA abundance remains significantly elevated for the rest of the time series (Fig. 3.3.1A). In contrast, *GPT2* expression decreased towards the end of the 6-hour period (Fig. 3.3.1B).

3.3.2 HL-induced genes within HL acclimation mutants

The concept of HL impacting HL acclimation genes was inverted by studying HL response genes within HL acclimation mutant plants. Alvarez-Fernandez *et al*. (2021) performed an RNA-seq on the HL acclimation mutant BBX32-10 and the WT Col-0 following 3.5 hours of HL exposure and a LL control. In addition, Alvarez-

Fernandez *et al*. (2021) performed a concurrent RNA-seq analysis on *hy5-2* plants exposed to both treatments. This study is the first to analyse this data (GSE158898). I focused on the expression of HL response genes in the *hy5-2* and BBX32-10 mutants. I defined a HL response gene by a rapid change in expression upon exposure to light which was verified using the WT (Col-0) experimental controls. *ELIP1*, *ELIP2* and *PsbS* were selected as they are classical HL response and NPQ marker genes (Kleine *et al*., 2007; Roach and Liszkay, 2012).

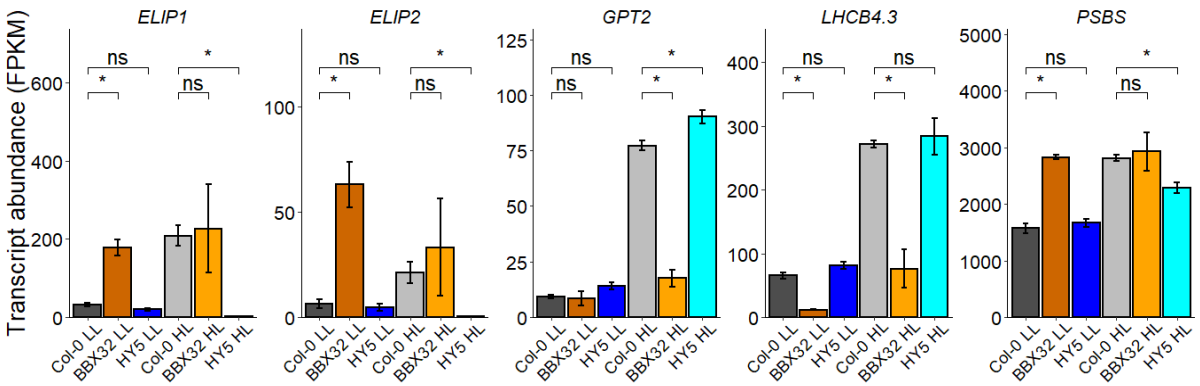

Figure 3.3.2: The expression of HL response and HL acclimation genes from the *BBX32-HY5* HL RNA-seq. Expression data from BBX32-10 (BBX32), *hy5-2* (HY5) or Col-0 under LL or HL conditions for 3.5 hours of exposure. Asterisks and bars show genes significantly changed in expression between the LL and HL groups of each genotype ($p < 0.05$; ANOVA).

ELIP1 and *ELIP2* had very similar expression profiles within the Col-0 controls; however, within the HL acclimation mutants, the expression profiles of the *ELIP* genes were very perturbed (Figure 3.3.2 [Page 71]). HL caused a significant increase in the expression of the *ELIP*s; however, this is not true within the HL acclimation mutants. *hy5-2 showed a* significantly decreased expression of *ELIP1*

and *ELIP2* in response to HL, with the expression values remaining close to the Col-0 LL values. BBX32-10 does not significantly alter the expression of the *ELIPs* upon HL exposure, but the expression values remain close to the Col-0 HL value.

The expression of *PsbS* corroborates the hypothesis that BBX32-10 is reacting as though experiencing HL at LL conditions (Figure 3.3.2 [Page 71]). *hy5-2* and Col-0 increased *PsbS* transcript levels in response to HL; however, BBX32-10 had an increased expression under LL maintained at HL. This maintained expression could have been due to the lowered PSII operational efficiency leading to high NPQ rates though this was not seen in *hy5-2* and did not increase in response to HL exposure (Alvarez-Fernandez *et al*., 2021).

BBX32-10 failed to increase the expression of the HL acclimation genes *LHCB4.3* and *GPT2* in response to HL; however, compared to HL response genes, HL acclimation genes were maintained at values similar to Col-0 LL instead of Col-0 HL. Alterations in light-harvesting super-complex composition and alterations in primary metabolism could reduce the ability to enhance photosynthetic capacity in response to HL (Albanese *et al*., 2016; Dyson *et al*., 2015). This alteration provides a strong hypothesis for the cause of the defective acclimation phenotype of BBX32-10. However, *hy5-2* did not significantly alter the expression profile of *LHCB4.3,* and there were only minimal changes to *GPT2* transcript levels. In *hy5-2,* the expression of these acclimation genes could be affected (post)-translationally, which would not be detected by RNA-seq. Alternatively, these differences could involve a separate signalling pathway from *BBX32-10*.

3.3.3 Conclusion

The term ‘response to light stress’ emphasises the threat posed by HL, whereas ‘HL acclimation initiation’ invokes the possible opportunity. Enhancing photosynthetic capacity takes several days; however, the first few hours of HL exposure increased the expression of HL acclimation genes (Figure 3.3.2 [Page 71]). The mutants impacted the expression of HL response genes; *ELIP1*, *ELIP2*, *GPT2*, *LHCB4.3* and *PSBS*, all of which display the same perturbed HL acclimation phenotype (Figure 3.3.2 [Page 71]). The initiation of HL acclimation and HL response are deeply intertwined processes that may be inseparable.

HL acclimation and HL response genes are strongly linked; however, there is no clear pattern of perturbation between the BBX32-10 and *hy5-2* HL acclimation mutants despite the similar HL acclimation phenotypes. Therefore, these mutants could have similar phenotypes due to convergence of distinct HL acclimation pathways or by manipulating the same pathway in different ways to create a similar phenotype. Future studies could test these hypotheses by performing large-scale analysis on the *BBX32-HY5* HL RNA-seq to identify if these mutations alter the transcriptome similarly. In addition, I could further search this data set to identify more HL acclimation genes, in particular, transcription factors which can impact the expression of many other genes to cause a cellular response.

3.4: Analysing HL acclimation defective transcriptomes

This section uses a *BBX32* HL RNA-seq data set, and a novel analysis of a parallel HY5 HL RNA-seq data set performed by Alvarez-Fernandez *et al*. (2021; GSE158898). This section aims to use these data sets to identify changes in the

transcriptome within BBX32-10 and *hy5-2* mutants that may cause defective HL acclimation phenotypes. This experiment used BBX32-10, *hy5-2* and Col-0 plants either maintained under growth light conditions (LL) or exposed to 1000 µmol m^{-2} s^{-1} of light for 3 ½ hours (HL), which had RNA extracted for analysis. The plants' RNA were extracted at the same point in their day/night cycle to mitigate changes in expression caused by the circadian rhythm. RNA-seq was performed on these samples and processed to determine significant differences between the expression of genes in different samples.

hy5-2 and BBX32-10 can be contrasted to Col-0 to identify the overlap of significantly altered genes between the HL acclimation defective mutants and the WT control. For this analysis, comparisons within LL or the HL treatment groups were used but not comparisons between LL and HL exposed treatment groups. Comparisons between the LL and HL treatment groups of the same genotype obscure changes in the expression of the mutant compared to the WT. When comparing the LL and HL treated groups of the same genotype, a gene that was significantly altered in expression by the mutant compared to the WT may not be able to be identified if changes between LL and HL treatment groups were similar.

This choice meant that the LL or HL data sets had to be used to make the mutant-WT comparisons, and the LL mutant-WT comparisons were selected instead of the HL mutant-WT comparisons. As BBX32-10 and *hy5-2* have a perturbed PSII operational efficiency on day 1, a study previously hypothesised that their altered cellular environments limit the ability to initiate HL acclimation in response to HL (Alvarez-Fernandez *et al*., 2021). Therefore, studying the steady-state transcriptome

differences under LL is critical to understanding how these plants respond to HL. However, the HL data set records the transcriptome after only 3.5 hours of HL exposure and therefore did not study the transcriptome of HL acclimated plants. Therefore, this section only uses the LL comparisons between the mutants and WT (Col-0) to highlight the mutants' expression changes. Furthermore, this section is interested in the transcriptional changes made by the HL acclimation mutants, not the changes made after a short HL exposure.

3.4.1 Protocol for analysis of the *BBX32-HY5* HL RNA-seq

An issue with RNA-seq is the overwhelming nature of the data sets. The *BBX32-HY5* HL RNA-seq data set contains the expression of 34218 genes of each of the 24 samples categorised into six groups. Without a clear analysis, the meaning of the results can be challenging to determine. Therefore, I devised a list of steps to focus the scope of this section and the specificity of the results. This set of steps governed the analysis of the *BBX32-HY5* HL RNA-seq:

- Isolate the significantly differentially expressed genes (DEGs) between mutant and Col-0 (Col) sets under LL conditions
- Identify the DEGs that were shared between the HY5 LL / Col LL and BBX32 LL / Col LL groups
- Determine DEGs that are either upregulated or downregulated in both HY5 LL / Col LL and BBX32 LL / Col LL groups
- Perform gene ontology (GO) analysis on the upregulated and downregulated DEG groups

- Extract transcription factor genes from the upregulated and downregulated DEG groups for individual gene analysis

These steps aim to find genes and pathways that are altered within *hy5-2* and BBX32-10 causing the similar HL acclimation phenotypes of these mutants. GO analysis is very useful for distinguishing pathways from large gene sets by labelling genes as belonging to different pathways. It calculates the significance of a pathway based on the number of genes belonging to the pathway, the number of pathways genes in the data set and the size of the data set. I identified upregulated and downregulated sets of pathways by performing this on groups of genes that were either upregulated or downregulated in both BBX32-10 and hy5-2 (compared to Col-0).

I further investigated the upregulated and downregulated data sets by isolating the transcription factors and co-factors in these groups. Alvarez-Fernandez *et al*. (2021) focused on transcription factors in the development of the HL TF network due to their encompassing nature over transcription, which can alter the cellular environment. Transcription factors were reasoned to have the ability to directly or indirectly control the expression of genes that bring about perturbed HL acclimation phenotypes (Alvarez-Fernandez *et al*., 2021). By isolating transcription factors, it is possible to identify a commonality with the HL TF network and interactions with its members.

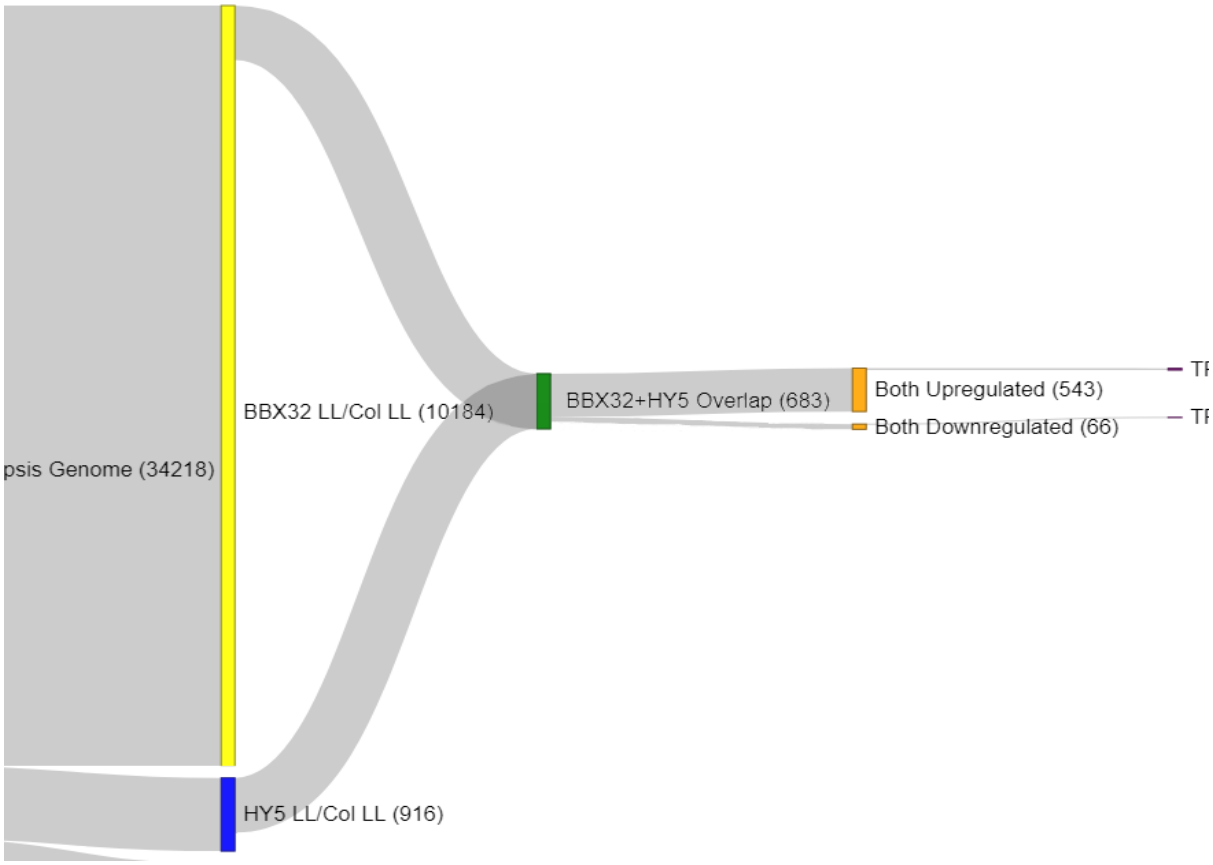

Figure 3.4.1: Schematic showing this section's steps on the *BBX32-HY5* HL RNA-seq to analyse this large data set. Numbers in brackets represent the number of genes or DEGs that are part of the associated group. *Arabidopsis* genome and Insignificant are not to scale.

3.4.2 DEG overlap between BBX32-10 and *hy5-2*

The first step was to isolate DEGs between BBX32-10 LL and Col-0 LL (BBX32 DEGs) and *hy5-2* LL and Col-0 (HY5 DEGs). I overlapped these lists to obtain a shared gene list between the BBX32 DEGs and HY5 DEGs. A far larger number of genes were significant between *BBX32-10* and Col-0 than in *hy5-2* and Col-0.

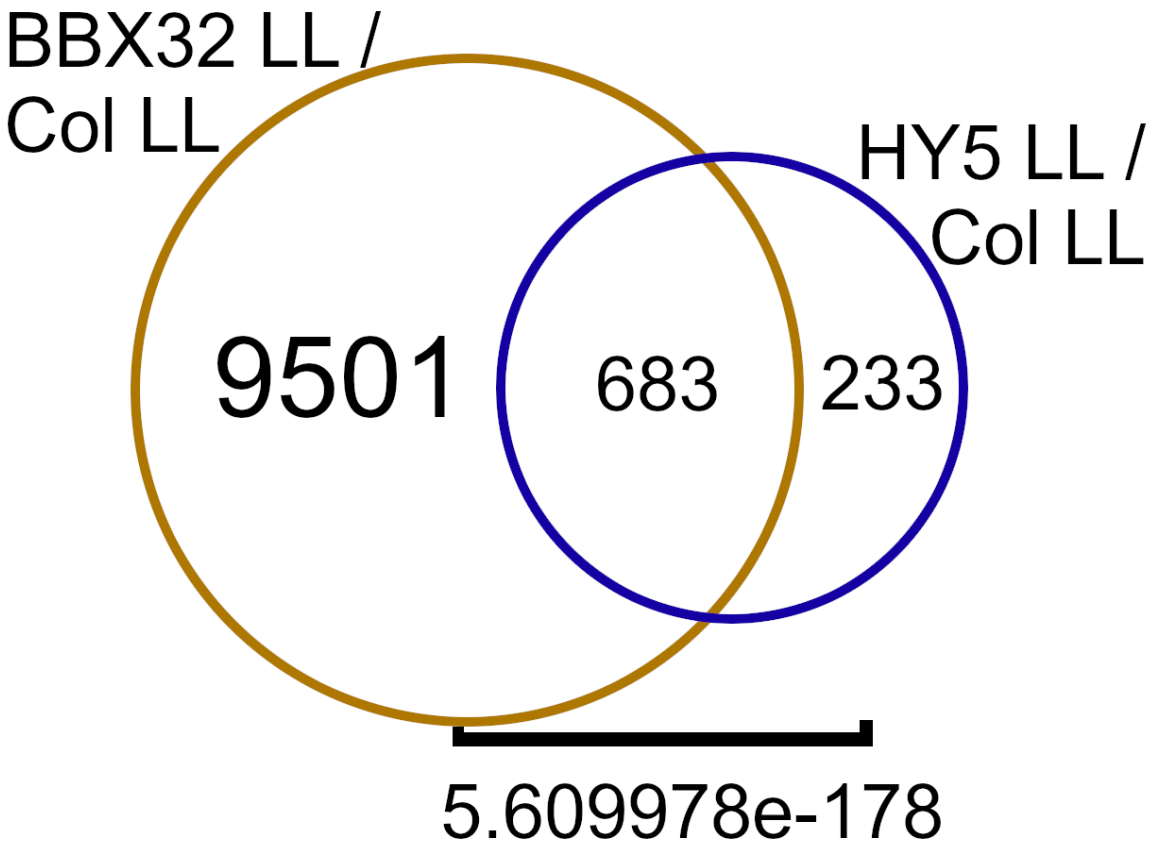

Figure 3.4.2: A Venn diagram showing the overlap between the DEGs (p < 0.05) of BBX32 LL / Col LL and HY5 LL / Col LL. The value at the bottom corresponds to the p-value of the likelihood of 683 genes of 916 HY5 LL / Col LL DEGs being present in the 10184 BBX32 LL / Col LL DEGs within an *Arabidopsis* genome containing 34218 genes (hypergeometric distribution test).

There is a very significant overlap between the HY5 and BBX32 DEGs. The genes within the shared group potentially contribute to the decreased PSII operational efficiency seen in *hy5-2* and BBX32-10 mutants. However, this still was not the greatest reduction in the number of genes possible. I was only interested in genes that have their expression altered in the same direction within the *hy5-2* and BBX32-

10 mutants, as these genes are more likely to be causal of the HL acclimation defective phenotype. Therefore, I created an overlap to capture the genes that are either both upregulated or both downregulated within BBX32-10 and *hy5-2* mutants compared to Col-0.

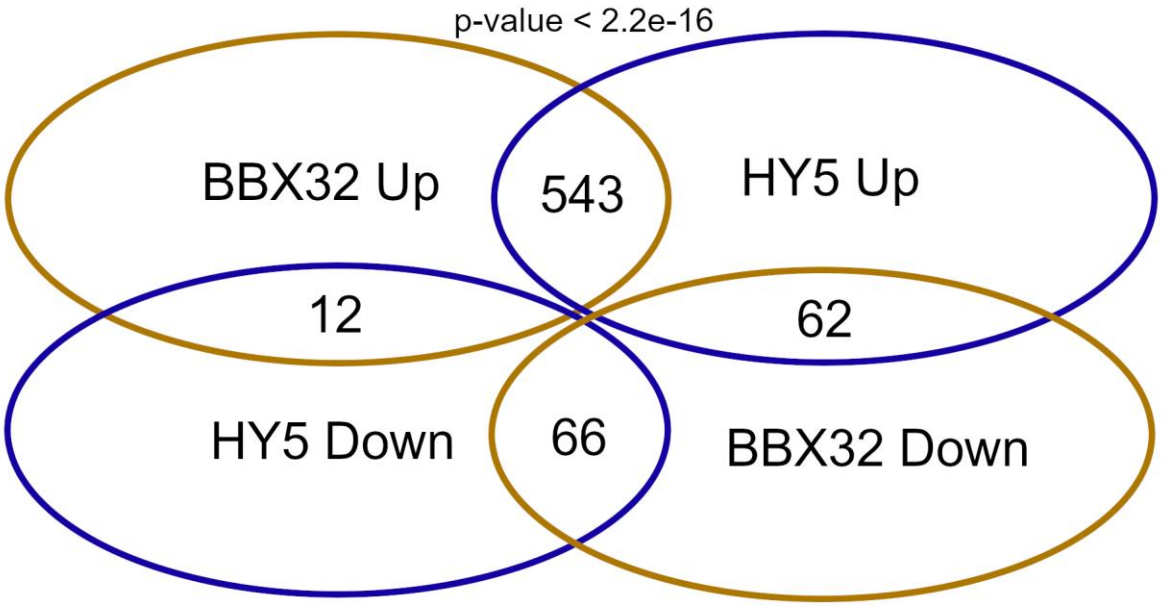

Figure 3.4.3: The relationship between the regulation of BBX32 LL / Col LL and HY5 LL / Col LL overlapping DEGs. DEGs were determined to have been upregulated (Up) or downregulated (Down) in both BBX32 LL / Col LL (BBX32) and HY5 LL / Col LL (HY5) and assigned to a pair of overlapping circles of the corresponding regulation. P-value was calculated using a Pearson's Chi-square test with Yates' continuity correction to evaluate if this alignment is random. A random distribution of genes would have an expected 25% of total common DEGs in each crossover.

I have found far more upregulated genes than downregulated ones when combining *hy5-2* and BBX32-10 DEG lists. BBX32, as it is not a transcription factor, does not directly affect the transcriptome but acts through other transcription factors. *HY5*

expression is significantly reduced in *hy5-2* and points to HY5 preventing the transcription of many genes by directly binding DNA or other interactions. The combination is interesting as HY5 is a positive regulator of light signalling, and BBX32 is a negative regulator (Goto *et al*., 1991; Holtan *et al*., 2011; Preuss *et al*., 2012)

More than 89% of the significantly altered genes match the regulatory direction between *hy5-2* and BBX32-10 (609/683; Figure 3.4.3 [Page 79]). This assortment is not random, as indicated by the low p-value. Therefore, the *hy5-2* and BBX32-10 mutations have similar impacts on the plant's transcriptome.

3.4.3 GO analysis of up and downregulated DEGs

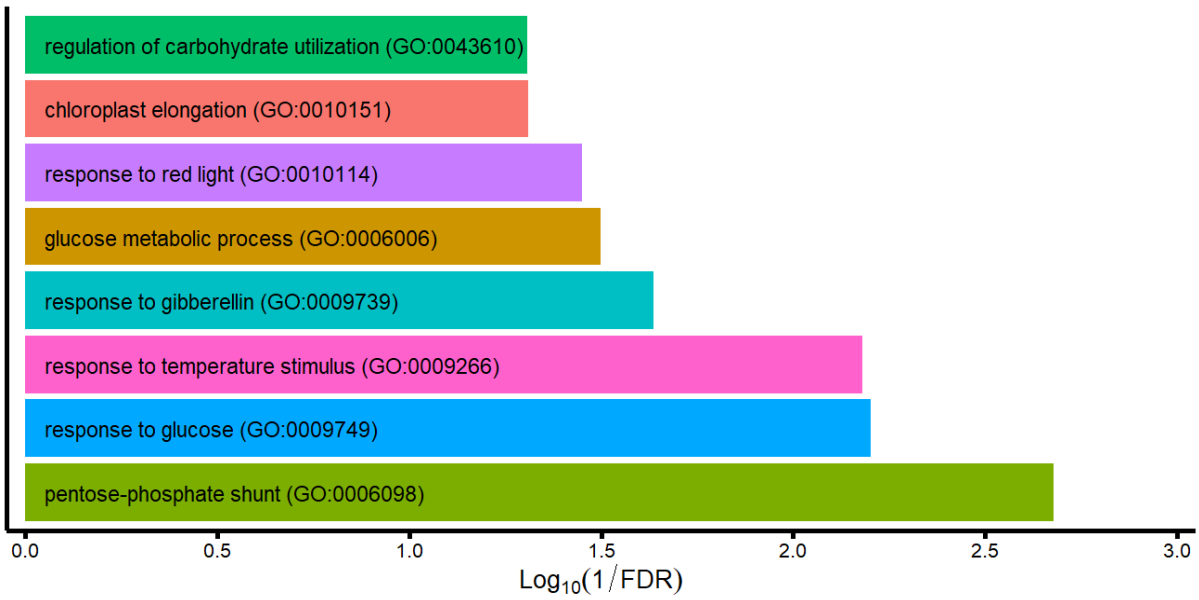

Figure 3.4.4: A subset of the GO analysis of the 543 DEGs upregulated by both *hy5-2* and BBX32-10 when compared to Col-0 under LL conditions. A false discovery rate was calculated from the p-value, which is transformed to provide a more readable scale.

I performed GO analysis on the upregulated and downregulated DEG groups from Figure 3.4.3 [Page 79]. This analysis focuses first on the upregulated DEG group. Upregulation of pentose-phosphate shunt (GO:0006098), regulation of carbohydrate utilisation (GO:0043610), glucose metabolic process (GO:0006006), and response to glucose (GO:0009749) GO terms hint at the dysfunction of glucose accumulation, transport or signalling within *hy5-2* and BBX32-10. This dysfunction is closely related to GPT2, a glucose 6-phosphate/ inorganic phosphate chloroplastic antiporter with a HL acclimation defective null mutant (Athanasiou *et al*., 2010; Dyson *et al*., 2015). However, BBX32-10 and *hy5-2* impacted the expression of *GPT2* in a very different manner (Figure 3.3.2 [Page 71]). This expression data diminishes the role of GPT2 in HL acclimation as both HL acclimation mutants positively alter processes related to GPT2 without necessitating similar alteration of *GPT2* expression (Athanasiou *et al*., 2010).

The processes invoked by the upregulated DEGs (Figure 3.4.4 [Page 80]) and *GPT2* centre around the movement of carbon, cellular partitioning, and primary metabolism. GPT2 and TRIOSE PHOSPHATE/PHOSPHATE TRANSLOCATOR (TPT) act as antiporters for inorganic phosphate and glucose-6-phosphate or glycerate 3-phosphate, respectively, decreasing their concentration gradients between chloroplast and cytosol (Gerhardt *et al*., 1987; Walters *et al*., 2004). HL causes sucrose accumulation, which diverts fixed carbon towards starch biosynthesis in the chloroplast, which also quickly accumulates (Gerhardt *et al*., 1987; Dyson *et al*., 2015). Plants lacking GPT2 or TPT have a decreased photosynthetic capacity compared to WT controls following HL acclimation (Walters

et al., 2004; Athanasiou *et al*., 2010). *gpt2-* plants do not accumulate starch within the chloroplast as quickly in response to HL as the WT (Dyson *et al*., 2015). This evidence indicates that altered compartment distributions of primary metabolites can negatively impact the enhancement of photosynthetic capacity in response to HL.

BBX32-10 and *hy5-2* upregulate genes involved in primary metabolism processes, indicating a change in the management of carbon made by these plants. As indicated by *GPT2* and *TPT* mutants, altering the distribution of primary metabolites can impact the enhancement of photosynthetic capacity in response to HL, as seen in the BBX32-10 and *hy5-2* mutants (Walters *et al*., 2004; Athanasiou *et al*., 2010; Alvarez-Fernandez *et al*., 2021).

Figure 3.4.3 [Page 79] also invokes response to temperature stimulus, which in the native environment is partially connected to light irradiance as leaf temperature increases when exposed to higher light irradiances such as from direct sunlight (Nelson and Bugbee, 2015). HL acclimation and temperature response pathways are evolutionarily intertwined due to the stimuli commonly occurring concurrently (Legris *et al*., 2017). HL acclimation genes *CRY1*, *COP1* and *HY5* are all mediators of temperature response during photomorphogenesis (Ma *et al*., 2016; Jang *et al*., 2015; Delker *et al*., 2014). Hypocotyls grow longer at high temperatures through the repression of *PIF4* in a HY5-dependent manner (Delker *et al*., 2014). However, *PIF4* does not influence HL acclimation (Delker *et al*., 2014; Alvarez-Fernandez *et al*., 2021). Previous HL acclimation experiments have attempted to control for leaf temperature; however, the divorce of light irradiance and leaf temperature may be impractical and deleterious to a plant's HL acclimation ability (Huang *et al*., 2019).

Response to gibberellin (gibberellic acid; GA) becomes interesting upon reviewing the transcription factors associated with the upregulated genes (Table 3.4.1 [Page 84]). GA suppresses the expression of the *ELIP* genes and the accumulation of the HY5 protein (Alabadí *et al*., 2008). I further explored the impact of GA in section 3.4.4 [Page 84]; however, first, GO analysis was performed on the downregulated gene group to determine if any linking or antagonistic GO groups were present.

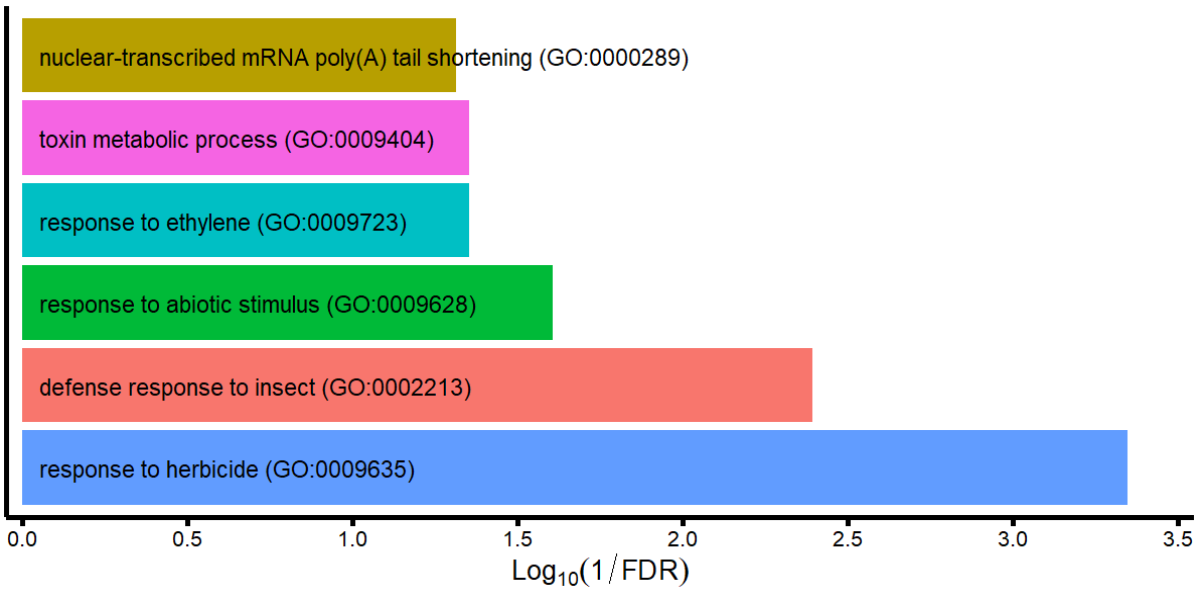

Figure 3.4.5: A subset of the GO analysis of the 66 DEGs downregulated by both *hy5-2* and BBX32-10 when compared to Col-0 under LL conditions. A false discovery rate is calculated and transformed to provide a readable scale.

I categorised toxin metabolic process, response to abiotic stimulus, defence response to insect and response to herbicide as altering defence response. Resource allocation may need to occur for *Arabidopsis* to acclimate to new HL conditions (Alvarez-Fernandez *et al*., 2021). For example, a plant could focus on building a new photosynthetic apparatus that requires energy; therefore, plants may

deprioritise non-essential systems. Response to ethylene also has a relationship to defence. Plants upregulate defence genes such as *PDF1.2a* upon applying exogenous ethylene and overexpression of ethylene-responsive genes (Anderson *et al*., 2004). Defence response and the impact on HL acclimation was explored further in Chapter 5 [Page 166].

3.4.4 Analysis of differentially expressed transcription factors

Transcription factors are essential proteins that control the expression of other genes. They bind to DNA to enhance or suppress transcription. These transcriptional changes alter the proteome initiating cellular changes. Transcription factors can enhance or suppress the genes of other transcription factor proteins, which causes a cascade of transcriptional alterations. *hy5-2* and BBX32-10 have perturbed transcriptional steady states due to their genetic modifications. By isolating transcription factors from the upregulated and downregulated DEGs lists, I can more comprehensively understand the changes *hy5-2* and BBX32-10 jointly made that may impact HL acclimation.

Table 3.4.1: The transcription (co-) factors found amongst the 543 DEGs upregulated in both BBX32 LL / Col LL and HY5 LL / Col LL. L2F, log_2 Fold change.

Locus Identifier	Primary Gene Symbol / Description	Other Gene Symbol	BBX32 LL/ Col LL L2F	HY5 LL/ Col LL L2F
AT4G24540	AGAMOUS-LIKE 24 (AGL24)		0.876159	0.52406
AT5G10140	FLOWERING LOCUS C (FLC)	AGAMOUS-LIKE 25 (AGL25)	2.68475	1.588334
AT2G37630	ASYMMETRIC LEAVES 1 (AS1)	MYB91	1.020169	0.436625
AT2G21320	B-BOX DOMAIN PROTEIN 18 (BBX18)		0.614886	0.420577
AT3G23210	BASIC HELIX-LOOP-HELIX 34 (bHLH34)	IRON DEFICIENCY TOLERANT1 (IDT1)	1.332531	0.632728
AT4G23750	CYTOKININ RESPONSE FACTOR 2 (CRF2)	TARGET OF MONOPTEROS 3 (TMO3)	1.461576	0.760488
AT5G56860	GATA, NITRATE-INDUCIBLE, CARBON METABOLISM-INVOLVED (GNC)	GATA TRANSCRIPTION FACTOR 21 (GATA21)	1.365924	0.334611
AT4G26150	CYTOKININ-RESPONSIVE GATA FACTOR 1 (CGA1)	GATA TRANSCRIPTION FACTOR 22 (GATA22)	2.056727	1.032083
AT4G34590	G-BOX BINDING FACTOR 6 (GBF6)	BASIC LEUCINE-ZIPPER 11 (ATBZIP11)	1.212279	0.588059
AT3G58070	GLABROUS INFLORESCENCE STEMS (GIS)		1.670375	0.649095
AT3G44750	HISTONE DEACETYLASE 3 (HDA3)	HISTONE DEACETYLASE 2A (HD2A)	0.700193	0.543037
AT3G57150	HOMOLOGUE OF NAP57 (NAP57)	C-REPEAT/DRE BINDING FACTOR 5 (CBF5)	0.813532	0.766096
AT5G49330	MYB DOMAIN PROTEIN 111 (MYB111)	PRODUCTION OF FLAVONOL GLYCOSIDES 3 (PFG3)	2.515197	1.001484
AT1G06180	MYB DOMAIN PROTEIN 13 (MYB13)		2.052117	0.999
AT3G12270	PROTEIN ARGININE METHYLTRANSFERASE 3 (PRMT3)		1.149086	0.697218
AT1G66350	RGA-LIKE 1 (RGL1)		0.512695	0.623754
AT3G03450	RGA-LIKE 2 (RGL2)		0.536081	0.485787
AT1G15100	RING-H2 FINGER A2A (RHA2A)		1.411728	0.865926
AT3G54990	SCHLAFMUTZE (SMZ)		1.343095	1.395472
AT2G23740	SU(VAR)3-9-RELATED PROTEIN 5 (SUVR5)		0.490054	0.386524
AT1G08290	WIP DOMAIN PROTEIN 3 (WIP3)		1.371108	1.489797
AT5G52010	C2H2-like zinc finger protein		0.516614	0.541638

BBX18 is the closest related gene to *BBX19*, a member of the HL TF network (further details on the BBX family see section 6.3 [Page 207]; Khanna *et al*., 2009; Alvarez-Fernandez *et al*., 2021). BBX19 acts with the evening complex to suppress *PIF4*, another member of the HL TF network, and *PIF5* expression (Wang *et al*., 2015). BBX18 also suppresses *PIF4* and *PIF5* expression in a temperature-dependent manner. In a mass yeast 2-hybrid experiment, BBX32 binds both BBX18 and BBX19. Both potentially have a similar bridging functionality between BBX32 and BBX4, which have been previously shown to have a protein link, however, the

specifics of this interaction has not yet been explored (Trigg *et al*., 2017; Tripathi *et al*., 2017). In addition, BBX18 can bind CONSTANS (CO; BBX1), a photoperiod gene with links to flowering, and COP1, a key regulator of photomorphogenesis and has also been implicated in HL acclimation, likely targeting BBX18 for degradation (Trigg *et al*., 2017; Ding *et al*., 2018; Alvarez-Fernandez *et al*., 2021).

AGAMOUS-LIKE 24 (AGL24) and *AGL25* are both type II MYOCYTE ENHANCER FACTOR2-like genes, and in *hy5-2* and BBX32-10 mutants are upregulated (Fatima *et al*., 2020). However, *AGL24* and *AGL25* are not the closest relatives within their gene family (Alvarez-Buylla *et al*., 2000). *AGL25* is known as *FLOWERING LOCUS C* (*FLC*) and acts as a central flowering and vernalisation repressor (Lee *et al*., 1994). Different alleles of *FLC* control and integrate signals into flowering time in different *Arabidopsis* ecotypes (Sanda and Amasino, 1996; Ferguson *et al*., 2019). FLC represses *SUPPRESSOR OF OVEREXPRESSION OF CONSTANS1 (SOC1*; *AGL20*), which co-upregulates with *AGL24* to promote flowering time (Michaels *et al*., 2003). A study found that during vernalisation, *AGL24* is activated and positively regulates flowering time (Michaels *et al*., 2003). BBX32 binds AGL24 directly in *Brassica rapa L. ssp. pekinensis* (Chinese cabbage) potentially disrupts the SOC1-AGL24 complex and increases flowering time (Guan-Peng *et al*., 2019; Chapter 4 [Page 125]; Tripathi *et al*., 2017).

GATA, NITRATE-INDUCIBLE, CARBON-METABOLISM INVOLVED (GNC; GATA21), and CYTOKININ RESPONSIVE GATA FACTOR1 (CGA1; GATA22) modulate chlorophyll biosynthesis and *GLUTAMATE SYNTHASE1* (*GLU1*) expression (Hudson *et al*., 2011). PIF3, a binding partner and repressor of HY5,

binds to the *GNC* and *CGA1* promoters and becomes upregulated by light following darkness (Chen *et al*., 2013; Hudson *et al*., 2011). *GNC* and *CGA1* cross-repress with *SOC1*; GNC and CGA1 bind to the *SOC1* promoter, and SOC1 binds to the *GNC* and *CGA1* promoters, integrating light signalling into flowering time (Richter *et al*., 2013). *GNC* and *CGA1* also act in a feedback loop to repress gibberellin (GA) signalling, a pathway implicated by the upregulated DEGs GO analysis (Richter *et al*., 2010; Figure 3.4.4 [Page 80]).

REPRESSOR OF GIBBERELLIN LIKE1 (RGL1) and RGL2 are DELLA proteins that act in the absence of GA (Wen and Chang, 2002; Lee *et al*., 2002). These proteins are closely related to GAI, whose gene is a member of the HL TF network produced by Alvarez-Fernandez *et al*. (2021). The repression of *FT* and *SOC1* by binding with RGL1 and RGL2 enhances the expression of *FLC* (Li *et al*., 2016). The key HL acclimation protein COP1 in complex with a SUPPRESSOR OF PHYA-105 (SPA; SPA1, SPA2, SPA3, SPA4) protein degrades RGL1 and RGL2 in a light and temperature-dependent manner (Blanco-Touriñán *et al*., 2020; Frerigmann *et al*., 2021). PIF3 and PIF4, another member of the HL TF network, are sequestered by RGL1 and RGL2 and prevented from interacting with other targets (Li *et al*., 2016).

In the joint *hy5-2* and BBX32-10 upregulated gene list, a large number of connections exists with HL acclimation genes and HL TF network members. Analysing the downregulated genes from Figure 3.4.3 [Page 79] may elucidate further connectivity within a growing gene network with connections to HL acclimation, productivity, and flowering time genes.

Table 3.4.2: The 66 DEGs downregulated in both BBX32 / Col and HY5 / Col under LL conditions which are transcription factors. L2F, log_2 Fold change.

Locus Identifier	Primary Gene Symbol / Description	Other gene symbol	BBX32 LL/ Col LL L2F	HY5 LL/ Col LL L2F
AT1G74930	Ethylene Response Factor 018 (ERF018)	ORA47	-1.21638	-1.41988
AT5G61590	Ethylene Response Factor 107 (ERF107)	DEWAX	-2.45181	-0.7422
AT1G71030	MYB-LIKE 2 (MYBL2)		-0.60417	-0.43558
AT1G69490	NAC-LIKE, ACTIVATED BY AP3/PI (NAP)	NAC029	-0.87862	-1.03642
AT1G06160	ETHYLENE RESPONSIVE FACTOR 59 (ERF59)	ORA59	-2.81715	-2.04814
AT1G68840	RELATED TO ABI3/VP1 2 (RAV2)	EDF2	-1.14813	-1.07719
AT2G38470	WRKY DNA-BINDING PROTEIN 33 (WRKY33)		-0.94015	-0.52143

ERF107 and NAP (NAC029) are both members of the HL TF network produced by Alvarez-Fernandez *et al*. (2021) and downregulated in BBX32-10 and *hy5-2* (Table 3.4.2 [Page 88]). NAP is a regulator of leaf senescence and integrates signals from RGA1, RGA2 and GA (Lei *et al*., 2019). TEMPRANILLO1 (TEM1), the closest homologue of RAV2, binds to the FT promoter and is increased in expression by GA (Fu *et al*., 2014). WRKY33 and ORA59 are defence genes in the necrotrophic pathogen response pathway (Huang *et al*., 2016). This correlation with defence was discussed further in Chapter 5 [Page 166].

The information gathered around the upregulated and downregulated genes (Table 3.4.1 [Page 84] and Table 3.4.2 [Page 88]) can be processed into a cohesive network centred around the HL acclimation genes *HY5*, *BBX32* and *COP1* (Figure 3.4.6 [Page 89]). The network is built solely out of interactions known already in the literature. It includes 3 (currently known) HL acclimation genes, 2 HL TF network members and 5 other genes that were suppressed in their expression by genes upregulated in both *hy5-2* and BBX32-10.

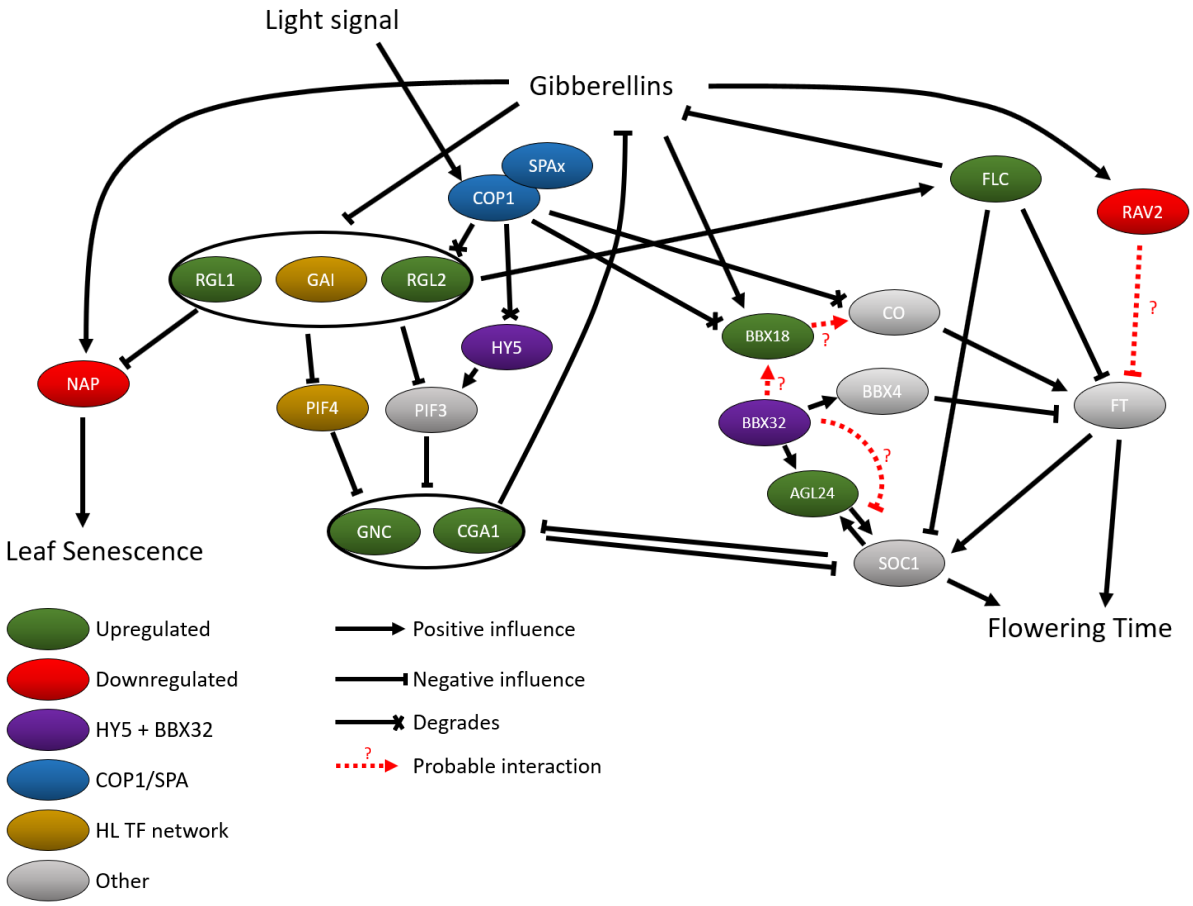

Figure 3.4.6: The interaction map of transcription factors, transcription co-factors, flowering time, light signalling and the phytohormone gibberellin. Arrows denote a positive interaction, lines ending in a flat bar show a repressing action and lines ending in a cross show the COP1/SPA E3 ligase complex degrading proteins. Circled genes are closely related where all of the interactions apply to all of the genes in the circle. Green, genes upregulated within BBX32-10 and *hy5-2* compared to Col-0 (all LL); Red, genes downregulated within BBX32-10 and *hy5-2* compared to Col-0 (all LL); Purple, BBX32 and HY5; Yellow, members of the HL TF network; Blue, members of the COP1/SPA complex (SPAx denotes SPA1, SPA2, SPA3 or SPA4); Grey, auxiliary genes to complete the network. Protein connections have been gathered from BioGrid (Oughtred *et al*., 2019) and from; Wen and Chang (2002), Lee *et al*. (2002), Michaels *et al*. (2003), Richter *et al*. (2010), Tripathi *et al*.

(2017), Trigg *et al*. (2017), Guan- Peng *et al*. (2019), Blanco-Touriñán *et al*. (2020), Frerigmann *et al*. (2021).

HY5 and BBX32 act in different parts of the interaction map (Figure 3.4.6 [Page 89]) though they potentially form a complex with bridging proteins such as BBX21 (Holtan *et al*., 2011). This connection joins the centre of the map and further increases the number of interactions. In addition, this map involves other systems that interact with HL acclimation, such as flowering time and leaf senescence (Athanasiou *et al*., 2010; Alvarez-Fernandez *et al*., 2021; Guo and Gan, 2006). However, it does not contain any genes that are known to control the expression of Calvin-Benson cycle genes or photosynthesis-associated nuclear genes (PhANGs), which are a group of nuclear-encoded genes coding for the proteins of the light-dependent reactions of photosynthesis (Miller *et al*., 2017; Lv *et al*., 2019).

The high number of HL TF network members associated with the interaction map genes indicates a connection to HL acclimation. However, it is unknown how the Figure 3.4.5 [Page 83] interaction map fits into HL acclimation. Understanding the HL TF network may assist in creating a direct connection to the PhANGs and HL acclimation.

3.4.5 Conclusion

Similarities between the *hy5-2* and BBX32-10 transcriptomes show that these mutants are most likely altering HL acclimation through the perturbation of the same pathway. *gpt2*-, *hy5-2,* and BBX32-10 HL acclimation mutants impact primary metabolism, although it is unclear whether this is the cause of the defective HL

acclimation phenotypes. Discovering new HL acclimation mutants may be used to verify the link between HL acclimation and primary metabolism.

This section culminated in developing an interaction map of genes related to HL acclimation, including the influence of members of the HL TF network from Alvarez-Fernandez *et al*. (2021). *GAI* and *PIF4* have direct connections to *BBX32*, the central hub of the HL TF network. Genes of the HL TF network can be directly tested by exposing null mutants of these genes to HL for five days and measuring their PSII operational efficiency (Alvarez-Fernandez *et al*., 2021). Further analysis of the HL TF network may yield more testable genes and interactions that impact HL acclimation.

3.5 Verifying the HL TF network

The HL TF network, as discussed previously, is a computer-generated network based on data gathered from plants that the study exposed to 0-6 hours of HL (Beal *et al*., 2005; Alvarez-Fernandez *et al*., 2021). The study exposed plants to HL and growth light conditions, and plants were taken for RNA extraction every 30 minutes, generating 13-time points. RNA was extracted from 4 samples per time point per condition generating 100 individual samples (0-hour time point not requiring a LL control). The study performed a microarray experiment on RNA samples, and the data was processed. Alvarez-Fernandez *et al*. (2021) processed the difference between HL and the control time series for each gene into a value and a cut-off assigned to remove less differentiated genes. The transcription (co-) factor genes and their HL time series values were input into a Variational Bayesian State-Space Model (VBSSM) to determine hidden states between the expression of these genes (Beal *et al*., 2005). The output of this program was the HL TF network.

Alvarez-Ferndez *et al*. (2021) identified that some of the transcription factors involved in the HL TF network contribute to Arabidopsis's HL response and hypothesised that more would also influence HL acclimation. However, many of these genes are known to initiate other processes; therefore, analysing these genes is necessary to identify members of the HL acclimation pathway. Alvarez-Fernandez *et al*. (2021) determined *BBX32* and *HY5* to play a key role in HL acclimation, but 44 other network members have not been tested. This test involves measuring the PSII operational efficiency using chlorophyll fluorescence as a substitute for the more destructive, expensive, and time-consuming process of directly measuring carbon assimilation.

The HL acclimation parameters used have a similar experimental design to the HL acclimation experiments from Alvarez-Fernandez *et al*. (2021). 4-6 week old plants were exposed to HL conditions (1000 µmol m^{-2} s^{-1}) for 4 hours to initiate HL acclimation. I repeated these HL conditions for 4 hours each day over five days, at which point the plant is HL acclimated. Plants have their PSII operational efficiency (Fq'/Fm') measured on day one following 4 hours of HL exposure and after the exposure on day 5.

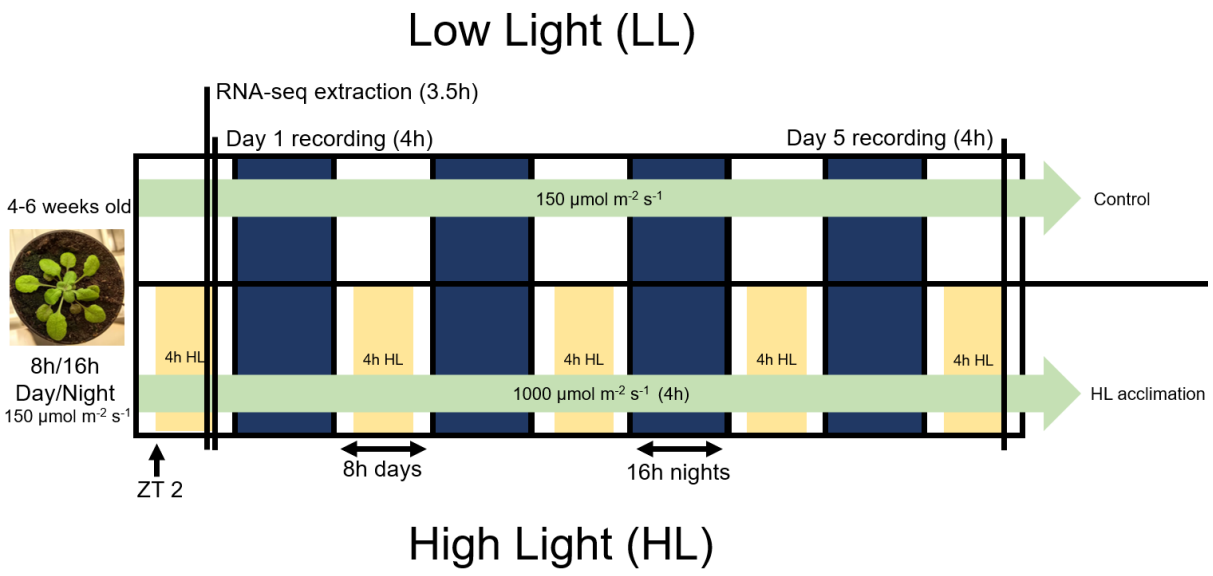

1859

1860 **Figure 3.5.1: Experimental design for *Arabidopsis* HL acclimation.** 4-6 week old
1861 *Arabidopsis* plants (grown at 8h/16h, day/night; 150 µmol m^{-2} s^{-1}) are either
1862 maintained at the same growth conditions (known as LL or control) or placed under
1863 increased light conditions (1000 µmol m^{-2} s^{-1}) at ZEITLUPE (ZT) 2 for 4 hours for five
1864 days (HL). RNA is extracted after 3.5 hours of HL or 3.5 h control conditions.
1865 Chlorophyll fluorescence measurements are taken after 4 hours of HL on the first
1866 day and after repeating the 4 hours of increased light conditions at ZT 2 for five days.
1867 Identical to Figure 7.3.2 [Page 281].

1868

1869 Due to limited resources, I could not analyse all network members within this
1870 chapter. A list of genes was selected based on the location within the network and
1871 having a direct connection to *BBX32*. *PIF4* had previously been studied by Alvarez-
1872 Fernandez *et al*. (2021), leaving 18 direct connections to *BBX32*. I added *BBX19* and
1873 *PIF7* to this list due to their secondary connection to *BBX32* and homology to other
1874 genes on the list (*BBX14*/ *BBX32* and *PIF4*, respectively). *SPA1* was studied
1875 separately in Chapter 4 [Page 125] due to its known light signalling properties and
1876 that it is not a transcription factor (Laubinger *et al*., 2004).

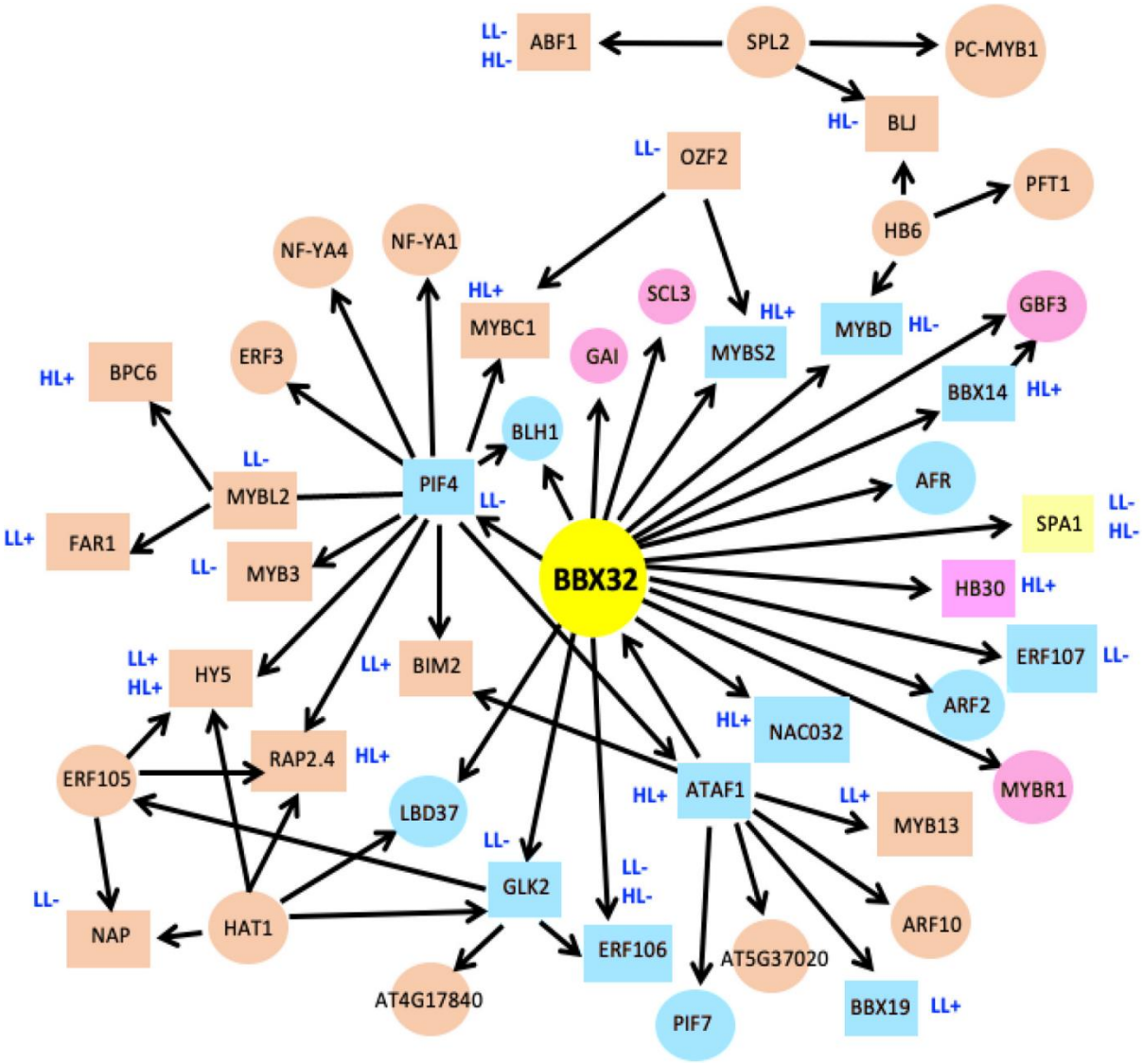

Figure 3.5.2: HL transcription factor network from Alvarez-Fernandez *et al*. (2021). Blue indicates direct connections with BBX32 and secondary connections that are close homologues with primary connections. Pink genes were unable to be studied. *SPA1* and *BBX32* (shown in yellow) are the only two genes in the network that do not encode transcription factors.

3.5.1 Transcriptional regulation of HL TF network members

Mutants of genes in pink were either unable to be obtained (*HB30*, *SCL3* and *MYBR1*), not able to be successfully germinated (*GBF3*) or only have mutants that are unsuitable for chlorophyll fluorescence measurements (*GAI*). This removal left 15 genes for study. These genes can be looked at within *BBX32-HY5* HL RNA-seq to identify transcript abundance changes induced by HL and within mutant plants that cannot acclimate to HL. The expression of *BBX32* and *HY5* genes was significantly perturbed within their respective mutants as expected (Figure 3.5.3 [Page 96]). *AFR* was excluded from Figure 3.5.3 [Page 96] due to the lack of traceable expression within any of the samples of the *BBX32-HY5* HL RNA-seq.

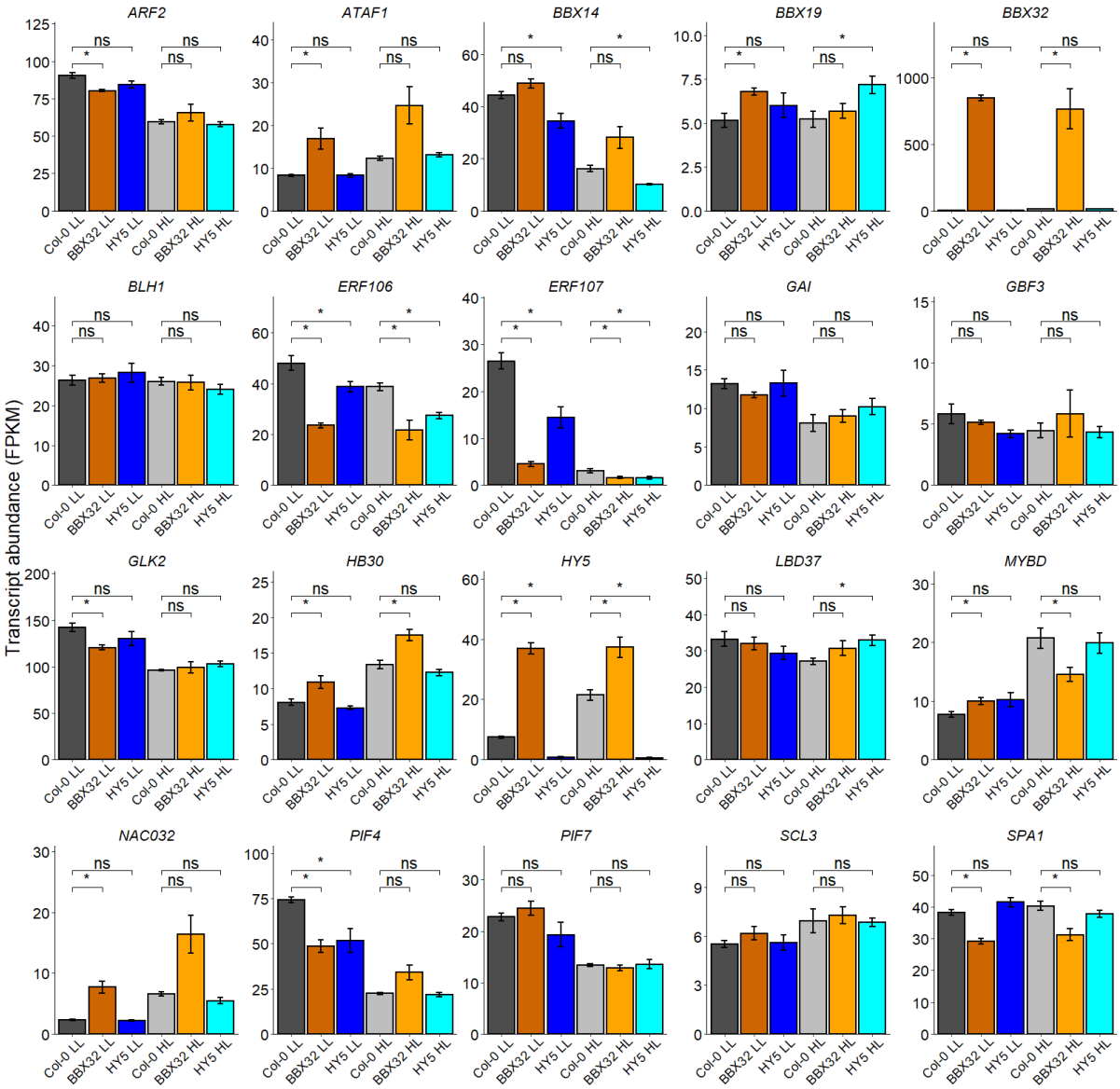

Figure 3.5.3: The expression of a selection of genes from the HL transcription factor network from the *BBX32-HY5* HL RNA-seq. Expression was obtained from BBX32-10 (BBX32), *hy5-2* (HY5) or Col-0 under LL or HL conditions for 3.5 hours of exposure. Asterisks and bars show genes significantly changed in expression between the LL and HL groups of each genotype ($p < 0.05$; ANOVA).

Some genes showed minimal changes when exposed to HL for 3.5 hours; *BBX19*, *BLH1*, *GBF3*, *LBD37*, *SCL3* and *SPA1* did not significantly change. *BLH1*, *GBF3*,

SCL3 and *SPA1* had no significant expression changes between the samples. *GLK2* and *PIF7* experience significant alterations in expression due to HL, although this was matched by both *hy5-2* and BBX32-10 with no significant changes within the light treatment groups (LL and HL). An exciting change in expression was the *HY5* gene in the BBX32-10. BBX32-10 plants over-expressed *HY5,* and 3.5 hours of HL did not impact this change. This data suggests that *BBX32* has some control over the expression of *HY5*.

3.5.2 Protein-protein linkage between the members of the HL TF network

This chapter's current model of HL acclimation is built around protein-protein interactions between CRY1, COP1 and HY5 (Figure 3.1.2 Page [67]). HY5 and BBX32 connect through a complex involving another BBX family member, BBX21 (Holtan *et al*., 2011). In addition, previous studies have conducted extensive large-scale yeast-two hybrid experiments on *Arabidopsis* transcription factors (Trigg *et al*., 2017). I gathered these connections from an online database called Biogrid (Oughtred *et al*., 2019) and arranged them into a single network by adding a limited number of other transcription factors and transcriptional regulators (Oughtred *et al*., 2019).

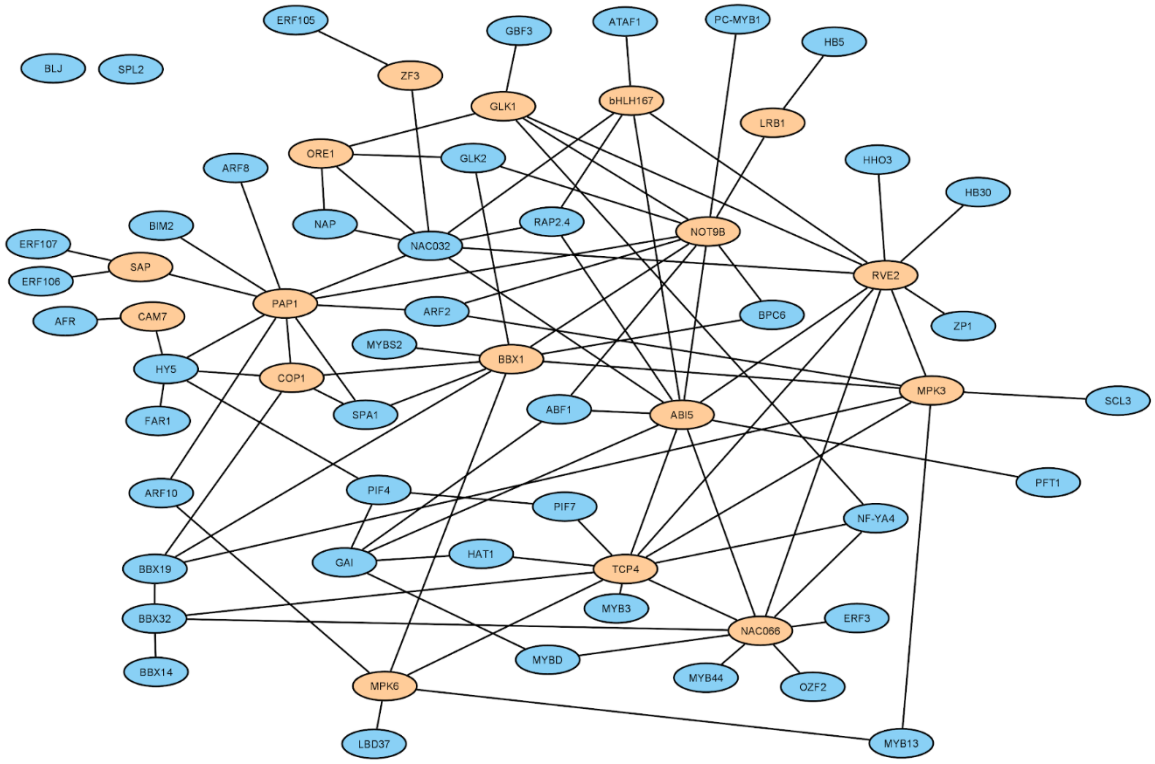

Figure 3.5.4: A transformation of the HL TF network where each connection represents a known protein-protein interaction. Information has been gathered from the BioGrid database (Oughtred *et al*., 2019). Genes from the HL transcription factor network are coloured blue, and genes added are coloured peach.

Many members of the HL TF network have known protein-protein binding with others, and I connected them using several non-member hub proteins. These non-member proteins like COP1, PAP1 and BBX1 (CO) are typically well studied. As many of these proteins directly interact, they could transduce a light signal to initiate HL acclimation. This protein-protein data is crucial information for building a HL acclimation regulatory network. Further exploring the HL TF network genes and

discovering which genes play a role in HL acclimation, fundamental interactions of this protein-protein network can be isolated.

3.5.3 HL acclimation phenotype of HL TF network members

HL acclimation experiments were carried out on plants with mutations of the gene of interest by the experimental design shown in Figure 3.5.1 [Page 93]. Plants were exposed to HL for 4 hours a day for five days, with chlorophyll fluorescence measurements taken after the HL exposure on day one and day 5. In addition, the Fq'/Fm' data for each measured PPFD was extracted and visualised.

Mutant plants of these genes were obtained from the National Arabidopsis Stock Centre (NASC; University of Nottingham) and were primarily SALK mutants (Table S3 [Page 337]). Some of the mutants had not been characterised in the literature before, limiting their usefulness. Not all T-DNA insertion lines (like SALK) produce a mutant that fails to accrue native levels of the target protein (Alonso *et al*., 2003). Without a HL acclimation phenotype, it would be impossible to tell the difference between a successful and an unsuccessful mutant. This methodology is not aiming to disprove the role of a HL TF network member within HL acclimation but to identify targets for further study.

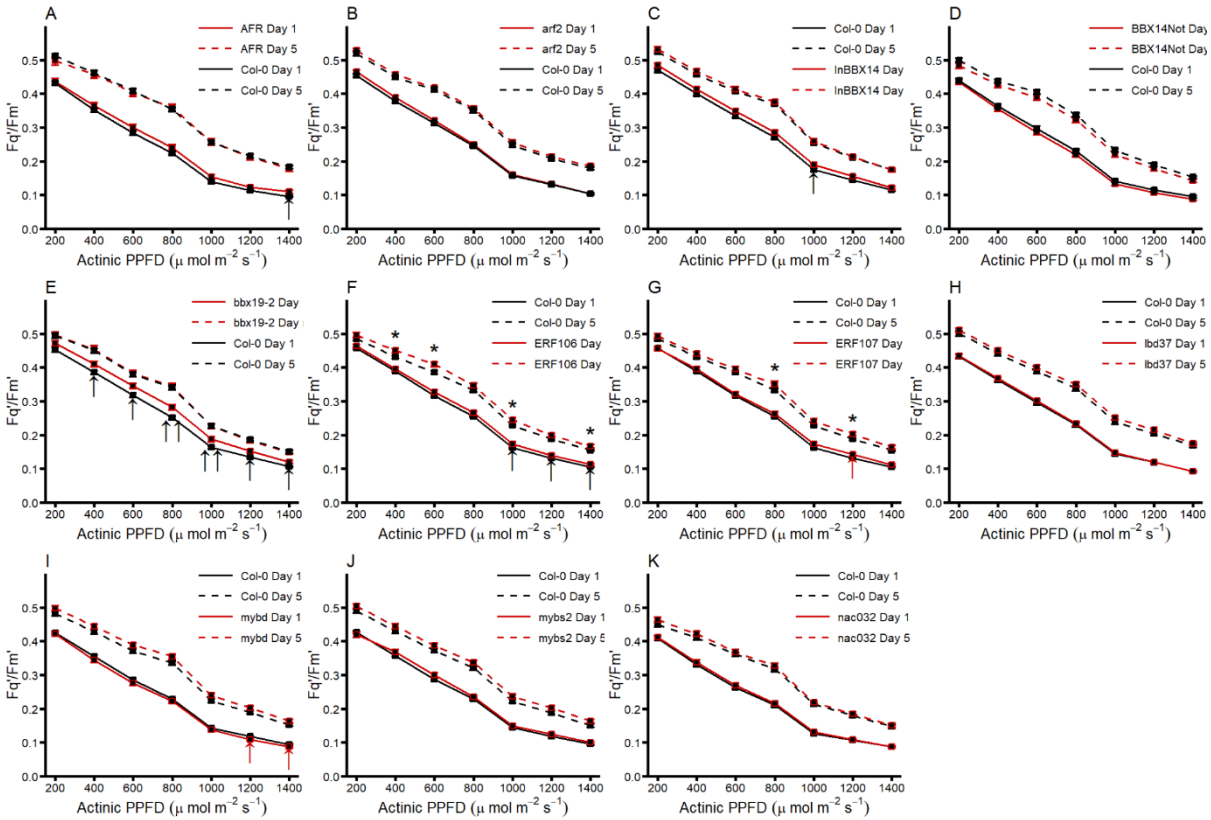

Figure 3.5.5: HL acclimation of *afr* (A), *arf2*(B), Induced BBX14 (InBBX14) (C), BBX14 Not induced (BBX14Not) (D), *bbx19-2* (E), *erf106* (F), *erf107* (G), *lbd37* (H), *mybd* (I), *mybs2* (J), *nac032* (K) and Col-0 plants. Fq'/Fm' was determined by chlorophyll fluorescence with an actinic PPFD range of 200 µmol m^{-2} s^{-1} to 1400 µmol m^{-2} s^{-1} at 200 µmol m^{-2} s^{-1} increments. Measurements were taken from 4-6 week old plants (n > 4) with a minimum of 6 mature leaves each (means ± SE). Arrows and asterisks denote a significant difference between the day 1 and day 5 values respectively of the mutants and Col-0 (ANOVA, post-hoc GH; */↑ = $p < 0.05$; **/↑↑ = $p < 0.005$).

I have shown that many HL TF network members do not have a HL acclimation phenotype when exposed to HL for five days. However, many of these genes are poorly studied and have close homologues. These homologues potentially have overlapping functionality that masks the effects of a T-DNA insertion mutation.

Therefore, I could not simply determine the role of these genes in HL acclimation using knockout mutants.

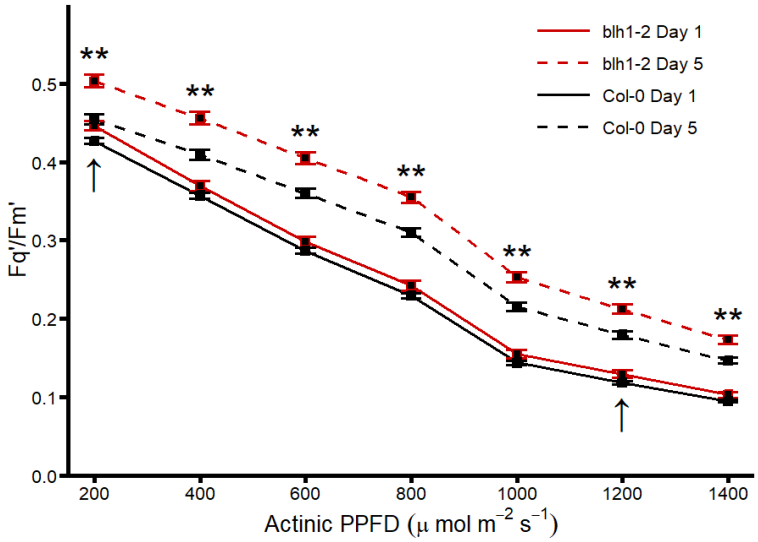

Figure 3.5.6: HL acclimation phenotype of *blh1-2* and Col-0 plants. Fq'/Fm' was determined by chlorophyll fluorescence with an actinic PPFD range of 200 µmol m^{-2} s^{-1} to 1400 µmol m^{-2} s^{-1} at 200 µmol m^{-2} s^{-1} increments. Measurements were taken from 4-6 week old plants (n > 4) with a minimum of 6 mature leaves each (means ± SE). Arrows and asterisks denote a significant difference between the day 1 and day 5 values respectively of the mutants and Col-0 (ANOVA, post-hoc GH; */↑ = p < 0.05; **/↑↑ = p < 0.005).

BLH1 is a homeodomain transcription factor known for impacting embryo sac development and ABA response during germination; however, its role in mature plants has not been elucidated (Pagnussat *et al*., 2007; Kim et al., 2013). The *BLH1* T-DNA insertion mutant (GK-114D09), also known as *blh1-2* (Pagnussat *et al*., 2007), does not have an impact on PSII operational efficiency on day 1; however, it

is significantly higher on day 5 (Figure 3.5.6 [Page 101]). It is unknown how *blh1-2* impacts PSII operational efficiency and HL acclimation.

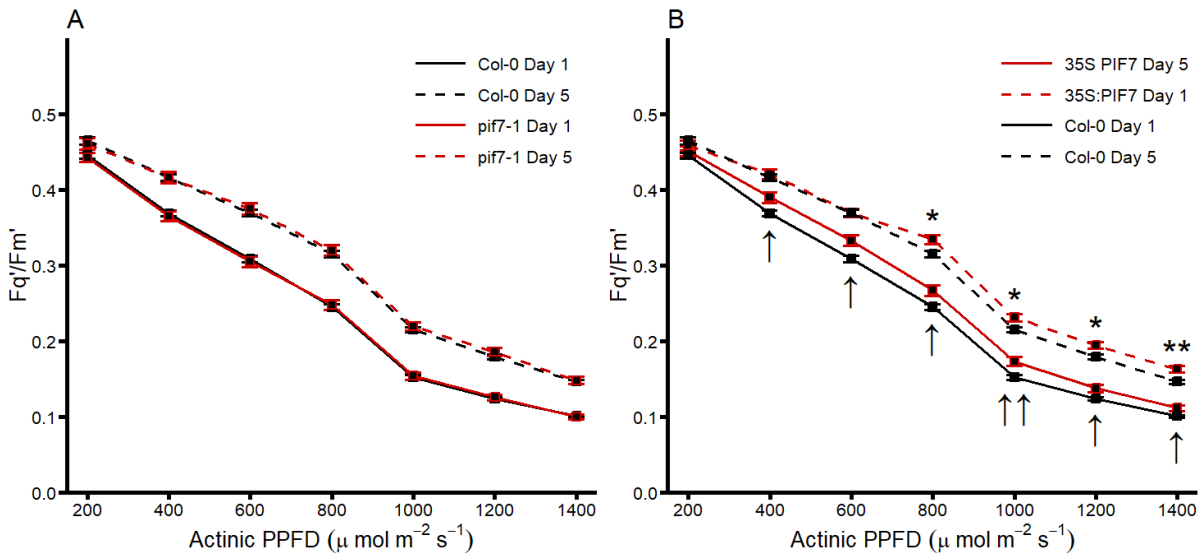

Figure 3.5.7: HL acclimation phenotype of *pif7-1* (A), 35S:PIF7 (B) and Col-0 plants. Fq'/Fm' was determined by chlorophyll fluorescence with an actinic PPFD range of 200 µmol m^{-2} s^{-1} to 1400 µmol m^{-2} s^{-1} at 200 µmol m^{-2} s^{-1} increments. Measurements were taken from 4-6 week old plants (n > 4) with a minimum of 6 mature leaves each (means ± SE). Arrows and asterisks denote a significant difference between the day 1 and day 5 values respectively of the mutants and Col-0 (ANOVA, post-hoc GH; */↑ = $p < 0.05$; **/↑↑ = $p < 0.005$).

pif7-1 does not have an altered HL acclimation phenotype, whereas 35S:PIF7 has a minor increase in PSII operational efficiency on days one and five. The lines formed from the 35S:PIF7 data are skewed on day one and day 5; The Fq'/Fm' is closer to the Col-0 values at lower PPFD levels than at higher PPFD levels. The higher PPFD levels gravitate towards being more significant.

The small changes in HL acclimation phenotype seen in 35S:PIF7 can be contrasted to the *pifQ* and *pif4-2* mutants analysed by Alvarez-Fernandez *et al*. (2021). *pifQ* is a quadruple knock-out mutant containing *pif1*, *pif3*, *pif4* and *pif5* and displayed a defective HL acclimation phenotype (Alvarez-Fernandez *et al*., 2021). A knock-out mutation of *pif7* is not included in the *pifQ* mutant, and it is unknown which of the mutations within *pifQ* contribute to the HL acclimation phenotype (Alvarez-Fernandez *et al*., 2021). *pif4-2* had an insignificant HL acclimation phenotype even though it is the only mutant gene in *pifQ* that's also a member of the HL TF network (Alvarez-Fernandez *et al*., 2021). Further experiments would be necessary to ascertain the combinations of *PIF* genes required to reveal the most severe HL acclimation phenotype and which *PIF* genes are involved in HL acclimation.

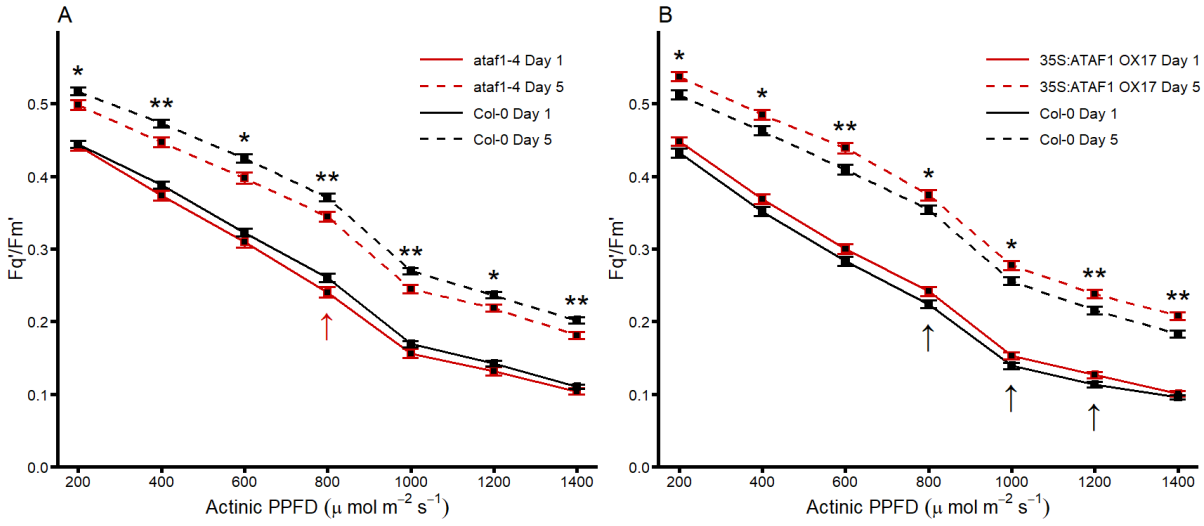

Figure 3.5.8: HL acclimation phenotype of *ataf1-4* (A), 35S:ATAF1 (B) and Col-0 plants. Fq'/Fm' was determined by chlorophyll fluorescence with an actinic PPFD range of 200 µmol m^{-2} s^{-1} to 1400 µmol m^{-2} s^{-1} at 200 µmol m^{-2} s^{-1} increments. Measurements were taken from 4-6 week old plants (n > 4) with a minimum of 6 mature leaves each (means ± SE). Arrows and asterisks denote a significant

difference between the day 1 and day 5 values respectively of the mutants and Col-0 (ANOVA, post-hoc GH; */↑ = $p < 0.05$; **/↑↑ = $p < 0.005$).

ataf1-4 and 35S:ATAF1 showed altered photosynthetic phenotypes upon exposure to HL. Neither were significantly different at most of the actinic PPFDs to Col-0 (WT) on day one; however, by five days of HL exposure, both show significance across all actinic PPFDs in an opposite fashion; *ataf1-4* increased less than Col-0 by day five and 35S:ATAF1 increased more. *ATAF1* is the closest homologue to *NAC032*, another HL TF network member that yielded no significant impact on the HL acclimation phenotype. A combination of these two mutants may yield a more robust HL acclimation phenotype than either alone due to a potential overlap in their functions.

ATAF1, ORE1 and the GLKs (GLK1 and GLK2) act as a regulatory unit to balance chloroplastic maintenance and leaf senescence gene expression (Garapati *et al*., 2015). *GLK2*, *ATAF1* and *NAP* (another leaf senescence regulator; implicated in the Figure 3.4.5 [Page 83] interaction map) are members of the HL TF network (Guo and Gan, 2006; Alvarez-Fernandez *et al*., 2021). This regulatory unit was further studied by analysing the HL acclimation phenotype of *GLK2* mutants.

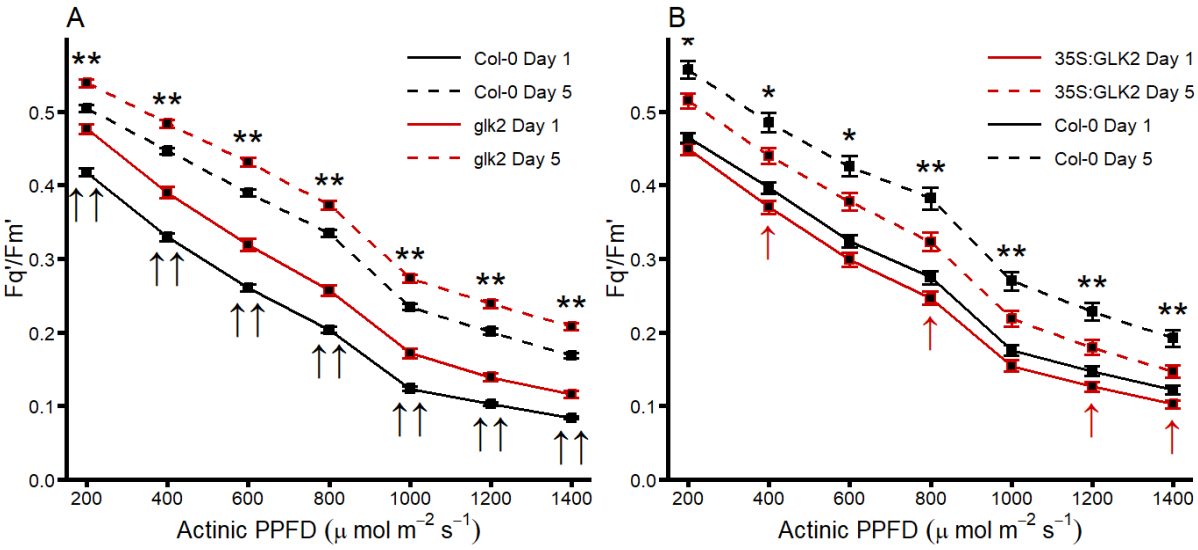

Figure 3.5.9: HL acclimation phenotype of *glk2* (A), 35S:GLK2 (B) and Col-0 plants. Fq'/Fm' was determined by chlorophyll fluorescence with an actinic PPFD range of 200 µmol m^{-2} s^{-1} to 1400 µmol m^{-2} s^{-1} at 200 µmol m^{-2} s^{-1} increments. Measurements were taken from 4-6 week old plants (n > 4) with a minimum of 6 mature leaves each (means ± SE). Arrows and asterisks denote a significant difference between the day 1 and day 5 values respectively of the mutants and Col-0 (ANOVA, post-hoc GH; */↑ = p < 0.05; **/↑↑ = p < 0.005).

glk2 showed a significant difference to Col-0 on day one and day five. The Fq'/Fm' of *glk2* plants was higher on day one and remained higher on day 5. The inverse was the case for 35S:GLK2; Fq'/Fm' of 35S:GLK2 was lower on days one and five. The difference between the day one and day five values of the *glk2* and 35S:GLK2 mutants were not significantly different from Col-0 day differences.

GLK2 is a transcription factor involved in chloroplast maintenance and impacts the expression of PhANGs by directly binding to their promoters (Waters *et al*., 2009). *GLK2* may provide the direct connection to enhancing photosynthetic capacity in

light acclimated plants. However, the *GOLDEN-LIKE2* gene family has two members: *GLK1* and *GLK2* (Fitter *et al*., 2002). These genes are commonly studied together within the double mutant *glk1glk2* (Yasumura *et al*., 2005; Murmu *et al*., 2013; Tokumaru *et al*., 2017; Lee *et al*., 2021; Zhang D *et al*., 2021; Zhao D *et al.,* 2021). I further analysed the effects of the *GLK* genes on HL acclimation in the next section (section 3.6 [Page 107]).

3.5.4 Conclusion

The majority of tested genes did not have a HL acclimation phenotype. Many of these genes are part of large gene families where they may have functional redundancies with other members. This redundancy would mask the gene's role in HL acclimation and make studying their roles more difficult. To further study the genes lacking a HL acclimation phenotype in their null mutant, an over-expressor could be sourced or created; however, this did not work in all cases in this section (*BBX14* and *PIF7*).

The HL acclimation genes *GLK2* and *ATAF1* discovered in this section are connected to the GLK1-ATAF1-ORE1 chloroplast maintenance/senescence module (Garapati *et al*., 2015). Garapati *et al*. (2015) treated *GLK1* and *GLK2* as completely redundant genes, and GLK2 (G2) can also heterodimerise with its close homologue GLK1 in maize (Rossini *et al*., 2001). If *GLK1* and *GLK2* are truly functionally redundant, *GLK1* should be able to compensate for the *glk2* mutant; however, the single *glk2* mutant has a strong HL acclimation phenotype (Figure 3.5.9 [Page

105105]). Repeating this analysis on different *GLK2* mutants and analysing *GLK1* mutants will further our understanding of the HL acclimation phenotype.

3.6: HL acclimation phenotype of *GOLDEN-LIKE2* mutants

The previous section (section 3.5 [Page 91]) discovered that *glk2* and 35S:GLK2 have HL acclimation phenotypes determined using chlorophyll fluorescence. I further explored the effects of *GLK2* on HL acclimation through the use of known *GLK1* and *GLK2* mutants, a new *GLK2* SALK mutant and GLK over-expressors.

GLK2 is a member of the *GOLDEN2-LIKE* family containing only two members: *GLK1* and *GLK2* (Fitter *et al*., 2002). *GLK1* and *GLK2* are completely functionally redundant (Rossini *et al*., 2001; Fitter *et al*., 2002; Yasumura *et al*., 2005; Waters *et al*., 2009; Murmu *et al*., 2013; Zhao D *et al*., 2021), and the overexpression of either gene rescues the phenotype of the double mutant, *glk1glk2* (Fitter *et al*., 2002). The only known difference between *GLK1* and *GLK2* is a pale green siliques phenotype of *glk2* plants, which is rescued through the overexpression of *GLK1* (Fitter *et al*., 2002). This phenotype is due to differences in compartmentalised expression between the genes (Fitter *et al*., 2002). The *glk1glk2* is often used to study as the double mutant *glk1glk2* or with the over-expressor 35S:GLK1 and is rarely assessed separately (Yasumura *et al*., 2005; Murmu *et al*., 2013; Garapati *et al*., 2015; Tokumaru *et al*., 2017; Lee *et al*., 2021; Zhang D *et al*., 2021; Zhao D *et al.,* 2021; Veciana *et al*., 2022).

3.6.1 GLK1 and GLK2 act in opposition to control acclimation and photosynthetic regulation

A second *GLK2* mutant was sought to confirm the HL acclimation phenotype of the *glk2* mutant. I identified a novel *GLK2* SALK T-DNA insertion, which was acquired for analysis (Alonso *et al*., 2003). This mutant, however, has not been studied before. Therefore, I obtained the commonly used *glk1glk2* mutant, and their HL acclimation phenotypes were analysed.

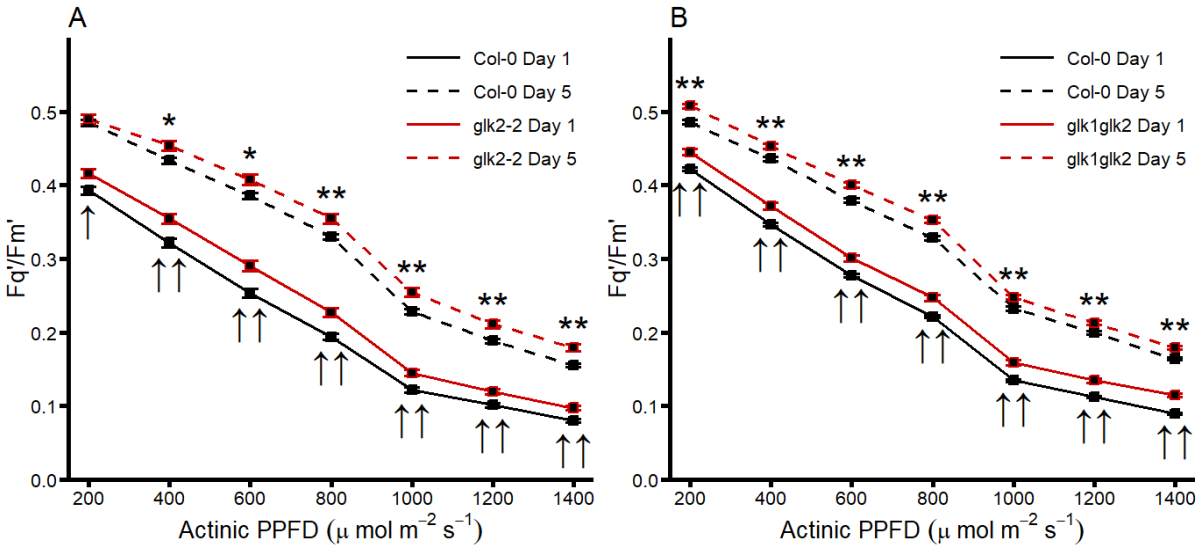

Figure 3.6.1: HL acclimation of *glk2-2* (A), *glk1glk2* (B) and Col-0 plants. Fq'/Fm' was determined by chlorophyll fluorescence with an actinic PPFD range of 200 µmol m^{-2} s^{-1} to 1400 µmol m^{-2} s^{-1} at 200 µmol m^{-2} s^{-1} increments. Measurements were taken from 4-6 week old plants (n > 4) with a minimum of 6 mature leaves each (means ± SE). Arrows and asterisks denote a significant difference between the day 1 and day 5 values respectively of the mutants and Col-0 (ANOVA, post-hoc GH; */↑ = $p < 0.05$; **/↑↑ = $p < 0.005$).

The SALK mutant of *GLK2* (SALK_117006; named here *glk2-2*) strongly impacts the HL acclimation ability. *glk2-2* does not have as strong of a phenotype as *glk2* though this is not unexpected as *glk2* has a transposon insertion in its first exon, whereas *glk2-2* has a T-DNA inserted into its fourth exon (Fitter *et al*., 2002; Alonso *et al*., 2003). *glk1glk2* has a weaker phenotype than *glk2;* however, it is still significant ($P < 0.005$). This phenotype is unexpected as if the *GLK1* and *GLK2* genes are indeed functionally redundant, then the *glk1glk2* mutant, in theory, should have a more robust phenotype than the *glk2* mutant. Following, I tested the *glk1* mutant and 35S:GLK1 mutants.

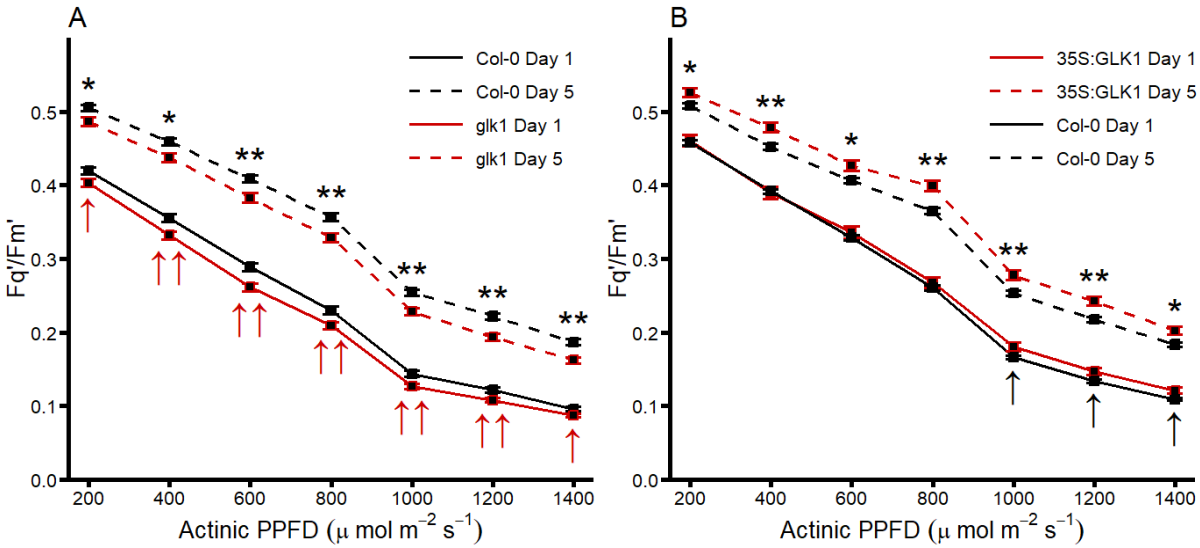

Figure 3.6.2: HL acclimation of *glk1* (A), 35S:GLK1 (B) Col-0 plants. Fq'/Fm' was determined by chlorophyll fluorescence with an actinic PPFD range of 200 µmol m^{-2} s^{-1} to 1400 µmol m^{-2} s^{-1} at 200 µmol m^{-2} s^{-1} increments. Measurements were taken from 4-6 week old plants ($n > 4$) with a minimum of 6 mature leaves each (means ± SE). Arrows and asterisks denote a significant difference between the day 1 and day 5 values respectively of the mutants and Col-0 (ANOVA, post-hoc GH; */↑ = $p < 0.05$; **/↑↑ = $p < 0.005$).

The single *glk1* mutant has lower Fq'/Fm' values on days one and five than Col-0 (WT). This finding is opposite in relation to the WT of the phenotype found in *glk2*. The *GLK1* over-expressor also has a similar the phenotypic pattern with*glk1,* as seen between *glk2* and 35S:GLK2*.* 35S:GLK1 does not have significance on day one but has a higher Fq'/Fm' on day 5 when compared to Col-0.

Data from a single actinic PPFD was selected to simplify the complexity of having many figures for the *GLK* mutants. I selected 800 µmol m^{-2} s^{-1} as the median of the seven PPFD steps. This selection means that each mutant only has two values: a day 1 Fq'/Fm' and a day 5 Fq'/Fm'. This data was plotted on a scatter diagram; however, information may have been lost due to subtle differences between experiments (reflected by the minor changes within Col-0 across experiments). So instead, a delta value was used, meaning that each of the Fq'/Fm' values had the Col-0 Fq'/Fm' of the day, and the experiment subtracted to create a ΔFq'/Fm'. These were plotted with day one on the x-axis and day five on the y-axis.

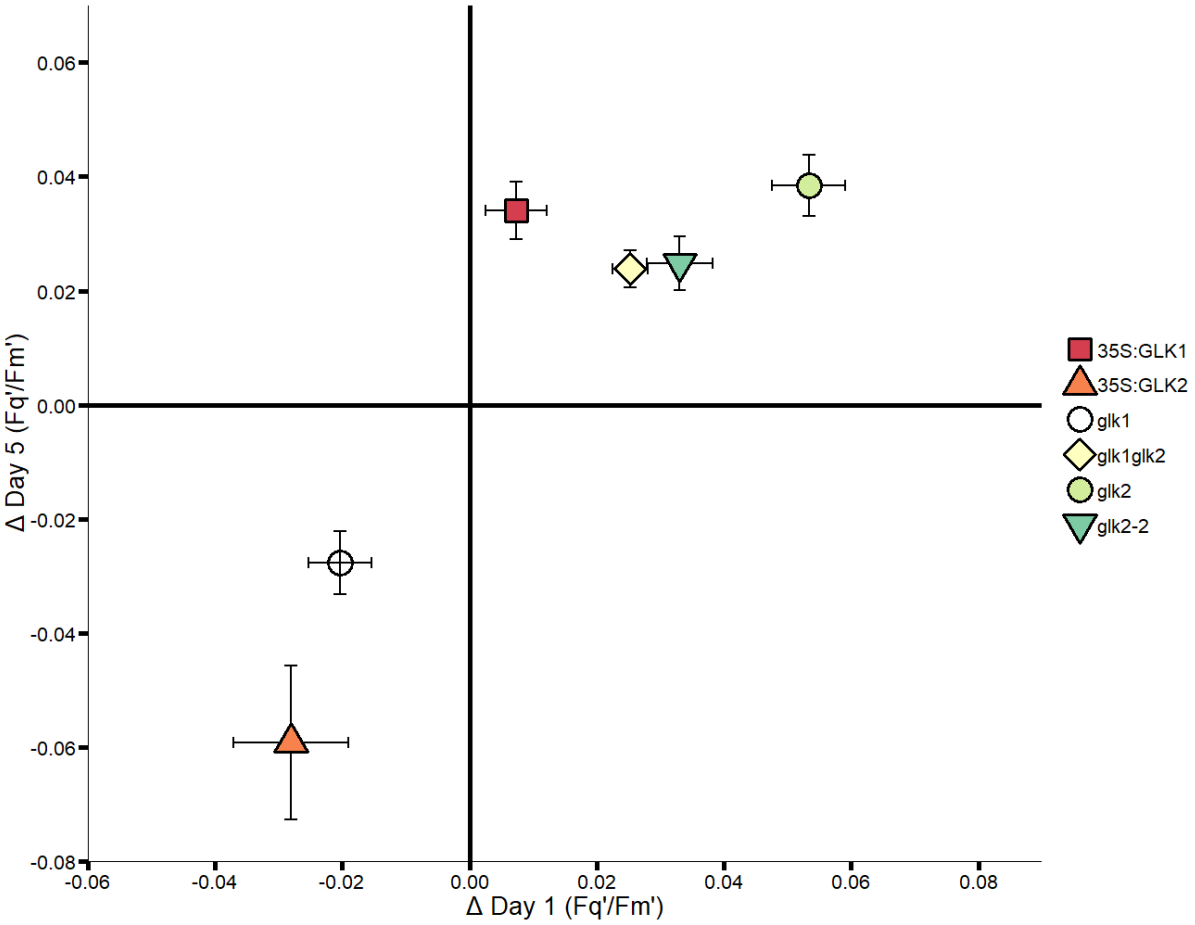

Figure 3.6.3: HL acclimation of 35S:GLK1, 35S:GLK2, *glk1*, *glk1glk2*, *glk2*, *glk2-2* and Col-0 plants. ΔFq'/Fm' is determined by chlorophyll fluorescence with a PPFD of 800 µmol m^{-2} s^{-1} minus the Col-0 (WT) value. Measurements were taken from 4-6 week old plants (n > 4) with a minimum of 6 mature leaves each (means ± SE).

Figure 3.6.3 [Page 111] uses delta values to eliminate the subtle experimental difference to look at each mutant without having to do so simultaneously. The mutants form a linear relationship between day one and day five. They also lie very close to the line Δday 1 = Δday 5 other than 35S:GLK1. 35S:GLK1 is not close to x = y due to its day one skew and lower change than its day five result.

3.6.2 The HL expression of GLK1 and GLK2

The expression *GLK1* and *GLK2* within Col-0, BBX32-10 and *hy5-2* plants may be interesting to look at to understand the linkage between *GLK1* and *GLK2* and HL acclimation. I used the HL *BBX32-HY5* HL RNA-seq and the HL time series; however, as *GLK2* was identified through the HL time-series, changes between HL and the control are expected. All the transcription factors selected as potentially part of the HL transcription factor network were altered in the HL time series.

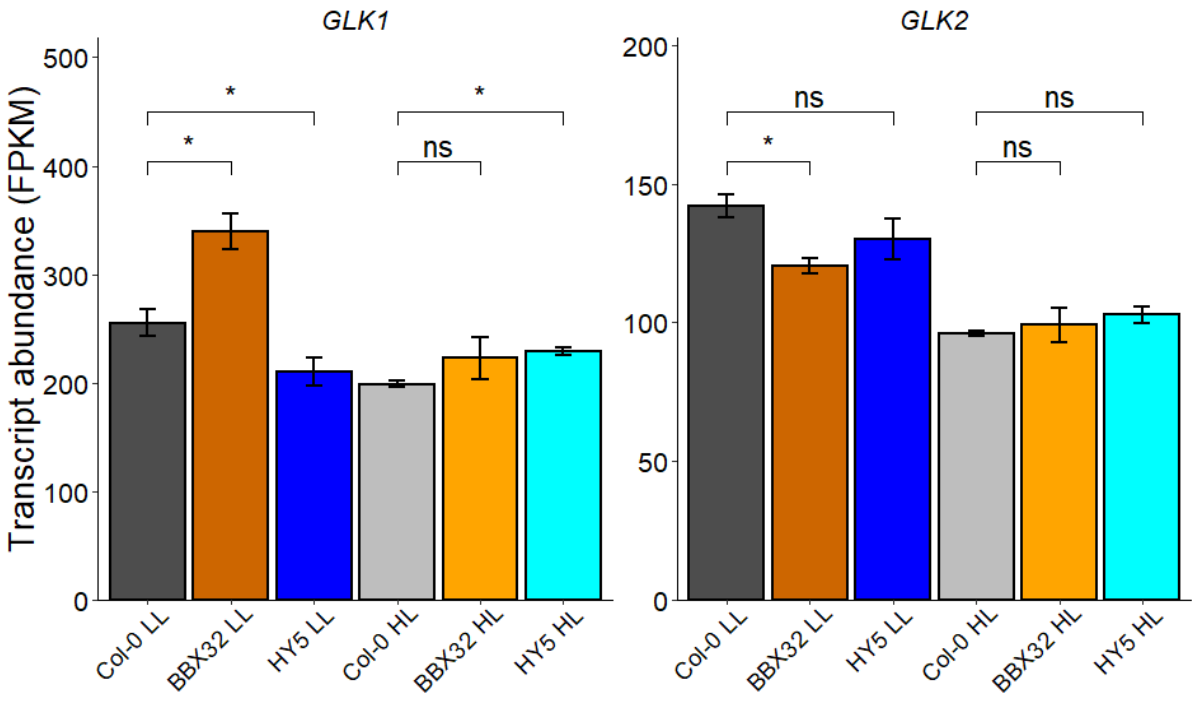

Figure 3.6.4: The expression of *GLK1 and GLK2* from the *BBX32-HY5* HL RNA-seq. Expression was obtained from BBX32-10 (BBX32), *hy5-2* (HY5) or Col-0 under LL or HL conditions for 3.5 hours of exposure. Asterisks and bars show genes significantly changed in expression between the LL and HL groups of each genotype ($p < 0.05$; ANOVA).

The GLKs showed minimal changes in transcript abundance between genotypes, decreasing all due to HL other than *hy5-2 GLK1,* which does not significantly change. This data exemplifies the stringent control *Arabidopsis* has over the expression of the *GLK* genes. I used the HL time-series microarray from Alvarez-Fernandez *et al*. (2021) to visualise the changes in expression of *GLK1* and *GLK2* caused by HL over time.

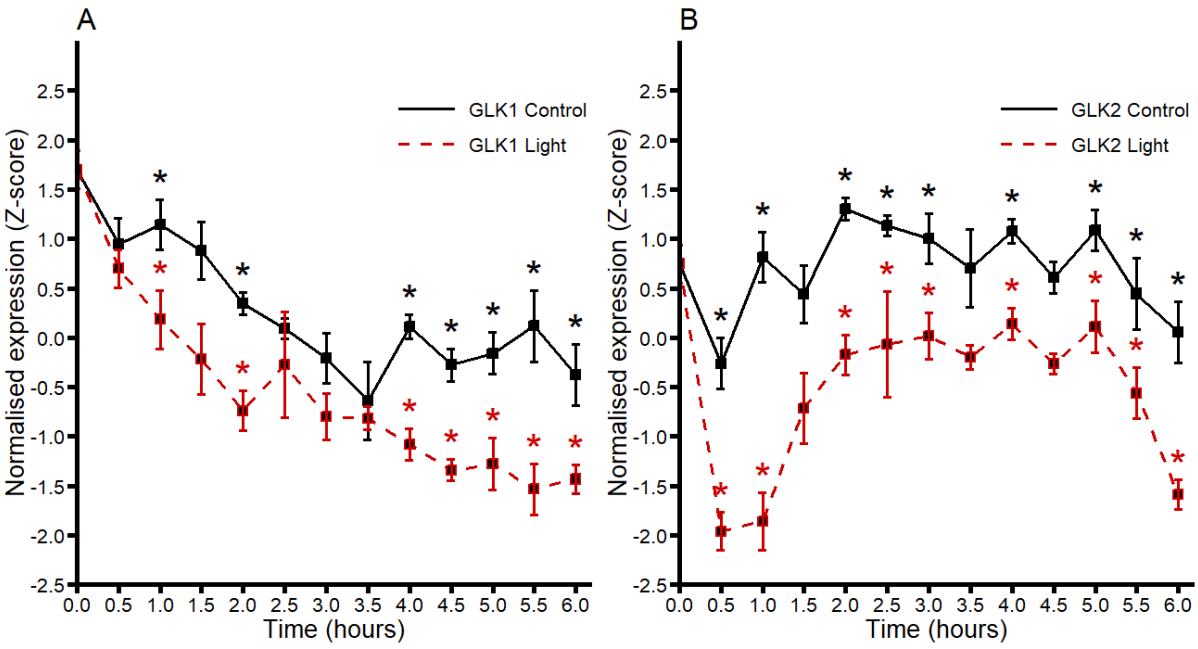

Figure 3.6.5: The expression *GLK1* (A) and *GLK2* (B) from the Alvarez-Fernandez *et al*. (2021) time-series acclimation microarray experiment. Asterisks and bars show time points significantly changed in expression between the control and light groups (n = 4; p < 0.05; ANOVA).

As seen in the RNA-seq, *GLK1* and *GLK2* within the microarray time series are decreased within the HL samples; however, there is a difference between the *GLK1* and *GLK2* expression profiles. *GLK2* drops significantly for the first hour of HL exposure, whereas *GLK1* exhibits a gradual decrease in expression (Figure 3.6.5

[Page 113]). This *GLK2* decrease would be entirely missed by the 3.5-hour time point of the RNA-seq. The early decrease most likely made *GLK2* a prime target for the VBSSM algorithm, which constructed the HL TF network (Alvarez-Fernandez *et al*., 2021).

3.6.3: Differentiating GLK1 and GLK2

GLK1 and *GLK2* have inverted HL acclimation phenotypes; however, the transcriptomic data does not explain how this is possible. Previous studies have analysed the promoter binding motifs of both GLK1 and GLK2 (Franco-Zorrilla *et al*., 2014; Zubo *et al*., 2018). Differences in promoter binding may identify different sets of genes regulated by GLK1 and GLK2.

Figure 3.6.6: Promoter binding motifs of GLK1 and GLK2. This image is modified from Franco-Zorrilla *et al*. (2014) and Zubo *et al*. (2018).

The promoter binding motifs of GLK1 and GLK2 are nearly identical (Figure 3.6.6 [Page 114]). Therefore, changes in promoter binding motif cannot be used to explain the differences in HL acclimation phenotype. It is unknown how the *GLK* genes interact with other HL acclimation genes, although some clues can be found in the literature. Analysing the *GLK* promoters for binding motifs of different transcription factors can help identify changes in expression seen in Figure 3.6.5 [Page 113]. For example, HY5 can bind to the promoter of only *GLK2* (Lee *et al*., 2007). However,

this interaction's importance is impossible to determine without further experimental analysis.

The amino acid sequences of the GLK*s* can also be studied to identify common domains and motifs. For example, many proteins use a VP motif to bind to the WD40 domain of COP1, including CRY1 and HY5 (Holm *et al*., 2002; Lau *et al*., 2019). A recent study identified the sequence for this motif to be far more plastic than initially thought (Lau *et al*., 2019). A VP motif exists of a core of valine and proline and a large anchor residue 2 to 3 amino acids upstream (Lau *et al*., 2019). In addition, some proteins, such as HY5, have a negatively charged residue (D or E) that can form a salt bridge with $COP1^{H528}$ *in vitro* (Osterlund *et al*., 2000; Lau *et al*., 2019).

GLK1 and GLK2 both have valine followed by proline in the centre of their amino acid sequence, and the small region surrounding this VP can be compared to other VP domains. Furthermore, the motifs of GLK1 and GLK2 are identical, which does not explain why the HL acclimation phenotypes are different. However, understanding how protein levels of GLK1 and GLK2 are controlled may be helpful.

Table 3.6.1: The VP motifs of GLK1 and GLK2 with comparable genes from Lau *et al*. (2019). The VP core is coloured in yellow, and the anchor residue is coloured in blue. In addition, data from proteins other than GLK1 and GLK2 has been gathered from Lau *et al*. (2019).

Protein	Start	-4	-3	-2	-1	0	1	2	3
HY5	39	E	I	R	R	V	P	E	F
BBX1 (CO)	366	G	Y	G	I	V	P	S	F
BBX4 (COL3)	287	G	F	G	V	V	P	S	F
CRY1	544	E	D	Q	M	V	P	S	I
GLK1	175	V	D	K	A	V	P	S	R
GLK2	169	V	D	K	A	V	P	S	R

This motif of GLK1 and GLK2 contains a lysine residue as their anchor residue. Lysine is positively charged like the arginine residue used by HY5 (Table 3.6.1 [Page 115]). By the primary structure, GLK1 and GLK2 appear to contain VP motifs though Hall *et al*. (1998) predicted this to be a TEA-like domain with the VP motif not aligning with the human and mouse *TEA* genes. This motif is highly conserved in plants; the *Zea mays ZmGLK1* and *GOLDEN2* (*ZmG2*) from which the gene family derives its name contains IDKAVPSR instead of VDKAVPSR found in *Arabidopsis* (Hall *et al*., 1998; Rossini *et al*., 2001): Valine (V) and isoleucine (I) are very similar hydrophobic amino acids. *Oryza sativa* (rice) *OsGLK1* and *OsGLk2* contained motifs identical to the *Zea mays* genes. Many of the clade I *GLK* genes in *Nicotiana tabacum L.* also contained motifs identical to *ZmG2* and *ZmGLK1* or *GLK1* and *GLK2* (Rossini *et al*., 2001; Qin *et al*., 2021).

Understanding the domains of GLK1 and GLK2 may help better determine the role of this potential VP motif. Alphafold is a system that predicts 3D structures of proteins by analysing their amino acid sequence (Jumper *et al*., 2021). GLK1 and GLK2 can

be extracted from the Alphafold database, and their structures can be analysed for potential domains.

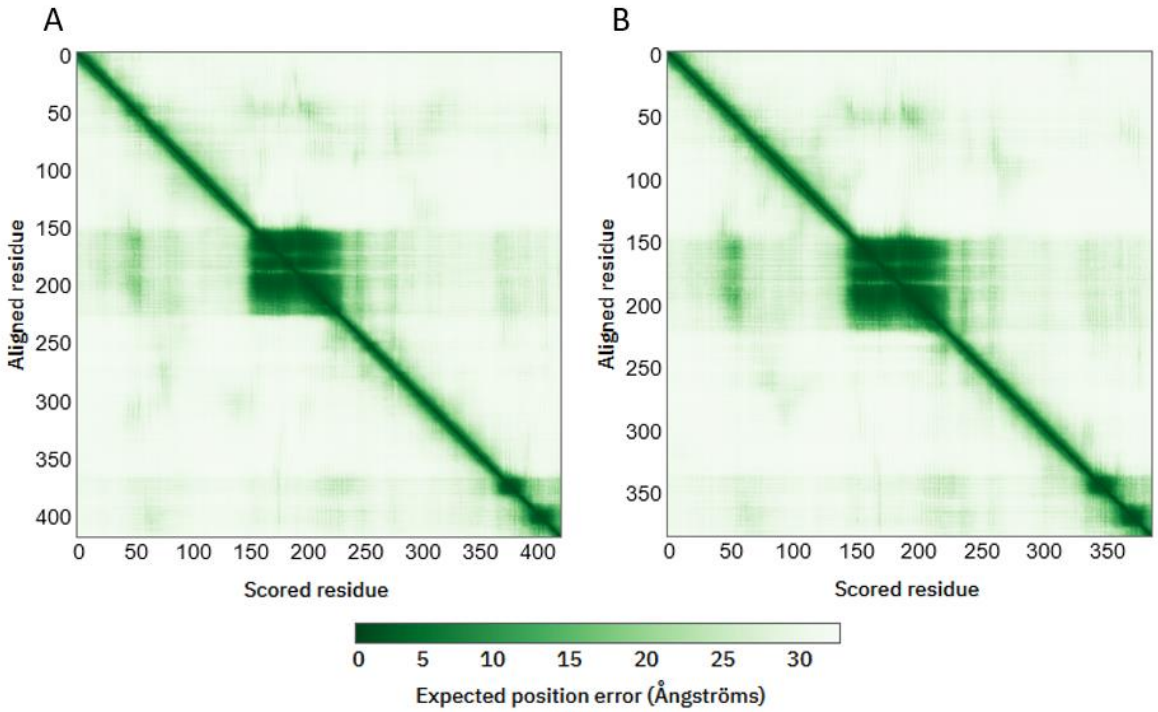

Figure 3.6.7: The expected position matrices (Å) of the residues of GLK1 (A) and GLK2 (B). Darker green colours indicate a lower expected position error between those residues.

GLK1 and GLK2 have a domain in the centre of their protein sequences, spanning the VP motif region. This VP motif is a region determined by alphafold (Jumper *et al*., 2021) to likely be a domain (dark green middle square; Figure 3.6.7 [Page 117]) due to the low expected position error between the residues indicating a region with a strong conformation. A low sequence error spans approximately 87 and 88 amino acids for GLK1 and GLK2, respectively (Figure 3.6.7 [Page 117]). GLK1 and GLK2 may have regulatory domains that interact with COP1. However, as GLK1 and GLK2 have identical VP motifs, this cannot be used to distinguish between them and their very different HL acclimation phenotypes.

3.6.4 Conclusion

Further studies are required to determine the difference between the photosynthetic regulation of *GLK1* and *GLK2*. The difference between the functionality of *Arabidopsis GLK1* and *GLK2* has not been seen before in the literature (Fitter *et al*., 2002; Waters *et al*., 2009; Wang *et al*., 2017), and therefore there are no considerable changes between the role of *GLK1* and *GLK2* outside of photosynthetic capacity. Future studies could play these genes against each other to fine-tune photosynthetic capacity similarly to the *ZmG2* and Zm*GLK1* genes of *Zea mays* which, through complementary compartmentalisation, specialise mesophyll and bundle sheath cells to optimise C4 photosynthesis (Hall *et al*., 1998; Rossini *et al*., 2001; analysed further in section 7.3.2 [Page 282]).

Continuing the analysis of the interaction between *GLK1* and *GLK2* may involve using RNA-seq like the ones performed by Alvarez-Fernandez *et al*. (2021). This experiment may yield further HL acclimation targets for analysis. The potential interaction between COP1 and GLK1 or GLK2 could be experimentally tested using co-immunoprecipitation or yeast 2-hybrid. The photosynthetic capacity of the *GLK* mutants could be measured directly along with other parameters such as yield (Athanasiou *et al*., 2010). These experiments would be necessary to prove if *GLK1* and *GLK2* are viable targets for increasing the photosynthetic capacity and yield of crop plants.

3.7: Discussion

Different environments provide different intensities of light that a plant can evolve towards to thrive better. For example, a plant reaching the top of a canopy will receive far higher light intensities than ones on a forest floor. However, new high light conditions can arise through many natural circumstances. Therefore, this increased light intensity provides a simultaneous and unavoidable risk and reward for a plant.

Crop plants have their environment manipulated by humans to increase their yields. These plants do not need an opportunity: humans maintain them in a constantly favourable environment. The light environment crop plants are exposed to is typically far more favourable, providing a target for genetic manipulation. Future studies could manipulate HL acclimation genes to suit crop plants better. Mutants of the HL acclimation genes *BBX32* and *GPT2* are already known to have altered yields (Preuss *et al*., 2012; Chapter 6 [Page 197]; Athanasiou *et al*., 2010). The HL TF network is a promising set of target genes to manipulate HL acclimation and photosynthetic capacity (Alvarez-Fernandez *et al*., 2021).

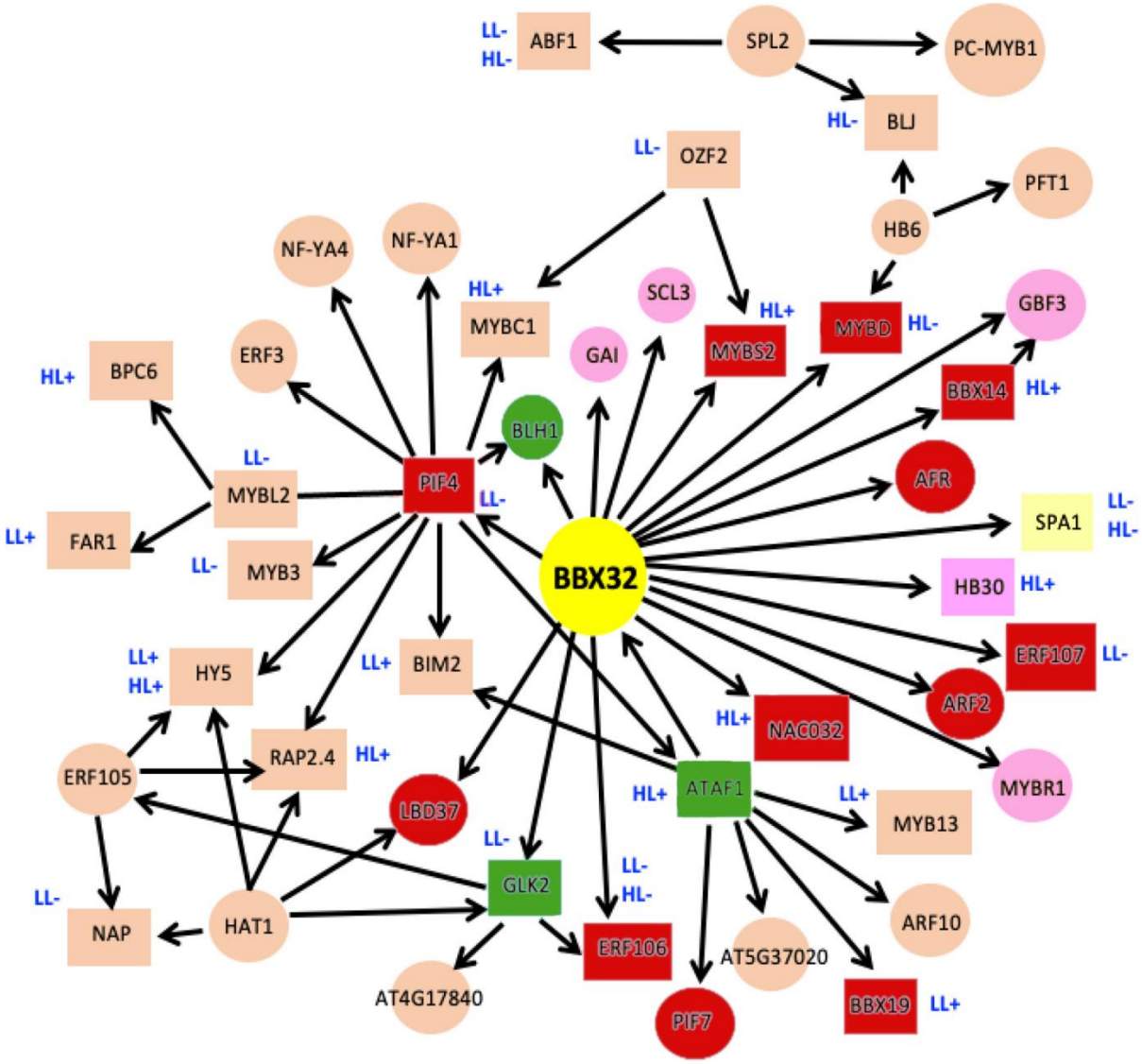

2318

2319 **Figure 3.7.1: HL transcription factor network from Alvarez-Fernandez *et al*.**

2320 **(2021).** Red indicates tested genes that did not show a perturbed acclimation

2321 phenotype. Green genes altered photosynthetic regulation or acclimation. Pink

2322 genes were unable to be studied. *SPA1* and *BBX32* (shown in yellow) are the only

2323 two genes in the network that do not encode transcription factors.

2324

2325 This chapter has shown that the HL TF network contains suitable candidate genes

2326 for further testing. HL acclimation genes like *GLK1* and *GLK2* are transcription

2327 factors that directly control the expression of PhANGs and are the first HL

2328 acclimation genes known to bind to the promoters of PhANGs (Waters *et al*., 2009).

Further experiments are required to identify how other HL acclimation genes interact with the GLKs. The *BBX32-HY5* HL RNA-seq did not identify any causal expression changes in *GLK1* or *GLK2* (Figure 3.6.4 [Page 112]). Therefore, short-term changes of expression may not be significant, and further study needs to be focused on the changes in protein levels and posttranslational modification of the GLK proteins.

Many of the genes within the HL TF network and HL acclimation genes have connections to photomorphogenesis (Holtan *et al*., 2011; Alvarez-Fernandez *et al*., 2021). Photoreceptors in *Arabidopsis* such as *CRY1* were discovered due to mutations causing elongated hypocotyls under blue light conditions (Wu and Spalding, 2007). Researchers named *COP1* for its constitutively photomorphogenic phenotype in the dark (Deng *et al*., 1991). These parallels also exist in the flowering time phenotype of *cry1* and *cop1* plants (McNellis *et al*., 1994; Bagnall *et al*., 1996). *BBX32* over-expressors have a later flowering time and longer hypocotyls than WT controls (Tripathi *et al*., 2017; Holtan *et al*., 2011). I drew these connections to compare different HL acclimation, flowering time and photomorphogenic phenotypes of HL acclimation mutants (Table 3.7.1 [Page 121]).

Table 3.7.1: The HL acclimation phenotype (Alvarez-Fernandez *et al*., 2021), photomorphogenic phenotype, flowering times and different HL acclimation mutants. (+) denotes a pre-acclimated phenotype, longer hypocotyls and later flowering, respectively, with the number of (+) being representative of the strength of the phenotype. (-) is used similarly to denote reduced HL acclimation ability, shorter hypocotyls, or an earlier flowering time. (*) indicates HL acclimation experiments performed either within this study or by Alvarez-Fernandez *et al*. (2021).

Mutant	HL acclimation phenotype*	Photomorphogenic phenotype	FT / Leaf No at FT phenotype (SD/LD)	Photomorphogenesis reference	Flowering time reference
cop1-4	+ + +	- - -	- / ~	Stacey *et al.* (2000)	McNellis *et al.* (1994)
cry1	- -	+ +	+ (12/12)	Wu and Spalding (2007)	Bagnall *et al.* (1996)
BBX32-OX	- - -	+ +	+ / +	Holtan *et al.* (2011)	Tripathi *et al.* (2017)
hy5-2	- - -	+++		Zhang *et al.* (2017)	
glk1	-	+		Martin *et al.* (2016)	
glk2	++				
glk1glk2	+		~ / -		Zubo *et al.* (2018)
35S:GLK1	+	-	+ / +	Martin *et al.* (2016)	Waters *et al.* (2008)
35S:GLK2	-		+ / +		Waters *et al.* (2008); *Zubo et al.* (2018)

Photomorphogenic, flowering time and HL acclimation phenotypes are aligned where an early flowering time and short hypocotyl are proportional to the severity of the pre-acclimated phenotype or *vice versa*. Furthermore, the over-expression of the *GLKs* increases flowering time in short- and long-day conditions (Waters *et al*., 2009). This data is evidence that flowering time and HL acclimation deviate before the *GLKs* or that post-translational modification systems are overwhelmed by over-expressed or ectopically expressed *GLK* transcript causing a change in the function of the proteins.

Leaf senescence phenotype is also related to HL acclimation, photomorphogenesis and flowering time. Overexpression of *AtBBX32* within *Glycine max* caused leaves to senesce earlier and pods to brown quicker (Preuss *et al*., 2012). GLK1 and GLK2 form a complex with the leaf senescence gene ORESERA1 (ORE1) and antagonistically regulate leaf senescence, driving *ATAF1* and *ORE1* while promoting chloroplast maintenance (Rauf *et al*., 2013; Garapati *et al*., 2015). Leaf senescence is not as simple to study as photomorphogenesis and flowering time; however, the phenotype is more complex than hypocotyls or time to bolt. Typically, leaf senescence is analysed by removing the rosette leaves and placing them in the

dark. Such experiments involve visual comparisons of the leaves over time and measurements of chlorophyll content (Song *et al*., 2014; Garapati *et al*., 2015). The other phenotypes described here can be explored non-destructively, making them more straightforward and widely studied.

The process of understanding HL acclimation can be started at the top, photoreceptors, and working down the signalling cascade to find genes such as the PhANGs and *FLOWERING LOCUS T* that have far more concise roles. Manipulating genes like the photoreceptors and *COP1* complexes often cause changes that are too systemically widespread to be helpful in crops. However, over-expressing particular genes such as the PhANG *LHCB1.1* cannot induce a significant enough change, or due to the importance of the gene, the plant attempts to compensate for its over-expression (Liu X *et al*., 2017). Studying transcription factors is very important as they have the potential to manipulate every gene in their regulatory network, which often includes other transcription factor genes. Plants pass signals through several transcription factors in a hierarchical fashion (Albihlal *et al*., 2018). However, these ‘lower’ transcription factor genes are elusive precisely because of how little of an effect they have, functional overlap with other genes or have very particular timings and triggers for expression. We can develop networks like the HL TF network to discover more genes in the signalling pathway and potentially identify points of functional divergence (Alvarez-Fernandez *et al*., 2021).

3.8: Conclusions of Chapter 3

- The transcriptomes of *hy5-2* and BBX32-10, which both had perturbed HL acclimation phenotypes, were found to be similar using RNA-seq.
- The HL acclimation phenotype of HL TF network genes were tested using related *Arabidopsis* plant lines and very few were found to be dismilar to the WT.
- *GLK1* and *GLK2*, which were previously described as functionally redundant, had distinct HL acclimation mutant phenotypes.

Chapter 4: The involvement of COP1/SPA complexes and red light signalling in HL acclimation

4.1: Introduction

Plants need to monitor their light environment to respond to HL. Photoreceptors (see section 1.4 [Page 26]) are activated by specific wavelengths of light and initiate signalling in response to the light environment (Lau and Deng, 2012). Many photoreceptors interact with CONSTITUTIVELY PHOTOMORPHOGENIC1 (COP1) to transduce light signals (Holtkotte *et al*., 2017; Paik *et al*., 2019; Lau and Deng, 2012; Wang and Lin, 2019; Ponnu and Hoecker, 2021). COP1, a central protein of the COP/DET/FUS complexes, targets specific proteins for degradation by ubiquitination and the 26S proteasome (Lau and Deng, 2012; Ponnu and Hoecker, 2021). Transcription factors are often targets of COP1 E3 ligase complexes such as the HL acclimation protein HY5 (Ang *et al*., 1998; Ponnu and Hoecker, 2021). *cop1-4* plants contain a single nucleotide polymorphism within the *COP1* gene causing a nonsense mutation leading to a partial *COP1* transcript (McNellis *et al*., 1994). *cop1-4* plants have a strong HL acclimation phenotype; *cop1-4* has a greater Fq'/Fm' on day 5 than the WT (Alvarez-Fernandez *et al*., 2021; Figure 4.1.1 [Page 126]). *cop1-4* also has a pre-acclimated phenotype as it has a greater Fq'/Fm' than the WT on day 1.

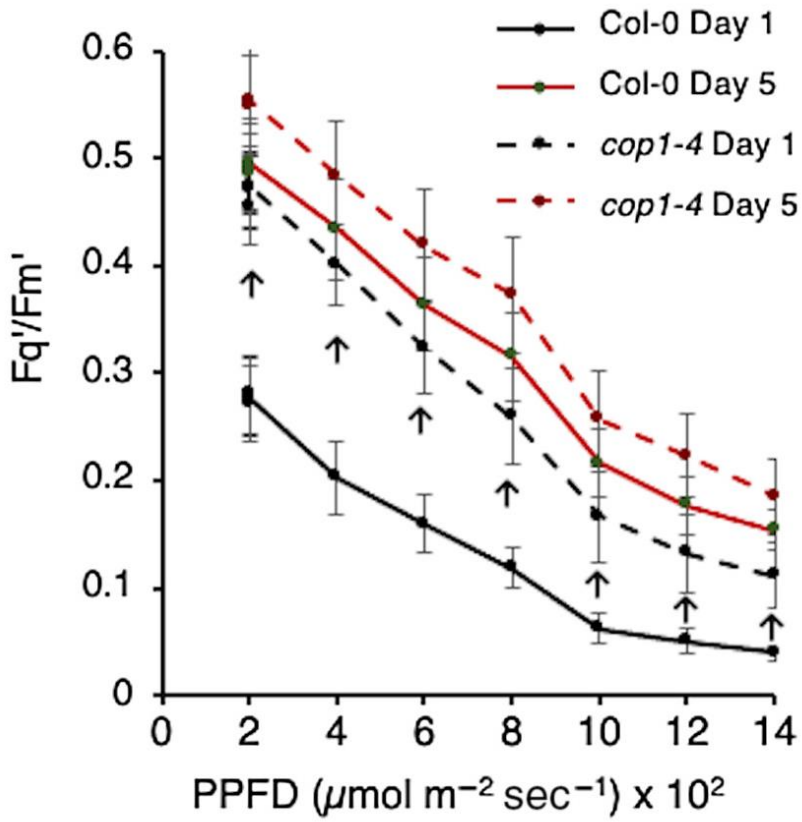

Figure 4.1.1: HL acclimation of *cop1-4* and Col-0 plants. Fq'/Fm' is determined by chlorophyll fluorescence with a PPFD range of 200 µmol m^{-2} s^{-1} to 1400 µmol m^{-2} s^{-1} at 200 µmol m^{-2} s^{-1} increments. Measurements were taken from 4-6 week old plants with a minimum of 6 mature leaves each (means ± SE). Arrows and asterisks denote a significant difference between the day 1 and day 5 values respectively of the mutants and Col-0 (ANOVA, Tukey post-hoc; */↑ = $p < 0.05$; **/↑↑ = $p < 0.005$). Modified from Alvarez-Fernandez *et al*. (2021).

The HL acclimation pathway appears similar to the photomorphogenic pathway as they contain the same proteins (CRY1, COP1 and HY5) when compared to flowering and circadian rhythm (Lau and Deng, 2012; Alvarez-Fernandez *et al*., 2021; see Chapter 3 [Page 63]). All of these processes are mediated by COP1 however the targets of COP1 specify the response. *HY5* is classically known for its role in

mediating photomorphogenesis however *HY5* also regulates HL acclimation (Ang *et al*., 1998; Alvarez-Fernandez *et al*., 2021).

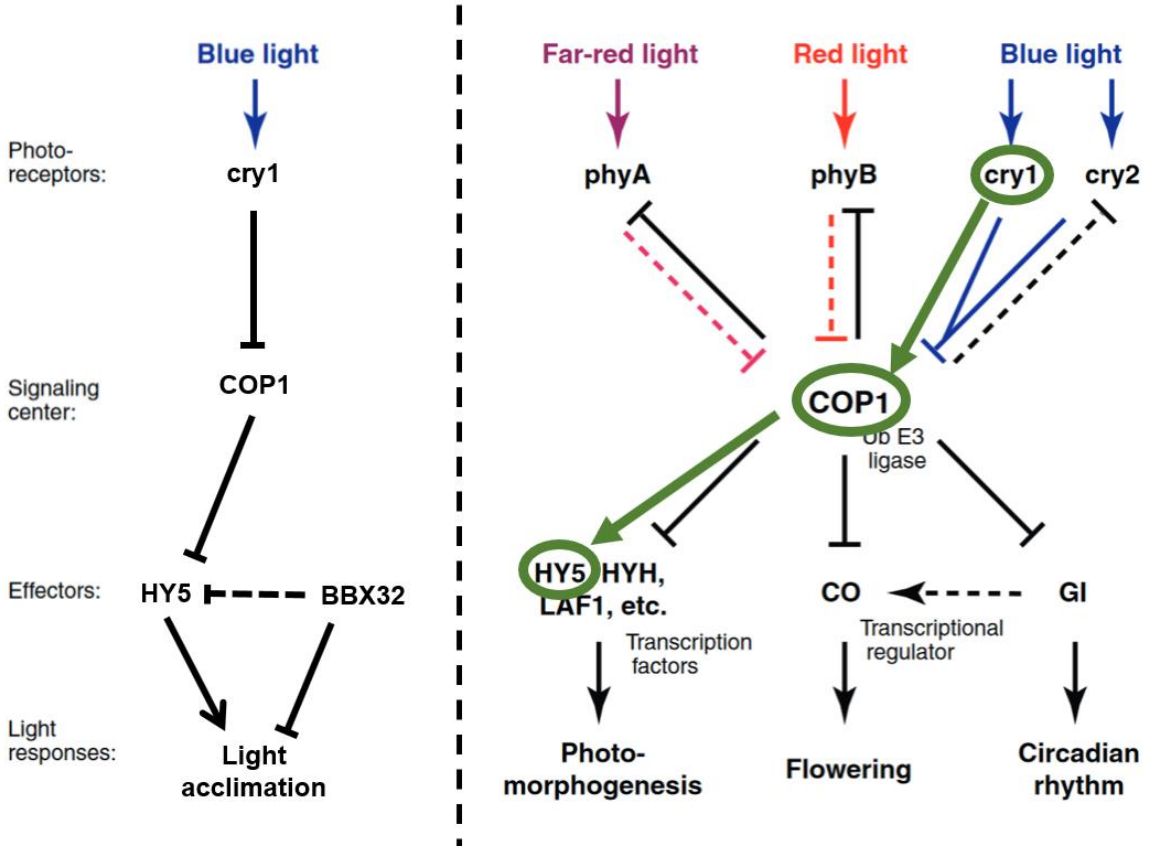

Figure 4.1.2: The current known pathway of HL acclimation with relation to the photomorphogenesis, flowering and circadian pathways. The left panel shows the predicted HL acclimation pathway from HL acclimation genes and their known interactions (Alvarez-Fernandez *et al*., 2021). Green arrows and circles overlay the HL acclimation genes discovered by Alvarez-Fernandez *et al*. (2021). Modified from Lau and Deng (2012).

One of the known COP/DET/FUS complexes, the COP10/DET1/DDB1 (CDD) complex, was found to not be involved in HL acclimation (Lau and Deng, 2012; Alvarez-Fernandez *et al*., 2021). The *det1-1* mutant did not have a HL acclimation

phenotype but does have a constitutively photomorphogenic (cop) phenotype similar to *cop1-4* (Alvarez-Fernandez *et al*., 2021). This unlinked the photomorphogenic regulation shown in Figure 4.1.2 [Page 127] from the HL acclimation phenotype (Chory *et al*., 1989). COP1 can form other COP/DET/FUS complexes, and these can be investigated to further understand the role of COP1 in HL acclimation (Lau and Deng, 2012).

SUPPRESSOR OF PHYA-105 1 (*SPA1*), was identified as a member of the HL TF network, a computer-generated network of genes that rapidly respond to HL, by Alvarez-Fernandez *et al*. (2021; Section 3.5 [Page 91]). This is despite *SPA1* not being a transcription factor or primarily known within the literature as a transcription co-factor (Hoecker *et al*., 1998). Its primary protein sequence, containing a WD40 motif like COP1, drove the initial exploration of SPA1 (Hoecker *et al*., 1998). However, SPA1 is involved in the interaction between COP1 and blue and red light photoreceptors (Holtkotte *et al*., 2017; Paik *et al*., 2019). The blue light photoreceptor *CRYPTOCHROME1* (*CRY1*) was identified as a positive regulator of HL acclimation (Alvarez-Fernandez *et al*., 2021). SPA1 can form a COP/DET/FUS complex with COP1 to transduce blue light signalling from CRY1 (Lau and Deng, 2012; Holtkotte *et al*., 2017). However, *SPA1* is part of a 4 gene family which the encoded proteins that can all interact with COP1 to form different COP1/SPA complexes (a type of COP/DET/FUS complex; Laubinger and Hoeker, 2003; Ponnu and Hoecker, 2021; Lau and Deng, 2012). Therefore, COP1/SPA complexes may have a role in HL acclimation. This hypothesis can be tested by analysing the HL acclimation phenotype of different *SPA* mutants.

COP/DET/FUS complexes do not only transduce blue light signals such as those from CRY1. Red light signalling is also transduced through COP/DET/FUS complexes (Paik *et al*., 2019). Alvarez-Fernandez *et al.* (2021) analysed a mutant of *PHYTOCHROME B* (*phyB*; Wester *et al*., 1994), a prominent red-light photoreceptor, but discovered it did not have a strong HL acclimation phenotype. However, this phenotype was theorised to be a consequence of the artificial light conditions involving far more blue light and therefore favouring a response from blue light photoreceptors such as CRY1 (Alvarez-Fernandez *et al*., 2021). A dominant gain-of-function allele of *phyB* was discovered to initiate a strong red-light response independent of light with a cop phenotype (Su and Lagarias, 2007). This mutant may be used to analyse the impact of red light on HL acclimation in the absence of strong red-light conditions.

This chapter aims to investigate the HL acclimation pathway prior to HL TF network, BBX32 and HY5 (see Chapter 3 [Page 63]). The HL acclimation and photomorphogenic pathways have been previously identified as overlapping (Alvarez-Fernandez *et al*., 2021). This can be used to expand the HL acclimation pathway by studying known photomorphogenic mutants whilst also identifying further differences between the pathways.

4.2: Methods

4.2.1: YHB microarray data set

The YHB is a dominant gain-of-function allele of PHYB, the red light photoreceptor. A YHB transgenic plant line was generated and a microarray data set created using

4-day-old plants grown in the dark (Su and Lagarias, 2007; Hu *et al*., 2009). This was downloaded from the supplementary data of Hu *et al*. (2009). The expression of target genes were extracted by searching the data set. By sorting the log_2 fold change in expression, sets of genes were extracted for GO analysis (section 2.4.5 [Page 52]).

4.2.2: Gas exchange on *spa123* and Col-0 plants

Gas exchange was performed on *spa123* and Col-0 plants following the methodology developed in section 2.2.6 [Page 40]. 8-week-old plants were used for the gas exchange experiments, as otherwise the *spa123* leaves would have been too small for the LiCor clamps. This was due to the rosette size and leaf size of the *spa123* plants being smaller than Col-0 (Figure 4.4.1 [Page 142]). Plants were grown in 5 cm pots as opposed to 6–well A5 propagation trays. This allows the plants to be separately positioned for use with the LiCor clamps.

4.2.3: RT-qPCR of *spa123*

spa123 and Col-0 plants (n > 3) were grown for 6 weeks under standard growth conditions (section 2.2.1 [Page 35]). HL exposure was conducted in a similar fashion to the Alvarez-Fernandez *et al*. (2021) RNA-seq methodology. Plants either were kept under standard growth conditions or exposed to a PPFD of 1000 µmol m^{-2} s^{-1} ± 100 µmol m^{-2} s^{-1} (HL; section 2.2.2 [Page 35]) for 3.5 hours. All plants had leaves taken for RNA extraction (section 2.3.2 [Page 43]), cDNA was synthesised (section 2.3.5 [Page 44]) and RT-qPCR was performed (section 2.3.6 [Page 45]) using primers designed to target specific cDNA sequences (section 2.3.4 [Page 44]). RT-

qPCR data was processed into gene expression relative to *PP2aA3* and manipulated using the $2^{--\Delta\Delta CT}$ methodology (section 2.3.6 [Page 45]; Livak and Schmittgen, 2001).

4.3: The impact of constitutive red light signalling on HL acclimation

The defective mutant of *PHYB*, a red light photoreceptor, does not have a perturbed HL acclimation phenotype (Alvarez-Fernandez *et al*., 2021). It is possible to mimic light signals using forms of photoreceptors that are constitutively active (Su and Lagarias, 2007). Y276 to H mutation of phyB (hereto known as YHB) is a constitutively active form of phyB that in darkness grows as though exposed to light, a cop phenotype (Hu *et al*., 2009). The constitutively active phyB displays changed steady state regulation of transcription and transcription factors to alter the cellular environment. This mutant can be considered to have a constitutively active form of phyB as opposed to the 'negative' defective phyB in *phyB-9* for HL acclimation experiments.

4.3.1: HL acclimation phenotype of constitutive *phyB*

The *phyB-9* mutant may not have exhibited a HL acclimation phenotype (Alvarez-Fernandez *et al*., 2021) due to functional redundancy also seen within other putative HL acclimation genes (as discussed in section 3.7 [Page 119]). Other phytochromes (phyC, phyD, phyE) are able to compensate for the lack of phyB (Li *et al*., 2011; Franklin *et al*., 2003; Whippo and Hangarter, 2004; Arana *et al*., 2014). Functional redundancy could have masked the HL acclimation role of phyB in the *phyB-9* mutant (Alvarez-Fernandez *et al*., 2021). YHB mimics the effects of red light exposure and therefore cannot be simply compensated for by functionally redundant

gene expression (Su and Lagarias, 2007; Hu *et al*., 2009). I performed a HL acclimation experiment on YHB plants to assess ability to enhance photosynthetic capacity in response to HL.

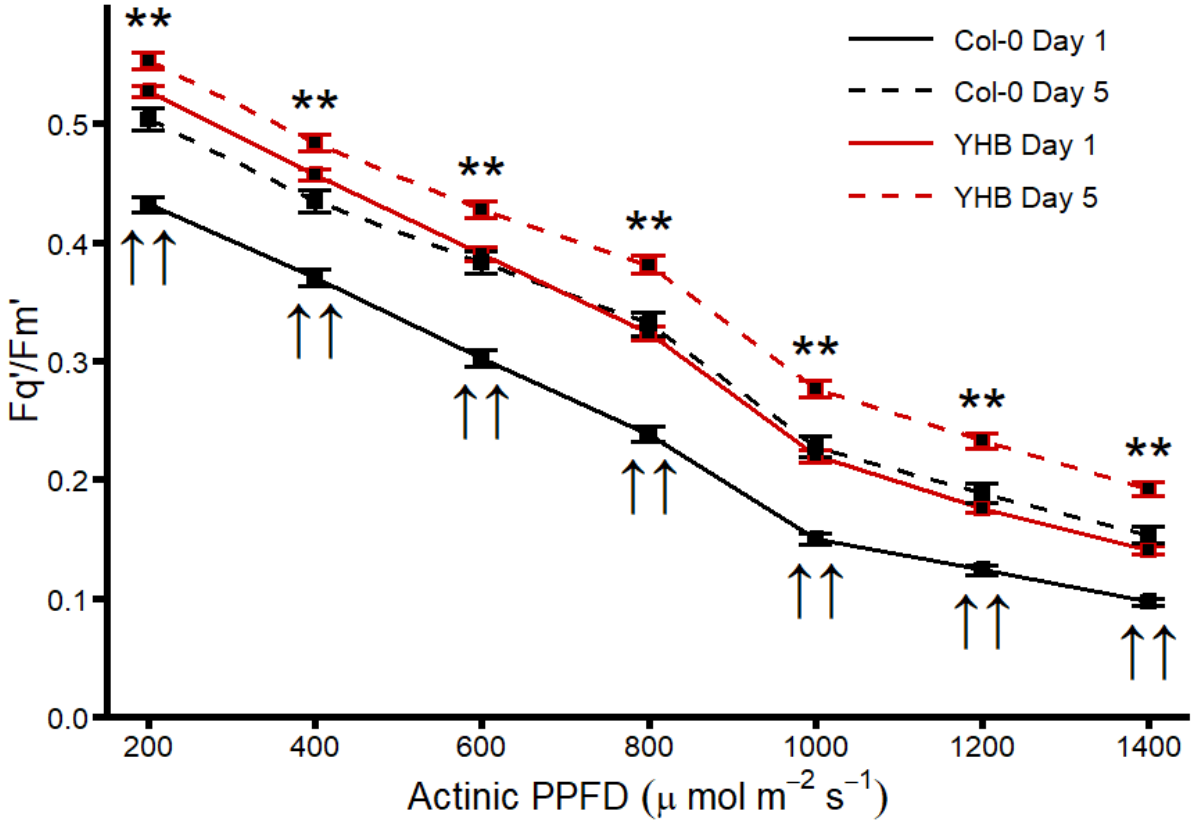

Figure 4.3.1: HL acclimation of YHB and Col-0 plants. Fq'/Fm' is determined by chlorophyll fluorescence with a light intensity range of 200 µmol m^{-2} s^{-1} to 1400 µmol m^{-2} s^{-1} at 200 µmol m^{-2} s^{-1} increments. Measurements were taken from 4-6 week old plants (n > 4) with a minimum of 6 mature leaves each (means ± SE). Arrows and asterisks denote a significant difference between the day 1 and day 5 values respectively of the mutants and Col-0 (ANOVA, post-hoc GH; */↑ = $p < 0.05$; **/↑↑ = $p < 0.005$).

After only a single day (4 hours) of HL exposure, the YHB mutant had a greater Fq'/Fm' at all measured PPFDs than Col-0. This is considered an accelerated acclimation phenotype (Alvarez-Fernandez *et al*., 2021). YHB has a similar HL acclimation phenotype to *cop1-4* (Alvarez-Fernandez *et al*., 2021). phyB, like CRY1, is involved in the direction of HL acclimation.

The mimicked red light signalling caused a new transcriptional steady state that enhanced PSII operational efficiency (Figure 4.3.1 [Page 132]). The PSII operational efficiency was also enhanced on day 5 however similarly to *cop1-4* this effect was lessened in comparison to the WT (Col-0; Alvarez-Fernandez *et al*., 2021). This may belie a rate limiting effect change away from light or an inherent limited photosynthetic property of *Arabidopsis* that may be reached or near-reached as to reduce the potential increase in Fq'/Fm' in response to HL.

Plants lacking *CRY1* have a strongly decreased Fq'/Fm' and a depressed HL acclimation phenotype however plants lacking *phyB* do not display a HL acclimation phenotype (Alvarez-Fernandez *et al*., 2021; Figure 4.3.1 [Page 132]). It may be through this interaction with CRY1 that YHB influences the HL acclimation phenotype. GO analysis can be performed on an RNA-seq data set of the YHB mutant to understand transcriptional changes that may bring about HL acclimation perturbation.

4.3.2: GO analysis of YHB

The transcriptome of YHB has been analysed however I used 4-day-old dark grown seedlings (Hu *et al*., 2009). This poses an issue for the interpretation of the results when applied to HL acclimation, a phenomenon studied primarily in mature plants (Athanasiou *et al*., 2010; Miller *et al*., 2017; Alvarez-Fernandez *et al*., 2021). YHB plants have de-etiolated at 4 days old in the dark, however by comparison the WT have not, which may imply further transcriptional changes (Su and Lagarias, 2007). However, these plants are exposed to the same conditions and the alterations in transcript abundance may indicate the steady state changes required of a pre-acclimated HL acclimation phenotype i.e., behave as if HL acclimated but having never been exposed to HL. Initially this hypothesis was tested through the analysis of specific genes linked with HL acclimation (Alvarez-Fernandez *et al*., 2021; Chapter 3 [Page 63]).

Table 4.3.1: The expression and significance of HL acclimation related genes from YHB seedling microarray and *BBX32-HY5* HL RNA-seq. These genes and the accompanying RNAseq data were taken from Chapter 3 (Figure 3.3.2 [Page 71]; Figure 3.4.6 [Page 89]; Table S4 [Page 337]). Red indicates a gene significantly decreased in expression and green indicates a gene significantly increased in expression. l2f, Log_2(Fold change); padj, adjusted p-value using BH correction.

Name	Gene locus	YHB/WT (l2f)	padj (YHB/WT)	Col-0 HL / LL (l2f)	padj (HL/LL)	BBX32/Col-0 (l2f)	padj (BBX32/Col)	HY5/Col-0 (l2f)	padj (HY5/Col)
BBX32	AT3G21150			2.192645131	0	8.122874	0	0.588719	0.08946
HY5	AT5G11260			1.533604255	1.85E-24	2.442638	0	-3.23541	0
PSBS	AT1G44575			0.841264355	3.28E-11	0.967608	0	0.191267	0.598486
ELIP1	AT3G22840	2.707753499	0.001648901	2.70E+00	0	2.586683	0	-0.62049	0.111475
ELIP2	AT4G14690			1.726203639	0.014565518	3.422162	0.0000000439	-0.38678	0.876146
GPT2	AT1G61800	2.102910829	6.36403E-05	3.101669616	1.96E-185	-0.06262	0.920729	0.741851	0.004197
LHCB4.3	AT2G40100			2.061982893	0	-2.37217	0	0.407431	0.128982
GLK1	AT2G20570			-0.348342115	0.000207168	0.549226	3.43E-05	-0.16128	0.670222
GLK2	AT5G44190	-2.26779883	1.48371E-07	-0.562793212	1.15E-07	-0.11491	0.407349	-0.01373	0.983364
GNC	AT5G56860			0.640354217	0	1.365924	4.11E-39	0.334611	0.029794
CGA1	AT4G26150	-4.736079762	2.21853E-10	2.945623015	0	2.056727	0	1.032083	0.0000000587
GAI	AT1G14920	1.174918085	1.92443E-06	-0.684380228	6.24E-04	-0.03873	0.80095	0.107902	0.834876
RGA	AT2G01570			0.035259922	0.807612277	0.010029	0.952491	0.300933	0.16271
RGL1	AT1G66350	2.548962225	3.77302E-07	0.119231576	0.575122133	0.512695	0.001212	0.623754	0.005434
RGL2	AT3G03450			1.088380087	8.09E-11	0.536081	0.000897	0.485787	0.017743
RGL3	AT5G17490	1.160813649	0.001735355	0.048230104	9.66E-01	0.975158	0.256484	0.000714	0.999885
FT	AT1G65480			0.32192727	NA	0.998627	NA	0.302019	NA
FLC	AT5G10140	-1.527683436	0.007944738	-0.075947724	0.949596504	2.68475	0.00000012	1.588334	0.030914
SOC1	AT2G45660			-0.713850643	0.000000593	-1.63162	0	-0.09725	0.869602
AGL24	AT4G24540			1.146580837	0	0.876159	0.00000000488	0.52406	0.03675
CO	AT5G15840			9.15E-07	0.9999996	1.294603	0.230295	0.323322	NA
COL3	AT2G24790			6.54E-02	0.574748149	0.19526	0.096762	-0.00693	0.990096
BBX18	AT2G21320	-2.229595984	7.42307E-07	1.167267672	2.46E-21	0.614886	2.40E-06	0.420577	0.038335
BBX19	AT4G38960	-1.666774632	1.57867E-07	0.013186463	0.959684571	0.526504	0.004306	0.339158	0.510206
PIF3	AT1G09530			0.139873527	0.513475023	0.377427	0.031539	0.075307	0.939122
PIF4	AT2G43010	-1.009884129	0.005735924	-1.718577351	0	-0.48869	0.0000198	-0.39583	0.277536

Some genes had missing expression data for the YHB microarray experiment (Hu *et al*., 2009). This could either be due to not being significant and therefore excluded from the Hu *et al*. (2009) or not being included on the microarray. The detected HL acclimation related genes followed a similar pattern of changes of expression to the changes of expression found within HL exposed plants (Table 4.3.1 [Page 134]). Notable exceptions are *GAI*, a DELLA gene and member of the HL TF network, and *CGA1*. The DELLA proteins interact with gibberellins (GA) and indicate higher GA levels (Alabadí *et al*., 2008). High GA levels halt photomorphogenesis and increase hypocotyl length in the dark (Alabadí *et al*., 2004). However, YHB has a constitutively photomorphogenic phenotype indicating a mis-regulation of GA that may impact HL acclimation in the adult plant (Su and Lagarias, 2007). Systems like the GA pathway can be explored through gene ontology analysis (GO analysis). Upregulated and downregulated by gene lists were created from the YHB microarray data set and analysed.

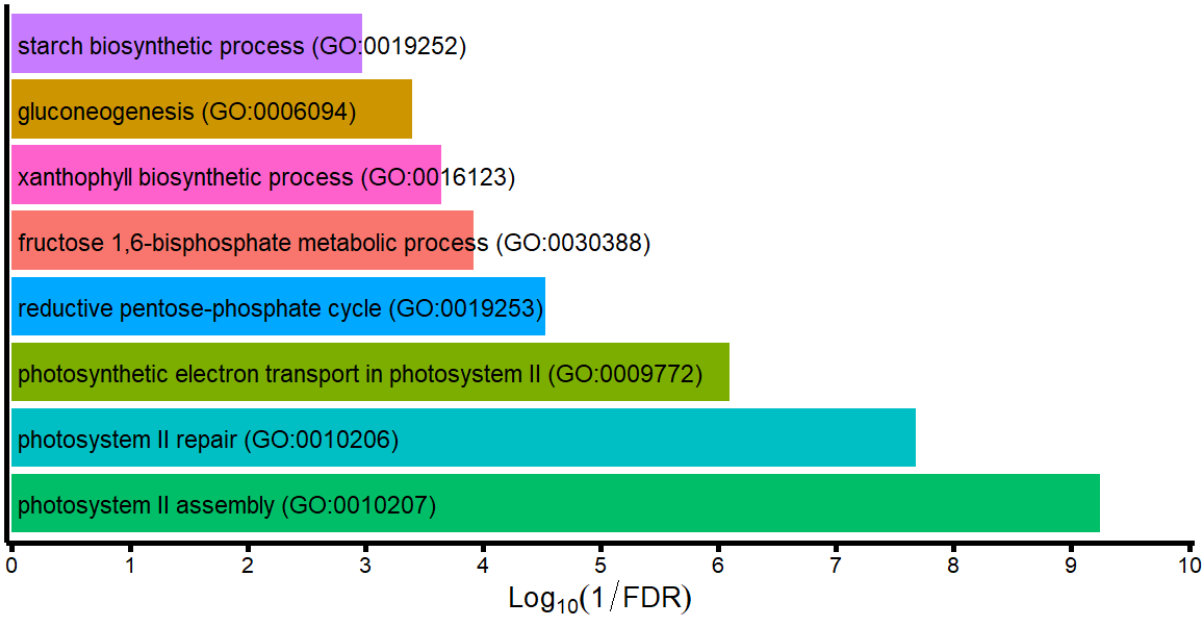

Figure 4.3.2: A subset of the GO analysis of the DEGs downregulated by both *hy5-2* and BBX32-10 when compared to Col-0 under LL conditions. A false discovery rate was calculated, and this transformed to provide a readable scale.

Pentose phosphate pathway was raised as a GO term of interest within the GO analysis of the *BBX32-HY5* HL RNA-seq within the gene set significantly upregulated within both BBX32-10 and *hy5-2* compared to Col-0 (section 3.4 [Page 73]). The reductive pentose phosphate pathway (a part of the Calvin cycle) was downregulated within YHB seedlings along with fructose 1,6-bisphosphate metabolic process, gluconeogenesis, and starch biosynthetic process (Figure 4.3.2 [Page 136]). This indicates a mis-regulation in glucose related processes similar to those seen within BBX32-10 and *hy5-2* (Section 3.4 [Page 73]).

Three different PSII associated GO terms were significantly downregulated by YHB (Figure 4.3.2 [Page 136]). This may be due to photomorphogenesis occurring in YHB

seedlings and down regulating PSII genes due to the lack of photosynthesis occurring in the dark and repair not being strongly required

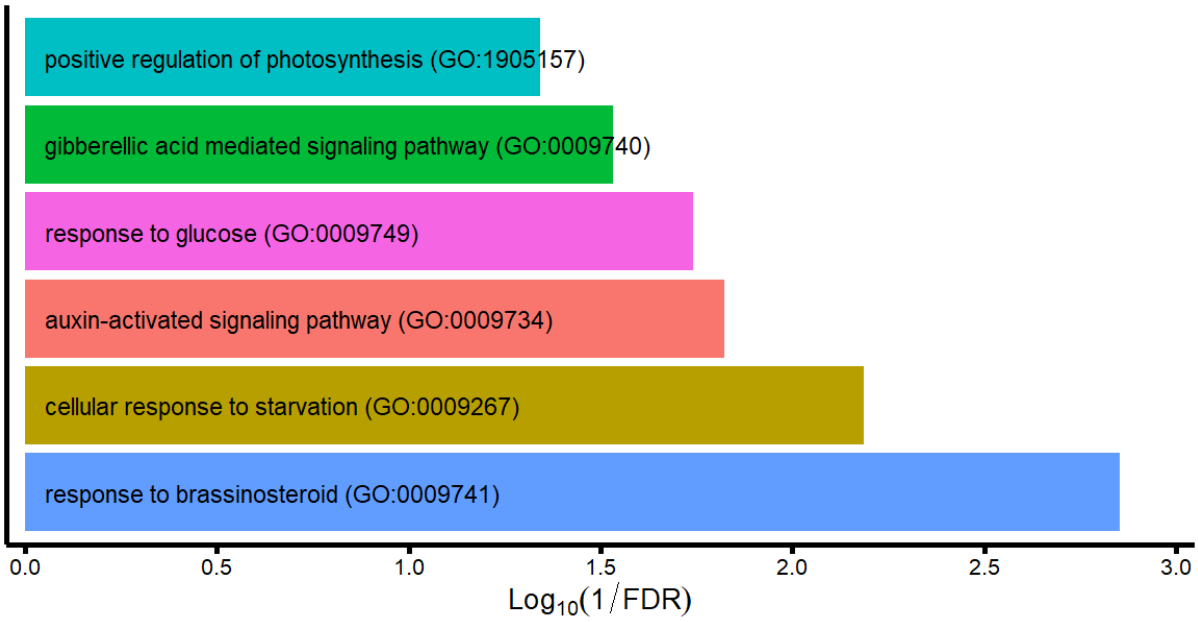

Figure 4.3.3: A subset of the GO analysis of the 1554 DEGs upregulated by both *hy5-2* and BBX32-10 when compared to Col-0 under LL conditions. A false discovery rate was calculated from the p value, and this is transformed to provide a more readable scale.

Response to glucose was upregulated in contrast to gluconeogenesis being downregulated. Plants maintain a strict control of glucose levels therefore this mis-regulation may be indicative of photosynthetic alterations (Dyson *et al*., 2015). Cellular response to starvation also fits into the narrative of primary carbon metabolism mis-regulation. YHB upregulated response to glucose, an energy source, while also signalling starvation. YHB also displays downregulation of the reductive pentose phosphate pathway, the part of the pathway for shunting glucose into the Calvin cycle (Wolosiuk *et al*., 1993).

HY5 controls the regulation of the auxin, GA and brassinosteroid pathways during photomorphogenesis (Gangappa and Botto, 2016). As active phyB suspends the degradation of HY5 by COP1 these signalling pathways are expected to be altered within YHB. GA was also an upregulated GO term within *hy5-2* and BBX32-10 though it is unknown how attributable GA mis-regulation in YHB seedlings would be to HL acclimation (section 3.4 [Page 73]).

4.3.3: Expression of photoreceptors

After the discovery of the HL acclimation mutant phenotype of YHB, the expression of photoreceptors were studied. The expression of photoreceptors within the HL acclimation mutants *hy5-2* and BBX32-10 from the *BBX32-HY5* HL RNA-seq to attempt to identify further photoreceptors involved in HL acclimation.

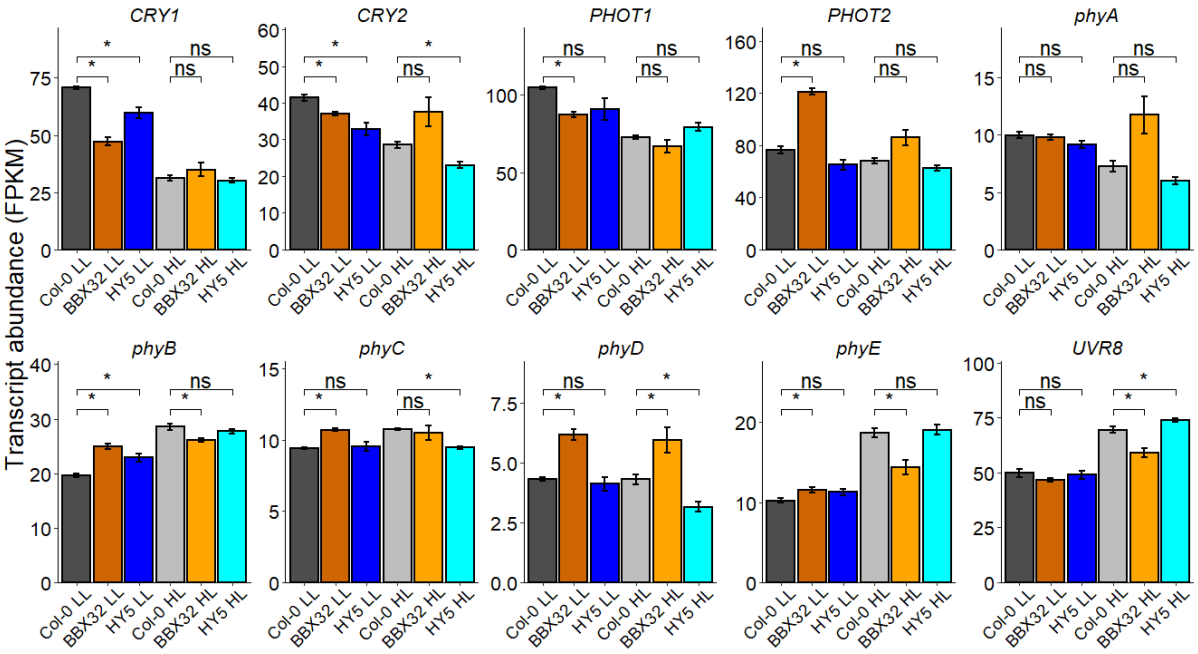

Figure 4.3.4: The expression of photoreceptor genes from the *BBX32-HY5* HL

RNA-seq. Expression was obtained from BBX32-10 (BBX32), *hy5-2* (HY5) or Col-0 under LL or HL conditions for 3.5 hours of exposure. Asterisks and bars show genes that were significantly changed in expression between the LL and HL groups of each genotype ($p < 0.05$; ANOVA).

CRY1 and *PHYB* both had a significantly altered expression in both BBX32-10 and *hy5-2* from the Col-0 control under LL conditions however *CRY2* does as well. None of the other photoreceptors have significantly altered expression in both mutants under LL conditions. Most of the photoreceptors are quickly altered in expression by HL; only *PHOT2*, *phyC* and *phyD* are not significantly altered in expression by exposure to HL. Most photoreceptors are perturbed in expression by 3.5 hours of HL. Within the HL exposed BBX32-10 and *hy5-2* plants, only one photoreceptor significantly changed in expression: *PHOT2* and *phyB* respectively. The HL acclimation mutants perturb the impact of HL on the expression of the photoreceptors potentially altering how these mutants understand their new HL environment.

4.3.4: Conclusion

phyB and CRY1 interact while phyB is in its inactive P_r state and therefore YHB, a permanently active mutant of PHYB, cannot interact with CRY1 (Hughes *et al*., 2012). A constitutively active CRY1 was also incapable of interacting with phyB (Hughes *et al*., 2012). phyB is capable of altering the HL acclimation pathway without interacting with CRY1.

The light intensity of the HL equipment used peaks in a region of the light spectrum that overlaps with the sensitivity of CRY1 indicating that CRY1 may be more influential under the conditions used (Araguirang *et al*., 2019; Figure S1 [Page 328]). More complex equipment would be required to test this hypothesis (discussed further in Section 4.6 [Page 160]).

phyB interacts with COP1 to alter the protein degradation rate of HY5 (Ang *et al*., 1998; Xu, 2020). There is also a known connection between HY5 and CRY1 but CRY1 does not directly mediate this interaction with COP1 (Kleine *et al*., 2007; Liu *et al*., 2011; Ponnu *et al*., 2019; Lau *et al*., 2019). Another protein is required to link the HL acclimation signalling pathway. The four *SPA* genes encoding members of the COP1/SPA E3 ligase complex complete the bridging of CRY1 and phyB to COP1 and HY5 (Ponnu *et al*., 2019). The next section studies the HL acclimation phenotype of different *SPA* mutants.

4.4: COP/SPA complexes control HL acclimation

The *SPA* genes are involved in the formation of the COP1/SPA E3 ligase complex that targets specific proteins for degradation by the 26S proteasome (Saijo *et al*., 2003). Many of the targets of COP1/SPA complexes are transcription factors like the HL acclimation protein HY5 (Saijo *et al*., 2003). The SPA proteins are required for a strong interaction between the known regulators of HL acclimation CRY1 and COP1 (Liu *et al*., 2011; Holtkotte *et al*., 2017; Alvarez-Fernandez *et al*., 2021). I hypothesised that HL acclimation signal transduction is through a CRY1-COP1/SPA-HY5 pathway. Due to known partial functional redundancies between the *SPA*

genes, a multiple *SPA* mutant was sought for a stronger HL acclimation phenotype (Alvarez-Fernandez *et al*., 2021).

4.4.1: HL acclimation phenotype of *SPA* mutants

I have extensively used the *spa123* (*spa1-7*, *spa2-1*, *spa3-1* triple mutant; Fittinghoff *et al*., 2006; Chen *et al*., 2016) as the quadruple spa mutant (*spa1 spa2 spa3 spa4*; henceforth known as *spaQ*) had a severely dwarfed phenotype as seen in Figure 4.4.1 [Page 142]. The size restricts the resolution of the leaves within chlorophyll fluorescence images. This made it impossible to distinguish between leaves and the meristem. Shoot apices were excluded from HL acclimation data sets due to possible morphological alterations in response to HL (section 2.2.3 [Page 36]; Athanasiou *et al*., 2010).

Figure 4.4.1: Size comparison of 6 week old *spaQ*, *spa123* and Col-0 plants grown under SD (8/16 hour day) at 150 µmol m^{-2} s^{-1}.

The *spa123* mutant was substituted for the *spaQ* mutant and the HL acclimation phenotype was tested using chlorophyll fluorescence. Strong HL acclimation phenotype of *spa123* was very similar to the strong phenotype of the *cop1-4* and YHB mutant. This was termed an accelerated acclimation phenotype by Alvarez-Fernandez *et al*. (2021). However, the increase between the day 1 and day 5 value of *spa123* was diminished compared to the Col-0 increase similar to the YHB mutant

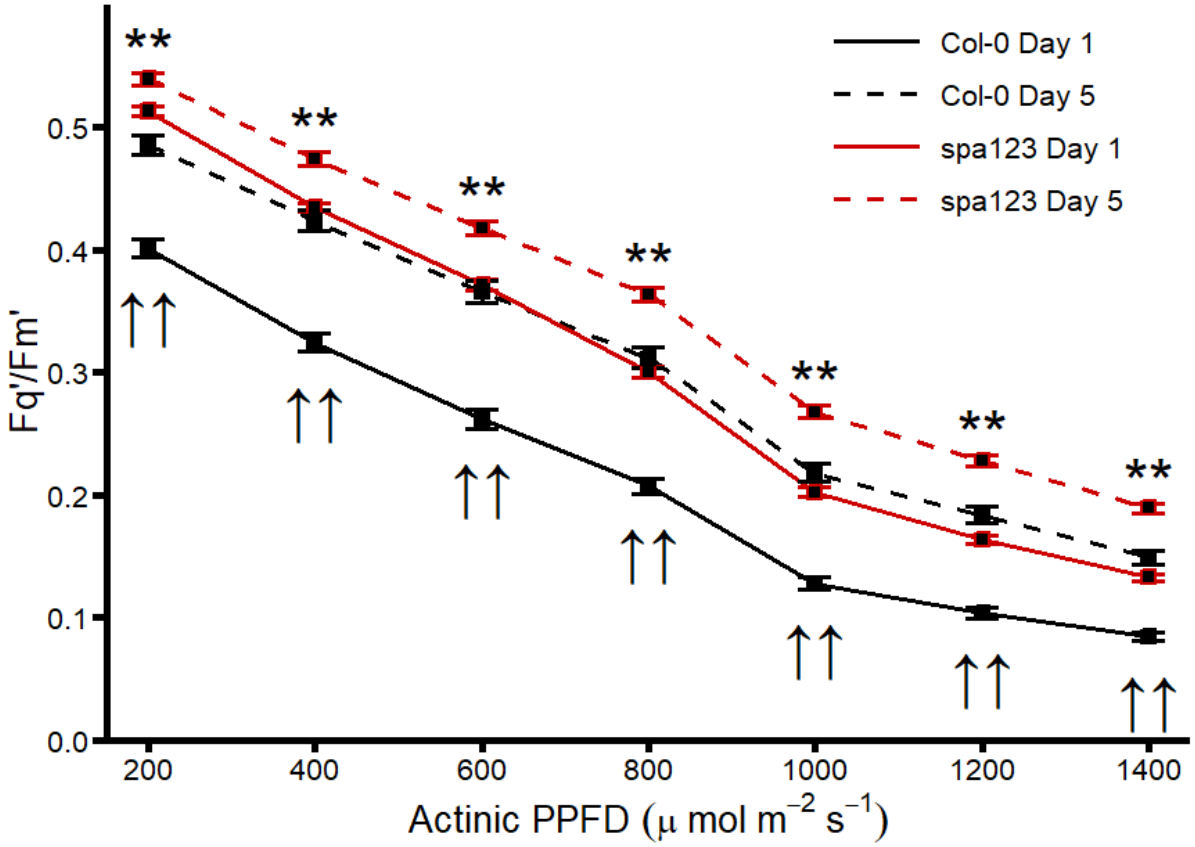

Figure 4.4.2: HL acclimation phenotype of *spa123* (*spa1-7*, *spa2-1*, *spa3-1* triple mutant) and Col-0 plants. Fq'/Fm' was determined by chlorophyll fluorescence with an actinic PPFD range of 200 µmol m^{-2} s^{-1} to 1400 µmol m^{-2} s^{-1} at 200 µmol m^{-2} s^{-1} increments. Measurements were taken from 4-6 week old plants (n > 4) with a minimum of 6 mature leaves each (means ± SE). Arrows and asterisks denote a significant difference between the day 1 and day 5 values respectively of the mutants and Col-0 (ANOVA, post-hoc GH; */↑ = $p < 0.05$; **/↑↑ = $p < 0.005$).

The diminished increase in Fq'/Fm' and the strength of the triple (and not quadruple) *spa* mutant prompted a full analysis of the HL acclimation phenotype. I aimed to study the rate of carbon assimilation under light and carbon dioxide limiting environments. However, measuring these rates would require older, larger plants. Therefore, the decision was made to repeat the chlorophyll fluorescence on the older plants. This presented the opportunity to analyse the Fq'/Fm' after each day of HL

exposure. A day 0 measurement was also taken to analyse the plant's PSII operational efficiency prior to any HL exposure.

Chlorophyll fluorescence measurements were performed across the 6 days: 5 days of HL exposure and a prior day 0 measurement with no HL exposure. Due to the high number of data points a single PPFD had to be selected for the analysis. 800 µmol m^{-2} s^{-1} was selected as it was the median increment.

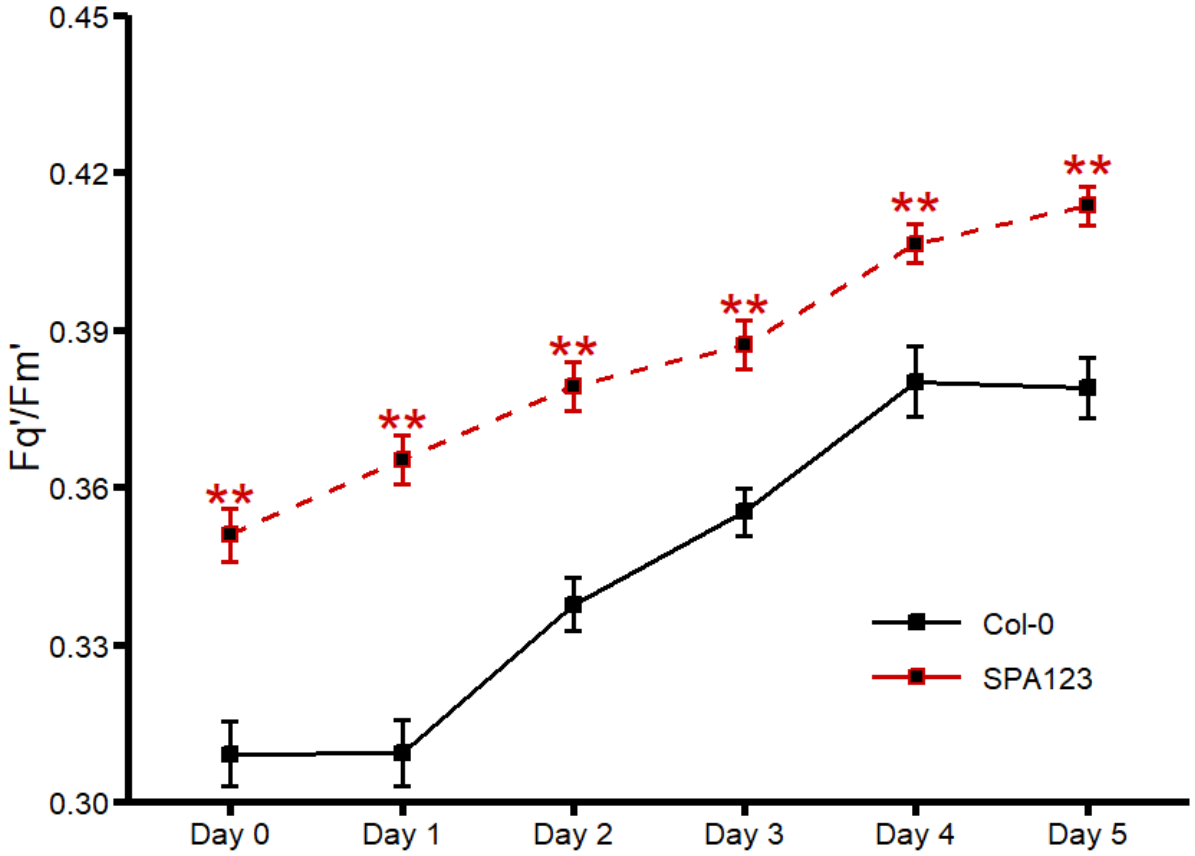

Figure 4.4.3: HL acclimation phenotype of *spa123* (*spa1-7*, *spa2-1*, *spa3-1* triple mutant) and Col-0 plants over 5 days of HL exposure. Fq'/Fm' was determined by chlorophyll fluorescence with an actinic PPFD of 800 µmol m^{-2} s^{-1}. Measurements were taken from 8 week old plants (n > 4) with a minimum of 10 mature leaves each (means ± SE). Arrows and asterisks denote a significant difference between the day 1 and day 5 values respectively of the mutants and Col-0 (ANOVA, post-hoc GH; */↑ = $p < 0.05$; **/↑↑ = $p < 0.005$).

spa123 had an increased Fq'/Fm' before any HL exposure on day 0. This was termed a pre-acclimated phenotype (Alvarez-Fernandez *et al*., 2021). *spa123* reacted faster to HL treatment than Col-0 and increased on day 1 unlike Col-0. By day 5, Col-0 stopped increasing Fq'/Fm'; its day 4 and day 5 Fq'/Fm' values were very similar however *spa123* showed a continued increase in Fq'/Fm' between day 4 and day 5. Col-0 appeared to cease HL acclimation by day 5 whereas it is unknown if *spa123* continues to increase Fq'/Fm' further. The rate of Fq'/Fm' increase of *spa123* was also less than Col-0. It would also be useful to look at other chlorophyll fluorescence parameters to understand what these early changes meant for other photosynthetic systems.

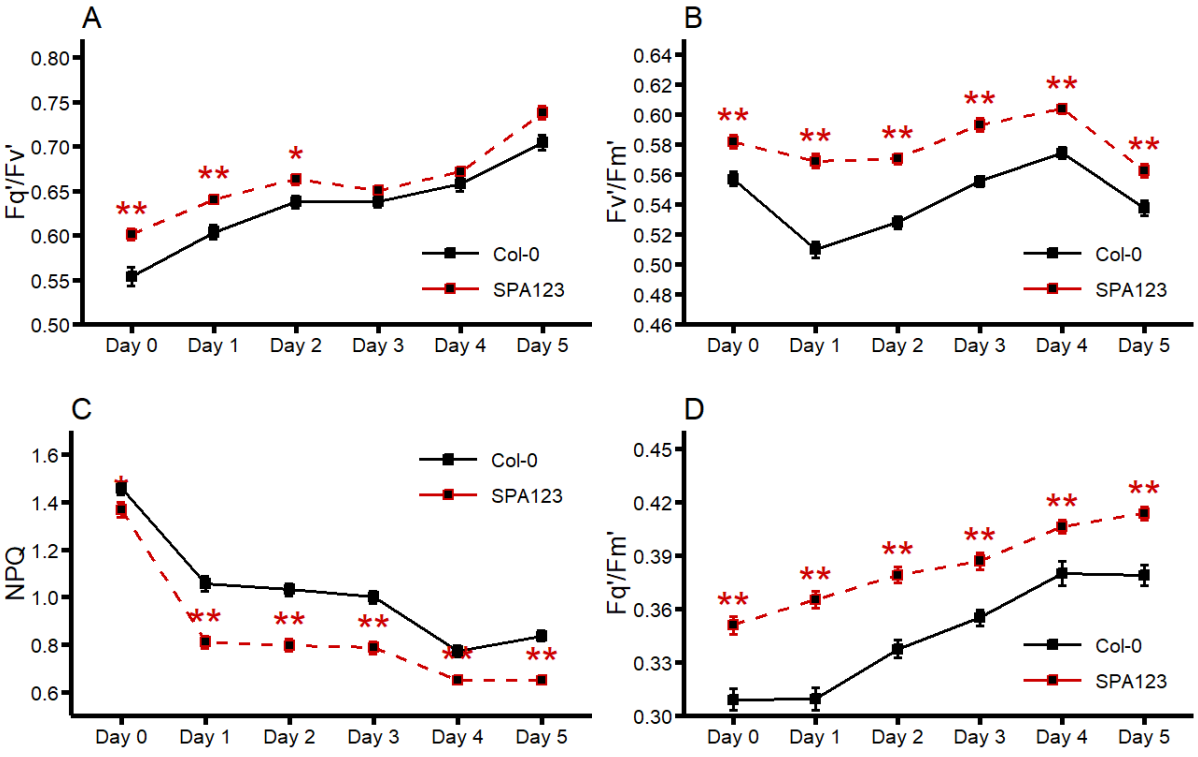

Figure 4.4.4: The chlorophyll fluorescence parameters (Baker, 2008) of *spa123* (*spa1-7*, *spa2-1*, *spa3-1* triple mutant) and Col-0 plants over 5 days of HL

exposure. Fq'/Fv' (PSII efficiency factor; A), Fv'/Fm' (PSII maximal efficiency; B), NPQ (Fm/Fm' -1; Non-photochemical quenching; C) and Fq'/Fm' (PSII operational efficiency; D) are determined by chlorophyll fluorescence with an actinic PPFD of 800 µmol m^{-2} s^{-1}. Measurements were taken from 8 week old plants (n > 4) with a minimum of 10 mature leaves each (means ± SE). Arrows and asterisks denote a significant difference between the mutants and Col-0 (ANOVA, post-hoc GH; */↑ = p < 0.05; **/↑↑ = p < 0.005).

The Col-0 data follows the results found within Alvarez-Fernandez *et al*. (2021) very closely. *spa123* had a reduced rate of NPQ compared to Col-0 throughout the time points. The photochemical quenching (qP; Fq'/Fv') was only significantly greater in *spa123* on day 0, day 1 and day 2. The maximum efficiency (Fv'/Fm') of *spa123* was significantly higher throughout the experiment. The reduced rate of NPQ may account for the greater Fq'/Fm' of *spa123* through the more useful dissipation through either enhanced primary metabolism or metabolic sinking of excess excitation energy.

4.4.2: Carbon assimilation phenotype of *spa123*

Chlorophyll fluorescence uses estimates of photosynthetic parameters and is an efficiency measurement; however, directly testing the rate of carbon assimilation provides more accurate measurements of photochemistry. Carbon assimilation can be measured in a light limiting or a carbon limiting environment. A light limiting environment was more applicable to HL acclimation although both environments were tested. *spa123* and Col-0 plants were grown to 8 weeks old for the increased

size required of the measurement apparatus. These plants were exposed to HL for 5 days before being measured.

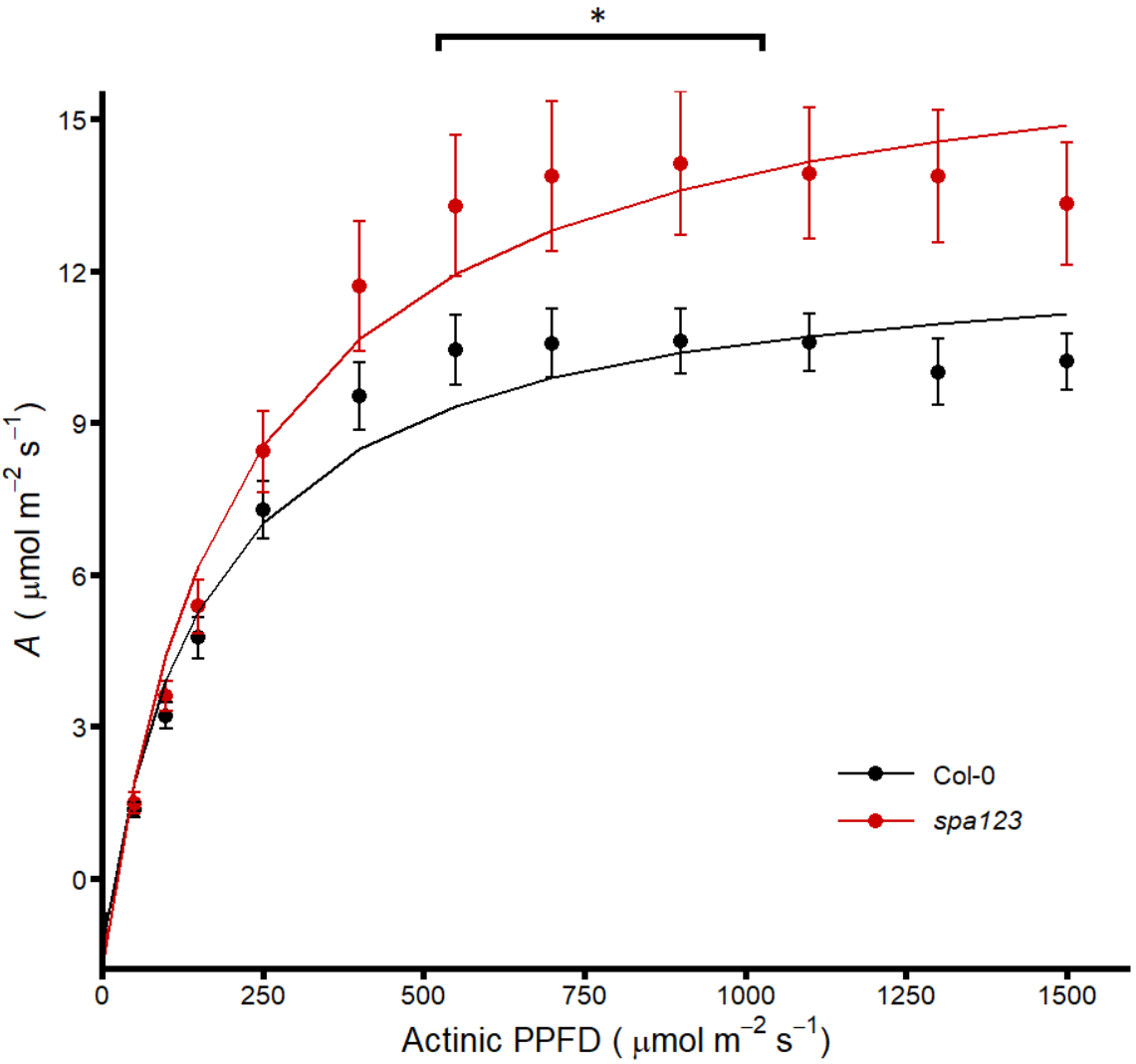

Figure 4.4.5: Carbon assimilation of *spa123* and Col-0 under a light limiting environment. 8 week old *spa123* and Col-0 plants (n > 4) were exposed to HL for 5 days and measurements were taken from a minimum of 5 plants for each genotype (means ± SE). The line was developed using an iterative optimisation model. The asterisk denotes a significant difference between the mutant and Col-0 (ANOVA; $p < 0.05$).

The carbon assimilation (A) of *spa123* was greater than Col-0 after 5 days of HL exposure and is significant between 500 and 1000 µmol m^{-2} s^{-1}. The carbon assimilation data supports the chlorophyll fluorescence measurements in Figure 4.4.2 [Page 143]. The carbon assimilation rate of *spa123* was also measured in a carbon limited environment.

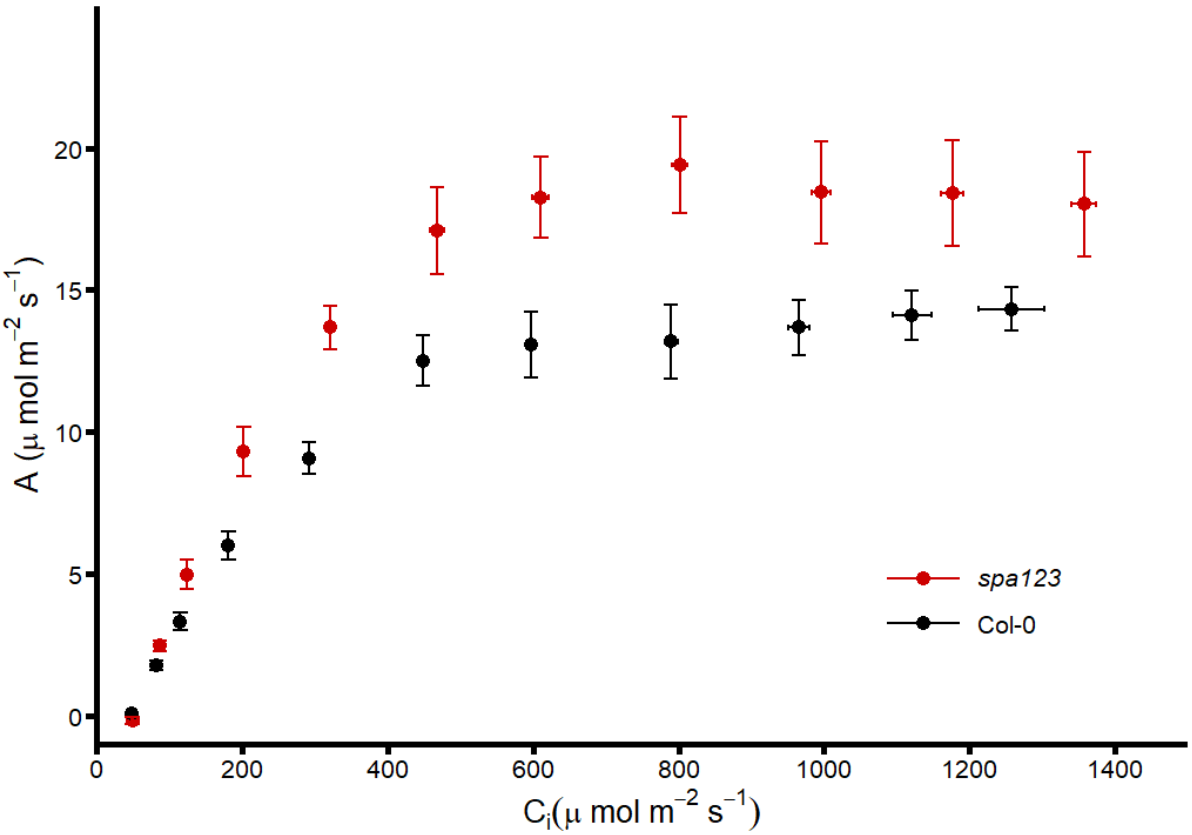

Figure 4.4.6: Carbon assimilation of *spa123* and Col-0 under a carbon limiting environment. 8 week old *spa123* and Col-0 plants (n > 4) were exposed to HL for 5 days and measurements were taken from a minimum of 5 plants for each genotype (means ± SE).

spa123 has an increased rate of carbon assimilation across all carbon dioxide concentrations above 100 ppm. Even under carbon limiting conditions *spa123* has

an increased rate of photosynthesis compared to Col-0. The significance is difficult to determine from an AC_i curve alone. An AC_i curve can be manipulated to calculate the J_{max} and $V_{c\,max}$. J_{max} is the maximum electron transport rate and the $V_{c\,max}$ is the maximum velocity of carboxylation (Kattge *et al*., 2009).

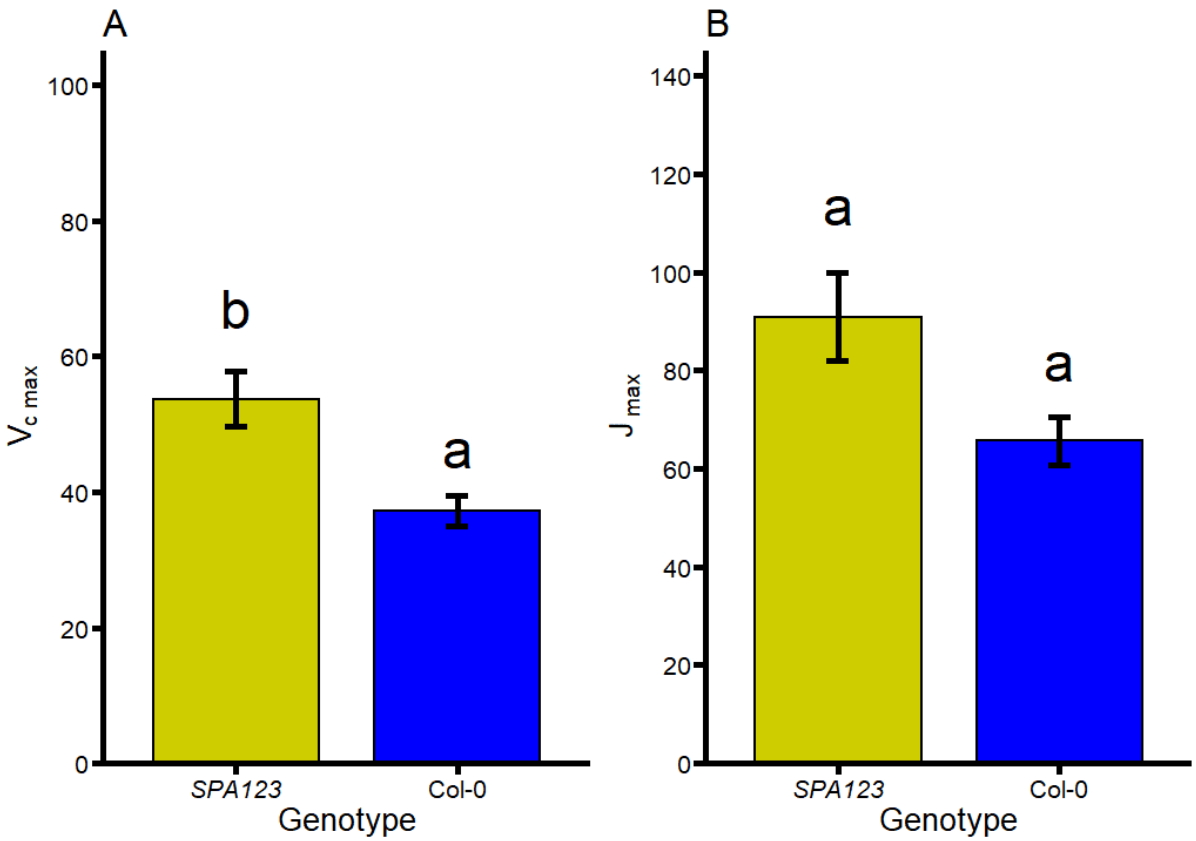

Figure 4.4.7: The maximum velocities of carboxylation (A; $V_{c\,max}$) and electron transport rate (B; J_{max}) of *spa123* and Col-0. *spa123* and Col-0 plants were exposed to HL conditions for 5 days and were tested for the rate of carbon assimilation across different CO_2 concentrations (AC_i; n >= 5 plants). Different letters above the bars indicate a significant difference between *spa123* and Col-0 ($p < 0.05$; ANOVA).

The J_{max} would be significant if a p value of 0.1 was used and an increased number of replicates may increase the significance. The stronger significance of the $V_{c\ max}$ denotes an impact on primary metabolism. This is similar to the *gpt2* mutant that alters the compartmental distribution of primary metabolites and disrupts HL acclimation. This is also similar to the GO terms discovered in the *BBX32-HY5* HL RNA-seq analysis that highlight changes to the Calvin cycle and pentose phosphate shunt (section 3.4 [Page 73]).

4.4.3: Regulation of HL acclimation genes in *spa123*

SPA proteins are involved in the COP1/SPA E3 ligase complex that targets proteins for degradation (Saijo *et al*., 2003). Transcription factors are targeted by the COP1/SPA complex, and this indirectly changes the steady state expression of specific target genes. RT-qPCR can be used to study the changes in expression of different HL acclimation related genes within the *spa123* mutant. RT-qPCR was performed on *spa123* and Col-0 from extracts of plants either maintained at growth conditions or exposed to HL for 3.5 hours. HL acclimation genes were selected for this experiment and primers were designed. The RT-qPCR data was transformed using *PP2A* as a control and are visualised in Figure 4.4.8 [Page 151].

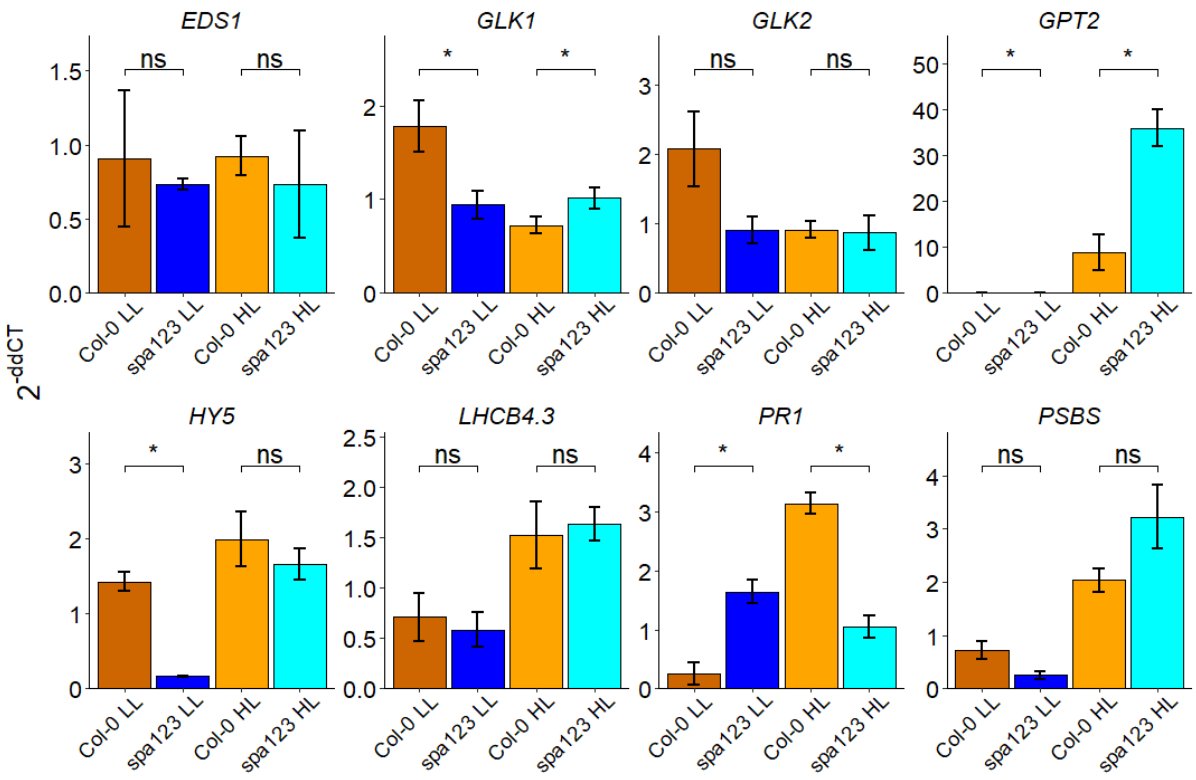

Figure 4.4.8: RT-qPCR of different HL acclimation related genes on *spa123* and Col-0 samples exposed LL or HL conditions. Expression data was manipulated using the double delta method with the expression of *PP2A* being used as a control ($p < 0.1$; ANOVA post-hoc Tukey HSD)

GPT2, a sugar transport gene crucial for HL acclimation (Athanasiou *et al*., 2010), was induced in expression by HL and this can be seen in Figure 4.4.8 [Page 151]. *GPT2* was significantly increased in expression under both LL and HL conditions within *spa123* (not visualised under LL conditions to the very low expression when compared to HL). *GPT2* expression can be used as an indicator of HL acclimation initiation (section 3.3 [Page 69], Athanasiou *et al*., 2010) and the clear increased expression within both *spa123* and Col-0 indicates that HL acclimation has been initiated.

Both of the *GLKs* were reduced in expression within *spa123* however only *GLK1* was significant. *HY5* was significantly decreased in expression in *spa123* under LL conditions compared to Col-0. This was in conflict with the phenotype of *hy5-2* having a reduced PSII operational efficiency on day 1 whereas *spa123* has an increased PSII operational efficiency (Alvarez-Fernandez *et al*., 2021). Under HL conditions, the *HY5* expression is not significantly different between *spa123* and Col-0. The alterations of expression of *EDS1* and *PR1* within *spa123* are explored further in Chapter 5 [Page 166].

4.4.4: Conclusion

There is a distinct alteration of the HL acclimation phenotype of the *spa123* mutant (Figure 4.4.2 [Page 143]). The chlorophyll fluorescence and carbon assimilation both show that *spa123* has a greater rate of photosynthesis than Col-0 after being exposed to HL for 5 days. Rosette size also plays a role in the rate of photosynthesis of the plant as a whole and as *spa123* has a smaller rosette size than Col-0 this may impact plant productivity (Figure 4.4.1 [Page 142]; Laubinger *et al*., 2004). The *SPA* single mutants have larger morphologies far closer to the size of the WT control (Laubinger *et al*., 2004) therefore these single mutants may be better suited for increasing plant productivity.

Functional differences exist between the *SPA* genes (Laubinger *et al*., 2004; Fittinghoff *et al*., 2006; Laubinger *et al*., 2006). *spa1* has a very early short day flowering time phenotype not shared by other *SPA* single mutants (Laubinger *et al*., 2006). The WT *SPA4* gene present in *spa123* was not able to recover the HL

acclimation phenotype and it is unclear whether other *SPA* genes could restore a WT HL acclimation phenotype. Therefore, I have continued by analysing the HL acclimation phenotypic changes within the *SPA* single mutants.

4.5: Analysis of *SPA* single mutants

The *SPA* genes are known to not have true functional redundancy (Laubinger *et al*., 2004; Laubinger *et al*., 2006; Fittinghoff *et al*., 2006). This is in contrast to HL acclimation genes *GLK1* and *GLK2* which prior to this experiment (section 3.6 [Page 107]) did not have any known functional distinction but have distinct HL acclimation phenotypes (Fitter *et al*., 2002; Tokumaru *et al*., 2017). As *spa123* has a HL acclimation phenotype (section 4.4 [Page 140]) it is known that *SPA4* is unable to compensate for the lack of *SPA1*, *SPA2* and *SPA3*. Therefore, multiple *SPA* genes are required for a WT HL acclimation phenotype. I, therefore, tested each of the *SPA* genes individually as single mutants for a perturbation in HL acclimation.

4.5.1: HL acclimation phenotype of *SPA* single mutants

The single mutant components of *spa123* were gathered along with *spa4-1* however *spa1-100* was used in place of *spa1-7* from the triple and quadruple mutants due to availability issues. The mature morphological phenotype (6 weeks old) was indistinguishable from the WT controls for all of the *SPA* single mutants. The *SPA* single mutants were subjected to HL for 5 days to test their HL acclimation phenotype.

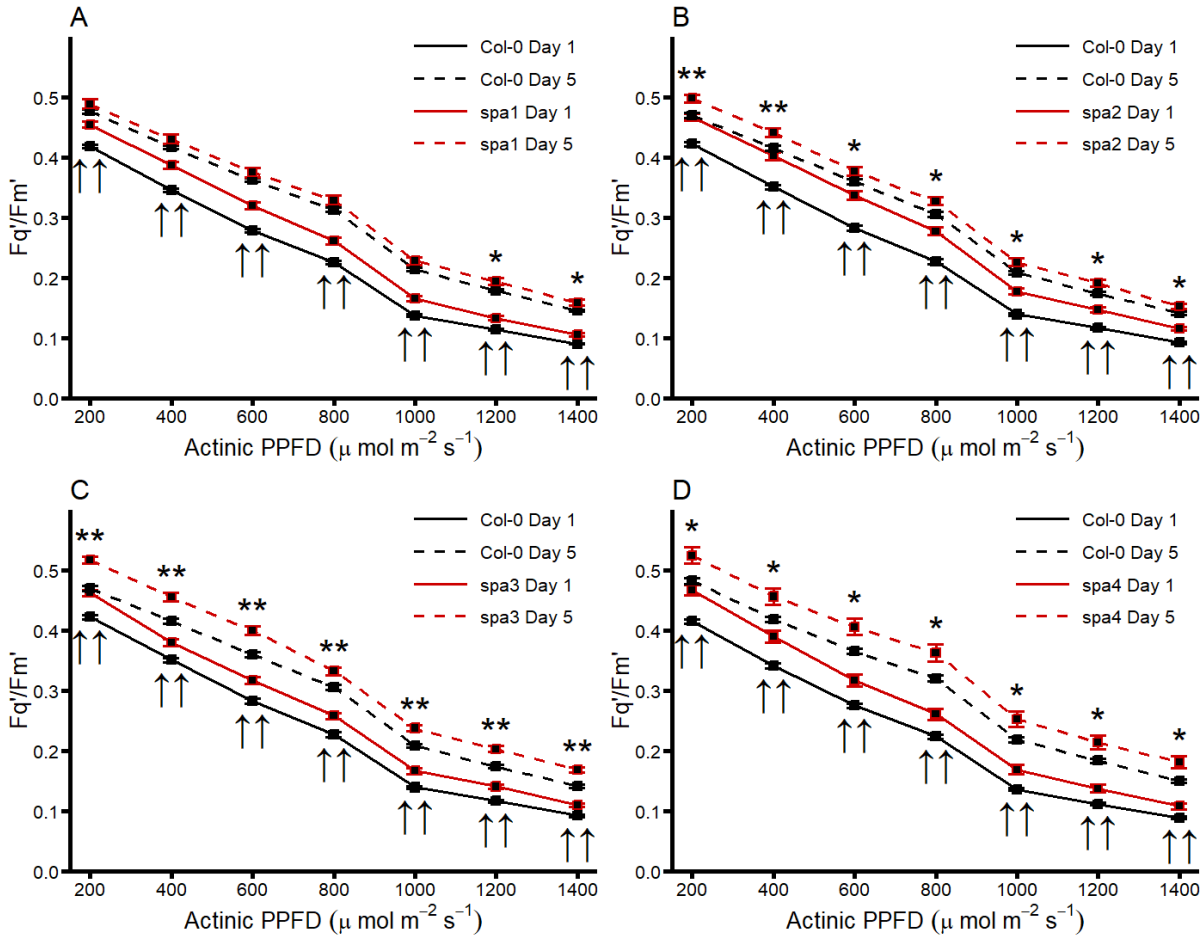

Figure 4.5.1: HL acclimation phenotype of *spa1-100* (A), *spa2-1* (B), *spa3-1* (C), *spa4-1* (D) and Col-0 plants over 5 days of HL exposure. Fq'/Fm' was determined by chlorophyll fluorescence with an actinic PPFD of 800 µmol m^{-2} s^{-1}. Measurements were taken from 8 week old plants (n > 4) with a minimum of 10 mature leaves each (means ± SE). Arrows and asterisks denote a significant difference between the day 1 and day 5 values respectively of the mutants and Col-0 (ANOVA, post-hoc GH; */↑ = p < 0.05; **/↑↑ = p < 0.005).

All of the *spa* single mutants had a degree of Fq'/Fm' perturbation on day 1 however *spa1* did not show a significant difference on day 5. *spa2*, *spa3* and *spa4* have a significantly increased Fq'/Fm' on both day 1 and day 5. A notable aspect was that *spa1* has the strongest SD flowering time phenotype and the weakest HL acclimation

phenotype (Ishikawa *et al*., 2006; Laubinger *et al*., 2006). *spa3* and *spa4* were the most impactful on the adult morphology however *spa2* also impacts HL acclimation strongly (Laubinger *et al*., 2004). These separate plots were combined into a single plot to visualise the differences between the *SPA* single mutants and the *spa123* triple mutant more easily.

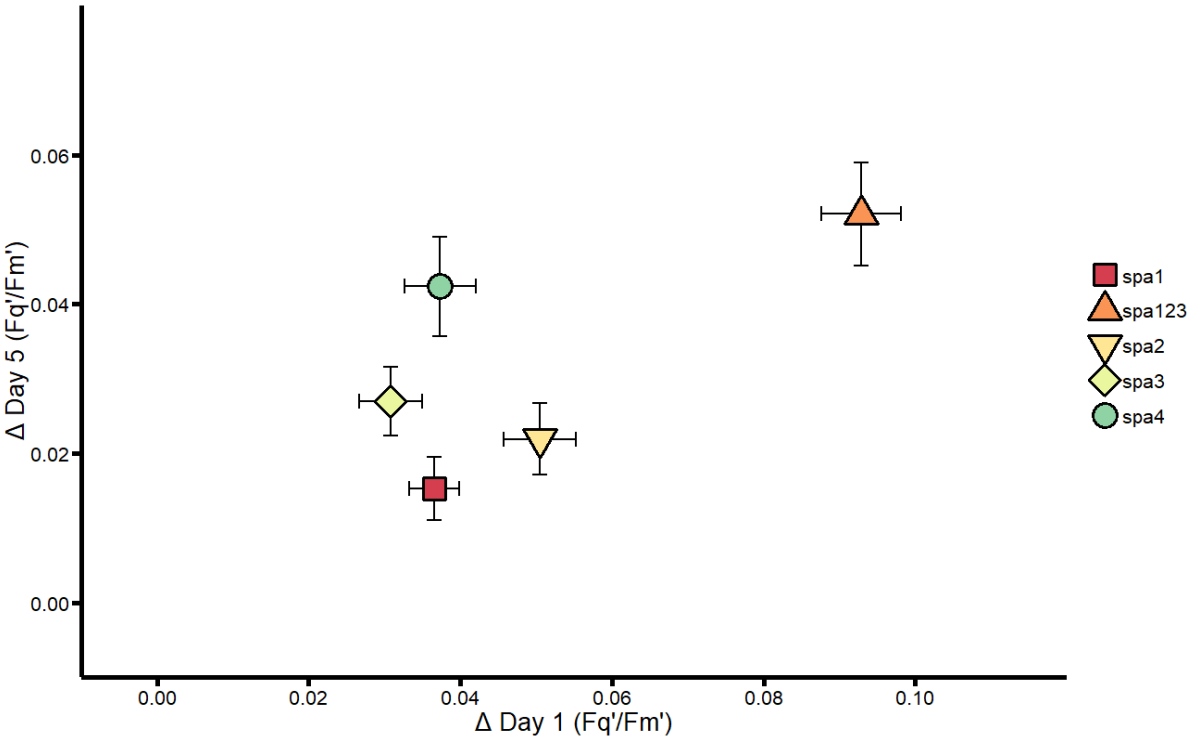

Figure 4.5.2: HL acclimation of *spa1*, *spa2*, *spa3*, *spa4*, *spa123* and Col-0 plants. ΔFq'/Fm' is determined by chlorophyll fluorescence with a PPFD of 800 µmol m^{-2} s^{-1} minus the Col-0 (WT) value. Measurements were taken from 4-6 week old plants (n > 4) with a minimum of 6 mature leaves each (means ± SE).

Only *spa3* and *spa4* are close to the line Δ Day 1 = Δ Day 5. The Δ Day 1 values were greater than Δ Day 5 values for *spa1*, *spa2* and *spa123* meaning that these mutants did not increase PSII operation efficiency in response to HL as much as the Col-0 control.

The theoretical Fq'/Fm' values of *spa123* can be calculated from the *spa1*, *spa2* and *spa3* mutants. If the *spa123* HL acclimation phenotype is additive, the *spa1*, *spa2* and *spa3* ΔFq'/Fm' values should sum to the ΔFq'/Fm' of *spa123*. This was done separately for day 1 and day 5.

Table 4.5.1: HL acclimation of spa1, spa2, spa3, spa123 and Col-0 plants. Fq'/Fm' is determined by chlorophyll fluorescence with a PPFD of 800 µmol m-2 s-1 minus the Col-0 (WT) value. Measurements were taken from 4-6 week old plants (n > 4) with a minimum of 6 mature leaves each (means ± SE). The theoretical Fq'/Fm' of *spa123* was calculated using the Fq'/Fm' values of Col-0 and the *spa1-100*, *spa2-1* and *spa3-1* single mutants. Each of the Fq'/Fm' of the single *SPA* mutants had the Col-0 Fq'/Fm' subtracted from it. These were added together and added to the Col-0 value to generate the theoretical value. This was performed for both day 1 and day 5. The theoretical and actual *spa123* Fq'/Fm' values are highlighted.

Mutant	Theoretical day 1 Fq'/Fm'	Actual day 1 Fq'/Fm'	Theoretical day 5 Fq'/Fm'	Actual day 5 Fq'/Fm'
Col-0		0.223 (±0.002)		0.313 (± 0.003)
spa1-100		0.262 (± 0.006)		0.328 (± 0.008)
spa2-1		0.278 (± 0.007)		0.328 (± 0.007)
spa3-1		0.258 (± 0.006)		0.333 (± 0.006)
spa123	0.352 (± 0.006)	0.300 (± 0.004)	0.363 (± 0.007)	0.364 (± 0.006)

The theoretical Fq'/Fm' of *spa123* on day 1 was greater than the actual *spa123* Fq'/Fm' value. The loss of *SPA1*, *SPA2* and *SPA3* genes has a greater impact than the loss of the combination of the individual genes on day 1. The Fq'/Fm' of *spa123*

is greater than the theoretical value. The day 5 theoretical value matched the actual *spa123* Fq'/Fm' value with a difference of 0.001: far less than either of the standard error values. This implies that the day 5 effect on Fq'/Fm' is additive. As these are estimates from separate experiments this is not the best methodology for testing additivity. However, performing these experiments at the same time would limit the number of plants

4.5.2: Expression of *SPA* genes in HL acclimation mutants

The regulation of the expression of the *SPA* genes is important due to the degradative nature of their encoded proteins (Saijo *et al*., 2003). As *SPA1* was identified as a member of the HL TF network the expression would be tested from a separate experiment. The reaction of the expression of the *SPA* genes to HL can be analysed from the *BBX32-HY5* HL RNA-seq. The expression within the HL acclimation mutants BBX32-10 and *hy5-2* may also be used to understand the defective HL acclimation phenotype.

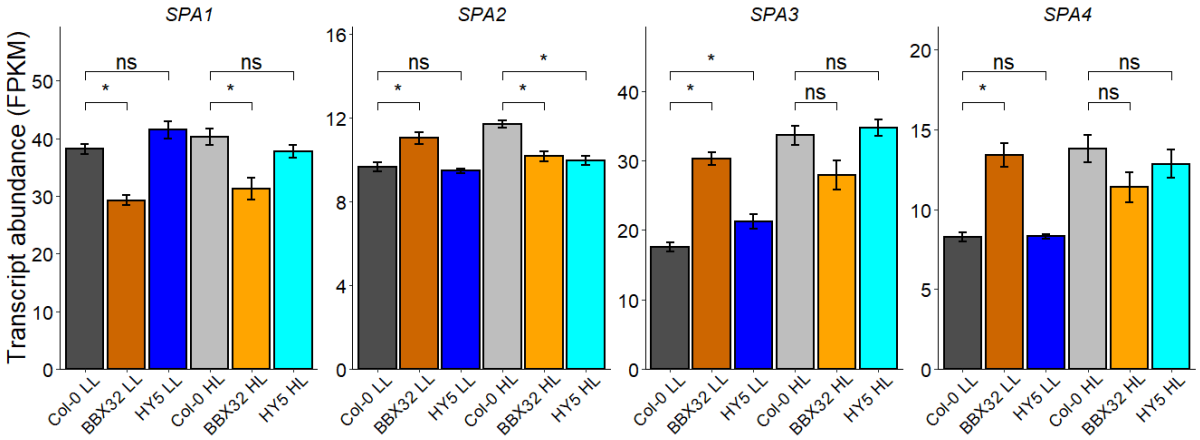

Figure 4.5.3: The expression of *SPA* genes from the *BBX32-HY5* HL RNA-seq. Expression was obtained from BBX32-10 (BBX32), *hy5-2* (HY5) or Col-0 under LL or

HL conditions for 3.5 hours of exposure. Asterisks and bars show genes that were significantly changed in expression between the LL and HL groups of each genotype ($p < 0.05$; ANOVA).

All of the *SPA* genes are significantly altered in expression by BBX32-10 when compared to the Col-0 control under LL conditions. *SPA1* is decreased and the other *SPA* genes are increased in expression. *hy5-2* only significantly impacted the expression of *SPA3* under LL conditions. Under HL conditions, BBX32-10 similarly decreased the expression of *SPA1* and both *hy5-2* and BBX32-10 decreased the expression of *SPA2*. It is interesting that *SPA1* is the only *SPA* gene decreased in BBX32-10 whilst the others are increased; however, as *hy5-2* does not follow the same pattern it cannot be hypothesised that this clearly impacts HL acclimation.

4.5.3: Conclusion

All the *SPA* single mutants other than *spa1* have a significant accelerated HL acclimation phenotype and all have a perturbed PSII operating efficiency on day 1 (Figure 4.5.1 [Page 154]). *SPA2*, *SPA3* and *SPA4* are also significantly increased in expression by HL whilst *SPA1* is not. The delineation between *SPA1* and *SPA2*, *SPA3* and *SPA4* has occurred repeatedly throughout this section and further study of a potential *spa234* mutant may be useful. This implies a separation of HL acclimation functionality of the different *SPA* genes, in particular *SPA1*, and an additive effect of *SPA1*, *SPA2* and *SPA3* to the strength of the *spa123* phenotype (Table 4.5.1 [Page 156]). Further studies would be needed to conclude for a statistical certainty that this effect is additive. The lower significance of the HL acclimation phenotype of the *SPA*

single mutants would make it difficult to significantly detect carbon assimilation rates different from wild type. However, it is clear that the *SPA* single mutants do not have redundant HL acclimation functionality but rather tend to have an additive effect.

Further experimentation into the *SPAs* would be required to understand the differences in functionality contributing to the HL acclimation phenotypes. An RNA-seq of the different *SPA* single mutants would detail the differences in the transcriptomes and how the *SPA* gene alters the steady state of gene regulation. The impact on other important phenotypic factors such as yield could also be studied. Elsewise, protein studies would be required to experimentally find protein targets of specific COP1/SPA complexes. The issue with this approach is that excluding auxiliary proteins there are 10 different COP1/SPA complexes of 2 COP1 proteins and any two SPA genes (Zhu *et al*., 2008; Figure 4.5.4 [Page 159]).

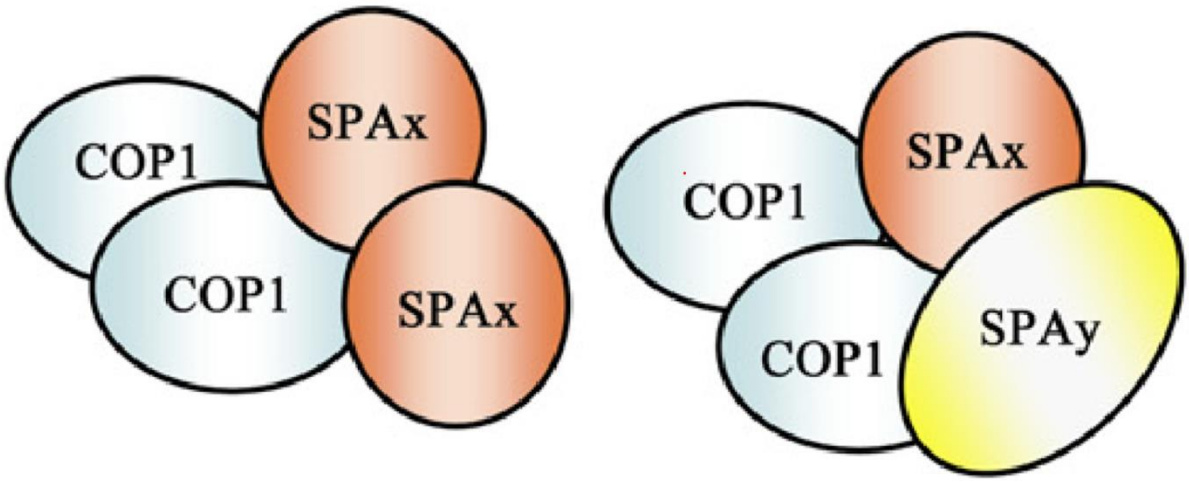

Figure 4.5.4: The possible configurations of the COP1/SPA complex. X and Y denote any SPA protein (SPA1-4). When x = y then the complex is considered

homogeneous and when x ≠ y the complex is heterogeneous. This image has been adapted from Zhu *et al*. (2008).

4.6: Discussion

This chapter identifies five new genes that impact HL acclimation: *SPA1*, *SPA2*, *SPA3*, *SPA4* and *phyB*. With the inclusion of *phyB*, red light signalling has been shown to be potentially involved in altering the HL acclimation phenotype. Red and blue light signalling are transduced by COP1/SPA complexes which are also involved in HL acclimation signalling (section 4.4 [Page 140]; section 4.5 [Page 153]). From this new information, a model was constructed of the new HL acclimation signalling pathway (Figure 4.6.1 [Page 161]).

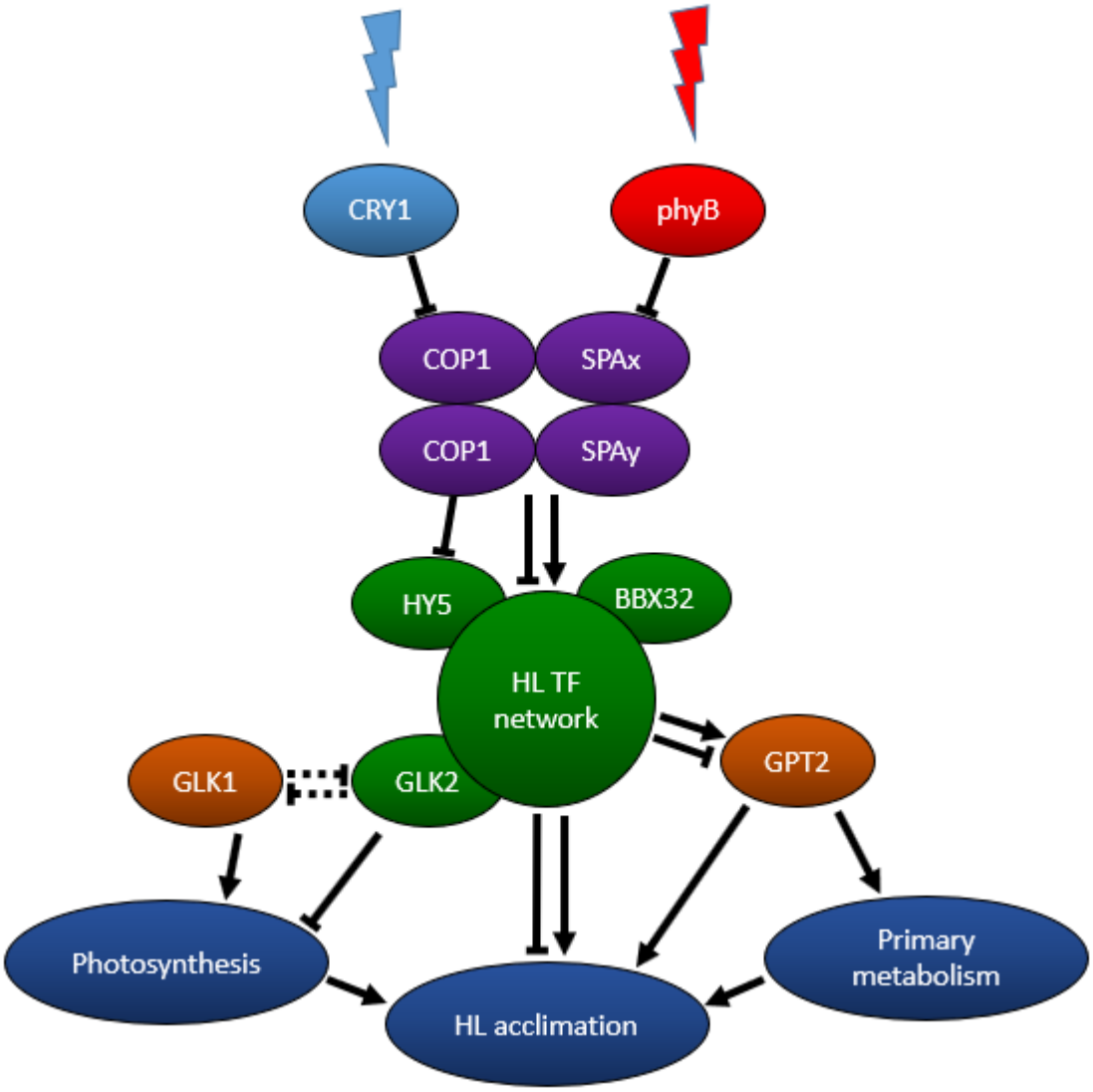

Figure 4.6.1: A model of known HL acclimation genes and their interactions. HY5, GLK2, BBX32 and SPA1 (within SPAx and SPAy) are a part of the HL TF network. Arrows indicate a positive interaction and blocked lines indicate negative interactions or degradation-based interactions. phyB and CRY1 are activated by red and blue light respectively (lightning bolts). The connection between CRY1 and phyB is not depicted due to the active forms not interacting.

It is possible that there are more photoreceptors that impact HL acclimation. CRY1 and phyB both have strong negative phenotypes whereas other type II phytochromes (phyC, phyD, phyE) have weaker phenotypes that may not produce such a strong constitutive HL acclimation phenotype (Sharrock and Clack, 2004; Li *et al*., 2011). Other photoreceptors may be capable of altering HL acclimation signalling.

To parallel YHB, HL acclimation of a constitutively active CRY1 mutant could have been analysed. There are two known constitutively active *CRY1* mutants: $CRY1^{W400A}$ and $CRY1^{G380R}$ (Gao *et al*., 2015). I attempted to obtain or recreate $CRY1^{W400A}$ however this was unsuccessful. This would have been a useful comparison between the *CRY1* and *phyB*.

YHB has a strong HL acclimation phenotype however *phyB-9* does not (Alvarez-Fernandez *et al*., 2021). There are some solutions to this apparent issue. The red light may not have been intense enough to saturate the phytochrome response in the lower leaf. The lack of saturation made the difference of HL acclimation phenotypes between *phyB-9* and the WT control insignificant. YHB, however, always has a saturated red light response (Su and Lagarias, 2007; Hu *et al*., 2009). Another explanation may be that other phytochromes were increased in expression to rescue the HL acclimation phenotype but do not have a strong impact on other *phyB-9* phenotypic effects such as morphology and photomorphogenesis (Yoshida *et al*., 2018).

The YHB phenotype may be related to the prominence of different *SPA* genes in various tissues. *SPA3* is far more prominent in adult plants than seedlings and *spa1* is the only *SPA* single mutant to have a strong flowering time phenotype (Fittinghoff *et al*., 2006; Laubinger *et al*., 2006; Table 4.6.1 [Page 163]). These potential photoreceptor binding affinities could change depending on the specific SPA proteins associated with the COP1/SPA complex and its ubiquitination targets. Potentially other phytochromes would be able to restore only the HL acclimation phenotype of *phyB-9*. Further study would be required to understand how photoreceptors interact with different COP1/SPA complexes.

Table 4.6.1: The HL acclimation phenotype, photomorphogenic phenotype, flowering times and of different HL acclimation mutants. (+) denotes a pre-acclimated phenotype, longer hypocotyls, and later flowering respectively with the number of (+) being representative of the strength of the phenotype. (-) is used similarly to denote a reduced HL acclimation ability, shorter hypocotyls, or an earlier flowering time respectively. (~) denotes no change from a wild-type control. (*) indicates the HL acclimation phenotypes were discovered within this section or Alvarez-Fernandez *et al*. (2021).

Mutant	HL acclimation phenotype*	Photomorphogenic phenotype	FT / Leaf No at FT phenotype (SD/LD)	Photomorphogenesis reference	Flowering time reference
cop1-4	+ + +	- - -	- / ~	Stacey *et al*. (2000)	McNellis *et al*. (1994)
cry1	- -	+ +	+ (12/12)	Wu and Spalding (2007)	Bagnall *et al*. (1996)
YHB	+ + +	- - -		Su and Lagarias (2007)	
spa123	+ + +	- - -	/ ~	Laubinger *et al*. (2004)	Hong-Li *et al*. (2011)
spa1	+	~	- - - / ~	Laubinger *et al*. (2004)	Laubinger *et al*. (2006)
spa2	+ +	~	~ / ~	Laubinger *et al*. (2004)	Laubinger *et al*. (2006)
spa3	+ +	~	~ / ~	Laubinger *et al*. (2003)	Laubinger *et al*. (2006)
spa4	+ +	~	~/ ~	Laubinger *et al*. (2003)	Laubinger *et al*. (2006)
BBX32-OX	- - -	+ +	+ / +	Holtan *et al*. (2011)	Tripathi *et al*. (2017)
hy5-2	- - -	+++		Zhang *et al*. (2017)	

SPA genes and photomorphogenesis and flowering time implies that different COP1/SPA complexes have different protein target affinities and therefore different regulatory patterns. *SPA1* is more involved in flowering time and response to far red light but doesn't have as strong of a role in HL acclimation (Laubinger *et al*., 2006). Several analytical methods can be used to further determine the roles of the different COP1/SPA complexes.

RNA-seq analysis can be performed on the *SPA* single mutants to understand the changes in steady state transcriptional regulation. The mis-regulated genes can be overlapped to attempt to understand the causes of the HL acclimation phenotype. They can also be contrasted to identify differences between the different *SPA* genes. Mutant plants overexpressing *SPA* genes may also be useful for a RNA-seq analysis. Instead of removing 4 potential COP1/SPA complexes, a strong over-expressor would potentially lead to the domination of a single COP1/SPA complex configuration consisting of two COP1 proteins and two SPA proteins encoded by the overexpressing gene.

Another methodology for testing the functionality of the *SPA* genes is by testing protein binding affinities of specific COP1/SPA complexes. Constructs could be designed containing *COP1* and *SPA* genes linked together to force a specific composition of the COP1/SPA complex *in planta*. Once inserted into *Arabidopsis*, this could be used to identify functionalities that the specific COP1/SPA complex impacts. This insertion may rescue the phenotype of near lethal mutations such as *cop1-4* and *spaQ*. The insertion could also be tagged to enable co-

immunoprecipitation experiments to identify binding protein partners that may impact HL acclimation.

The interaction between light and HL acclimation can be investigated through further experimentation on photoreceptors and the COP1/SPA complexes however the usefulness outside of broadening knowledge on the subject is debatable. The COP1/SPA may be manipulated to increase yield, due to the increased rate of photosynthesis of *spa123* (Figure 4.4.6 [Page 148]; Figure 4.4.7 [Page 149]). However, this yield increase is doubtful due to the number of other functions the *SPAs* impact (Laubinger *et al*., 2003; Laubinger *et al*., 2004; Table 4.6.1 [Page 163]). Yield improvements within *BBX32* mutants have been discovered which is further down the pathway (Preuss *et al*., 2012). Investigating *BBX32* to determine why it can improve yield is likely to be more productive than further study of the *SPA* genes.

4.7: Conclusions of Chapter 4

- YHB, a consistutive red light signalling line, had a perturbed HL acclimation phenotype
- The *spa123* triple mutant had an accelerated HL acclimation phenotype and a greater carbon assimilation rate per area than the WT.
- Single SPA mutants also had a perturbed HL acclimation phenotype, and this may be an additive effect.

Chapter 5: Impacts of light acclimation on phytohormones and defence response

5.1: Introduction

Phytohormones are signalling chemicals that play key roles in the regulation of growth and development in plants (Müller and Munné-Bosch, 2021). They coordinate systemic environmental and stress responses including light responses such as photosynthesis and photomorphogenesis (Müller and Munné-Bosch, 2021; Lau and Deng, 2012). The COP1-HY5 system exists at the confluence between light and phytohormone signalling and are both critical HL acclimation genes (Vandenbussche *et al*., 2007; Gangappa and Botto, 2016; Blanco-Touriñán *et al*., 2020; Alvarez-Fernandez *et al*., 2021; Müller and Munné-Bosch, 2021). Phytohormones also coordinate the response to pathogen and herbivorous attack (Cao *et al*., 1997; Wu *et al*., 2012; Liu *et al*., 2015). This chapter analyses the changes in phytohormone coordination and pathogenic defences in relation to HL acclimation and the genes *HY5* and *BBX32*.

HY5 and COP1/SPA complexes integrate signals from the phytohormones; brassinosteroids (BR), cytokinins, gibberellins (GA) and jasmonates (JA) (Müller and Munné-Bosch, 2021). HY5 physically interacts with the key regulator of abscisic acid (ABA) signalling ABA-INSENSITIVE5 (ABI5) and plants overexpressing *HY5* are hypersensitive to ABA (Bhagat *et al*., 2021). Along with integrating HL signals, BBX32 also transduces signals from BR by interacting with PIF3 (Ravindran *et al*., 2021). GA inhibits DELLA protein activity which inhibits the activity of PIF3 (Alabadí

et al., 2008). This increases the levels of HY5; a key HL acclimation gene (Alvarez-Fernandez *et al*., 2021). JAs decrease the rate of GA-initiated DELLA degradation (Yang *et al*., 2012).

Phytohormone mutants alter photosynthesis through changes in gene expression and related feedback loops. Cytokinin-insensitive mutants perturb the regulation of nuclear and plastid photosynthesis-associated gene expression (Danilova *et al*., 2017; Müller and Munné-Bosch, 2021). SA biogenesis mutant *sid2* had a reduced Fq'/Fm' compared to the WT control (Mateo *et al*., 2006).

Increased light is known to alter the concentrations of certain phytohormones. The concentration of SA was increased within plants exposed to new higher light conditions (Mühlenbock *et al*., 2008). Huang *et al*. (2019) exposed seedlings to increased light conditions and transcriptomic analysis was performed. This data set has applicability issues to HL acclimation due to the use of seedlings and constant light; however, it was discovered that ABA and JA were both significantly perturbed (Huang *et al*., 2019).

Phytohormone GO terms were significant from the *BBX32-HY5* HL RNA-seq (Chapter 3 [Page 63]). The "Response to GA" was significant from the list of DEGs downregulated by both BBX32-10 and *hy5-2* (Section 3.4 [Page 73]). The *DELLA* genes are suppressed by GA levels and two of these genes, *RGL1* and *RGL2*, were upregulated within BBX32-10 and *hy5-2* (Hauvermale *et al*., 2012; Figure 3.4.4 [Page 80]). *GAI* is a member of the HL TF network and was the first *DELLA* gene to be discovered (Koorneef *et al*., 1985). The DEGs upregulated in both BBX32-10 and

hy5-2 produced “Response to ethylene” as a significant GO term (Figure 3.4.5 [Page 83]).

Analysis of the *Arabidopsis* mutants containing a constitutively active *phyB* gene, a red light photoreceptor, was found to have a perturbed light acclimation phenotype (Section 4.3 [Page 131]). A microarray experiment was performed on this mutant by Hu *et al*. (2009) and GO analysis was performed on this data set (Section 4.3 [Page 131]). YHB had three significantly altered phytohormone GO terms using the upregulated DEGs list (Figure 4.3.3 [Page 137]). “Response to brassinosteroid”, “Gibberellic acid (GA) mediated signalling pathway” and “Auxin-activated signalling pathway” were significant GO terms of this upregulated gene list. However, as seedlings were used for the microarray analysis, it is difficult to determine if these effects would occur in mature plants such as those used throughout this study. These alterations in phytohormone regulation prompted analysis of widespread changes in phytohormone response using the *BBX32-HY5* HL RNA-seq data set.

Pathogen and herbivorous attack initiates change in the regulation of phytohormones to initiate a defensive reaction (Mühlenbock *et al*., 2008; Broekgaarden *et al*., 2015). SA and JA are traditionally viewed as the defence-centric phytohormones however ethylene and ABA also have a role in defence (Broekgaarden et al., 2015). Photoinhibition, excess light-driven programmed cell death, was also driven through a similar pathway involving ethylene and the SA-promoting EDS1-PAD4 module (Mühlenbock *et al*., 2008; Cui *et al*., 2017). Plants exposed to increased light conditions had an increased resistance to certain pathogens. Excess light exposed plants were more resistant to pathogenic infection by Pseudomonas syringae (pv.

tomato DC3000) than control plants (Mühlenbock *et al*., 2008). This was hypothesised to be linked to the increase in SA caused by the increased light conditions.

This chapter aims to further the understanding of the link between phytohormones, defence and light acclimation. This involves analysing the expression of phytohormone marker genes and 'response to' phytohormone gene groups from the BBX32-HY5 HL RNA-seq data set (Alvarez-Fernandez *et al*., 2021). The light acclimation ability of phytohormone and defence mutants could also be used to understand the converse impacts.

5.2: Methods

5.2.1: 'Response to' phytohormone GO analysis

The 'Response to' different phytohormone analysis was performed following the methodology outlined in section 2.4.6 [Page 53]. This methodology was employed to gain an understanding of the change in concentration of the different phytohormones immediately following HL acclimation initiation. Smaller changes most likely wouldn't be clear however it was hoped that any large changes in phytohormone responses could be identified for further analysis.

5.2.2: SA spraying of *Arabidopsis thaliana*

Spraying of *Arabidopsis* with 10 mM SA was carried out following the methodology outlined in section 2.3.7 [Page 41]. 10 mM SA is in great excess, however the plants were not checked for infiltration of the SA solution for example using RT-qPCR.

5.2.3: Infiltration of Arabidopsis with *Pseudomonas syringae*

6-week-old *Arabidopsis thaliana* plants were infiltrated with *Pseudomonas syringae pv. Tomato* (DC3000) using the methodology outlined in section 2.3.13 [Page 49]. The syringe methodology was used instead of a vacuum infiltration methodology. Vacuum infiltration requires a vacuum to be pulled on plants coated in the infiltrating bacteria. The removal of the vacuum causes an inrush of air which pulls some of the bacterial cells into the intercellular space of the leaf. This methodology is quite damaging to the whole plant when compared to the syringe method. The *Pseudomonas* infection was aimed to be paired with HL acclimation in future experimentation and damaging the whole plant was deemed unacceptable.

5.2.4: EDS1-PAD4 module RNA-seq

Cui *et* al., (2017) created an *Arabidopsis* plant transformed with 35S:EDS1 and 17β-oestradiol inducible *PAD4*. A comparison was performed between induced and mock plants using RNA-seq. RNA extracts were taken 6, 12 and 24 hours post induction/mock. The count table for this experiment was downloaded from the GEO database (GSE80585) and processed using DeSeq2 (section 2.4.3 [Page 51]). Significant genes were discovered using the RStudio (section 2.4.1 [Page 51]) and processed according to the time point of their significance (6, 12, and 24 hours post induction).

5.3: Phytohormones and defence in *BBX32* mutant plants

This section aims to analyse the changes in response to phytohormones within HL exposed plants and HL acclimation mutants and to further explore the implications of these alterations. There are many phytohormones that can be studied so a method

was developed to analyse changes in the 'Response to' phytohormone GO groups using the *BBX32-HY5* HL RNA-seq data set. The LL data sets of *hy5-2* and BBX32-10 and Col-0 HL were compared to Col-0 LL data set to analyse changes caused by the HL acclimation and HL acclimation mutants.

5.3.1: Analysis of phytohormone response to light acclimation

Each of the 'Response to' phytohormone GO terms have an associated gene list which can be analysed. Each of these gene lists were gathered (Table S1 [Page 337]). The $\log_2$ fold change of each of these genes from BBX32-10 LL, *hy5-2* (HY5) LL and Col-0 HL all compared to Col-0 LL were gathered and these were plotted as a box plot (Figure 5.3.1 [Page 171]).

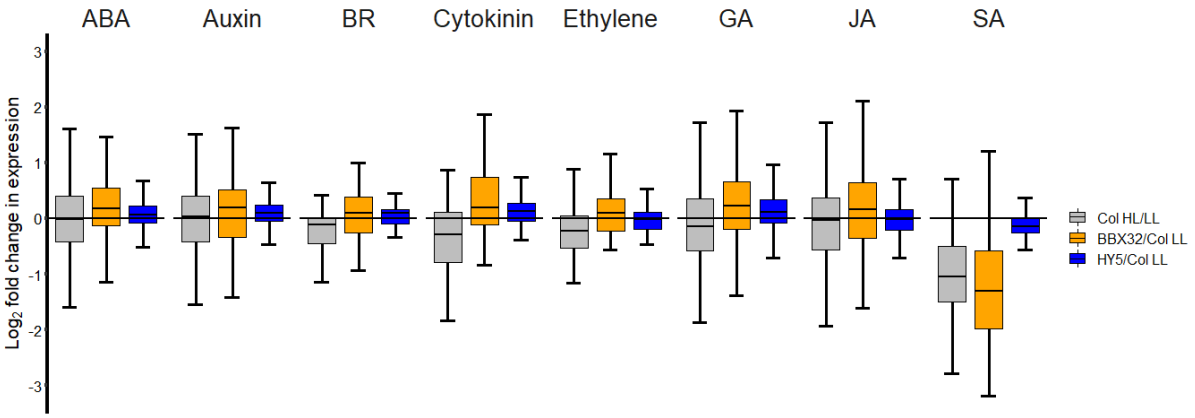

Figure 5.3.1: The mean change in expression of 'Response to' phytohormone groups within BBX32-10, *hy5-2* and Col-0 HL when compared to a Col-0 LL control. Expression was obtained from BBX32-10 (BBX32), *hy5-2* (HY5) or Col-0 under LL or HL conditions for 3.5 hours of exposure.

Most of the 'Response to' phytohormone groups had a $\log_2$ fold change close to 0 indicating no overall mean change to the mean expression in Col-0 LL. However, SA

response compared to Col-0 LL was strongly decreased within Col-0 HL and BBX32-10. This change was not apparent within *hy5-2* mutants. The light driven SA response may be mediated through *BBX32*. The impact of SA can be directly measured by measuring the light acclimation phenotype of SA treated plants.

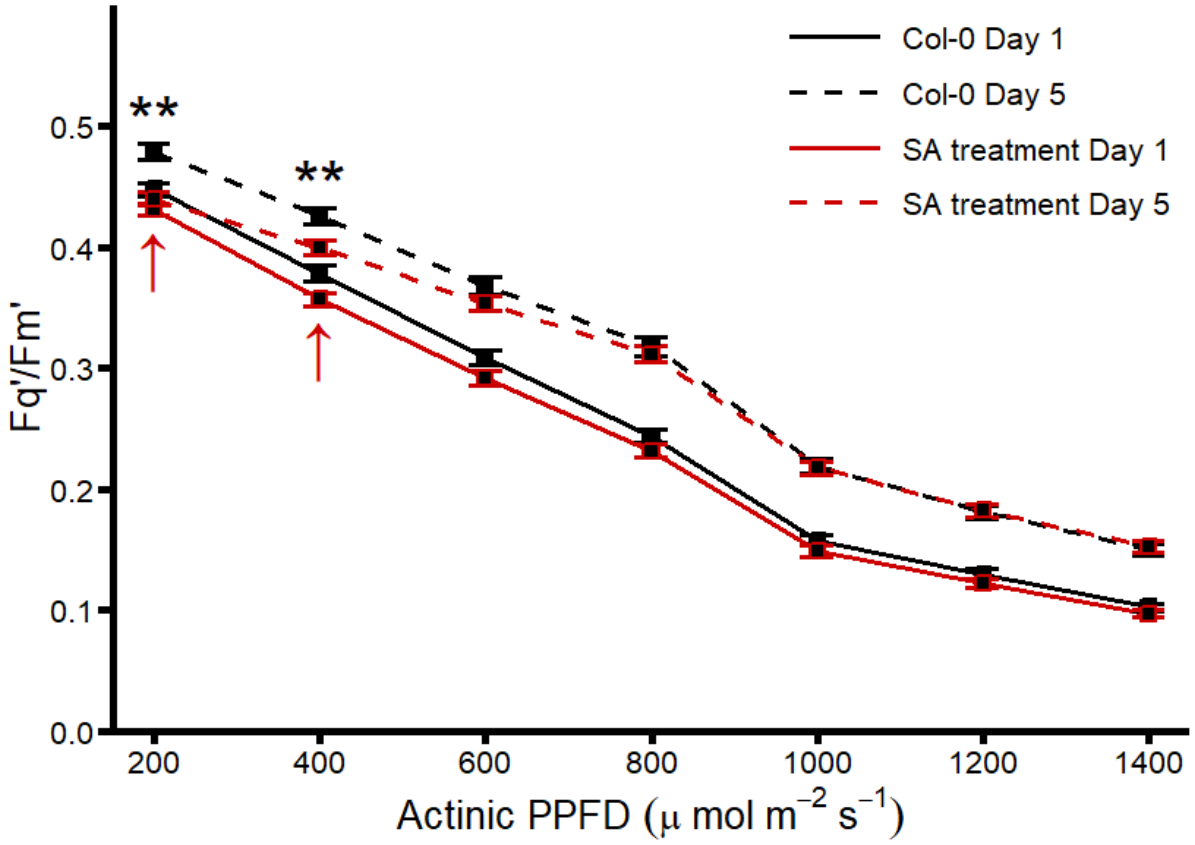

Figure 5.3.2: HL acclimation of SA-treated and control Col-0 plants. SA treated plants were sprayed with 10 µmol SA and 0.001 % trizol-100 in water and control plants were sprayed with 0.001 % trizol-100 in water. Plants were sprayed each day prior to light exposure. Fq'/Fm' is determined by chlorophyll fluorescence with a light intensity range of 200 µmol m^{-2} s^{-1} to 1400 µmol m^{-2} s^{-1} at 200 µmol m^{-2} s^{-1} increments. Measurements were taken from 4-6 week old plants with a minimum of 6 mature leaves each (means ± SE). Arrows and asterisks denote a significant difference

between the day 1 and day 5 values respectively of the mutants and Col-0 (ANOVA, post-hoc GH; */↑ = $p < 0.05$; **/↑↑ = $p < 0.005$).

The SA treatment did not appear to significantly alter the HL acclimation ability of the plants. The only significant changes between SA treated and control plants were small changes at lower PPFDs (200 and 400 µmol m^{-2} s^{-1}). The infiltration of the SA solution was not confirmed by a methodology such as RT-qPCR however as the SA was in great excess this wasn't deemed necessary. If the SA-treated plants had a strong HL acclimation phenotype, a RT-qPCR experiment to ascertain the response of SA induced genes, such as *PR1*, would have become necessary.

SA is required for a robust response to pathogens and induces systemic acquired resistance (SAR; Cao *et al*., 1997; Kesarwani *et al*., 2007; Wu *et al*., 2012). Reducing SA response may centre around altering resource allocation away from defence and towards altering the composition of the photosynthetic apparatus (Alvarez-Fernandez *et al*., 2021). The expression of SA marker genes can be analysed to identify probable changes in SA levels.

5.3.2: The expression of defence genes in light acclimation mutants

The PATHOGENESIS-RELATED genes (*PR* genes) respond quickly in increased expression to various, typically biotrophic, pathogens (Lawton *et al*., 1994; Cameron *et al*., 1999; Ali *et al*., 2018). This increase is mediated through a pathway involving SA (Lawton *et al*., 1994).

SA dependent systemic acquired resistance (SAR) can be identified using the expression of the *PR* genes (*PR1*, *PR2* and *PR5*) as marker genes (Hamamouch *et al*., 2011; Ali *et al*., 2018). *PR3* and *PR4* are excluded from this list as their expression is driven in a JA-dependent manner as opposed to an SA-dependent manner (Hamamouch *et al*., 2011).

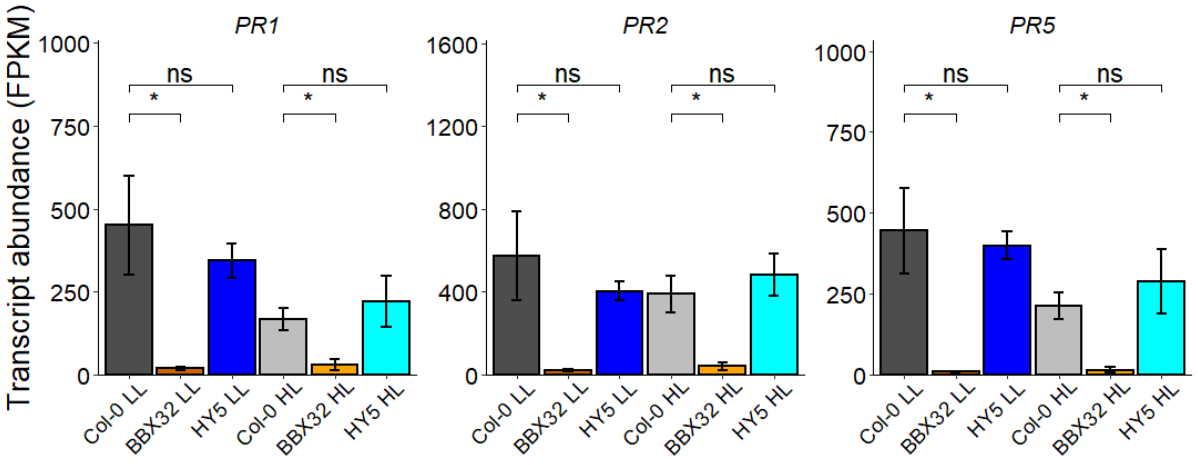

Figure 5.3.3: The expression of *PR* genes from the *BBX32-HY5* HL RNA-seq. Expression was obtained from BBX32-10 (BBX32), *hy5-2* (HY5) or Col-0 under LL or HL conditions for 3.5 hours of exposure. Asterisks and bars show genes that were significantly changed in expression between the LL and HL groups of each genotype ($p < 0.05$; ANOVA).

There was a clear decrease in the expression of the *PR* genes in BBX32-10 which was not found in the *hy5-2* mutant. This change was specific to the BBX32-10 mutant however the drop in *PR1* expression was also significant between Col-0 LL and Col-0 HL. HL had an impact on the expression of *PR1* however this change was not as strong as the effects of *BBX32* overexpression across all of the SA dependent *PR* genes.

The response to SA signalling was decreased however it is unknown how BBX32-10 and HL decrease SA levels. The rate limiting step of SA production is catalysed through the *ISOCHORISMATE SYNTHASE* genes and their expression is closely linked to SA production (Wildermuth *et al*., 2001; Garcion *et al*., 2008). The NPR proteins act as SA receptors and impact the expression of the *PR* genes (Zhang *et al*., 2006; Wu *et al*., 2012). NPR1 positively regulates SAR response whereas NPR3 and NPR4 negatively regulate it (Zhang *et al*., 2006; Wu *et al*., 2012). The expression of the *ICS* and *NPR* genes from the *BBX32-HY5* HL RNA-seq were analysed.

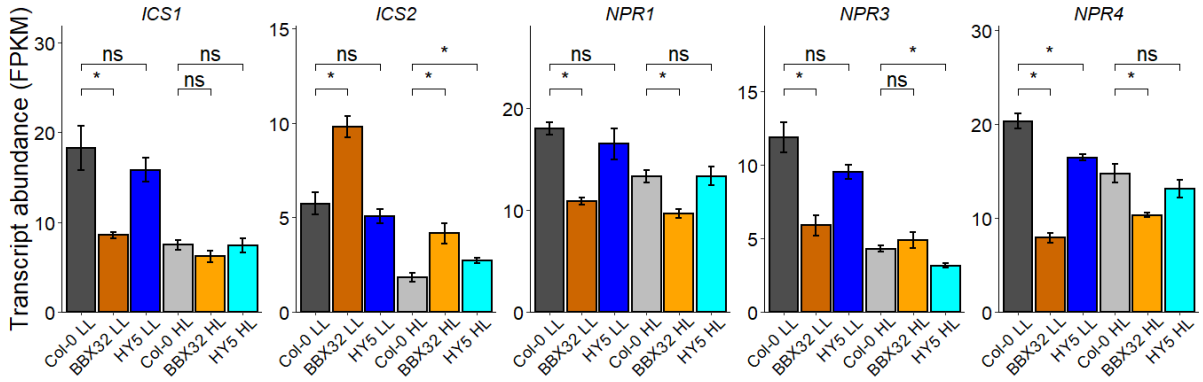

Figure 5.3.4: The expression of the NPR and ICS genes from the *BBX32-HY5* HL RNA-seq. Expression was obtained from BBX32-10 (BBX32), *hy5-2* (HY5) or Col-0 under LL or HL conditions for 3.5 hours of exposure. Asterisks and bars show genes that were significantly changed in expression between the LL and HL groups of each genotype ($p < 0.05$; ANOVA).

ICS2 significantly increased in expression in BBX32-10 however *ICS1* significantly decreased (Figure 5.3.4 [Page 175]). However, *ICS2* is less responsible for SA production than *ICS1* (Garcion *et al*., 2008). Both *ICS1* and *ICS2* decreased in

expression in response to HL implying a decrease in SA production under HL conditions. *NPR1*, *NPR3* and *NPR4* transcript levels were all significantly decreased by *BBX32* overexpression and by HL (Figure 5.3.4 [Page 175]). This matched the mean decrease in the “response to SA" GO group genes (Figure 5.3.1 [Page 171]).

To further understand the alteration of defence mechanisms by *BBX32* and HL, JA defence pathways were also analysed. PLANT DEFENSIN genes (*PDF* genes) coordinate defences and specifically have antifungal properties (Osborn *et al*., 1995; Stotz *et al*., 2009; Sher Khan *et al*., 2019). These genes are driven by the JA pathway and Figure 5.3.1 [Page 171] showed no clear change in the “response to JA” GO term mean expression. However, as these genes also coordinate defence, it was considered useful to understand if HL and *BBX32* impact other defence mechanisms or just those driven by SA. The expression of the *PDF* genes can be analysed from the *BBX32-HY5* HL RNA-seq to compare against the *PR* genes.

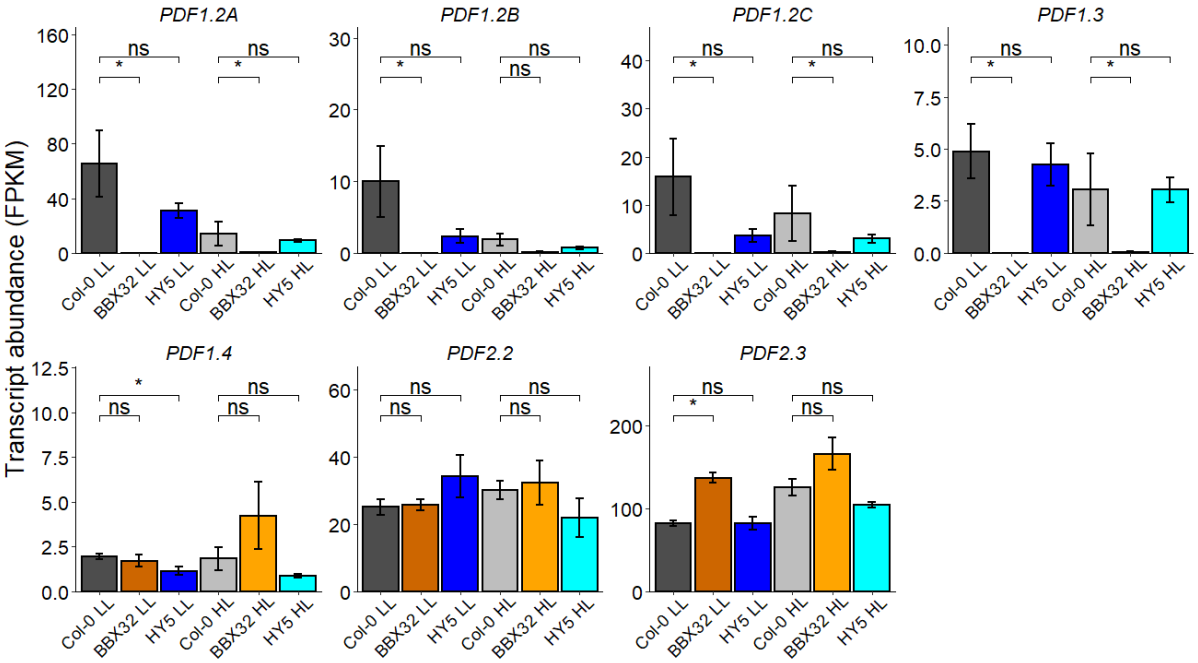

Figure 5.3.5: The expression of *PDF* genes from the *BBX32-HY5* HL RNA-seq.

Expression was obtained from BBX32-10 (BBX32), *hy5-2* (HY5) or Col-0 under LL or HL conditions for 3.5 hours of exposure. Asterisks and bars show genes that were significantly changed in expression between the LL and HL groups of each genotype ($p < 0.05$; ANOVA).

Not all of the *PDF* genes were detected in the *BBX32-HY5* RNA-seq and these were excluded from the analysis in Figure 5.3.5 [Page 176]. Very few or no reads of *PDF1.2A*, *PDF1.2B*, *PDF1.2C* and *PDF1.3* were recorded in the BBX32-10 mutants under both LL and HL conditions. *BBX32* overexpression therefore suppresses the expression of both SA and JA signalling defence genes.

The plant defence heterodimer EDS1-PAD4 regulates the response to bacteria and fungi upstream of SA induction (Cui *et al*., 2017). The EDS1-PAD4 module is also capable of initiating a defence response in plants deficient in SA biosynthesis (Straus *et al*., 2010; Cui *et al*., 2017). The ability of HL and *BBX32* to modulate a defence response independent of SA induction may explain the repression of JA mediated *PDF* genes.

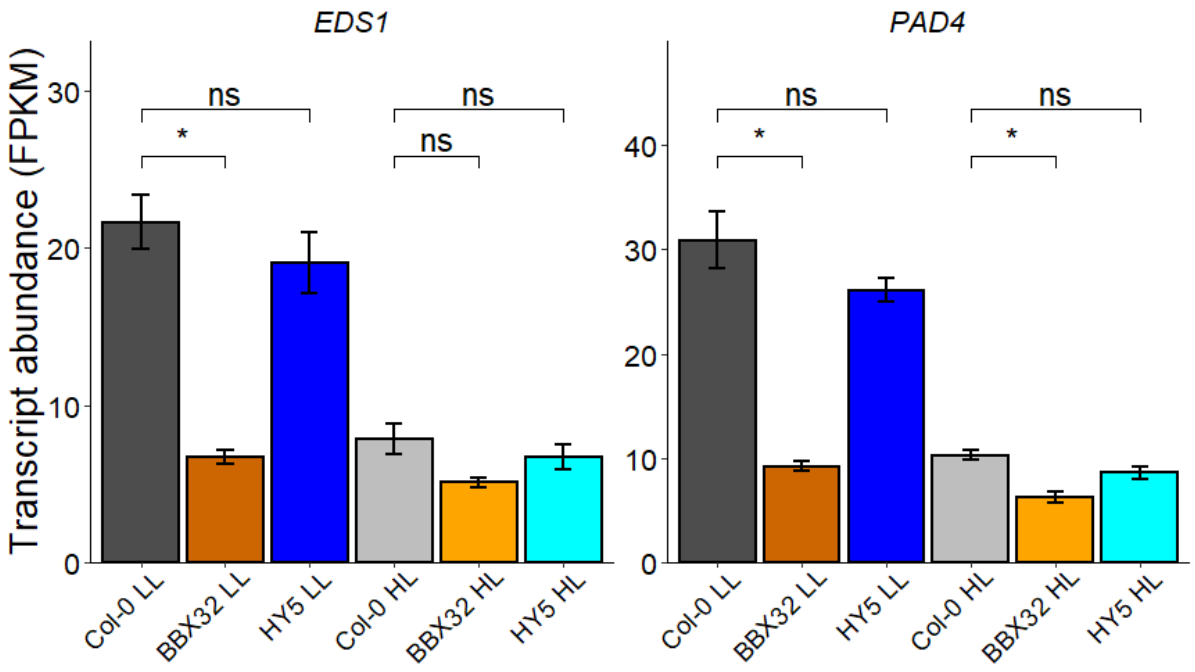

Figure 5.3.6: The expression of EDS1 and PAD4 genes from the *BBX32-HY5* HL RNA-seq. Expression was obtained from BBX32-10 (BBX32), *hy5-2* (HY5) or Col-0 under LL or HL conditions for 3.5 hours of exposure. Asterisks and bars show genes that were significantly changed in expression between the LL and HL groups of each genotype ($p < 0.05$; ANOVA).

There is a similar decrease in the expression of *PAD4* and *EDS1* by BBX32-10 and HL. The expression profiles of *PAD4* and *EDS1* are very similar which is potentially due to their combined functionalities (Wagner *et al*., 2013; Cui *et al*., 2017). All of these changes can be analysed further in the HL microarray experiment performed by Alvarez-Fernandez *et al*. (2021) to understand how the expression of these genes are impacted by HL over time. *PR1* and the significant *PDF* genes (*PDF1.2a* - *PDF1.3*) do not have CATMA references and therefore cannot be analysed. *PDF1.1*, an undetected gene in the *BBX32-HY5* HL RNA-seq, was substituted for the missing *PDF* genes.

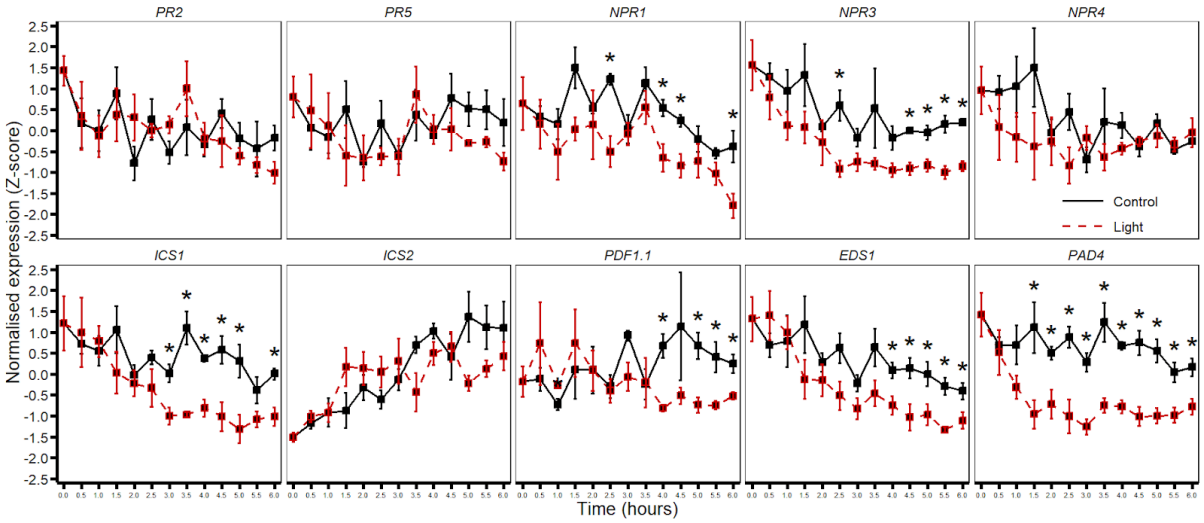

Figure 5.3.7: The expression defence related genes from the Alvarez-Fernandez *et al*. (2021) time series acclimation microarray experiment. Asterisks and bars show time points that were significantly changed in expression between the control and light groups (n = 4; $p < 0.05$; ANOVA).

PR2, *PR5*, *NPR4* and *ICS2* displayed no significant changes of expression at any time point. However, the other genes only had significantly decreased expression changes and no significantly increased expression changes. HL and *BBX32* altered defence response which has impacted SA response. Many of the analysed genes associated within defence are suppressed by HL and *BBX32* overexpression. Therefore, a hypothesis was developed that predicted that BBX32-10 plants were more vulnerable to infection. This can be tested directly by infecting the plants with a pathogen and measuring the rate of proliferation.

5.3.3: *Pseudomonas* infection of *BBX32* over-expressor mutants

The bacterium *Pseudomonas syringae* (DC3000) induces the SA pathway to bring about systemic acquired resistance in *Arabidopsis thaliana* (Yalpani *et al*., 1991; Cao

et al., 1997). Mutations that disrupt the SA and defence pathways alter the ability to reduce the proliferation of pathogens such as *Pseudomonas syringae* (Cao *et al*., 1997; Wildermuth *et al*., 2001; Cui *et al*., 2017). Analysing the defensive capabilities of HL exposed plants would be very difficult as *Arabidopsis* is easier to infect with *Pseudomonas* soon after dawn (Liu *et al*., 2015). 4 hours of HL exposure would make infiltration far more difficult therefore *BBX32* mutants were used as a substitute for HL. Expression of defence related genes were perturbed in BBX32-10 in the *BBX32-HY5* HL RNA-seq data set, and which is similar to the HL exposed plants when both are compared to Col-0 LL (Figure 5.3.3 [Page 174]; Figure 5.3.4 [Page 175]; Figure 5.3.5 [Page 176]; Figure 5.3.6 [Page 178]). This can be tested through infecting BBX32-10, BBX32-12*,* and Col-0 with *Pseudomonas syringae* and measuring the rapidity of bacterial proliferation.

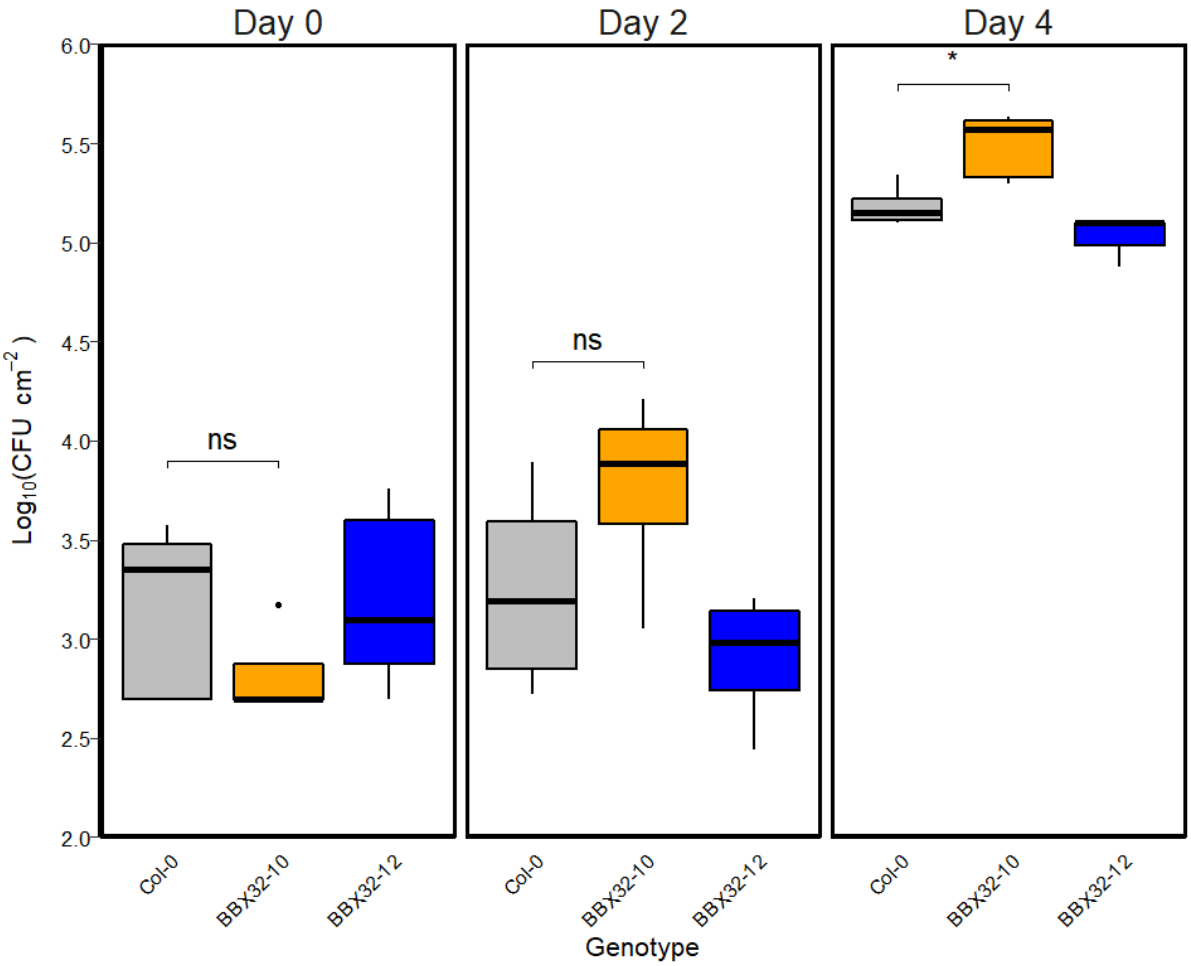

Figure 5.3.8: Colony forming units (CFU) per cm^2 of *Pseudomonas syringae pv. tomato* (DC3000; *Pst*) produced over 4 days of infection of different *Arabidopsis thaliana* genotypes. Plants were grown under short day (8:16, day: night) conditions with 150 µmol m^{-2} s^{-1} of light for 6 weeks were infected by *Pst*. at OD = 0.00002 (n = 5). Extracts were taken immediately after infection (day 0), day 2 and day 4 and diluted in series before being allowed to grow on LB plates for 48 hours (asterisks denote $p < 0.05$).

There was an increased number of colony forming units (CFU) per cm^2 in the extracts from the BBX32-10 mutant compared to Col-0 (Figure 5.3.7 [Page 179]). Therefore, it was concluded that the BBX32-10 genotype is more vulnerable to

Pseudomonas syringae infection than the Col-0 control. BBX32-12 did not have a significant impact on *Pseudomonas* proliferation possibly due to the lower *BBX32* expression in this genotype compared with BBX32-10 (Holtan *et al*., 2011).

5.3.4: Conclusion

HL exposure reduced the expression of many defence-centric genes associated with SA and JA (Figure 5.3.3 [Page 174]; Figure 5.3.4 [Page 175]; Figure 5.3.5 [Page 176]; Figure 5.3.6 [Page 178]). This change in expression was mimicked in the BBX32-10 plants but to an increased degree. BBX32-10 plants had a very limited to undetectable expression of many *PDF* and *PR* genes (Figure 5.3.3 [Page 174]; Figure 5.3.5 [Page 176]). The defensive capability against *Pst* infection of BBX32-10 was also diminished (Figure 5.3.8 [Page 181]). In the next section, I aimed to test the converse, the HL acclimation ability of defence response mutants.

5.4: The impact of defence on HL acclimation

This section aims to test the light acclimation ability of some of the integral defence genes in the SA pathway. Spraying plants with SA did not perturb light acclimation however it has not been determined if genes in the SA-dependent defence pathway can impact light acclimation. Mutants of genes that drive the SA pathway may have a role in defence impacting HL acclimation or being integral to the HL acclimation pathway in a defence-independent manner. HL acclimation experiments were performed on different defence mutants to test these hypotheses.

5.4.1: HL acclimation phenotype of defence response mutants

NPR1 is required for SA induced *PR* gene expression and was significantly reduced in expression by BBX32-10 and HL (Figure 5.3.3 [Page 174]). *NPR3* and *NPR4* are homologues of *NPR1* with similar SA binding properties however they negatively impact SA induction and *PR* gene expression (Cao *et al*., 1997; Fu *et al*., 2012; Ding *et al*., 2018). These genes were analysed as the double mutant *npr3npr4* as this combination displays a stronger perturbation in SA response (Ding *et al*., 2018). *NPR* gene mutants can be experimented upon to test their HL acclimation phenotype.

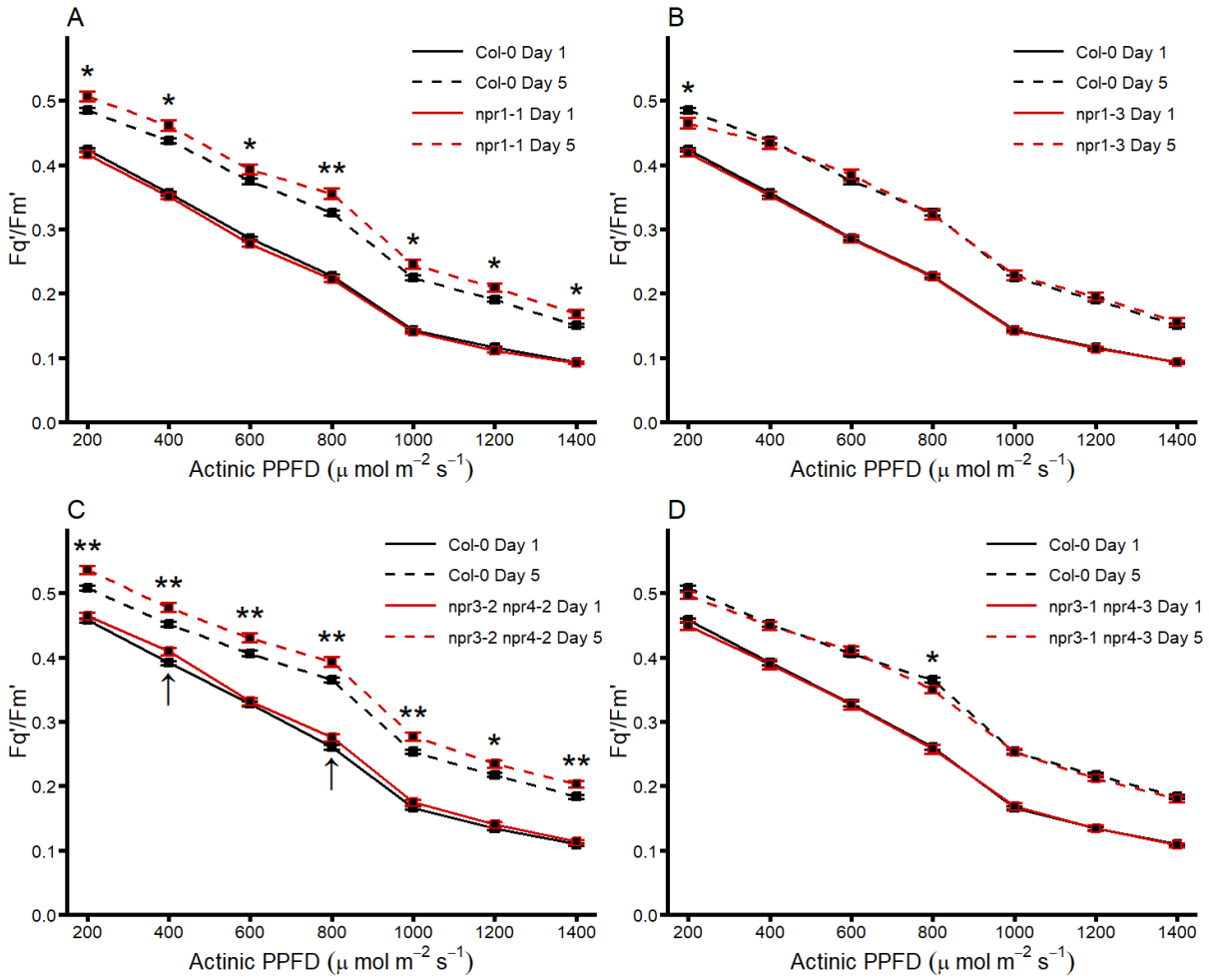

Figure 5.4.1: Acclimation of *npr1-1* (A), *npr1-3* (B), *npr3-2 npr4-2* (C), *npr3-1 npr4-3* (D) and Col-0 plants. Fq'/Fm' was determined by chlorophyll fluorescence

with a light intensity range of 200 µmol m^{-2} s^{-1} to 1400 µmol m^{-2} s^{-1} at 200 µmol m^{-2} s^{-1} increments. Measurements were taken from 4–6-week-old plants with a minimum of 6 mature leaves each (means ± SE). Arrows and asterisks denote a significant difference between the day 1 and day 5 values respectively of the mutants and Col-0 (ANOVA, post-hoc GH; */↑ = $p < 0.05$; **/↑↑ = $p < 0.005$).

The *npr1-1* allele had a slightly significant impact on day 5 however *npr1-3* did not have a perturbed light acclimation phenotype (Figure 5.4.1 [Page 183]). A similar effect was seen between the *npr3npr4* mutants. Both *npr1* mutants were created by EMS mutagenesis and the *npr3npr4* mutants were generated through T-DNA insertion (*npr3-2 npr4-2*) and fast neutron-mutagenesis (*npr3-1 npr4-3*) and crossing (Zhang *et al*., 2006). The effect on light acclimation of the *npr1* and *npr3npr4* mutations would have opposite effects due to their inverse effects on SA and *PR* gene expression (Ding *et al*., 2018). Therefore, I have concluded that the *NPR* genes had no effect on HL acclimation.

The *sid2-2* mutant has a disrupted *ICS1* gene which catalyses the conversion of chorismate to isochorismate (Wildermuth *et al*., 2001). This is the rate-limiting step of SA production (Gaille *et al*., 2003). Disruption of *ICS1* significantly reduces the production of SA and impairs the coordination of defence response to pathogens (Wildermuth *et al*., 2001; Block *et al*., 2005). To test the role of SA in light acclimation, *sid2-2* was exposed to HL conditions and chlorophyll fluorescence measurements were conducted.

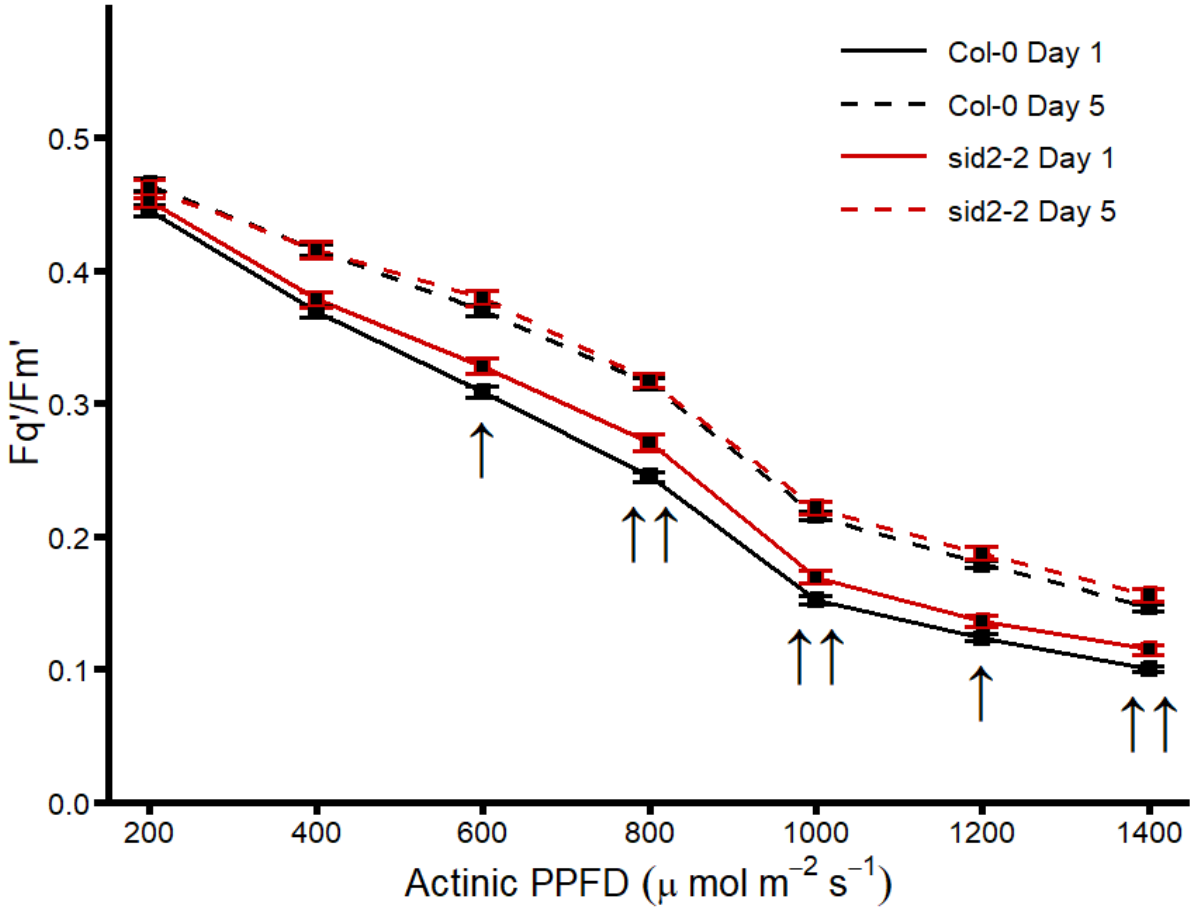

Figure 5.4.2: HL Acclimation of *sid2-2* and Col-0 plants. Fq'/Fm' was determined by chlorophyll fluorescence with a light intensity range of 200 µmol m^{-2} s^{-1} to 1400 µmol m^{-2} s^{-1} at 200 µmol m^{-2} s^{-1} increments. Measurements were taken from 4-6 week old plants with a minimum of 6 mature leaves each (means ± SE). Arrows and asterisks denote a significant difference between the day 1 and day 5 values respectively of the mutants and Col-0 (ANOVA, post-hoc GH; */↑ = $p < 0.05$; **/↑↑ = $p < 0.005$).

sid2-2 had a weakly significant change in Fq'/Fm' on day 1 however no change was found on day 5. *sid2-2* had a skew in Fq'/Fm' on day 1 that was very similar but inverted to the skew seen in SA treated plants (Figure 5.3.2 [Page 172]). Manipulating genes further up the SA pathway may yield stronger results. However,

an increased susceptibility to pathogen infection does not necessarily mean an altered capability to undergo HL acclimation.

The EDS1-PAD4 heterodimer module acts upstream of SA to regulate defence. Perturbation of defence against *Pseudomonas syringae pv. tomato* (DC3000) and *PR1* expression requires the overexpression of both *PAD4* and *EDS1* (Cui *et al*., 2017). If the EDS1-PAD4 module impacts HL acclimation, the perturbation of either *PAD4* or *EDS1* would be expected to yield very similar impacts on the HL acclimation phenotype.

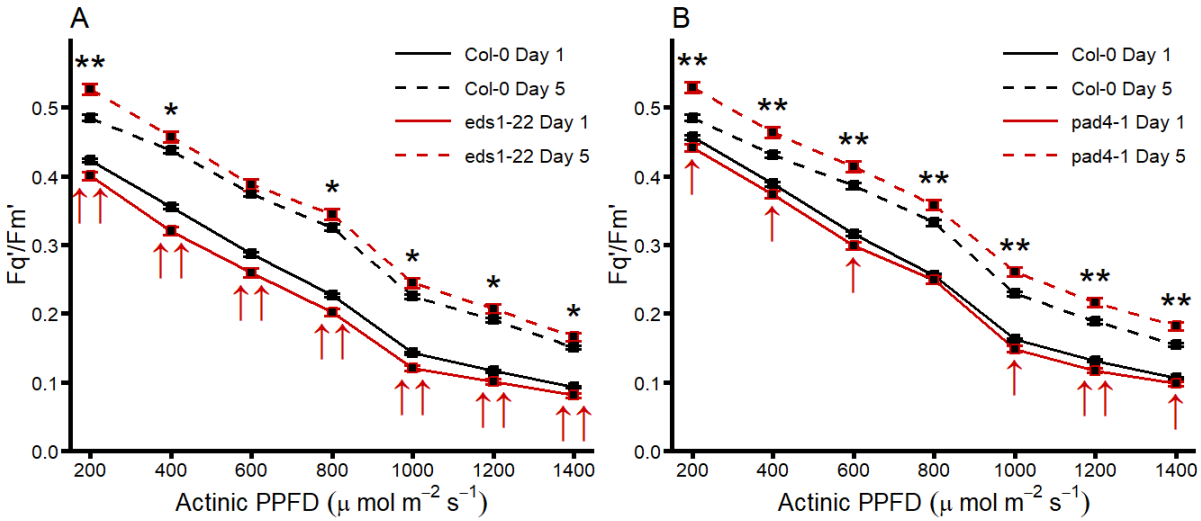

Figure 5.4.3: Acclimation of *eds1-22* (A), *pad4-1* (B) and Col-0 plants. Fq'/Fm' was determined by chlorophyll fluorescence with a light intensity range of 200 µmol m^{-2} s^{-1} to 1400 µmol m^{-2} s^{-1} at 200 µmol m^{-2} s^{-1} increments. Measurements were taken from 4–6-week-old plants with a minimum of 6 mature leaves each (means ± SE). Arrows and asterisks denote a significant difference between the day 1 and day 5 values respectively of the mutants and Col-0 (ANOVA, post-hoc GH; */↑ = $p < 0.05$; **/↑↑ = $p < 0.005$).

pad4-1 and *eds1-22* have very similar HL acclimation phenotypes (Figure 5.4.3 [Page 186]). The Fq'/Fm' was slightly reduced on day 1 but slightly increased on day 5 for both mutants (Figure 5.4.2 [Page 185). The similar phenotypes suggest a similar mechanism and therefore implicates the EDS1-PAD4 module as the cause. Analysis of gene expression in *EDS1* and *PAD4* mutant plants would be useful to determine how the EDS1-PAD4 module impacts on HL acclimation. Cui *et al*. (2017) performed an RNA-seq upon plants overexpressing *EDS1* with an inducible *PAD4* gene. This data set was analysed to identify light acclimation genes.

5.4.2: Genes induced by the EDS1-PAD4 module

Cui *et al*. (2017) induced *PAD4* expression in plant overexpressing *EDS1* and RNA-seq was performed on samples extracted 6, 12 and 24 hours post-induction. The data set analysed was reprocessed from the raw reads using Deseq2 to obtain genes that were both upregulated and downregulated and their corresponding p-adjust values (BH; v1.34.0; section 2.4.3 [Page 51] ; Love *et al*., 2014).

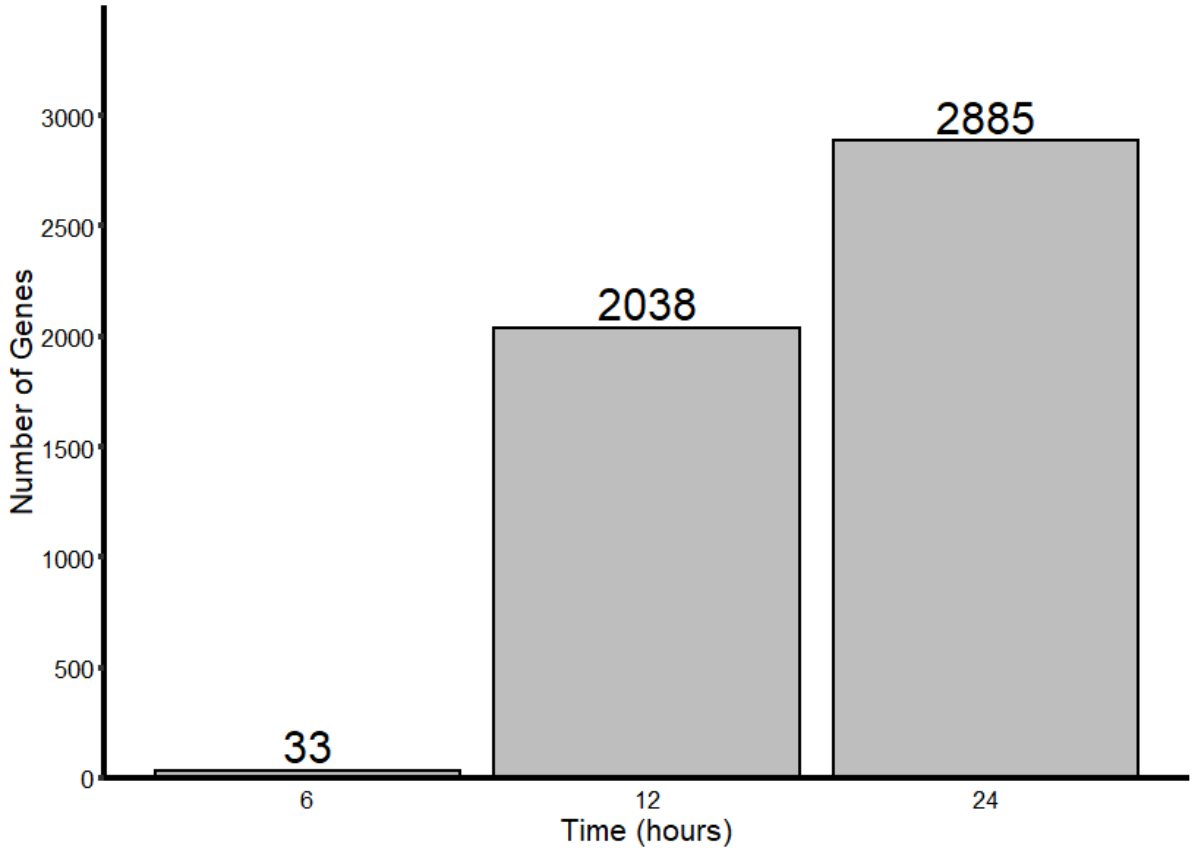

Figure 5.4.4: The number of significant differentially expressed genes after *PAD4* induction in inducible *PAD4* 35S:EDS1 plants compared to WT controls. Data was obtained from an RNA-seq performed in Cui *et al*., (2017) and reprocessed (p adjusted value < 0.05; post-hoc BH).

A provisional analysis revealed a number of HL acclimation genes with altered expression between the induced mutant and controls. The light acclimation gene *LHCB4.3* was one of the 33 genes significant at 6 hours and was repressed in expression (Figure 5.4.3 [Page 186]; Table S4 [Page 337]). At the 12-hour time point, *GLK2*, a HL acclimation gene (section 3.6 [Page 107]), was the 10th most significantly differentially expressed gene. *GNC* was significantly upregulated within both BBX32-10 and *hy5-2* (section 3.4 [Page 73]) and was highly significant at the 12-hour time point. *SIGMA FACTORA* (*SIGA*) and *SIGMA FACTOR BINDING*

PROTEIN1 (*SIB1*) are also in the top 100 most differentially expressed genes at the 12-hour time point and these genes drive chloroplastic photosynthetic-gene expression (Tanaka *et al*., 1997; Lv *et al*., 2019). The decision was made to analyse the expression changes of many different light acclimation associated genes across all the time points measured in the *EDS1-PAD4* induced RNA-seq data set.

Table 5.4.1: The change in expression of light acclimation associated genes 6, 12 and 24 hours after *PAD4* induction in 35S:EDS1 plants compared to WT control. Green indicates a significantly increased expression and red indicates a significant decrease in expression at the given time point.

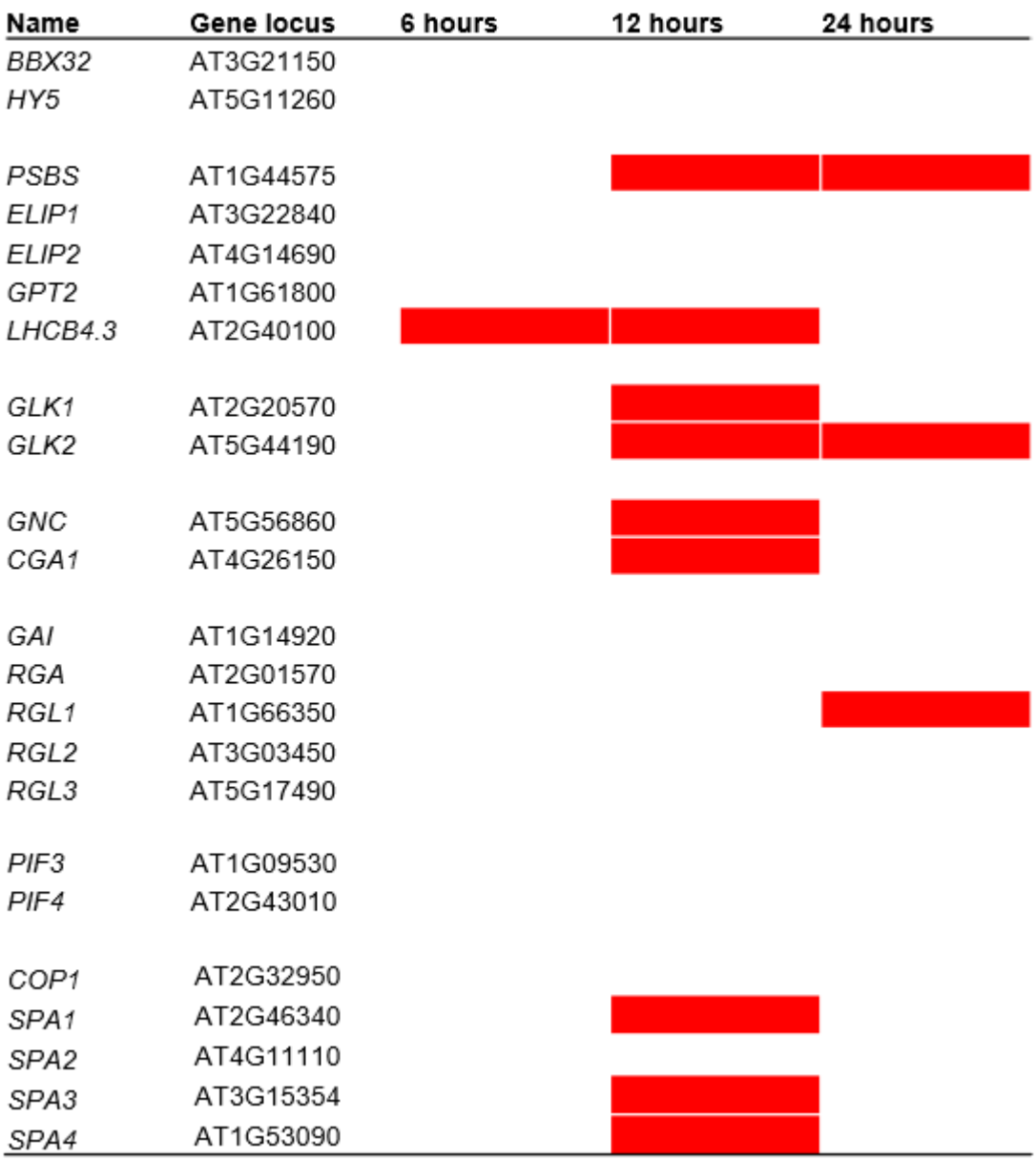

All the analysed light acclimation associated genes were either not significantly altered by the induction of *PAD4* expression in 35S:EDS1 plants or were significantly downregulated as indicated by the red blocks within Table 5.4.1 [Page 189]; none of the genes analysed were significantly upregulated. Much of the network acts to negatively regulate downstream network members (Figure 4.6.1 [Page 161]) such as the discovered relationship between the *GLK* genes however no light acclimation genes analysed were upregulated (Table 5.4.1 [Page 189]).

This table is highly comparable to Figure 5.3.8 [Page 181] which showed the only significant decreases in expression of many defence associated genes in response to HL. In Table 5.4.1 [Page 189], many HL acclimation associated genes were significantly decreased in expression by the induction of *PAD4* and none were significantly increased (Table 5.4.1 [Page 189]).

5.4.3: Conclusion

None of the defence mutants analysed had a strong HL acclimation phenotype. *eds1-22* and *pad4-1* exhibited the strongest light acclimation phenotypes however these were not nearly as strong as light acclimation phenotypes of genes discovered previously (Chapter 3 [Page 63]; Chapter 4 [Page 125]; Athanasiou *et al*., 2010; Alvarez-Fernandez *et al*., 2021). The EDS1-PAD4 module was capable of altering the light acclimation pathway however the entry point to the pathway remains unknown. Through the impact in expression, it appears the EDS1-PAD4 module does not impact the light acclimation pathway prior to *HY5* and *BBX32* on a transcriptional level but does impact some HL acclimation genes. The impact of the EDS1-PAD4 module, however, could not be discerned through the HL acclimation methodology (section 2.2.2 [Page 35]).

5.5: Discussion

During HL acclimation, *Arabidopsis thaliana* appears to reduce its own defensive capabilities (Alvarez-Fernandez *et al*., 2021). However, perturbing these defensive pathways had a very limited impact on light acclimation ability. Defence and light acclimation are important traits for plant productivity and their interconnectedness is

not yet well understood. The reasons why this relationship could be beneficial are further explored within this discussion.

5.5.1: HL and *BBX32* overexpression depress defence

There appears to be a contradiction in between the light acclimation and defence capabilities of *Arabidopsis thaliana*. Defensive genes are repressed in both HL exposed and BBX32-10 plants when compared to the control but not in *hy5-2*. Considering that HL promotes HL acclimation and *BBX32* overexpression represses light acclimation, why do they have similarly perturbed defensive capabilities? This is exacerbated by the lack of involvement of *HY5*.

This may allude to the functionality of *BBX32* in light acclimation. The true role of *BBX32* is unknown however it acts as a negative regulator of photomorphogenesis through *HY5* (Holtan *et al*., 2011). This pathway potentially uses BBX21 as an adaptor to interact with HY5 and repress photomorphogenesis (Holtan *et al*., 2011). The interaction between BBX32 and other BBX proteins is discussed further during Chapter 6 [Page 197] and Chapter 7 [Page 260] however it is relevant here to understand how BBX32 interacts with other proteins.

Holtan *et al*. (2011) hypothesised that BBX32 uses bridging proteins to link influence transcription. The *TCP* genes connect developmental, hormonal and defence processes and some are capable of binding to BBX32 (Zhang *et al*., 2018; Li *et al*., 2018; Trigg *et al*., 2017). BBX32 is capable of forming a protein-protein connection with TCP2, TCP4, TCP7, TCP13 and TCP14 (Trigg *et al*., 2017). TCP13 interacts with EDS1 and TCP14 interacts with NPR1 (Altmann *et al*., 2020; Li *et al*., 2018). By

binding both of these, BBX32 could repress SAR in a similar manner to photomorphogenesis (Holtan *et al*., 2011). The functionality of BBX32 could be explained through this set of interactions. During HL exposure, BBX32 could play a role in the suppression of these SAR responses. Protein binding affinity and co-immunoprecipitation studies may be used to determine BBX32-centric complex composition. This functionality is discussed further in Chapter 7 [Page 260].

5.5.2: Impact of defence on light acclimation

SA does not cause any strong alterations to light acclimation ability. SA treatment causes a slight skew in Fq'/Fm' possibly due to minor alterations in PSII complex composition however these changes are not great in scale (Figure 5.3.2 [Page 172]). *sid2-2* interestingly showed a very similar but inverted phenotype possibly due to the inverted changes in SA levels (Figure 5.4.2 [Page 185]). A larger change was seen in *eds1-22* and *pad4-1* however these were still very minimal when compared to light acclimation mutants such as BBX32-10 and *hy5-2* (Figure 5.4.2 [Page 185]; Alvarez-Fernandez *et al*., 2021). This was different when analysing the effects of the EDS1-PAD4 module when overexpressed (Table 5.4.1 [Page 189]).

The EDS1-PAD4 module caused a significant decrease in the expression of many light acclimation associated genes (Table 5.4.1 [Page 189]). This was a similar manner to the widespread depression in the defence gene expression caused by HL and BBX32-10 (Figure 5.3.3 [Page 174]; Figure 5.3.4 [Page 175]; Figure 5.3.5 [Page 176]; Figure 5.3.6 [Page 178]; Figure 5.3.7 [Page 179]). The EDS1-PAD4 module decreases the expression of both negative regulators of light acclimation such as

SPA1, *SPA3*, *SPA4* and *GLK2* and positive regulators such as *LHCB4.3* and *GLK1*. BBX32-10 suppressed defence in a similar manner by downregulating negative regulators of the SA pathway such as *NPR3* and *NPR4* and positive regulators such as *ICS1* and *NPR1* (Figure 5.3.4 [Page 175]). There appears to be a strong counteraction between the expression of defence and light acclimation associated genes. Further studies on the light acclimation ability of mutants such as *EDS1-PAD4* over-expressors may be useful for determining how light acclimation is impacted by SA signalling and defence.

5.5.3: Differences between HL and excess light

Prior to this study, excess light was found to increase the SA level in plants (Mühlenbock *et al*., 2008). However, this appears to be in direct contradiction to the decrease in mean expression of the “response to SA” GO group upon exposure to HL (Figure 5.3.1 [Page 171]). There appears to be a difference in the increased light conditions applied in the Mühlenbock *et al*. (2008) experiments and those performed in this study and Alvarez-Fernandez *et al*. (2021). These have been termed excess light and HL respectively.

The excess light conditions applied in Mühlenbock *et al*. (2008) caused large-scale photoinhibition whereas HL caused very limited irreversible photoinhibition (Alvarez-Fernandez *et al*., 2021). The plants exposed to HL were successfully coping with new challenging conditions whereas the plants exposed to excess light were not and therefore this caused photoinhibition and cell death (Mühlenbock *et al*., 2008). This difference between excess light and HL could completely change the SA response.

This links to an idea proposed by Mullineaux and Baker (2010) of a threshold between reversible and irreversible physiological damage caused by environmental stress centred around ROS signalling.

The distinction between the reversibility of stress revolved around ROS production, which is linked to SA, in response to stress. Light stress is innately tied to ROS signalling through excess excitation energy transfer generating singlet oxygen ($^1O_2$; Laloi *et al*., 2007). $^1O_2$ causes photooxidative damage to the PSII reaction centres and activates JA and SA signalling pathways through EDS1 (Ochsenbein *et al*., 2006). Overwhelming $^1O_2$ production causes cellular necrosis and reduced $^1O_2$ can signal the initiation of controlled cell death. Cellular and environmental sources of superoxide ($O_2^{\cdot-}$) radicals signal anti-cell death pathways which are integrated with $^1O_2$ signalling by EDS1 (Laloi *et al*., 2007; Straus *et al*., 2010). Light signalling can be integrated into the cell death responses through the balance of pro-cell death /$^1O_2$ oxygen and anti-cell death /superoxide anion pathways.

Excess light appeared to overwhelm the O_2^- production and anti-cell death signalling capabilities of the plant initiating widespread cell death. HL does not appear able to perturb $^1O_2$ signalling strongly enough to cause widespread photooxidative damage and increased SA signalling. SA signalling is therefore free to be depressed to reallocate resources towards HL acclimation (Mühlenbock *et al*., 2008; Alvarez-Fernandez *et al*., 2021).

5.5.4: Conclusion

The defences of *Arabidopsis thaliana* are perturbed upon exposure to HL. HL acclimation mutant BBX32-10 appeared to independently drive this pathway (Figure 5.3.3 [Page 174]; Figure 5.3.4 [Page 175]; Figure 5.3.5 [Page 176]; Figure 5.3.6 [Page 178]). Conversely, defence mutants did not show strong HL acclimation phenotypes, but some mutants showed perturbed HL acclimation gene expression (Table 5.4.1 [Page 189]). This may have implications on the intersections between defence, response to HL and resource allocation plants have evolved to endure in their natural environments.

5.6: Conclusions of Chapter 5

- BBX32-10 had a perturbated regulation of transcription of salicylic acid-related genes.
- BBX32-10 was more sensitive to *Pseudomonas syringae* infection than the WT.
- Mutants of the defence genes *EDS1* and *PAD4* had a perturbed HL acclimation phenotypes.

Chapter 6 – The modification of *BBX32* with *CRISPR/CAS9*

6.1: Introduction

BBX32 is a HL acclimation gene and plants overexpressing *BBX32* were significantly impaired in HL acclimation (Alvarez-Fernandez *et al*., 2021). The T-DNA mutant *bbx32-1*, however, had an accelerated but clearly weaker HL acclimation phenotype compared to the over-expressor BBX32-10 (Figure 6.1.1 [Page 197]; Alvarez-Fernandez *et al*., 2021). Holtan *et al*. (2011) found a truncated *BBX32* transcript in the *bbx32-1* mutant which increased in abundance after 1 hour of red light treatment. This chapter explores the relatively weaker HL acclimation phenotype of *bbx32-1* through analysis of the *BBX32* gene and development of novel *BBX32* mutants.

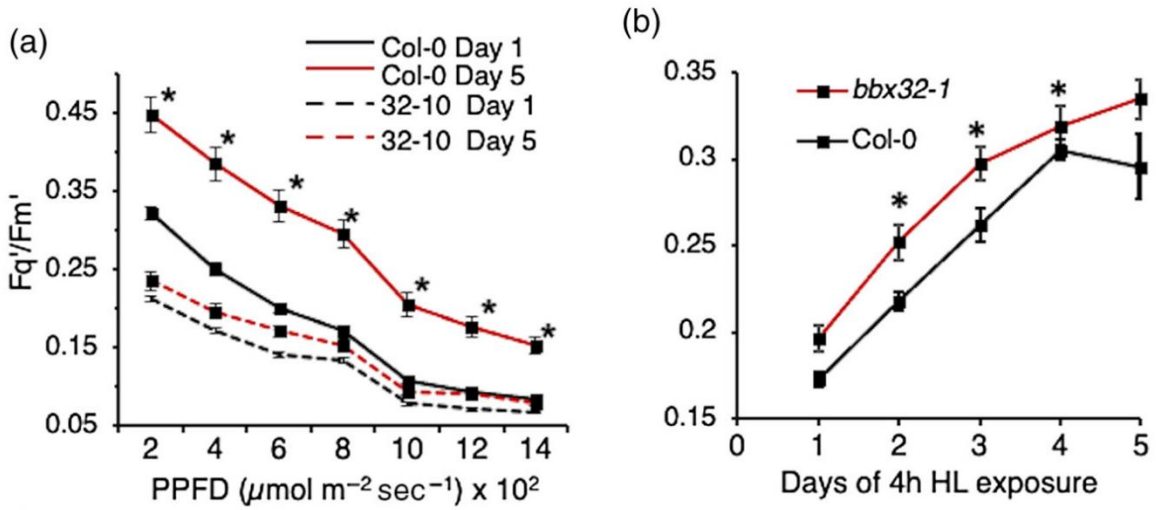

Figure 6.1.1: HL acclimation of BBX32-10 (32-10; a), *bbx32-1* (b) and Col-0 plants. Fq'/Fm' is determined by chlorophyll fluorescence with a light intensity range of 200 µmol m^{-2} s^{-1} to 1400 µmol m^{-2} s^{-1} at 200 µmol m^{-2} s^{-1} increments. All PPFDs

measured were displayed in (a) and only 800 µmol m^{-2} s^{-1} is displayed in (b). Asterisks denote a significant difference between the day 1 and day 5 values respectively of the mutants and Col-0 (ANOVA, post-hoc Tukey HSD; * = $p < 0.01$). Modified from Alvarez-Fernandez *et al*. (2021).

6.1.1: Structure and evolution of BBX32

The BBX family has been analysed within more than 40 species of plants (Khanna *et al*., 2009; Table S5 [Page 338]). The family was first studied as a whole by Khanna *et al*. (2009) in *Arabidopsis thaliana*. A set of five structural groups were discovered with BBX32 being placed into structure group V denoting a lack of a CCT or B-box2 domain (Khanna *et al*., 2009).

BBX32 was initially called EMF1-INTERACTING PROTEIN6 (EIP6) for its role in binding the key floral repressor EMBRYONIC FLOWERING1 (Park *et al*., 2011). In this Park *et al*. (2011), the BBX32 structure was further determined using yeast two-hybrid. The interaction between EMF1 and BBX32 was hypothesised to be causal to the late flowering phenotype of *BBX32* over-expressors (Park *et al*., 2011; Tripathi *et al*., 2017). Different regions of the *BBX32* gene were used to determine the location of the EMF1-binding domain (Fig. 6.1.2).

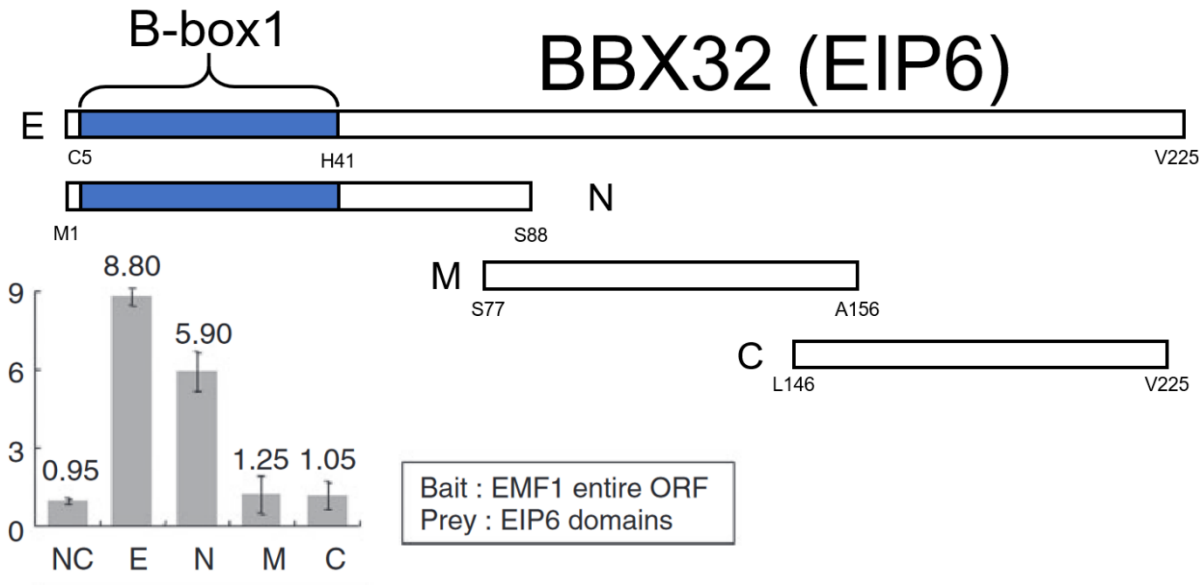

Figure 6.1.2: The yeast two-hybrid binding affinities between regions of the BBX32 (EIP6) and EMF1 from Park *et al*. (2011). The regions of the BBX32 denote the different regions used in the yeast two-hybrid experiment. Figure was modified from Park *et al*. (2011; NC, negative control; E, entire protein; N, N-terminus; M, middle; C, C-terminus).

The EMF1-BBX32 interaction only required a region of the BBX32 protein including the B-box1 domain. The whole sequence, however, has a greater β-galactosidase activity than the N-terminus region alone (Figure 6.1.1 [Page 197]). This suggests that more of the sequence is involved in the interaction than the first 88 amino acids. Park *et al*. (2011) also tested smaller regions of the N-terminus of BBX32 closer to the size of the B-box1 domain (C5 - H41).

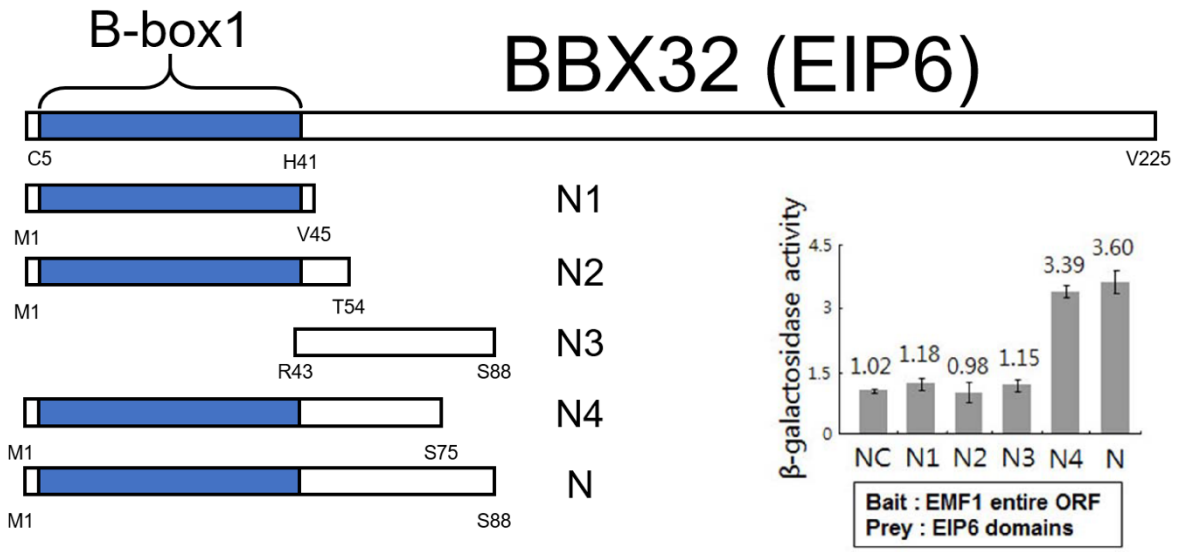

3753

3754 **Figure 6.1.3: The yeast two-hybrid binding affinities different sections of the N-**
3755 **terminus of BBX32 (EIP6) and EMF1 from Park *et al*. (2011).** The regions of the
3756 BBX32 denote the different regions used in the yeast two-hybrid experiment. Figure
3757 was modified from Park *et al*. (2011; NC, negative control; N, N-terminus).

3758

3759 Supplemental data indicated that the B-box1 domain of BBX32 could not bind EMF1
3760 using only the first 45 or 54 amino acids of the BBX32 sequence. Only when the first
3761 75 residues were used did the partial BBX32 sequence have a comparable β-
3762 galactosidase to the previously tested sequence of the N-terminus (1 - 88). The
3763 traditional B-box1 domain of BBX32 could not solely coordinate the binding between
3764 BBX32 and EMF1. This theory was be expanded upon further throughout this
3765 chapter.

3766

3767 BBX32 is capable of binding BBX4 (a.k.a. COL3) among other BBX genes (Tripathi
3768 *et al*., 2017). BBX32 bound both the N and C terminals of BBX4 and both co-
3769 localised to the nuclear speckles *in vivo*. Through combined action, BBX4 and
3770 BBX32 suppressed the expression of *FT*, a key flowering regulator and over-

expressors of both had a late flowering time (Tripathi *et al*., 2017). The joint co-localisation and suppression lead to the theory that BBX4 and BBX32 formed a complex to regulate gene expression.

6.1.2: Potential deficiencies in the *bbx32-1* mutant

The Khanna group in collaboration with the Preuss group at Monsanto studied the role of *BBX32* in light signalling (Holtan *et al*., 2011). Holtan *et al*. (2011) developed two novel *BBX32* over-expressors (BBX32-10 and BBX32-12) and characterised a T-DNA insertion mutant (*bbx32-1*). The over-expressors, in particular BBX32-10, had a far stronger hypocotyl length and growth time course phenotype. RT-qPCR highlighted that *bbx32-1* contained a truncated *BBX32* transcript and the level of this truncated transcript increased in response to red light (Holtan *et al*., 2011).

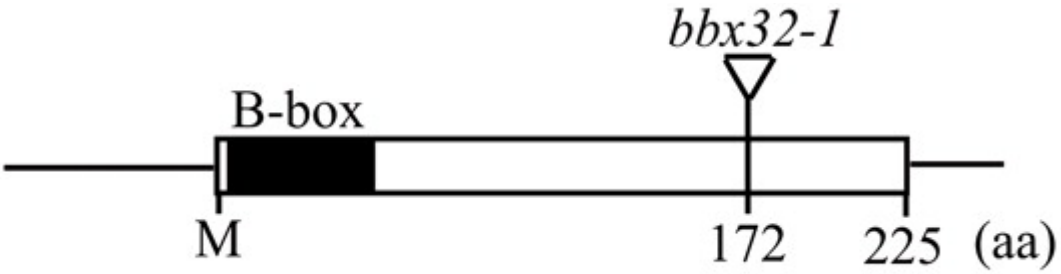

Figure 6.1.4: The structure of BBX32 with the insertion point of the T-DNA in the *BBX32* gene. Modified from Holtan *et al*. (2011).

This truncated *BBX32* transcript prompted here the idea that the *bbx32-1* mutant has only a partially defective *BBX32* gene. The only known structural domain of BBX32 was the B-box1 domain at the very beginning of the amino acid sequence (Khanna *et al*., 2009; Holtan *et al*., 2011; Park *et al*., 2011). No other domains are currently known. This means that a large proportion of the *BBX32* gene is intact in the *bbx32-*

1 and concerns were expressed over a truncated transcript having an impact on the phenotype (Holtan *et al*., 2011; Alvarez-Fernandez *et al*., 2021).

The Preuss and Khanna groups further explored the role of *BBX32* and its homologues within the crop plant *Glycine max* (soybean; Preuss *et al*., 2012; Khanna *et al*., 2009). *Glycine max* overexpressing *Arabidopsis thaliana BBX32* had up to a 14 % greater yield in field trials. However, the performance of the generated lines varied wildly, and many had a significantly depressed yield. Preuss *et al*. (2012) explained the yield changes by concluding that circadian and senescence changes were responsible. The circadian phenotype of two selected greater yield lines had a negligible difference in the expression of central clock genes. The senescence of the leaves and maturation of the pods of these two lines appeared to be delayed, 10 and 3 days respectively. However, a non-quantitative methodology was used for measuring these factors. These explanations did not provide a conclusive explanation for the yield increases in *BBX32* over-expressing *Glycine max* plants. This is discussed further in Chapter 7 [Page 260].

6.1.3: Genome editing with CRISPR/CAS9

Clustered, regularly interspaced, short palindromic repeat (CRISPR)/ CRISPR associated protein 9 (CAS9) is an adaptive immunological bacterial system for targeting and destroying previously encountered foreign DNA (Ceasar *et al*., 2016). CAS9 incorporates a short RNA strand called a guide RNA (gRNA) to target a specific sequence. Once identified, the sequence is cut, and the encoding gene is disrupted. This break may be improperly repaired by non-homologous end joining

(NHEJ) leading to an altered sequence. This system can be used in genetic engineering to create *in vivo* mutations in target genes without the eventual lineage containing any transgenes (Ordon *et al*., 2020). I have used CAS9 as it quickly generates guided but non-specific mutations that can be used as an allelic series.

A partially functioning BBX32 protein may be produced within the *bbx32-1* mutant. The HL acclimation phenotype of *bbx32-1* was weaker than the positive HL acclimation phenotypes of *cop1-4, spa123* and YHB (Alvarez-Fernandez *et al*., 2021; Chapter 4 [Page 125]). The BBX32-10 and BBX32-12 mutants also have some of the strongest known negative HL acclimation phenotypes and the *bbx32-1* could be expected to have an opposite phenotype. There are no other *bbx32* mutants to explore the strength of the *bbx32-1* phenotype therefore a CRISPR/CAS9 system was employed to create a novel *BBX32* allelic series. A novel mutant may be lethal due to a potentially strong constitutively photomorphogenic phenotype like those seen in *COP1* and *spaQ* mutants.

This section aims to develop an allelic series of *BBX32* using CRISPR/CAS9. The structure and evolution of *BBX32* was studied to develop and optimise gRNA design for the targeting of specific locations on the *BBX32* gene. The CAS9 construct selected allowed the use of multiple gRNAs and contained advanced selection technologies to simplify the generation of an allelic series (Ordon *et al*., 2020). Finally, *BBX32-CAS9* mutants were sequenced and were subjected to phenotypic analysis.

6.2: Methods

6.2.1: Analysing the structure of BBX32

The BBX32 amino acid sequence was obtained from Uniprot (Q9LJB7). The sequence was submitted to Phyre 2.0 and viewed in the alphafold database (section 2.4.7 [Page 53]). These analytical methodologies only use the primary sequence of the protein to generate secondary and tertiary structures. Phyre 2.0 does this by using known X-ray crystal structures and sequence homology (Kelley *et al*., 2015). Alphafold uses the DeepMind AI to predict protein structure (Jumper *et al*., 2021).

Neither of these methodologies can be used to determine the true *in vivo* structure of the BBX32 protein, however they are useful for predicting domains and regions of the protein structure. Analysing protein structures computationally can be useful for proteins with disordered regions, like BBX32, which resist the crystallisation required for X-ray crystallography.

6.2.2: Designing guides for CRISPR/ CAS9

Guide RNAs (gRNAs) were designed following the methodology presented in section 2.5.3 [Page 58]. Multiple tools were used to analyse the *BBX32* gene to find suitable gRNAs to validate the on and off-site targeting. It was assumed that if all of these tools agreed on the usefulness of a gRNA then it was more likely to work in practice.

gRNAs were selected not only by their on-site and off-site target scores but also where on the *BBX32* gene they would target. CAS9 cleaves DNA near the gRNA target sequence. Cleavage of the DNA often results in improper DNA repair and

therefore mutations in the DNA sequence. Targeting regions that have been identified to be a part of a structural domain may cause the CAS9 to alter that part of the gene and potentially lose its functionality. By placing cuts near each other, the CAS9 may cleave in two places on the same DNA strand which may become omitted during replication. Frame shifting the C-terminal can be done at various points along the gene by introducing or removing a number of nucleotides not divisible by three. This would remove the part of the protein after the perturbation and may also result in an early stop codon.

All of these methods can be employed at the same time with a CAS9 T-DNA construct that allows multiple gRNAs. The chosen construct pDGE277 (described in Ordon *et al*., 2020) can employ 1, 2, 4 or 8 gRNAs. At least two gRNAs would have to be used to direct region cleavage, but the other methods only require single gRNAs.

6.2.3: Building the *BBX32-CAS9* T-DNA construct

Golden Gate cloning was performed to create both the shuttle vectors and the final CAS9 T-DNA. This was done following the methodology outlined in section 2.5.4 [Page 59]. A completed T-DNA was capable of being produced over 7 working days.

6.2.4: Transformation of *Arabidopsis* plants

Transformation of Col-0 plants was conducted following the methodology outlined in section 2.5.6 [Page 61]. The floral inoculation methodology was selected for its higher transformational efficiency than the traditional floral dipping method (Narusaka *et al*., 2010). The floral inoculation requires a lower volume of

Agrobacterium culture than the floral dipping method as the inoculate is pipetted directly onto the buds as opposed to dipping the whole plant in the inoculum.

6.2.5: Selection of homozygous *bbx32* mutant plants

The progeny on plants inoculated with transformed *Agrobacterium* containing the *BBX32-CAS9* plasmid were grown on ½ MS agar plates containing hygromycin (25 mg/L) following methodology outlined in section 2.6.1 [Page 62]. The plants that survived the hygromycin selection were transferred to soil and allowed to grow and set seed under standard growth conditions (section 2.2.1 [Page 35]). During this generation (T_1), the CAS9 had a potential to edit the *BBX32* gene.

The next generation required the removal of the *CAS9* T-DNA to discontinue the perturbations of the *BBX32*. The FAST cassette was used to identify seeds containing the *CAS9* T-DNA by following the methodology outlined in section 2.6.2 [Page 62]. Seeds that did not have an RFP luminescence were grown under standard growth conditions (section 2.2.1 [Page 35]). These plants were labelled as M_2 instead of T_2 as they did not contain T-DNA.

M_2 and M_3 plants had leaves taken for DNA extraction (section 2.3.1 [Page 42]) and PCR was performed using the BBX32F and BBX32R primers (section 2.3.3 [Page 43]; Table S6 [Page 338]). The PCR product was sent to Eurofins (Luxembourg, Luxembourg) with the BBX32seq primer (Table S6 [Page 338]) for sequencing with their TubeSeq Service. Results were received in FASTA format, and the sequence could be analysed for alterations.

6.2.6: Phenotypic analysis of novel *bbx32* mutants

Phenotypic analysis was conducted on the novel *bbx32* mutants that were discovered by the previous steps. Hypocotyl experiments were conducted following the methodology outlined in section 2.2.4 [Page 39]. HL acclimation experiments were also conducted following the methodology outlined in section 2.2.2 [Page 35] and chlorophyll fluorescence measurements were taken (section 2.2.3 [Page 36]).

6.3: Structural and evolutionary analysis of *BBX32*

This section sets out to gather information on the structure and function of *BBX32* in order to develop suitable gRNAs for the CAS9-mediated generation of a *BBX32* mutant allelic series. Structural and evolutionary information can be used to identify conserved sequences that may possess functionality. These may be targeted by CAS9 to generate specific mutants and therefore analyse the phenotype of *BBX32* mutants with perturbed forms of these regions thus relating structural domains of wild-type BBX32 to their influence on whole plant phenotypes.

6.3.1: Analysing the *bbx32-1* mutant phenotype

This section analysed other phenotypic traits of the *bbx32-1* mutant compared to the BBX32-10 and BBX32-12 over-expressors. The HL acclimation phenotype of the *bbx32-1* mutant was not as impactful as the BBX32-10 and BBX32-12 over-expressors and therefore if the *bbx32-1* mutant is weak *bbx32* allele then other phenotypic traits should also be relatively inversely weak compared to the over-expressors.

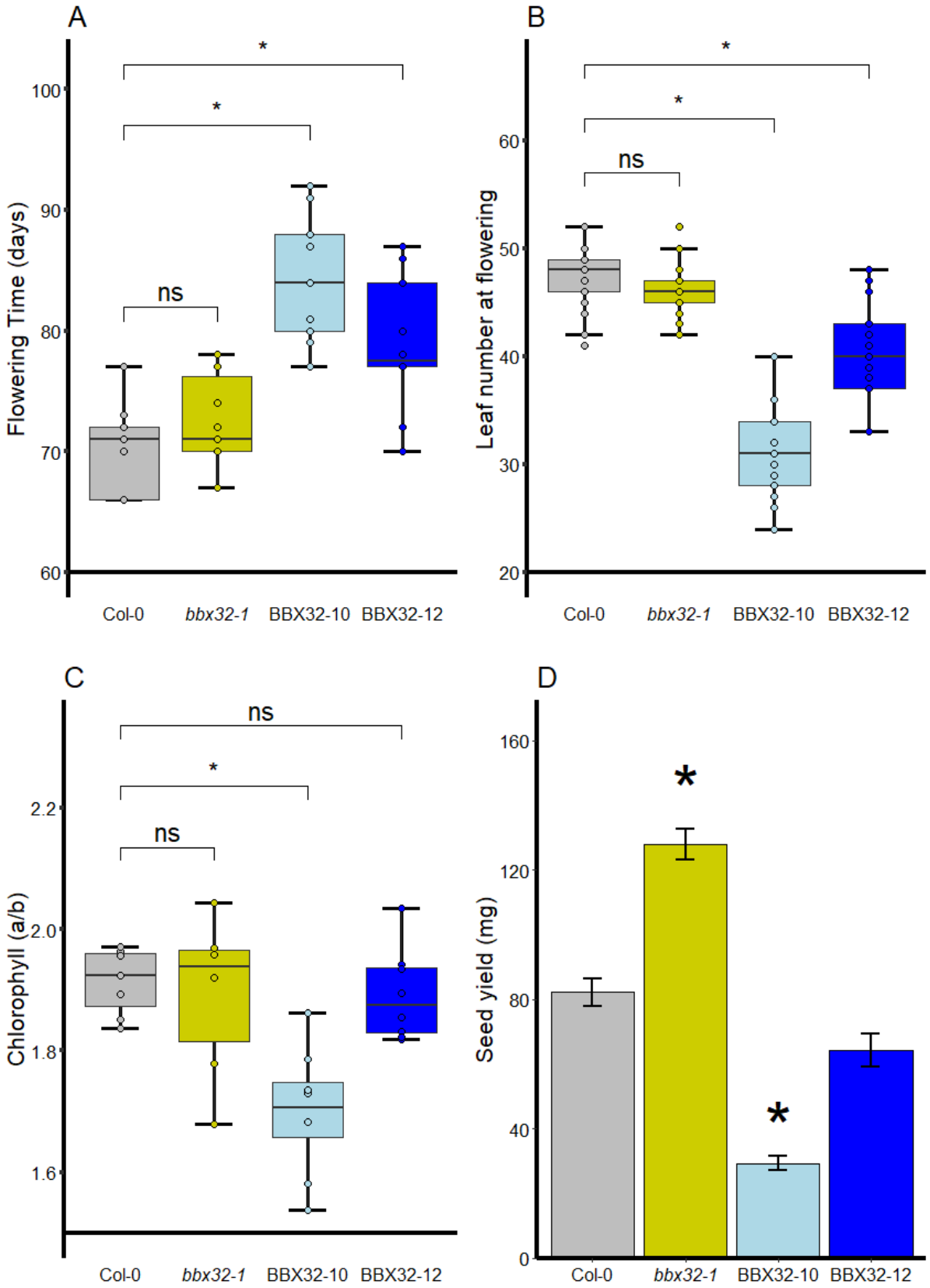

Figure 6.3.1: Flowering time (A), leaf number at flowering (B), chlorophyll (a/b) ratio (C) and seed yield (D) of *BBX32* mutant and over-expressors. Asterisks

denote significance between Col-0 (WT) and the indicated mutant (ANOVA; $p < 0.05$).

Flowering time, leaf number at flowering time, chlorophyll (a/b) ratio and seed yield were analysed. The only significantly different phenotype measured of *bbx32-1* was the seed yield. BBX32-10, however, had a significantly different phenotype in all of the measured traits. I attempted to create a *BBX32* mutant without the truncated transcript using CRISPR CAS9 *in vivo* gene editing. This process began with analysing the structure and evolution of *BBX32* and the *BBX* family to find suitable targets for CAS9.

6.3.2: Computer generated 3D models of BBX32

As seen in Figure 6.3.1 [Page 208], there was a large region of the BBX32 protein with no known domain or structure. Many tools exist that can be used to analyse the primary sequence of a protein to detect and build a potential protein structure. Phyre 2.0 uses sequence homology detection software to build a 3D structure from a database of known protein structures (Kelley *et al*., 2015). The sequence of *Arabidopsis thaliana* BBX32 was analysed, and the 3D structure was visualised (Figure 6.3.3 [Page 211]).

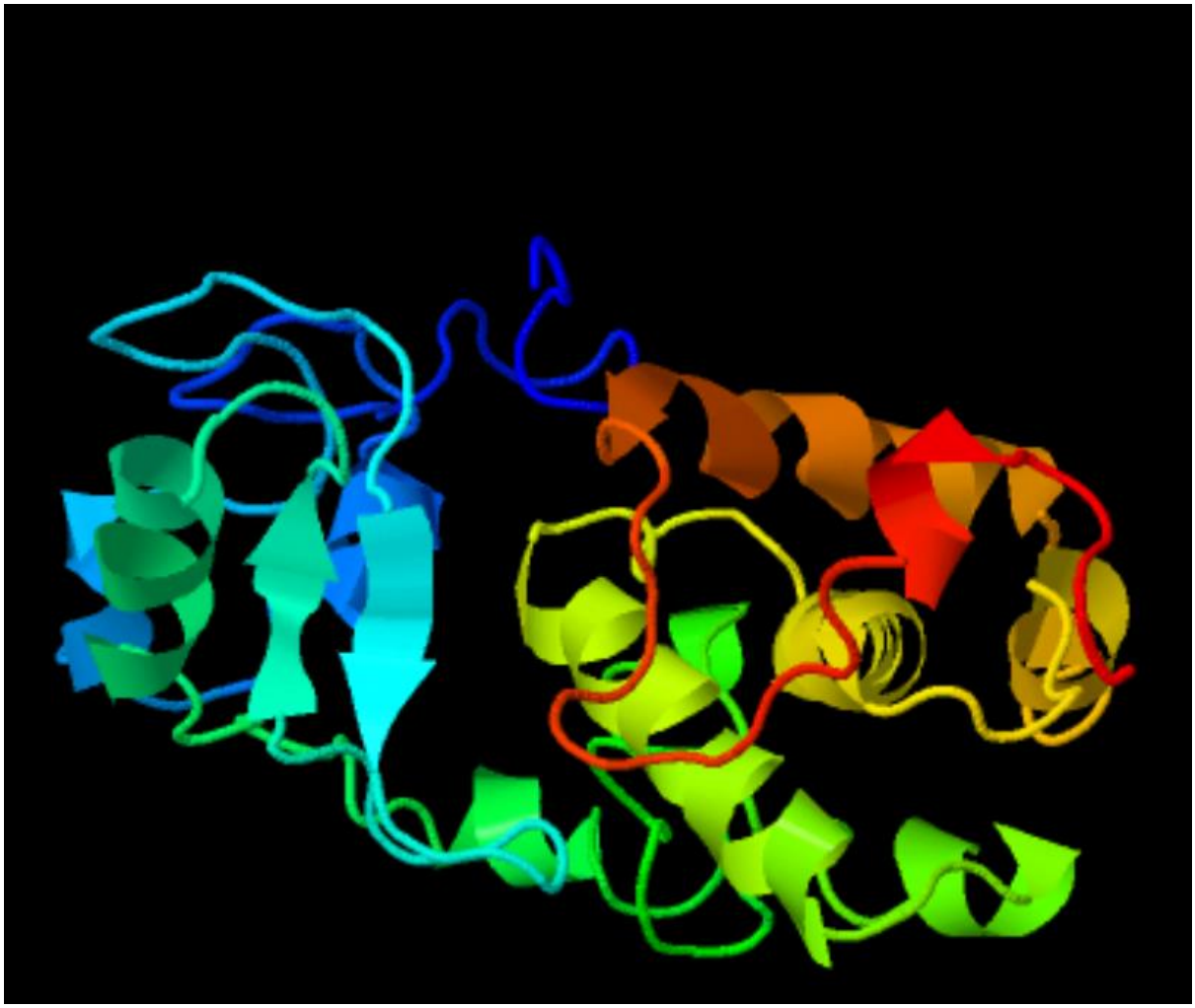

Figure 6.3.2: Modelled output of the BBX32 sequence processed through Phyre 2.0. The N terminal was displayed as dark blue transitioning to the red C terminal. The B-box 1 was displayed on the left and the novel domain was shown on the right.

Phyre 2.0 correctly identified the B-box1 domain basing its confidence on the human MID1 protein that also contains a B-box domain (95.0 %). However, the analysis also identified a second domain with a lower confidence (78.8 %). This domain can be seen on the right of Figure 6.3.3 [Page 211] and contains 5 alpha helices. Phyre 2.0 identified the human TRANSCRIPTION INITIATION FACTORIIb (TFIIb) as having homology with a novel C-terminal domain of BBX32. This homology is specifically

with one of the two core (cyclin-like) domains of HsTFIIb. TFIIb is a general transcription factor existing in all eukaryotic life forms and is involved in forming the pre-initiation complex (PIC) and recruiting RNA POLYMERASEII. Other methodologies were also used to corroborate these findings.

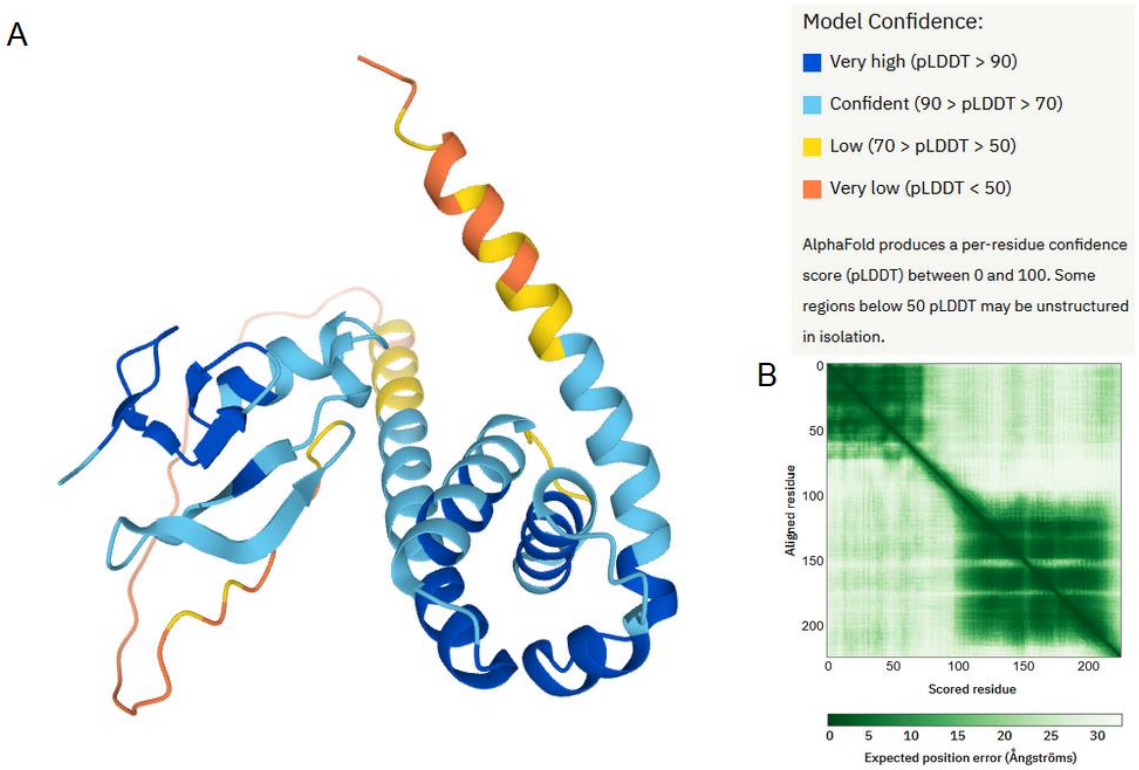

Figure 6.3.3: The Alphafold predicted 3D structure (A) and predicted alignment error (B) of BBX32. Blue represents a higher confidence and orange a lower confidence of the model. The B-box domain was on the left and the novel domain was on the right. The predicted alignment error (B) of BBX32 where darker greens indicate a greater coordination between the aligned and scored residues.

Alphafold uses the DeepMind AI to predict the 3D structures of proteins from primary sequences (Jumper *et al*., 2021). The novel domain of 5 alpha helices also appears in the Alphafold predicted structure. There was a high coordination (Figure 6.3.3B

[Page 211]) within the B-box1 domain and the novel domain as shown by the dark green colours in the predicted alignment error graph.

The B-box1 domain has very high coordination between the N-terminal and S75 however the B-box1 domain ends at H41. This matches the results found by Park *et al*. (2011) using yeast-two hybrid on BBX32 / EIP6. The B-box1 domain may be larger than originally thought and this should be considered when planning CAS9 guide RNAs (gRNAs).

The five alpha helices of the novel domain can be identified from the four light green lines delineating the larger dark region of the predicted alignment error graph (Figure 6.3.3B [Page 211]). The predicted alignment error graph (Figure 6.3.3B [Page 211]) also shows a relatively high coordination between the B-box1 and novel domain as indicated by the green regions in the top right and bottom left of the figure. This was separated by a region of relatively less coordination between S78 and T95. The T-DNA insertion site of *bbx32-1* occurs within the novel domain and may be causing the phenotype of the *bbx32-1* even with a truncated transcript (Holtan *et al*., 2011).

6.3.3: B-box structure of BBX32

The *BBX32* genes were identified from different species including *Bryophyta*, *Marchantiophyta*, *Lycophyta*, Gymnosperms and Angiosperms. Other earlier diverging species were too difficult to identify due to their sequence dissimilarity to *Arabidopsis thaliana BBX32* (*AtBBX32*). In the case where there were multiple *BBX32* genes, the one with the highest homology to *AtBBX32* was used. From this data gathering, the *BBX32* homologous gene(s) of 46 species were identified and

analysed, however only representative species were shown to simplify the tables presented. These species and the represented groups were:

- *Arabidopsis thaliana* and *Brassica oleracea* (wild cabbage) - *Brassicaceae* family.
- *Solanum chilense* (tomato) and *Glycine soja* (wild soybean) - other eudicots.
- *Zea mays* - monocots
- *Picea abies*- gymnosperms
- *Selaginella moellendorffii* - *Lycophyta* (vascular plants)
- *Physcomitrella patens* - *Bryophyta* (mosses)

Table 6.3.1: The amino acid sequence of the B-box1 domain of the BBX32 homologous protein from representative different plant species. Sequences were aligned using clustalW and manual manipulation. Asterisks denote a perfect alignment of a given amino acid.

Species	Start	1	2	3	4	5	6	7	8	9	10	11	12	13	14	15	16	17	18	19	20	21	22	23	24	25	26	27	28	29	30	31	32	33	34	35	36	37
Arabidopsis thaliana	5	C	E	L	C	G	A	E	A	D	L	H	C	A	A	D	S	A	F	L	C	R	S	C	D	A	K	F	H	A	S	N	F	L	F	A	R	H
Brassica oleracea	5	C	E	L	C	G	A	E	A	D	L	H	C	A	A	D	S	A	F	L	C	R	S	C	D	A	K	F	H	A	S	N	I	L	F	S	R	H
Solanum chilense	9	C	E	L	C	N	D	Q	A	A	L	F	C	P	S	D	S	A	F	L	C	F	H	C	D	A	K	V	H	Q	A	N	F	L	V	A	R	H
Glycine soja	6	C	E	L	C	H	Q	L	A	S	L	Y	C	P	S	D	S	A	F	L	C	F	H	C	D	A	A	V	H	A	A	N	F	L	V	A	R	H
Zea mays	12	C	E	L	C	G	A	P	A	A	V	H	C	A	A	D	E	A	F	L	C	A	A	C	D	A	K	V	H	G	A	N	F	L	A	S	R	H
Picea abies	9	C	E	L	C	S	N	E	A	A	L	H	C	E	A	D	S	A	N	L	C	F	K	C	D	A	N	V	H	G	V	N	F	L	V	A	R	H
Selaginella moellendorfii	7	C	E	L	C	Q	V	R	A	A	V	Y	C	C	A	D	E	A	Y	L	C	W	K	C	D	S	K	V	H	G	A	N	F	I	V	A	R	H
Physcomitrella patens	8	C	E	L	C	D	G	V	A	D	L	Y	C	A	A	D	E	A	H	I	C	W	T	C	D	A	K	V	H	S	A	N	F	L	V	A	R	H

There were 15 amino acids of the 37 comprising the traditional B-box1 from Khanna *et al*. (2009) were conserved between all of *BBX32* genes analysed (n = 46; Table S7 [Page 338]). No insertions or deletions were discovered in the B-box1 of any of the analysed homologous BBX*32* genes (n=46). This region was determined to be highly conserved. The region downstream from the traditional B-box1 domain was

also analysed in accordance with the yeast-two hybrid data from Park *et al*. (2011) and the predicted alignment error graph (Figure 6.3.3B [Page 211]).

Table 6.3.2: The amino acid sequence of the post-B-box1 region of the BBX32 protein from different representative plant species. Sequences were aligned using clustalW and manual manipulation. Asterisks denote a perfect alignment of a given amino acid.

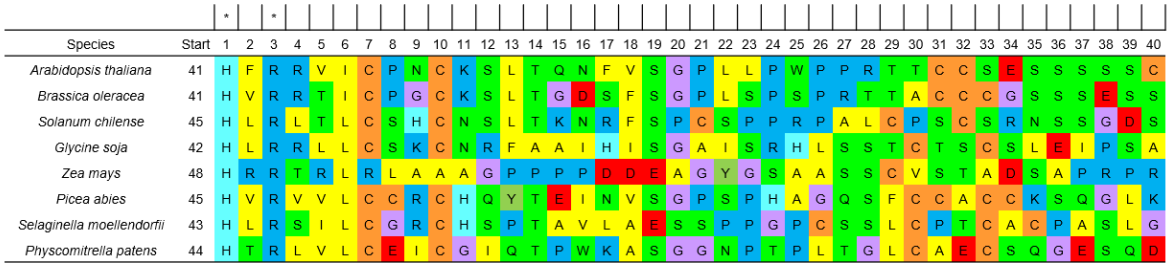

Species	Start	1	2	3	4	5	6	7	8	9	10	11	12	13	14	15	16	17	18	19	20	21	22	23	24	25	26	27	28	29	30	31	32	33	34	35	36	37	38	39	40
Arabidopsis thaliana	41	H	F	R	R	V	I	C	P	N	C	K	S	L	T	Q	N	F	V	S	G	P	L	L	P	W	P	P	R	T	T	C	C	S	E	S	S	S	S	S	C
Brassica oleracea	41	H	V	R	R	T	I	C	P	G	C	K	S	L	T	G	D	S	F	S	G	P	L	S	P	S	P	R	T	T	A	C	C	C	G	S	S	S	E	S	S
Solanum chilense	45	H	L	R	L	T	L	C	S	H	C	N	S	L	T	K	N	R	F	S	P	C	S	P	P	R	P	A	L	C	P	S	C	S	R	N	S	S	G	D	S
Glycine soja	42	H	L	R	R	L	L	C	S	K	C	N	R	F	A	A	I	H	I	S	G	A	I	S	R	H	L	S	S	T	C	T	S	C	S	L	E	I	P	S	A
Zea mays	48	H	R	R	T	R	L	R	L	A	A	A	G	P	P	P	P	D	D	E	A	G	Y	G	S	A	A	S	S	C	V	S	T	A	D	S	A	P	R	P	R
Picea abies	45	H	V	R	V	V	L	C	C	R	C	H	Q	Y	T	E	I	N	V	S	G	P	S	P	H	A	G	Q	S	F	C	C	A	C	C	K	S	Q	G	L	K
Selaginella moellendorfii	43	H	L	R	S	I	L	C	G	R	C	H	S	P	T	A	V	L	A	E	S	S	P	P	G	P	C	S	S	L	C	P	T	C	A	C	P	A	S	L	G
Physcomitrella patens	44	H	T	R	L	V	L	C	E	I	C	G	I	Q	T	P	W	K	A	S	G	G	N	P	T	P	L	T	G	L	C	A	E	C	S	Q	G	E	S	Q	D

The region after the traditional B-box 1 was not as highly conserved and only one arginine (R43) was conserved throughout all of the *BBX32* genes. However, 2 cysteines were highly conserved throughout many of the BBX32 sequences including in non-vascular plants. This was missing in the *Poaceae* family (such as maize, wheat and rice) but existed in other monocots such as *Elaeis guineensis* (oil palm). This appeared to align with the first two cysteines of the B-box2 of other BBX proteins (analysed further in Table 6.3.4 [Page 218]). More cysteines existed further downstream from the first pair within a serine-rich region; however, these didn't fully align and only formed a region of greater numbers of cysteines between 29 - 33 (Table 6.3.2 [Page 214]).

The novel BBX32 domain was also analysed across the gathered species to determine if it consistently appeared. Figure 6.3.4 [Page 215] shows that the novel

domain exists throughout all of the analysed species and was also highly conserved. Residues with a white background had a greater than 50 % conservation across all species. This accounted for 39 of 107 residues in *Arabidopsis thaliana*, 40 of 106 in *Glycine soja* and 32 of 103 residues in *Zea mays*. The high conservation indicates a conserved functionality.

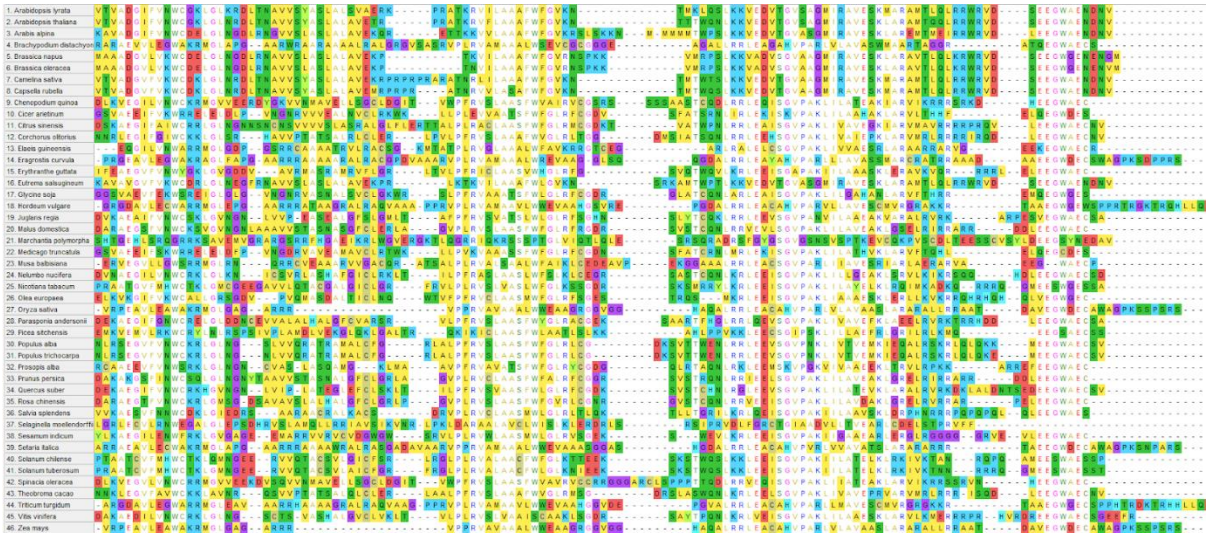

Figure 6.3.4: The novel domain of BBX32 across 46 different species. The residues with a white background have greater than 50 % conservation across the analysed species. Sequences were aligned using ClustalW and displayed within MEGA X.

AtBBX32 does not contain a VP motif; a motif that allows the binding of the light acclimation regulator COP1. However, close analysis of the other BBX32 sequences revealed a VP pair with a greater than 50 % conservation across the 46 analysed species. These potential VP motifs can be compared against known VP motifs to determine if they are consistent with the structure of a VP motif.

Table 6.3.3: The VP motifs of BBX proteins with comparable genes from Lau *et al*. (2019). The VP core was coloured in yellow, and the anchor residue was coloured in blue. Data from proteins other than the BBX proteins were gathered from Lau *et al*. (2019).

Protein (species)	Start	-4	-3	-2	-1	0	1	2	3
Arabidopsis thaliana	184	D	V	T	G	V	S	A	G
Brassica oleracea	181	D	V	S	G	V	A	A	G
Solanum chilense	222	E	I	S	G	V	P	A	K
Glycine soja	210	A	I	S	G	V	P	A	K
Zea mays	372	A	C	A	H	V	P	A	R
Picea abies	294	E	C	S	G	I	P	S	K
Selaginella moellendorfii	235	R	C	T	G	I	A	A	D
Physcomitrella patens	365	G	C	A	G	V	S	T	R
AtHY5	39	E	I	R	R	V	P	E	F
AtBBX1 (CO)	366	G	Y	G	I	V	P	S	F
AtBBX4 (COL3)	287	G	F	G	V	V	P	S	F
AtCRY1	544	E	D	Q	M	V	P	S	I

Most species outside of the *Brassicaceae* family have a potential VP motif towards the end of the novel domain. It appears that the ancestor of the *Brassicaceae* family lost the VP pair of BBX32. *Erythranthe guttata* also lost its potential VP motif whereas it was maintained in its nearest analysed relative *Olea europaea* (Olive). The VP pair was very highly conserved nevertheless it has still been lost multiple times over many millions of years.

On the AtBBX32 Alphafold model, the TGVS sequence (in Table 6.3.3 [Page 216) formed the turn between the fourth and fifth alpha helices. The potential VP motif of other BBX32 sequences was also found between the fourth and fifth alpha helices in

other species within the Alphafold database: *Oryza sativa subsp. japonica*, *Zea mays* and *Glycine max* (*Glycine soja* and *Glycine max* BBX32 have a 100 % identity). It may be that this is a conserved turn sequence. However, the turn exists on the surface of these models and therefore could be interacted with by another protein such as COP1.

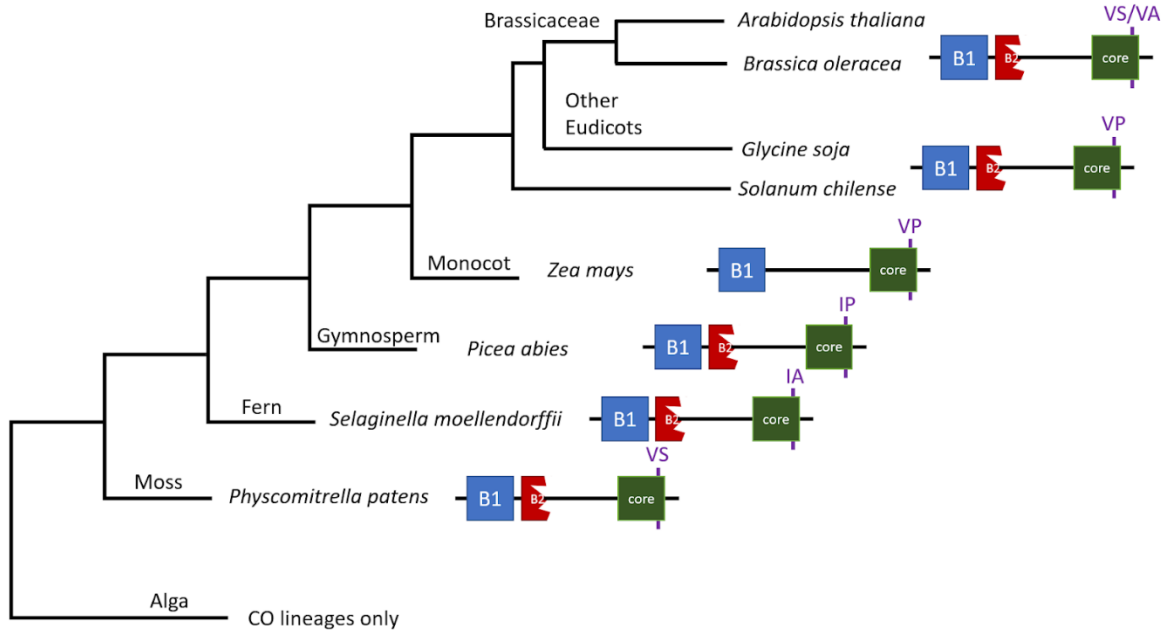

Figure 6.3.5: A phylogenetic tree (n = 46) showing the structural evolution of BBX32. Alongside each species name was a representation of the structure of the BBX32 protein within that species. B-box 1 was shown as B1 (blue), the partial B-box two was shown as a broken B2 box (red) and the novel HsTFIIb core-like domain was labelled core (green). A dash (purple) through the core-like domain shows a potential VP motif absent in the *Brassicaceae*.

The knowledge gathered on the evolution of *BBX32* was formed into a pseudo-phylogenetic tree with protein structures. The BBX32 protein structure most likely first appeared in the common ancestor of land plants due to the lack of BBX32 in

algae. This ancestor would have existed between 515 and 470 million years ago (Morris *et al*., 2018). *BBX32* genes and by extension the whole *BBX* family are very old, exist across all land plant species analysed and are highly conserved.

6.3.4: Evolution of the BBX family

I analysed the structure and evolution of the whole *BBX* family. The cysteine pair after B-box1 from BBX32 was thought to potentially align with B-box2 from other BBX proteins. The BBX sequences from *Arabidopsis thaliana* were gathered and aligned for analysis.

Table 6.3.4: The B-box2 domain BBX family (excluding BBX14 - BBX17 as they do not contain B-box2) of *Arabidopsis thaliana*. This was aligned using clustalW and with manual adjustments.

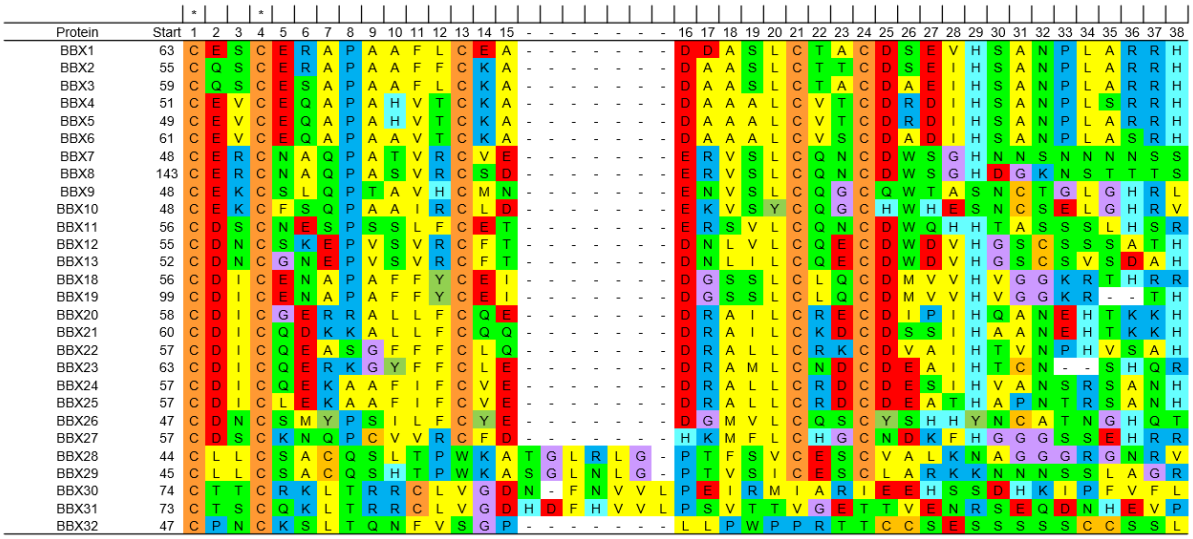

Protein	Start
BBX1	63
BBX2	55
BBX3	59
BBX4	51
BBX5	49
BBX6	61
BBX7	48
BBX8	143
BBX9	48
BBX10	48
BBX11	56
BBX12	55
BBX13	52
BBX18	56
BBX19	99
BBX20	58
BBX21	60
BBX22	57
BBX23	63
BBX24	57
BBX25	57
BBX26	47
BBX27	57
BBX28	44
BBX29	45
BBX30	74
BBX31	73
BBX32	47

The structure group V BBX family was previously noted as not having the B-box2 domain (Khanna *et al*., 2009). The two cysteines following B-box1 of BBX26 - BBX32 align with B-box2 of BBX1 - BBX13 and BBX18 - BBX25 (1 and 4). However, BBX26

and BBX27 strongly align with B-box2 for the full length of the domain. The first coordinating H residue of BBX26 appears 1 earlier in the sequence (28), similarly to BBX11. The second coordinating H residue in both BBX26 and BBX27 appears 2 earlier (36), similarly to BBX9, BBX10 and BBX11. It would be safe to conclude that BBX26 and BBX27 both have a second undiscovered B-box2 domain.

BBX28 and BBX29 also contain the second cysteine pair of the B-box2 domain (21 and 24) but lack the cysteine-aspartate pair and contain no histidine residues in the region. BBX30, BBX31 and BBX32 do not align with the B-box2 domain after the first cysteine pair.

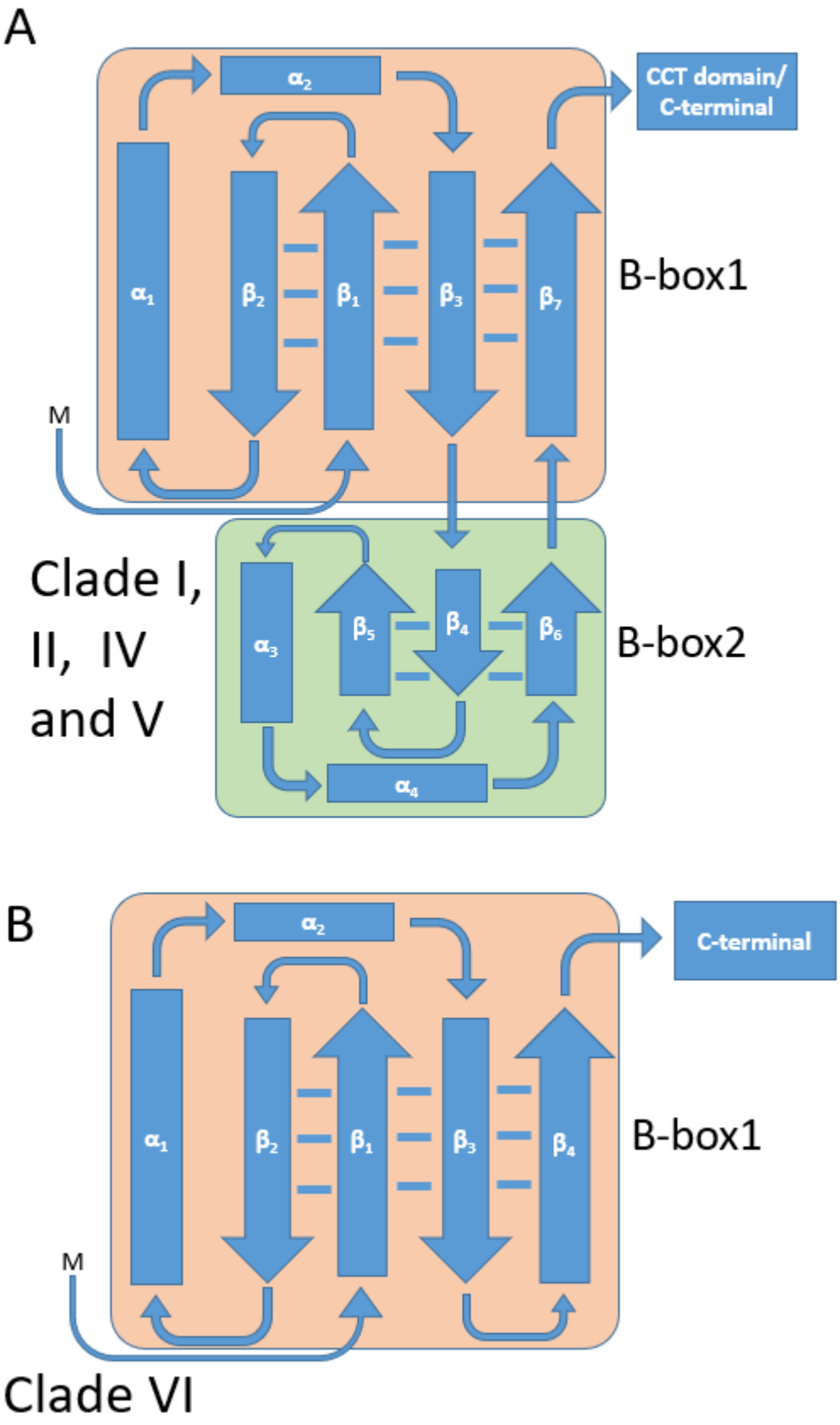

4124

4125 **Figure 6.3.6: The B-box structure of Clade I, II, IV and V (A) and Clade VI BBX**

4126 **family proteins.** The BBX family structures were analysed using the Alphafold

database and compiled. This represents the structure of the BBX proteins of these clades excluding BBX23 and BBX26 from Clade IV and V respectively. Large rectangles represent alpha helices, thick arrows represent beta sheets, thin arrows represent the amino acid sequence and N>C direction. Small rectangles represent bonds between the beta sheets. Green and orange boxes surrounding represent B-box1 and B-box2 respectively.

The second cysteine pair of BBX28 - BBX32 coordinated the turn between β_3 and β_4 of the B-box1 domain according to the Alphafold predicted structure. In BBX28 - BBX31, a fifth beta sheet of a lower confidence was formed by the model, and this may represent a more malleable part of the structure. In BBX32, this role was taken by C71 coordinating with C47 and C50. This also aligns with the EMF1-BBX32 yeast-two hybrid data which not only did find a strong β-Galactosidase activity between EMF1 and 1 - 54 of BBX32 but did also for 1 - 75 of BBX32 (Park *et al*., 2011).

Due to the issues found with BBX26 and BBX27, a repeat of the phylogenetic analysis performed by Khanna *et al*. (2009) was conducted. The phylogenetic tree, the structures and other general information was placed into a single figure. New clades were assigned based on this data.

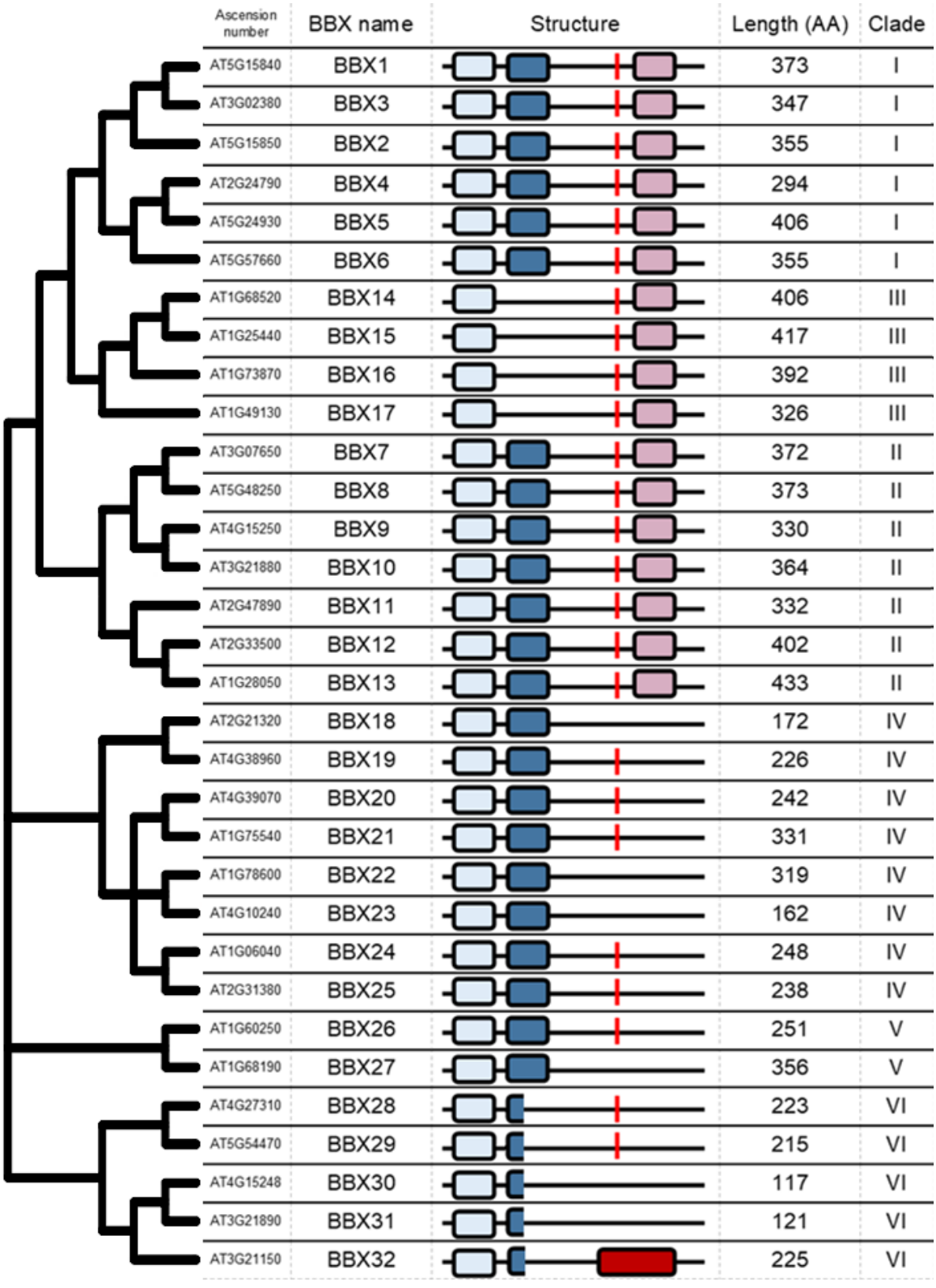

Figure 6.3.7: A list of the Arabidopsis thaliana BBX family members with their ascension numbers (Gangappa and Botto, 2014). Within the structure column, light blue represents B-box 1, dark blue represents B-box 2, a red dash represents

the presence of at least one VP motif, pink represents a CCT domain and dark red represents a novel BBX32 domain. Clades are given based on a maximum likelihood phylogenetic tree of the BBX family (Figure S2 [Page 330]) with the clade number given in ascending order starting from the lowest BBX member of the clade. The phylogenetic tree was a maximum likelihood tree using the JTT model with 500 bootstrap replicates. The order of the BBX proteins were based on their position within the tree.

The greatest change was the separation of BBX26 and BBX27 into their own clade, labelled as Clade V. BBX28 - BBX32 form the new clade VI. Potential VP motifs were also identified in BBX28 and BBX29. The BBX32 novel domain was also added. Clade I was determined by the phylogenetic analysis to be closer to Clade III than Clade II. It was not possible to determine the way the clades IV, V and VI split from Clades I, II and II from the *Arabidopsis thaliana* genes. The sequences of *BBX* from other species were also gathered for analysis.

Clade I was determined to be closer to Clade III when a large-scale analysis was performed on 9 species (species from Figure 6.3.5 [Page 217] and *Klebsormidium nitens*; Figure S3 [Page 332]). In this analysis, *Arabidopsis* BBX26 formed the outgroup and Clade V was made up of BBX27 and its homologues. The model couldn’t strongly separate Clade II and Clade V. Clade IV divided up into 4 subclades (Clade IVa - IVd) and *Klebsormidium nitens* KnBBX6 was modelled as being not specifically related to any of the subclades and as a descendant of the parent of all of Clade IV. A similar situation occurred with Clade VI where BBX28 and BBX29 divided from BBX30 - BBX32. However, the most distant member of Clade

VI, KnBBX7, has the novel domain insinuating that all of Clade VI are descendant from an ancestor containing the novel domain.

Lyu *et al*. (2020) identified the BBX family members within *Prunus avium* (sweet cherry). They showed that *Prunus avium* has 15 BBX family members. The Group V members are similar to the Clade VI *Arabidopsis BBX* genes by protein structure and three of these genes were discovered. Wang *et al*. (2021) drew together a lot of calculable information about BBX proteins including the molecular weight and isoelectric point. Of the three *BBX* genes that were similar to clade VI, two of them had greater isoelectric points than the other (4.51, 9.09, 9.32). Lyu *et al*. (2020) also analysed the theoretical isoelectric point (pI) of *BBX* genes of *Arabidopsis thaliana,* and an identical phenomenon was observed. I repeated this analysis for 7 different flowering plant species including *Arabidopsis thaliana*. An outgroup analysis was also performed on the gymnosperm *Picea abies*, the vascular plant *Selaginella moellendorffii* and the charophyte *Klebsormidium nitens*. This brought the total to 10 species.

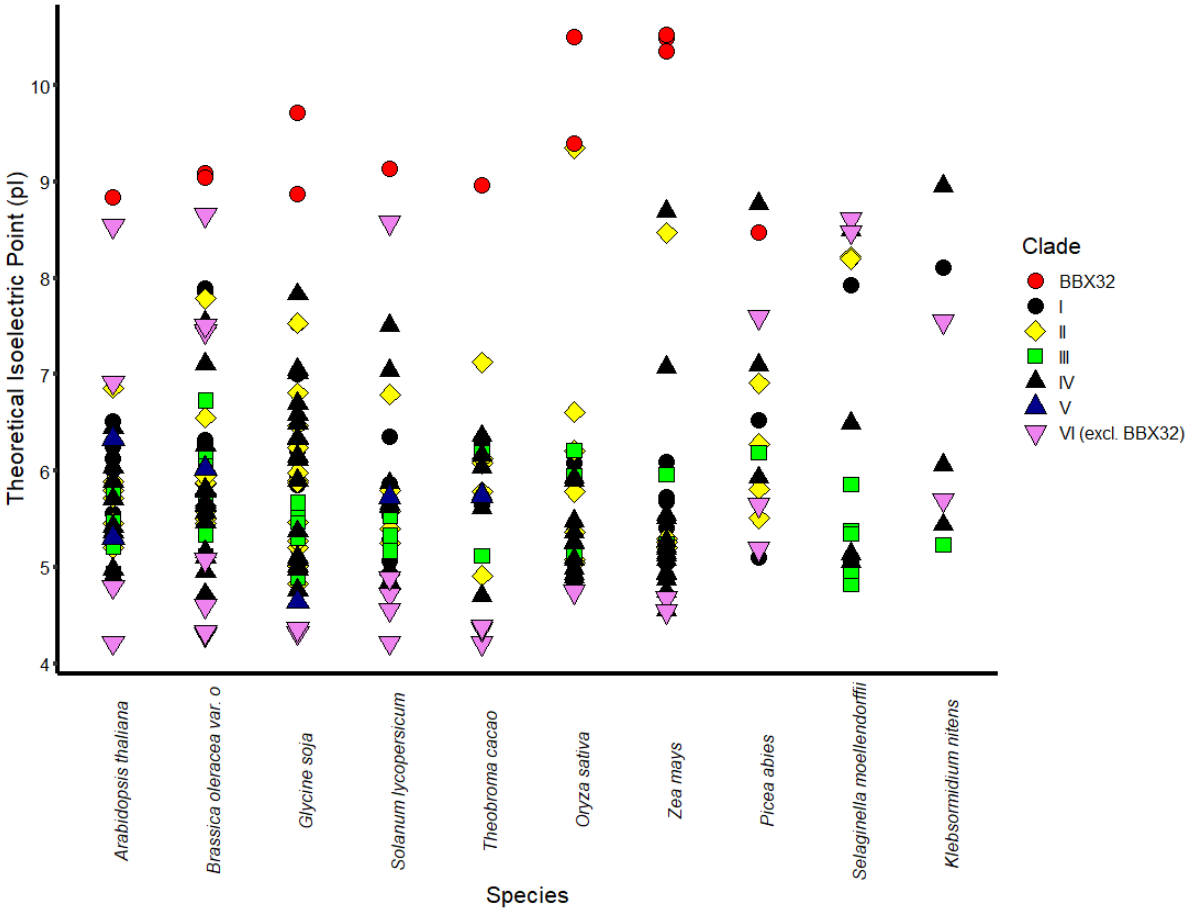

Figure 6.3.8: The calculated theoretical isoelectric point (pI) of the BBX family members by clade of different species. BBX32 has been separated from clade VI to be shown individually.

5 eudicots and 2 monocots were studied and the *BBX32* gene was identified using the core-like domain and B-box1 similarities. All of these species identified a BBX32 homologue as having the greatest pI. Some species had multiple BBX32 homologues; for these species no other BBX protein had a greater pI than any of these BBX32 homologues. BBX32 consistently has the highest pI of any BBX family protein.

Picea abies identified a *BBX32* homologue as having the second highest pI. *Selaginella moellendorffii* and *Klebsormidium nitens* did not have a *BBX* family member that wasn't closer related to another *BBX* gene than *BBX32*. However, when both of the proteins closest to BBX32 were run through the Phyre 2.0 algorithm, they both output a similar result to *Arabidopsis* BBX32 including the novel TFIIb core-like domain. The clade VI BBX proteins in *Selaginella moellendorffii* also have the highest theoretical isoelectric point.

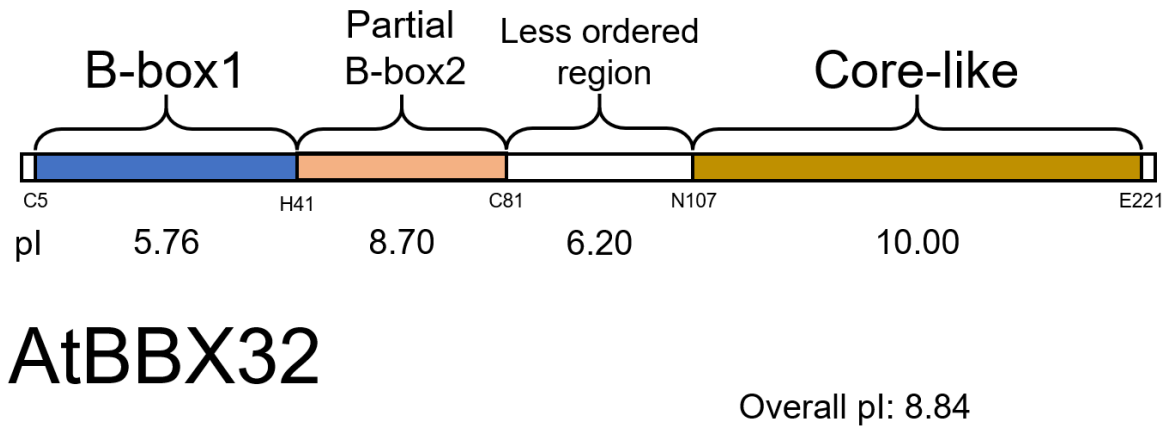

Figure 6.3.9: The theoretical isoelectric point (pI) of different regions of the *Arabidopsis thaliana* BBX32 protein.

The AtBBX32 protein sequence was divided up by its newly discovered regions and each of these were analysed for their theoretical isoelectric point (pI). The different sections of the BBX32 protein have wildly different theoretical isoelectric points. The novel domain core-like region of BBX32 had a very high pI whereas the B-box1 domain has a pI of 5.76 which was far closer to the BBX family average (Figure 6.3.7 [Page 222]; Figure 6.3.6 [Page 220]). This provides further evidence to the difference between *BBX32* and the rest of the *BBX* family members.

6.3.5: Intra-family connectivity of the BBX family

Most members of the BBX family can form protein bonds with other BBX family members (Holtan *et al*., 2011; Trigg *et al*., 2017; Tripathi *et al*., 2017). Certain BBX family members can bind more than others. This was analysed and many of the BBX family were found to be involved in a large-scale transcription factor binding analysis (Trigg *et al*., 2017). These known connections can be formed into a network.

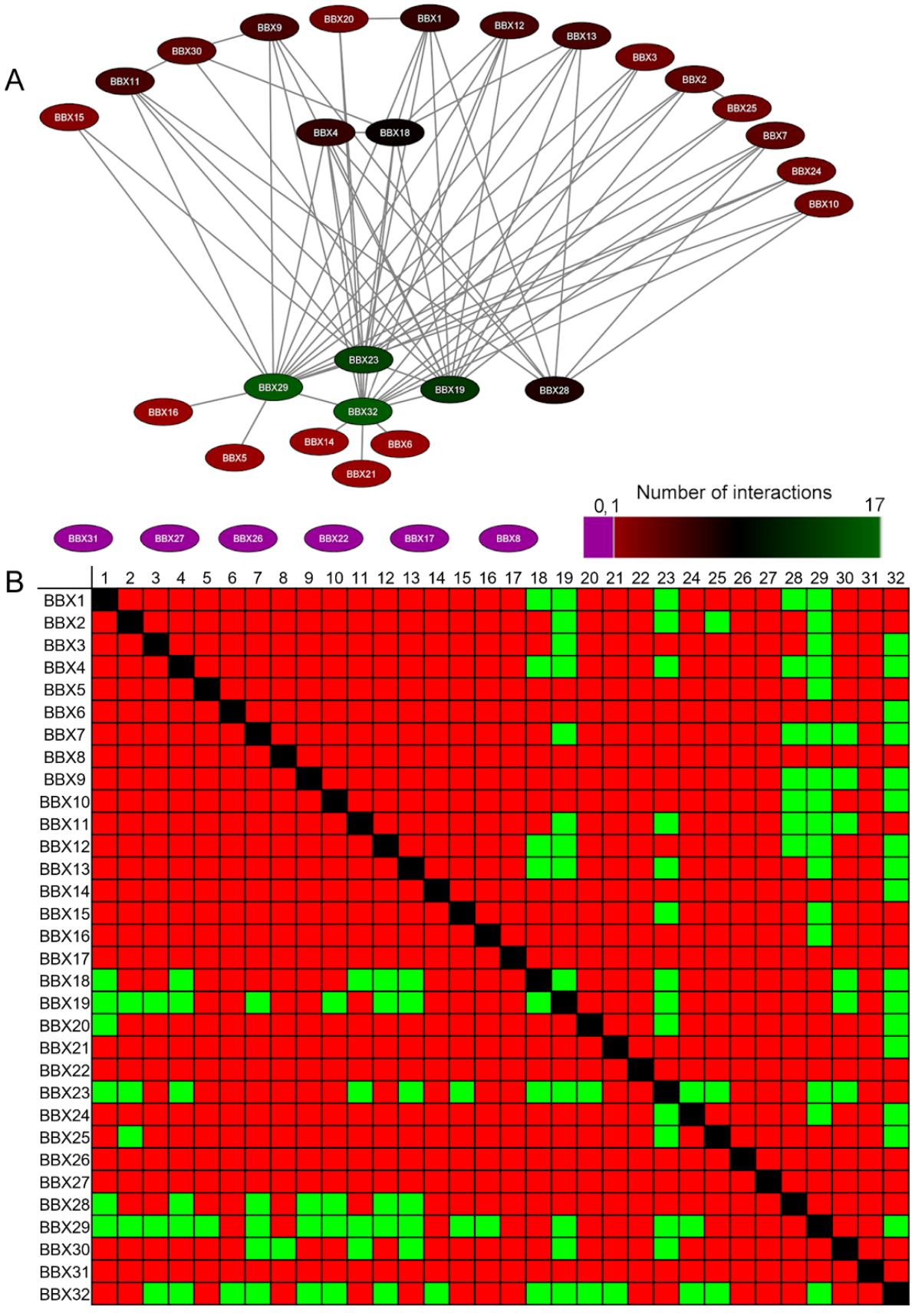
A
BBX9
BBX20
BBX1
BBX12
BBX13
BBX30
BBX3
BBX11
BBX2
BBX15
BBX25
BBX4
BBX18
BBX7
BBX24
BBX10
BBX23
BBX29
BBX19
BBX28
BBX16
BBX32
BBX14
BBX6
BBX5
BBX21
Number of interactions
0, 1
17
BBX31
BBX27
BBX26
BBX22
BBX17
BBX8
B
1 2 3 4 5 6 7 8 9 10 11 12 13 14 15 16 17 18 19 20 21 22 23 24 25 26 27 28 29 30 31 32
BBX1
BBX2
BBX3
BBX4
BBX5
BBX6
BBX7
BBX8
BBX9
BBX10
BBX11
BBX12
BBX13
BBX14
BBX15
BBX16
BBX17
BBX18
BBX19
BBX20
BBX21
BBX22
BBX23
BBX24
BBX25
BBX26
BBX27
BBX28
BBX29
BBX30
BBX31
BBX32

4232

Figure 6.3.10: The interaction network between the BBX family members. Data was extracted from the BioGrid database with most of the interactions being based on high-throughput *in vitro* yeast two-hybrid experimental data (Trigg *et al*., 2017). (A) shows the interactions as a network where colour scales with interaction number. (B) displays the same data but as a grid where green denotes an interaction and red indicates no known interaction.

The *Arabidopsis* BBX family is highly connected however it only takes 4 BBX proteins to completely connect every family member that does interact: BBX19, BBX28, BBX29 and BBX32 (Figure 6.3.10A [Page 229]). BBX29 has the highest number of interactions at 17 followed by BBX32 at 15. Interestingly, there are no interactions discovered between any of the members of clades I, II, or III (Figure 6.3.10B [Page 229]). These happen to be the BBX family members with DNA-binding CCT domains (Figure 6.3.7 [Page 222]).

Holtan *et al*. (2011) postulated that BBX32 suppresses the action of HY5 using BBX21 as an intermediary. However, BBX32 can interact with many BBX family members (Figure 6.3.10 [Page 229]). The BioGrid database can also be used to analyse the primary and secondary bridging connections (requiring one or two other BBX family proteins respectively) between HY5 and BBX32 and these can be formed into a network.

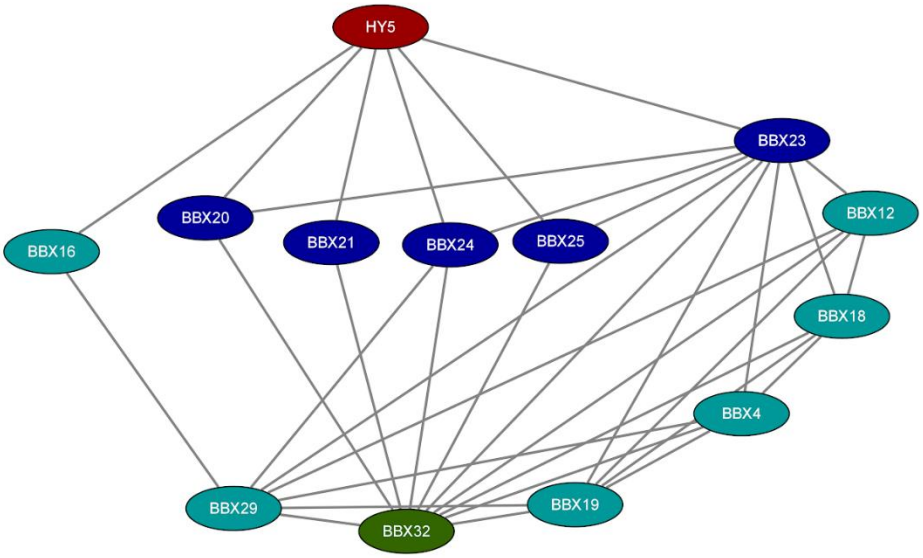

Figure 6.3.11: Interactions between HY5 and BBX32 involving other members of the BBX family. Data was adapted from the BioGrid database. Interactions involving only one linking protein are shown in dark blue. Interactions requiring two proteins to bridge between BBX32 and HY5 are shown in turquoise.

There are many different connections that BBX32 can form to bridge to HY5. BBX20, BBX21, BBX23, BBX24 and BBX25 (all from Clade IV) bind both HY5 and BBX32 (Figure 6.3.11 [Page 230]). It is possible that the removal of any one of these intermediary proteins would not disrupt the ability of BBX32 to impact the functionality of HY5.

6.3.6: Conclusion

The structure of BBX32 was discovered to be far more complex than originally published (Khanna *et al*., 2009; Holtan *et al*., 2011). The potential novel domain may have an as yet undescribed causal relationship to the functions of BBX32. I have

found that *BBX32* is very well conserved amongst flowering plant species and exists throughout all embryophytes examined. Within this section, I have created a base of information that was further used to develop gRNAs for a *BBX32-CAS9* allelic series.

6.4: Generation of a BBX32 allelic series using CRISPR CAS9

The generation of a *BBX32* allelic series requires a full analysis of the *BBX32* gene and the protein. The coding region of the gene was analysed in the previous section however the 5'UTR was not included. The whole sequence can then be analysed to find guide RNA (gRNA) target sites for use in the CAS9 construct.

6.4.1: Creating gRNAs for *BBX32*

Prior to designing the gRNAs for *BBX32*, further analysis was conducted on the non-coding regions of the gene. The expression of BBX32 may be post-transcriptionally controlled, shown by the rapid change in BBX32 mRNA quantity upon exposure to HL even when expressed from the cauliflower mosaic virus (CaMV) 35S promoter (Alvarez-Fernandez *et al*., 2021). The gene was submitted to a mirRNA BLAST algorithm to detect any miRNA target sites (Kozomara and Griffiths-Jones, 2011). A single weak miRNA target site was found to exist in the 5'UTR (Figure 6.4.1 [Page 232]). This could be targeted with CAS9 to analyse the phenotype of a mutant plant missing this potential target site.

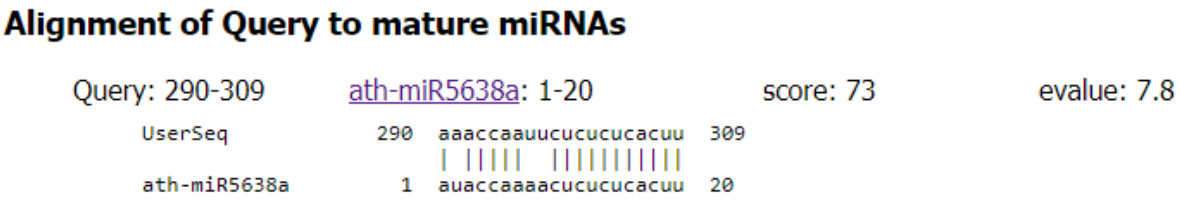

4291

4292 **Figure 6.4.1: The alignment of *BBX32* cDNA and miR5638a.** The sequence of

4293 *BBX32* was submitted to miRBase, a BLAST algorithm, to be compared against

4294 mature miRNAs (Kozomara and Griffiths-Jones, 2011).

4295

4296 Many tools exist to aid in the design of CRISPR CAS9 gRNAs. The *BBX32* gene was

4297 inputted to several different CRISPR/CAS9 tool programs; Synthego (Robb, 2019),

4298 CRISPR-P 2.0 (Liu H *et al*., 2017), Deskgen (Hough *et al*., 2016), and Benchling

4299 (San Francisco, California). Using multiple tools allowed the gRNAs selected to be

4300 cross-checked for on and off-site targeting. A very large number of potential gRNAs

4301 existed, and these were analysed to shortlist gRNAs that target specific regions of

4302 the *BBX32* gene and have good on and off-site targeting.

4303

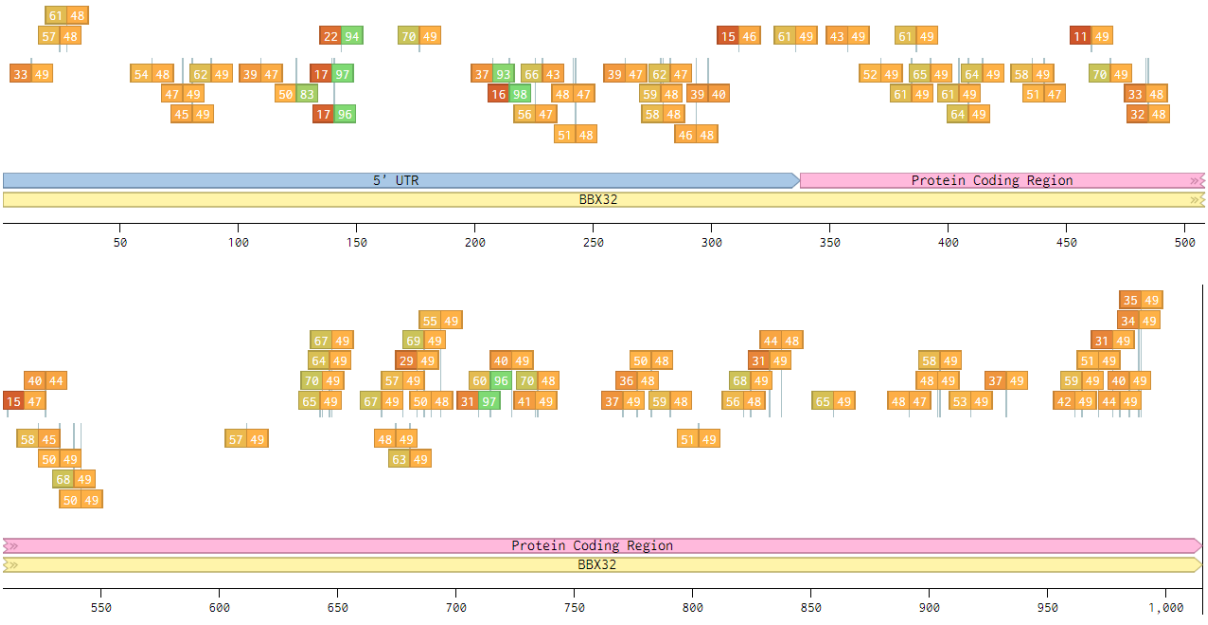

4304

Figure 6.4.2: Locations of CRISPR CAS9 guide RNA (gRNA) target sites on the *BBX32* gene. Numbers indicate on-target score (left; Doench *et al*., 2016) and off-target score (Hsu *et al*., 2013) where higher numbers indicate better targeting (Benchling, 2022).

The Benchling tool shows 90 potential gRNAs within the 5'UTR and coding region of *BBX32*. The gRNAs were constrained to a length of 20 base pairs and targeting NGG in accordance with the CAS9 being used. The T-DNA could be loaded with between 1 and 8 gRNAs (Ordon *et al*., 2020). A balance was sought between creating *BBX32* alleles with specific single mutations and an allelic series with many altered locations. I have used 4 gRNAs to attempt to cleave a section of the *BBX32* gene to disrupt B-box1 and potentially the ATG start codon.

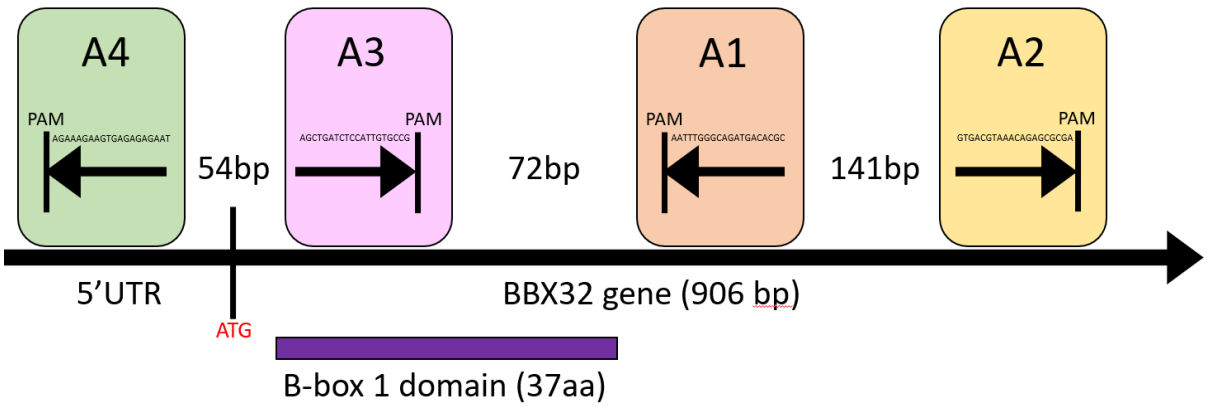

Figure 6.4.3: The 4 selected gRNAs labelled A1 - A4 at their target site location on the *BBX32* gene. Protospacer adjacent motif (PAM) indicates the CAS9 cleavage site with the arrow showing the directionality relative to the gRNA sequence. The base pair (bp) numbers indicate the distance between the gRNAs.

Each gRNA was chosen to specifically target a part of the *BBX32* gene. The cut site is typically around 3 - 4 base pairs upstream of the PAM site (opposite direction from the arrow). The gRNA selected target the following regions of the *BBX32* gene:

- A1 targets just prior to the two cysteines that align with the first two cysteines of the B-box2 domain of other BBX family members (Table 6.3.4 [Page 218]).
- A2 targets a region prior to the potential novel domain (Figure 6.3.4 [Page 215])
- A3 targets between the third cysteine and the first asparagine of the B-box1 domain (Table 6.3.1 [Page 213])
- A4 targets the centre potential miRNA site (Figure 6.4.1 [Page 232]).

Cutting at multiple target sites has the chance to remove larger portions of the *BBX32* gene. These gRNAs were placed into shuttle plasmids before being added to the pDGE277 backbone. These genetic manipulations used the restriction enzymes BpiI and BsaI respectively both with the Golden Gate methodology (section 2.5.4 [Page 59]). The schematic of the CAS9 plasmid, pDGE277, can be seen in Figure 6.4.4 [Page 234].

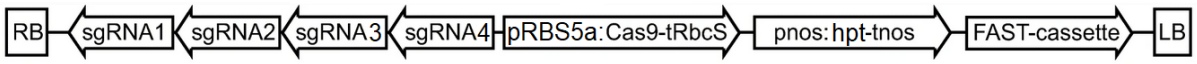

Figure 6.4.4: Schematic of the *BBX32-CAS9* T-DNA construct designed by Ordon *et al*. (2020). sgRNA 1-4 represent the selected gRNAs labelled A1 - A4. *pRBS5a:CAS9-tRbcS* is the *CAS9* construct driven by the *RBS5a* promoter and terminated by *trbs E9*. pnos:hpt-tnos provides hygromycin resistance and the FAST-cassette targets RFP tagged OLE1 to the seed coating for simplified selection (Shimada *et al*., 2010). Modified from Ordon *et al*. (2020).

The pDGE277 plasmid incorporates two different selection methods. *pnos:hpt:tnos* gives an *Arabidopsis* plant the ability to grow on agarose plates containing the aminoglycoside antibiotic hygromycin. Transformants can be quickly identified by growing the T_0 seed on MS media containing hygromycin. The FAST-cassette encodes an OLEOSIN1 (OLE1) protein fused with RED FLUORESCENT PROTEIN (RPF) driven by the *OLE1* promoter (Shimada *et al*., 2010). This tagged protein is abundant in the seed coating allowing swift identification of transgenic seed.

CAS9 only needs to be transiently expressed in the plant genome to cut the *BBX32* gene. If the CAS9 T-DNA remains in the plant, changes in the *BBX32* gene may continuously occur creating different somatic mutations which are both difficult to sequence and the phenotype becomes difficult to interpret. The plant would also become more susceptible to off-site mutations. Therefore, after only a single generation, the T-DNA needs to be segregated out of the *BBX32* mutant lines. The FAST-cassette enables the selection of seeds that do not contain the T-DNA.

6.4.2: Infiltration and selection of *CAS9-BBX32* plants

Col-0 ecotype *Arabidopsis thaliana* plants were transformed using the floral inoculation method with *Agrobacterium tumefaciens* containing the completed *BBX32-CAS9* T-DNA (section 2.5.5 [Page 60]). These plants were allowed to grow, set seed, and senesce. Seeds from the transformed plants (T_0) were grown on hygromycin selection plates (section 2.6.1 [Page 62]).

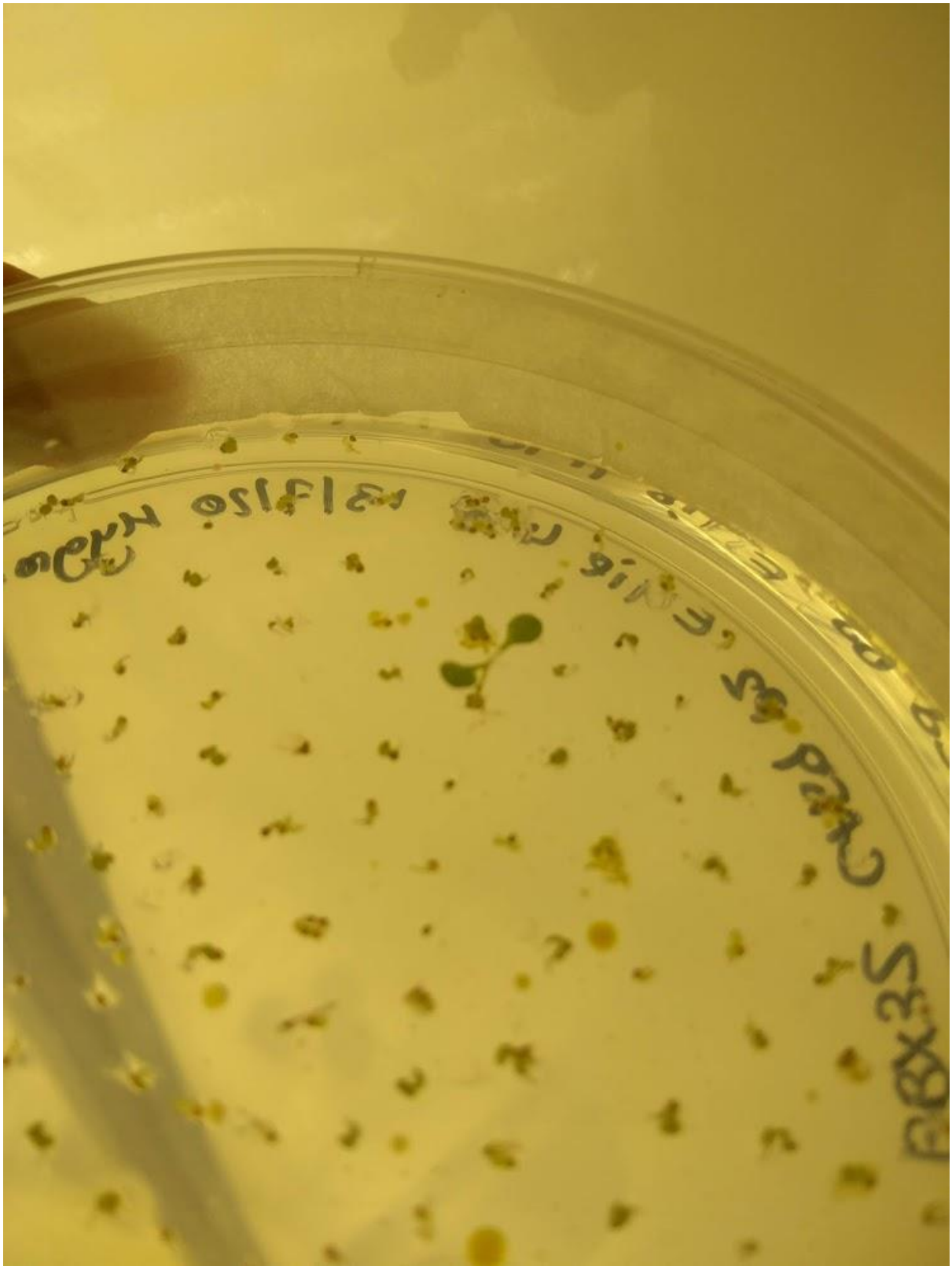

Figure 6.4.5: Progeny of C*AS9-BBX32* inoculated plants growing on hygromycin MS plates.

Only seeds transformed by the *CAS9-BBX32* T-DNA with the hygromycin resistance gene were able to grow. 62 T_1 plants were recovered from hygromycin-containing MS plates, and these were transplanted onto soil after 2 - 3 weeks of growth.

Figure 6.4.6: Putative transformed *Arabidopsis* plants selected from hygromycin-containing medium transferred to soil.

Plants were allowed to grow on soil, flower, set seed and senesce. The seed was separated and illuminated under RFP fluorescent lighting and filtered images were captured.

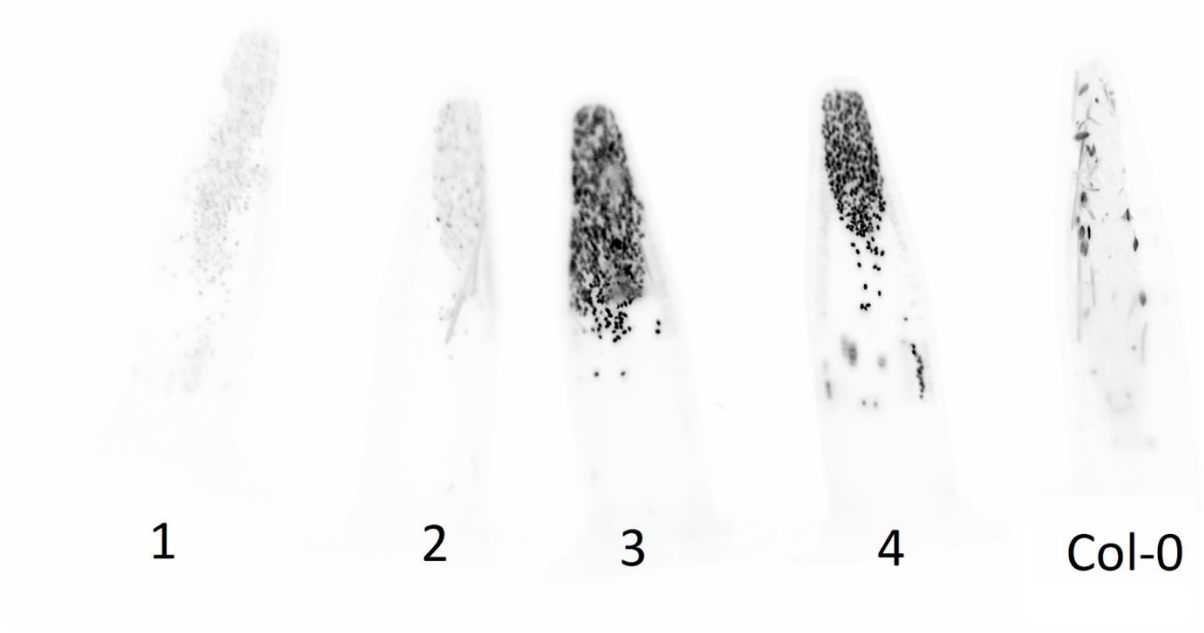

Figure 6.4.7: Negative images of the RFP-containing *CAS9-BBX32* mutant and Col-0 seeds.

Only chaff, which has some background bioluminescence, can be seen in the Col-0 tube and the seeds appear as a single mass. The RFP positive seeds however can be individually identified. Some of the seeds of T_1 plants are brighter than others. This can be seen between the more muted seed packets of 1 and 2 compared to 3 and 4. This is most likely related to the quantity of OLE1-RFP in the seed coating and may have a relationship with the expression of *CAS9*.

The *BBX32-CAS9* seeds which would germinate into M_2 plants were placed on thin agar wells to prevent movement between imaging and selection. Grayscale and RFP detecting images were taken and placed side-by-side in Figure 6.4.8 [Page 239] (section 2.6.2 [Page 62]).

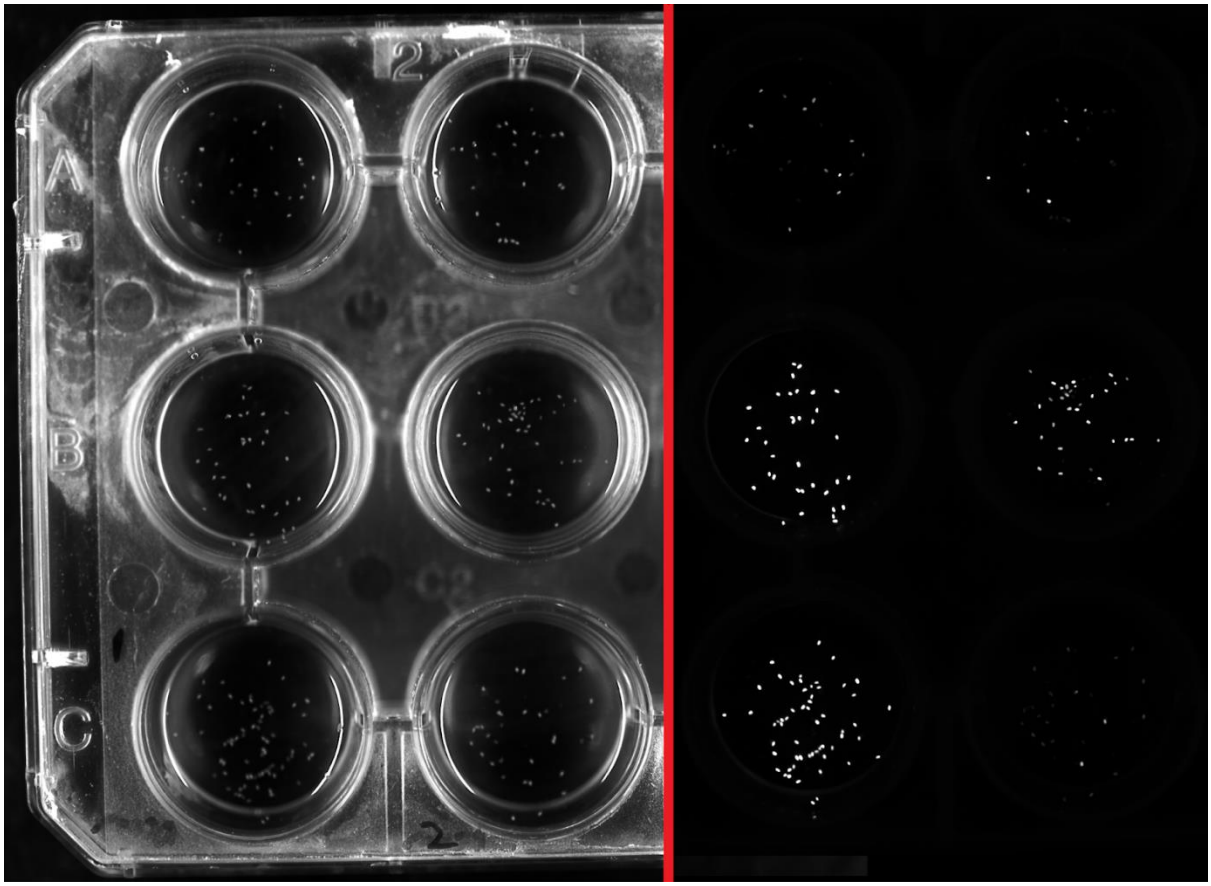

Figure 6.4.8: Grayscale (left) and RFP fluorescent (right) images of *BBX32-CAS9* seed of T_1 plants.

Some seed batches had very weak RFP luminescence and therefore these batches were omitted to prevent false negatives. Bright seed batches were analysed and carried forward to M_2. Of the bright seed batches, seeds that were visible under the grayscale but did not have corresponding RFP fluorescence were determined to be RFP negative. These seeds were selected for and grown under standard growth conditions (section 2.2.1 [Page 35]). These plants may have been edited by CAS9 but would likely not contain the *CAS9-BBX32* –hyg^R T-DNA and if so, would not be further edited.

The plants were grown, and once large enough DNA was extracted. The M_2 generation was allowed to reproduce, and those seeds were grown and also had DNA extracted. PCR was performed on the M_2 parents and the M_3 progeny to identify mutant *BBX32* alleles. Large changes in allele size would be apparent in multiple bands on a gel after electrophoresis.

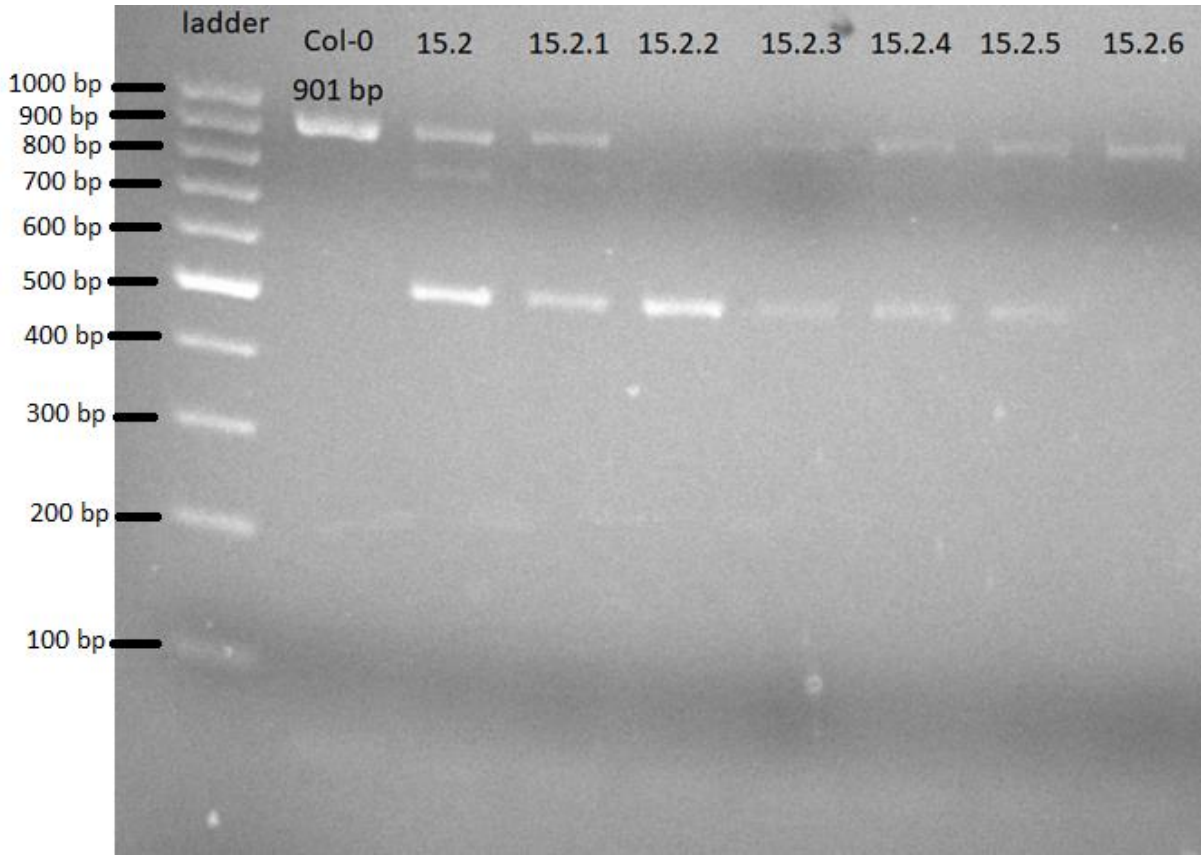

Figure 6.4.9: Gel electrophoresis of PCR products performed on Col-0, 15.2 M_2 and its M_3 progeny 15.2.1 - 15.2.6. PCR was performed using BBX32F and BBX32R primers (Table S6 [Page 338]). The genotype, ladder and expected size of the Col-0 band have been superimposed on the image of the agarose gel above the respective lane.

Col-0 produced a DNA band of approximately 900 base pairs which is very similar to the predicted band size of 901 base pairs. The M_2 parent 15.2 had three DNA bands of approximately 900, 800 and 500. The M_3 progeny 15.2.1, 15.2.3, 15.2.4 and 15.2.5 all had identical DNA bands. Whereas 15.2.2 and 15.2.6 only had the 500 bp and 900 bp bands respectively. The 800 bp band does not appear independently and may therefore be the result of heterologous hybridisation between the 500 and 900 bp DNA strands.

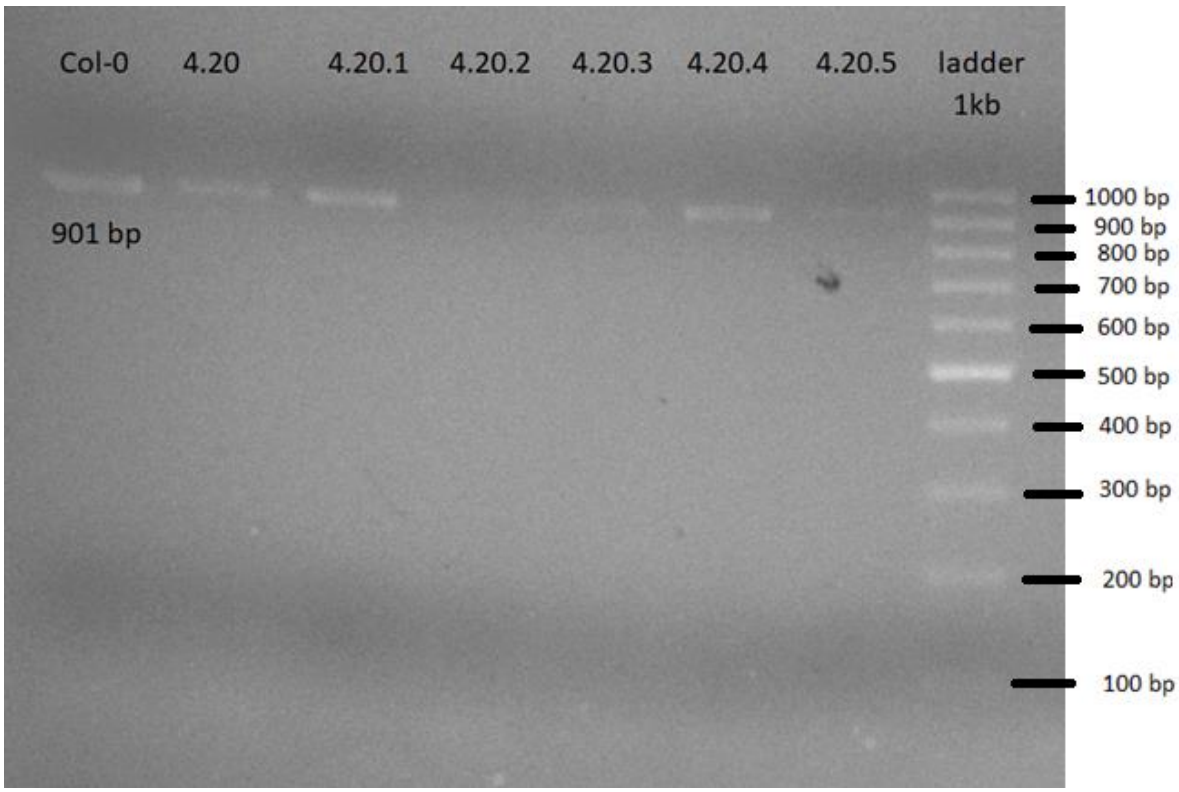

Figure 6.4.10: Gel electrophoresis of PCR products performed on Col-0, 4.20 M_2 and its M_3 progeny 4.20.1 - 4.20.5. PCR was performed using BBX32F and BBX32R primers (Table S6 [Page 338]). The genotype, ladder and expected size of the Col-0 band have been superimposed on the image of the agarose gel above the respective lane.

The M_2 4.20 and its M_3 children did not display bands that deviated far from the 900 bp Col-0 band. The parent 4.20 band appears very slightly higher than the Col-0 band and 4.20.5 also appears to be larger than the 900 bp ladder band. However, it was difficult to determine if these were due to imperfections in the agarose gel or true slight differences. PCR product samples from 4.20 and 15.2 and their progeny were used in DNA sequencing. A sequencing primer was selected close to but not overlapping the forward PCR primer.

6.4.3: Sequencing of *BBX32-CAS9* mutants

The *BBX32* PCR product of Col-0, 15.2.2, 15.2.6, 4.20 parent and the 4.20 M_3 progeny only displayed a single DNA band on the agarose gels (Figure:6.4.8 [Page 239]; Figure:6.4.9 [Page 240]) The PCR products were analysed using DNA sequencing. The *BBX32* sequence of Col-0 was completely identical to the sequence on the NCBI BLAST database and was used as a WT comparison (Figure S4 [Page 333]).

Sanger DNA sequencing is conducted progressing from the 5’ end towards the 3’ end and requires the individual DNA strands within the sample to be nearly all identical for good signal and base identification. 15.2 and 4.20 were revealed to be heterozygotes as the two alleles within 15.2 and 4.20 led to two different sequences DNA in the samples. Clear base recognition and therefore DNA sequencing failed once a deviation between the two sorts of DNA strands were reached. The homozygous M_3 progeny were simple to isolate from 15.2 due to the clear band size

differences (Figure 6.4.8 [Page 239]). Several 4.20 M_3 progeny were analysed to obtain both of the alleles as homozygotes.

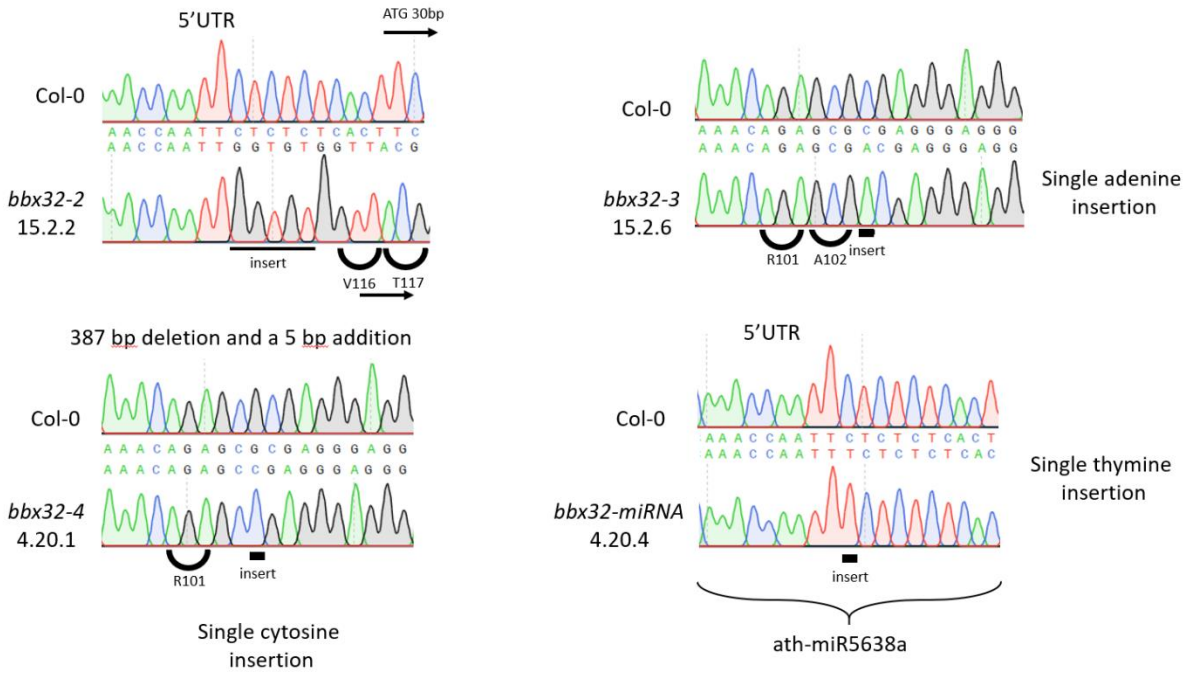

Figure 6.4.11: Partial sequences of CAS9 altered *BBX32* genes compared to the Col-0 *BBX32* gene. The partial sequence identifies the differences compared to the Col-0 *BBX32* gene.

The *BBX32* PCR product from 15.2.2 was identified as only containing the ~500 bp DNA band (Figure 6.4.9 [Page 240]). This band was calculated using the DNA sequence product to be 528 bp in length. This is significantly shorter than the 901 bp length of the Col-0 *BBX32* PCR product. 15.2.2 contained a 378 bp deletion and a 5 bp addition at the same point starting in the 5'UTR. In relation to the gRNAs, the region between A4 and A2 was missing in 15.2.2. This missing region includes the ATG start codon and the entire B-box1 domain. Two in-frame start codons exist in the remainder of the sequence however these only produce sequences of 21 and 35 amino acids in length. This product is too short to encompass the full length of the

novel domain (Figure 6.3.3 [Page 211]). 15.2.2 does not appear to contain an operational form of the *BBX32* gene and is labelled henceforth *bbx32-2*.

15.2.6 was homozygous for the other 15.2 allele which appeared to be the same length as the Col-0 band. However, 15.2.6 contained a single adenine addition. This addition caused a frame-shift mutation within R103 seemingly caused by the A2 gRNA. This shifted the potential novel domain out-of-frame. This was a useful mutation for testing the functionality of the potential novel domain. The 15.2.6 mutant was labelled *bbx32-3*.

4.20.1 and 4.20.4 both also contain a single base pair addition in the *BBX32* gene. The addition within 4.20.1 was at a very similar point to the *bbx32-3* addition inserting a cytosine two base pairs earlier in the codon for A102. 4.20.1 was labelled *bbx32-4* and was predicted to be very similar to the *bbx32-3* allele. The single thymine insertion within 4.20.4 was found to be within the potential miRNA target site and results in the miRNA BLAST no longer discovering a miRNA target site within the *BBX32* gene. If the miRNA target site has an impact on the *BBX32*, this would most likely be disrupted within 4.20.4. 4.20.4 was labelled *bbx32-miRNA*.

6.4.4: Conclusion

Four new *BBX32* mutants were developed using CAS9. More mutants could be developed by growing and analysing more M_2 plants. However, these mutants were deemed sufficient to test the phenotype of both a *BBX32* deficient mutant and a

mutant missing the novel *BBX32* domain. In the next section, I aimed to explore the phenotype of these mutants in comparison to WT and the known *bbx32-1* mutant.

6.5: Testing novel *BBX32-CAS9* mutants

The development of novel *BBX32* mutants necessitated testing methodologies that could be used to compare them to both Col-0 and *bbx32-1*. Holtan *et al*. (2011) identified that *bbx32-1* had shorter hypocotyls than the WT control under low fluence rates. The novel *BBX32* mutants were initially tested for hypocotyl length in the dark. The light acclimation phenotypes were also very important to test.

6.5.1: Photomorphogenic phenotype of *BBX32* mutants

Seeds that would grow into M_4 plants were placed onto ½ MS agar plates and forced to germinate with 4 days of stratification and 16 hours of exposure to white light. The plates were then placed in the dark and at a vertical angle so the plants would grow up the agar over the course of 7 days. The seedlings were imaged, and hypocotyl lengths were measured using ImageJ (section 2.2.4 [Page 39]). The mutant hypocotyl lengths were compared with *bbx32-1* and Col-0 to find significant differences in hypocotyl length.

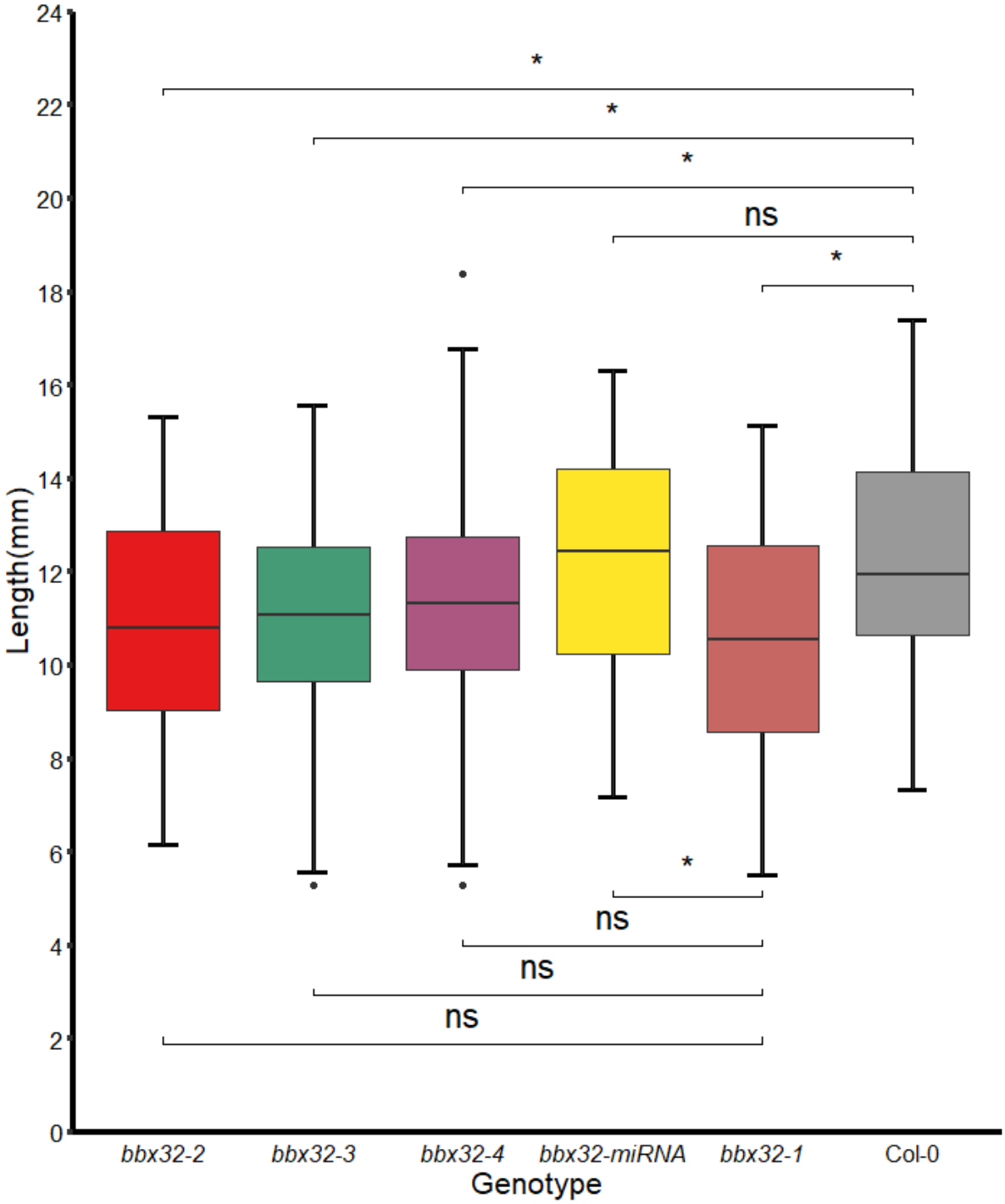

Figure 6.5.1: Hypocotyl lengths of different *BBX32-CAS9* mutants compared to Col-0. Plants were grown under darkness following 16 hours of 150 µmol m^{-2} s^{-1} for 7 days. Asterisks indicate significance between the *CAS9-BBX32* lines and Col-0 (top) or *bbx32-1* (bottom; ANOVA; $p < 0.005$; $n > 50$). The hypocotyl data presented was merged from two separate experiments.

The hypocotyl length of *bbx32-1* was significantly shorter than that of Col-0 as did 3 of the 4 novel *BBX32-CAS9* mutants, *i.e., bbx32-2*, *bbx32-3* and *bbx32-4* all had significantly shorter hypocotyls than Col-0. The *BBX32* mutants *bbx32-1*, *bbx32-2*, *bbx32-3,* and *bbx32-4* were not significantly different from one another. However, *bbx32-miRNA* was not significantly different to Col-0 and was significantly longer than *bbx32-1*.

The hypocotyl lengths of the genotypes formed two clear groups. The mutants were either significantly different to *bbx32-1* or Col-0 but not both. *bbx32-2, bbx32-3* and *bbx32-4* formed an in-group with *bbx32-1* whereas *bbx32-miRNA* formed an in-group with Col-0. The *bbx32-miRNA* mutant was not analysed further.

6.5.2: HL acclimation phenotype of *BBX32* mutants

Alvarez-Fernandez *et al*., (2021) showed that *bbx32-1* had a significantly increased PSII operational efficiency after 2, 3 and 4 days of HL exposure compared to Col-0. This experiment was repeated by with a higher number of plants and significance on day 1 and low significance day 5 were discovered (Figure 6.5.2 [Page 248]). The HL acclimation phenotype of *bbx32-2*, *bbx32-3* and *bbx32-4* were also analysed.

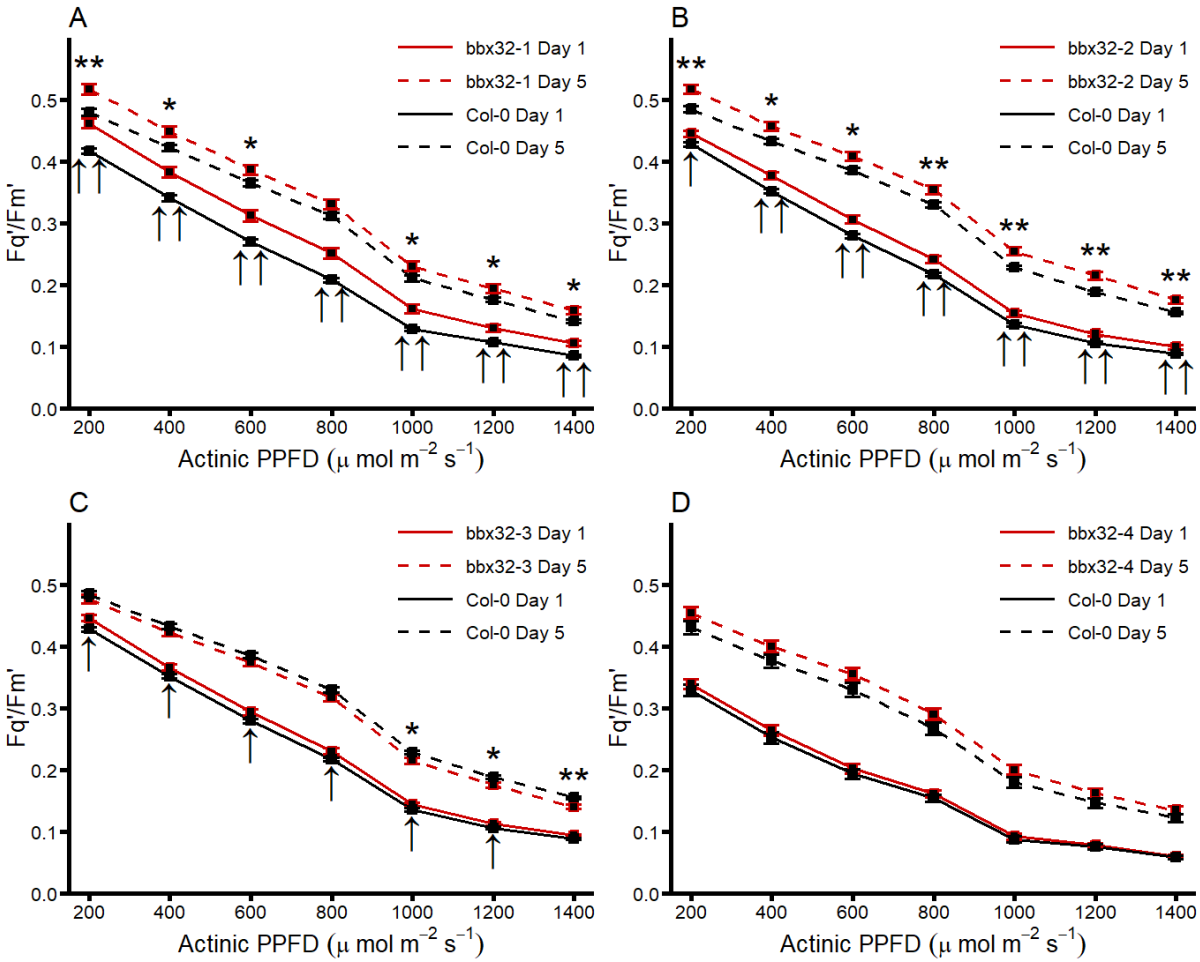

Figure 6.5.2: HL Acclimation of *bbx32-1* (A), *bbx32-2* (B), *bbx32-3* (C), *bbx32-4* (D), and Col-0 plants. Fq'/Fm' is determined by chlorophyll fluorescence with a light intensity range of 200 µmol m^{-2} s^{-1} to 1400 µmol m^{-2} s^{-1} at 200 µmol m^{-2} s^{-1} increments. Measurements were taken from 4-6 week old plants with a minimum of 6 mature leaves each (means ± SE). Arrows and asterisks denote a significant difference between the day 1 and day 5 values respectively of the mutants and Col-0 (ANOVA, post-hoc GH; */↑ = $p < 0.05$; **/↑↑ = $p < 0.005$).

bbx32-2 had the most significant phenotype on day 5. However, there was minimal difference between *bbx32-1* and *bbx32-2*. These mutant phenotypes appear to be very similar. The mutants *bbx32-3* and *bbx32-4* had either very minimal significant or no significant differences to Col-0 on both measured days. *bbx32-3* and *bbx32-4* had

significantly shorter hypocotyls but did not have a light acclimation phenotype like that seen in the *bbx32-1* and *bbx32-2* mutants. This analysis was repeated with measurements taken every day on the representative of each of these two groups (*bbx32-2* and *bbx32-3*).

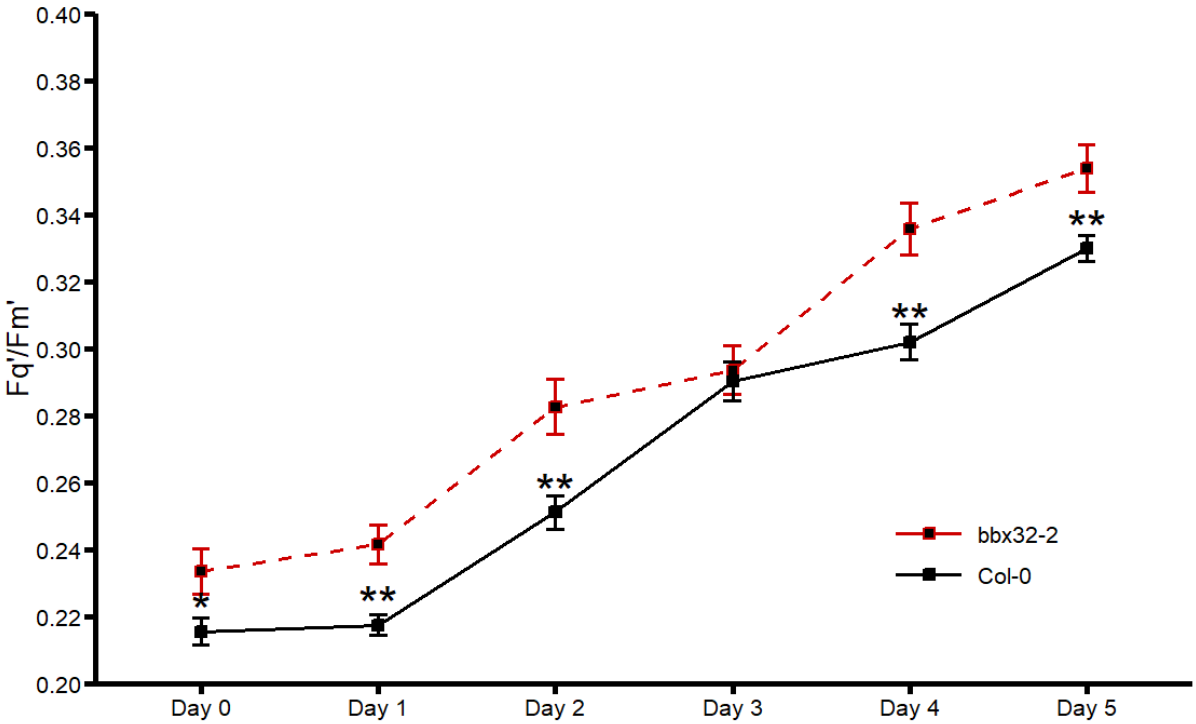

Figure 6.5.3: HL Acclimation of *bbx32-2* and Col-0 plants over 5 days of HL exposure. Fq'/Fm' is determined by chlorophyll fluorescence with a light intensity of 800 µmol m^{-2} s^{-1}. Measurements were taken from 8 week old plants with a minimum of 10 mature leaves each (means ± SE). Arrows and asterisks denote a significant difference between the mutants and Col-0 (ANOVA, post-hoc GH; */↑ = $p < 0.05$; **/↑↑ = $p < 0.005$).

The light acclimation phenotype of *bbx32-2* over the course of 5 days was very similar to the phenotype of *bbx32-1* found by Alvarez-Fernandez *et al*. (2021) with the least significant days being day 1 and day 5 (assuming that day 3 is an

anomalous result). Unlike Alvarez-Fernandez *et al*. (2021), a day 0 result prior to any HL exposure was also recorded. The day 0 measurement showed that *bbx32-2* had a pre-acclimated light acclimation phenotype. It had a slight increase in Fq'/Fm' compared to Col-0 with no HL exposure.

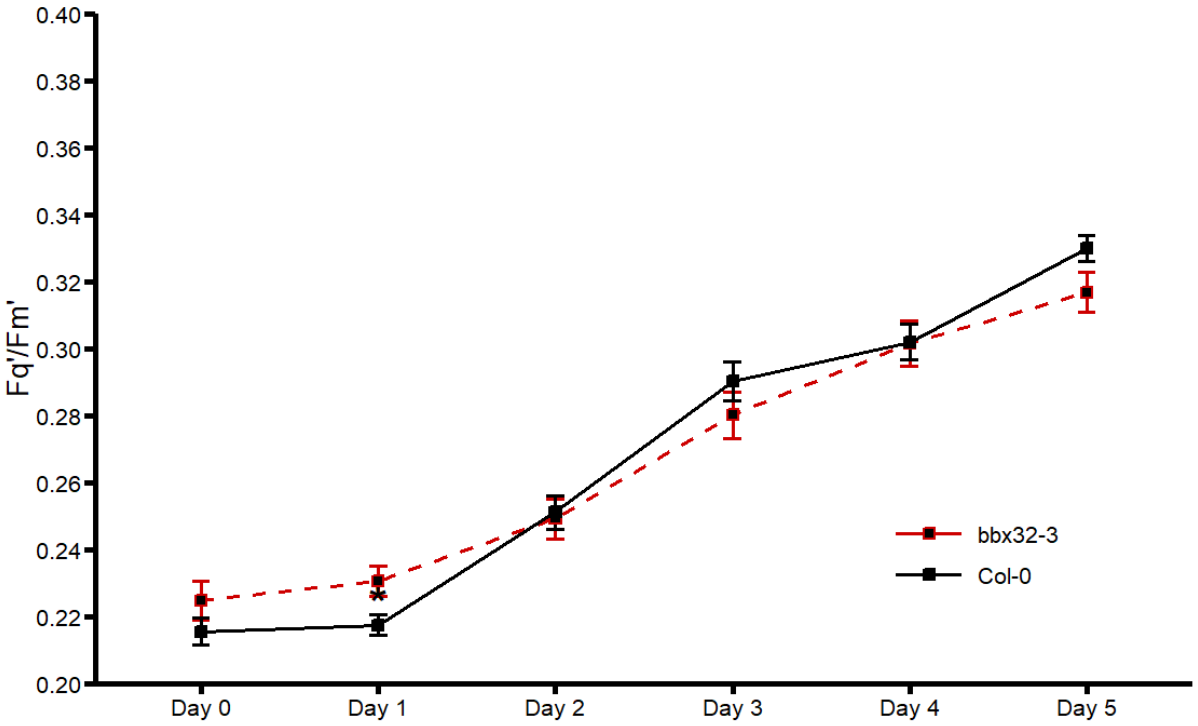

Figure 6.5.4: HL Acclimation of *bbx32-2* and Col-0 plants over 5 days of HL exposure. Fq'/Fm' is determined by chlorophyll fluorescence with a light intensity of 800 µmol m^{-2} s^{-1}. Measurements were taken from 8 week old plants with a minimum of 10 mature leaves each (means ± SE). Arrows and asterisks denote a significant difference between the mutants and Col-0 (ANOVA, post-hoc GH; */↑ = $p < 0.05$; **/↑↑ = $p < 0.005$).

bbx32-3 did not have a significantly different Fq'/Fm' to Col-0 on any day measured at the PPFD of 800 µmol m^{-2} s^{-1} other than a minor significant difference on day 1.

This matched the results seen in Figure 6.5.1 [Page 246]. *bbx32-3* did not have a significant light acclimation phenotype.

6.5.3: Conclusion

A differentiation has occurred between two groups of *BBX32* mutants. One group contains *bbx32-1* and *bbx32-2* which have both light acclimation phenotypes and hypocotyl phenotypes. The other group, *bbx32-3* and *bbx32-4*, however, only have a hypocotyl phenotype and not the light acclimation phenotype. The differentiation between these phenotypes is explored further in 6.6: Discussion.

6.6: Discussion

This section discovered a potential C-terminal domain of BBX32 and developed four novel *BBX32* mutants. The evolution revealed that *BBX32* is a very well conserved gene implying that its functionality may be well conserved. The overlap of HL acclimation and hypocotyl phenotypes of the novel *BBX32* mutants were more complex than originally expected. The integration of these ideas were further explored in this section.

6.6.1: The evolution of the BBX family

I conducted two separate analyses on the phylogenetic structure of the *BBX* family. One of these analyses included only the *Arabidopsis* genes and the second included 251 *BBX* genes gathered from 8 species including *Arabidopsis* Table S9 [Page 338]. The clade distinctions made between the two were very similar. I have concluded that the BBX family within *Arabidopsis thaliana* can be placed into 6 clades. However, much of the scientific literature uses only 5 structural groups. This stems

back to Khanna *et al*. (2009) who first catalogued the BBX family in *Arabidopsis thaliana*. This chapter attempted to replicate the phylogenetic tree found by Khanna *et al*. (2009) however this was unsuccessful. The reason this finding was not reproducible was due to the use of Bayesian inference phylogeny by Khanna *et al*. (2009) whereas I have created a maximum likelihood tree. The Bayesian inference phylogenetic methodology provides prior knowledge about the potential phylogenetic tree to the algorithm. It is only useful when prior knowledge exists or is assumed about the phylogeny. Khanna *et al*. (2009) does not state what prior knowledge was passed to the Bayesian inference phylogenetic tree. However, the only assumption that makes sense is that the five structural classifications created by Khanna *et al*. (2009) were passed to the Bayesian inference phylogenetic algorithm. This would have forced the combination of Clade V and Clade VI: BBX26 and BBX27 would have been grouped with BBX28 - BBX32.

Arabidopsis BBX26 was modelled as the outgroup to the large-scale *BBX* family analysis. Lyu *et al*. (2020) did not find *BBX26* gene expression and no transcript for *BBX26* was recovered from the *BBX32-HY5* RNA-seq (Alvarez-Fernandez *et al*., 2021). *BBX26* may not have been functional for a period of time and had been mutagenised. On analysis of the supplemental data of Khanna *et al*. (2009), the second cysteine pair of B-box2 of BBX26 and BBX27 were also clearly visible in supplemental Figure 1 (of Khanna *et al*., 2009) and aligned with the B-box2 domain of Clade I, II, III and IV BBX proteins. However, these B-box2 domains were not counted as such.

Much of the scientific literature that references Khanna *et al*. (2009) uses 5 structural groups and forces them upon the BBX family (Huang *et al*., 2012; Crocco and Botto, 2013; Chu *et al*., 2016; Cao *et al*., 2017; Liu *et al*., 2018; Cao *et al*., 2019; Shalmani *et al*., 2019; Wei *et al*., 2020; Bu *et al*., 2021; Feng *et al*., 2021; Hou *et al*., 2021; Liping *et al*., 2021; Ma *et al*., 2021; Singh *et al*., 2021; Ye *et al*., 2021; Zhao J *et al*., 2021; Zhang X *et al*., 2021; Zheng *et al*., 2021; Yu *et al*., 2022 and in review: Gangappa and Botto, 2014; Talar and Kiełbowicz-Matuk, 2021). Many analyses also show clear deviation of BBX26 and BBX27 from Clade VI in phylogenetic trees (Cao *et al*., 2017; Cao *et al*., 2019; Shalamani *et al*., 2019; Bu *et al*., 2021; Ma *et al*., 2021; Ye *et al*., 2021; Singh *et al*., 2021; Zhang X *et al*., 2021; Zhao J *et al*., 2021; Zheng *et al*., 2021). Zou *et al*. (2018) shows a deviation between BBX26-BBX27 from Clade VI splitting early on in the phylogeny. Wen *et al*. (2020) clusters *Petunia hybrida* BBX family members into 6 groups and places BBX27 into the 6th group. Shalmani *et al*. (2018) identifies 6 sub-families of *BBX* genes in *Rosacea* species.

The number of clades of the BBX family is subjective. I placed the *Arabidopsis thaliana* BBX family into 6 clades, but they could have been divided further. It was significant that I found that Clade V and Clade VI, formerly structure group V, could not be reconciled without the inclusion of Clade IV. BBX26 and BBX27 have a B-box2 domain that is mostly missing in BBX28 - BBX32.

The ancestor of all Clade VI members may have contained the novel TFIIb core-like domain. KnBBX7 was found to be an outgroup to all of Clade VI, but it also contained a similar domain to the novel domain of BBX32. It is possible that BBX28,

BBX29, BBX30 and BBX31 lost this domain in two separate events (section 7.1.3 [Page 267]).

6.6.2: The BBX32 novel domain

The potential novel domain of BBX32 was identified from the primary sequence by two separate algorithms. Both BBX32 models have a zinc-coordinating B-box domain and a novel domain formed of 5 alpha helices that resembles a cyclin or a core-like domain of TFIIb. Similarly, TFIIb has an N-terminal zinc-binding motif that's used to coordinate the formation of RNA polymerase II of the composition Cys-X_{2}-Cys-X_{17}-Cys-X_{2}-Cys (Nikolov *et al*., 1995). Every BBX32 homologue I have analysed had a very similar structure: Cys-X_{2}-Cys-X_{15}-Cys-X_{2}-Cys.

The two extreme differences in pI also belie the differences in functionalities. The B-box1 domain of BBX32 has a pI that is similar to the average pI of the BBX family; however, the novel domain has high pI. A high pI results in a positively charged protein. This may relate to DNA binding affinity however Holtan *et al*. (2011) found that BBX32 did not have any although it did not explain the methodology for that conclusion. The BBX binding may be non-specific like TFIIb and therefore be far more difficult to detect (Nikolov *et al*., 1995). This could be tested using fixed BBX32 proteins, potentially with binding partners, and analysing random DNA fragment binding.

BBX32 is a negative transcriptional regulator and BBX32 is structurally very similar to TFIIb, a positive general transcription factor (Figure 6.3.2 [Page 210]; Orphanides *et al*., 1996). There may be a relationship or competition between the functionalities

of BBX32 and TFIIb. The functionality of BBX32 may be to selectively interfere with formation of the pre-initiation complex, preventing transcription. Yeast-two hybrid could be used to identify if BBX32 is capable of binding with any proteins in the PIC.

Tripathi *et al*. (2017) found that the suppression of *FT* expression by BBX4 (COL3) and BBX32 required both proteins. This mechanism may provide an initial insight into the activity of BBX32. As shown in Figure 6.3.10 [Page 241], BBX32 binds 15 out of the 31 other BBX family members. Many of these binding partners in the Clades I, II, III and IV are capable of binding DNA and altering transcription (Gangappa and Botto, 2014; Cao *et al*., 2017). The BBX4-BBX32 mechanism could be used as a model to study many other interactions involving BBX32.

6.6.3: Development of *BBX32-CAS9* mutants

The development of the *BBX32-CAS9* mutants ran into issues. The number of plants used was far higher than necessary. 62 T_1 plants were grown to maturity from hygromycin resistant transformed seedlings with an initial batch being entirely lost due to Covid restrictions. Of these 62 T_1 plants only the first 47 were analysed. 132 M_2 plants were grown with many failing to reach maturity due to ongoing pest issues. There were also concerns over knockout lethality that were eventually disproven with the discovery of the *bbx32-2* homozygote however the concern drove scepticism over the scale of the pest issue. 64 M_2 plants reached maturity and produced seed of which 25 of them were tested using qPCR - high resolution melting to identify differences between alleles and therefore heterozygosity of the *BBX32* alleles.

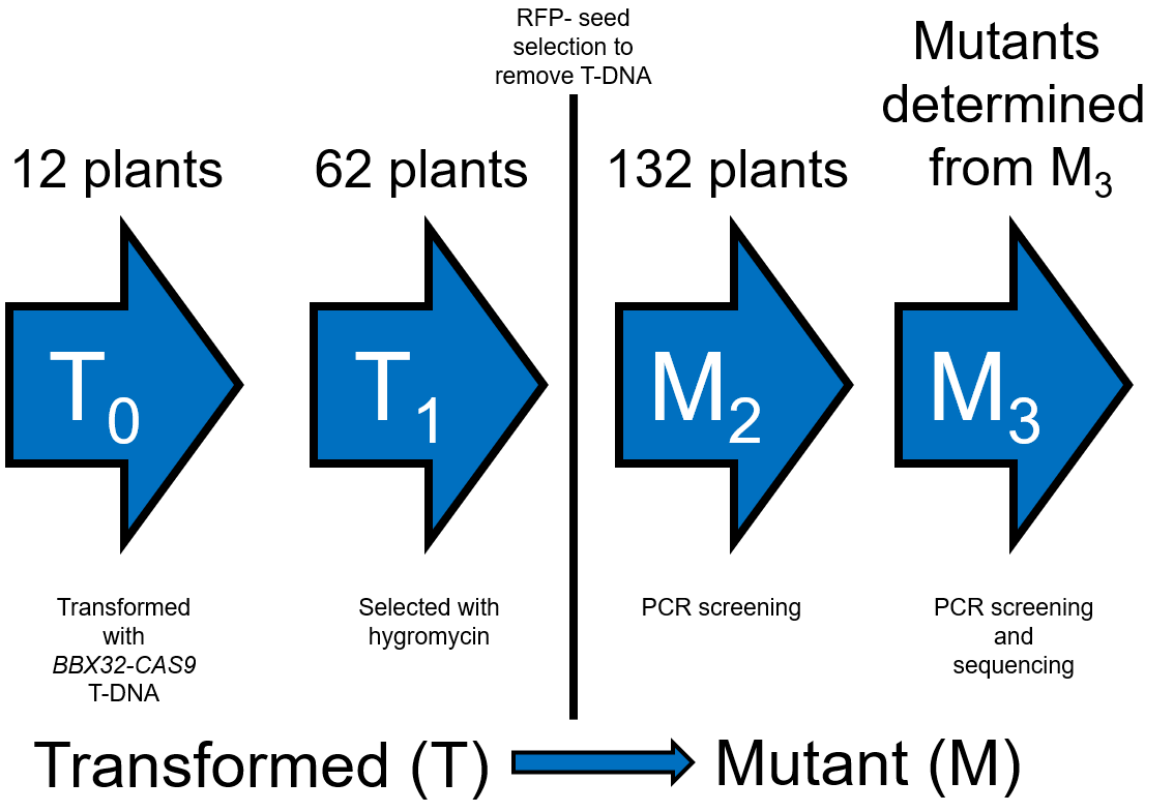

Figure 6.6.1: Workflow diagram for the breeding and selection of *BBX32-CAS9* plants. RFP- progeny of T_1 plants gives rise to a generation lacking T-DNA and therefore termed M_2 and M_3 and not T_2 and T_3.

I attempted to use qPCR - high resolution melting to determine subtle changes in the *BBX32* alleles of M_2 plants. This method works by measuring the melting curve of DNA strands. Heterozygotes should have a lower melting peak as two DNA strands of different sequences have fewer hydrogen bonds and therefore a lower melting temperature. These attempts appeared to yield positive results however upon sequencing the *BBX32* alleles in the T_3 progeny some were found to only have WT *BBX32* alleles such as 6.8.

qPCR high resolution melting did lead to the serendipitous discovery of the *bbx32-2* allele. Large scale changes in the *BBX32* gene were rarely detected with the *bbx32-2* allele being discovered during PCR of the 15.2 and its progeny. The second allele of 15.2 was also mutated and was isolated as the *bbx32-3* mutant. Curiously, 20.4.4 was also homozygous for an identical allele. This mutation can be attributed to the A2 gRNA. The A2 gRNA contributed to 3 of the 4 *BBX32-CAS9* mutants studied though it didn't have the strongest specificity or efficiency score of the selected guides (Table S8 [Page 338]). The other allele of 20.4 had a band that was smaller by approximately 70 bp however it was unable to be recovered after testing 17 M_3 progeny.

If this experiment was to be conducted again, far fewer T_1 and M_2 plants would be used. The M_2 plants did not necessarily have the same *BBX32* alleles as their siblings due to the action of CAS9. Pest issues would also be far more manageable with a smaller cohort of plants. A smaller group of M_2 plants could all be extracted and tested for *BBX32* gene size or just directly sequenced. The M_3 plants could be grown knowing that they all contain mutant alleles. This experiment could also be expanded starting by analysing further M_2 plants.

6.6.4: Phenotype of the *BBX32-CAS9* mutants

The hypocotyl length phenotype indicates that the functionality of BBX32 does not depend on the novel domain. *bbx32-1* had a very low level of expression (Holtan *et al*., 2011) and the ATG of the *BBX32* gene in *bbx32-2* was missing. Therefore, these mutants have been determined to have far less mature BBX32 protein. *bbx32-3* and *bbx32-4* had an out-of-frame novel domain which is likely to be missing in the mature

protein. All these mutants had a similarly perturbed hypocotyl phenotype to *bbx32-1* and *bbx32-2* (Holtan *et al*., 2011). However, unlike *bbx32-1* and *bbx32-2*, *bbx32-3* and *bbx32-4* did not have a HL acclimation phenotype (Figure 6.5.2 [Page 248]). The B-box1 domain alone was able to rescue the HL acclimation phenotype but not the hypocotyl phenotype. This implies a separate mode of action of BBX32 for these different phenotypes.

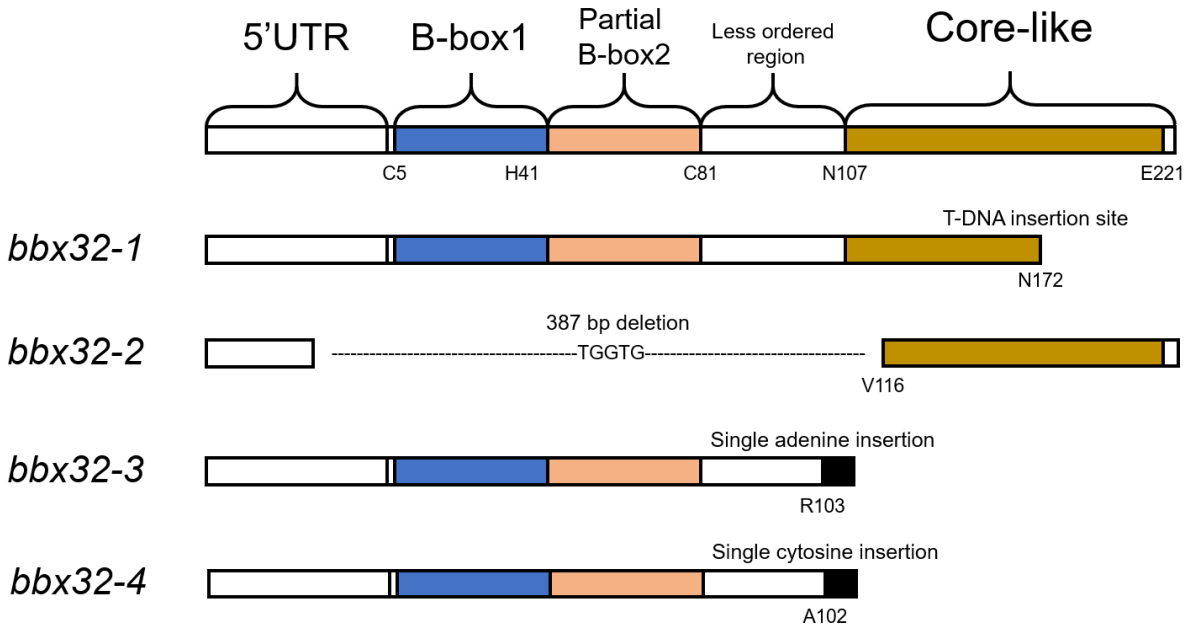

Figure 6.6.2: Schematic of *BBX32* and the mutants *bbx32-1* (Holtan *et al*., 2011), *bbx32-2*, *bbx32-3* and *bbx32-4*.

Holtan *et al*. (2011) suggested the mode of action of BBX32 is through a BBX bridge to HY5. *hy5-2* has both a strong hypocotyl and HL acclimation phenotype (Srivastava *et al*., 2015; Alvarez-Fernandez *et al*., 2021). The separation of the light acclimation and hypocotyl phenotypes are difficult to reconcile due to the similar transcriptomics of the BBX32-10 and *hy5-2* mutants found in section 3.4 [Page 73]. This differentiation is discussed further in Chapter 7 [Page 259].

6.6.5: Conclusion

This chapter studied the structure and evolution of the *BBX* family and discovered a novel domain of *BBX32*. This influenced the development of new *BBX32* mutants using CAS9. However, the phenotypically strongest mutant, *bbx32-2*, could not be phenotypically differentiated from the previously studied T-DNA mutant *bbx32-1*. Further experimentation into the novel *BBX32* mutants could focus on the specific BBX32 binding partners and the impact of the novel domain on this functionality to understand the differentiation between the light acclimation and hypocotyl phenotypes.

6.7: Conclusions of Chapter 6

- A new potential domain of BBX32 was discovered in the C-terminus region using computational methods.
- Due to a truncated *BBX32* transcript in *bbx32-1*, novel mutants of *BBX32* were generated using CRISPR/CAS9.
- A novel CAS9 mutant missing the ATG start codon, *bbx32-2*, had similar HL acclimation and hypocotyl phenotypes to *bbx32-1*.

Chapter 7 – General Discussion

7.1: The function of *BBX32*

The *bbx32-1* mutant was predicted to not harbour a null *BBX32* allele due to the T-DNA insertion site being late into the protein coding region of the gene (Figure 6.1.4 [Page 201]). The position of the SALK T-DNA insertion at N172 in the *bbx32-1* mutant did not impact the previously only known B-box1 domain (Figure 6.1.4 [Page 201]; Holtan *et al*., 2011). There was also a lack of any other mutants with a T-DNA located within the *BBX32* gene available (Alonso *et al*., 2003). Holtan *et al*. (2011) also were able to isolate a truncated *BBX32* transcript using non-spanning primers to amplify it from cDNA (Holtan *et al*., 2011). This harmonised with the relatively weaker phenotype of *bbx32-1* compared to the over-expressing 35S:BBX32 lines BBX32-10 and BBX32-12 (Holtan *et al*., 2011; Alvarez-Fernandez *et al*., 2021). This applied to HL acclimation (Alvarez-Fernandez *et al*., 2021; Figure 1.3.2 [Page 25]) and photomorphogenesis (Holtan *et al*., 2011).

Early on into the development of the novel *BBX32* mutants (section 6.1.3 [Page 202]), I predicted a mutant missing any *BBX32* transcript would be lethal in a similar fashion to many *COP1* mutants since, like *COP1* mutants, the *bbx32-1* mutant has a short hypocotyl phenotype (Stacey *et al*., 2000). The CRISPR/Cas9 gene editing strategy was designed to accommodate for a possible lethality by generating heterozygous *bbx32* mutants. Indeed, many of the M_2 generation contained two distinct *BBX32* alleles (Figure 6.4.10 [Page 241]; Figure 6.4.11 [Page 243]). It was hoped to recover a mutant that was incapable of segregating one of the homozygous

daughters and determining a lethal allele from the parent. This didn't come to fruition with the discovery of the *bbx32-2* mutant which was missing the start codon of *BBX32* (Figure 6.6.2 [Page 258]). *bbx32-2* is most probably a complete knock out of *BBX32.* Further study into gene expression and protein levels would be needed to confirm this supposition. However, this is considered likely as this start codon is missing (Figure 6.6.2 [Page 258]) with no other early in frame methionine (ATG) to potentially start translation.

7.1.1: Domains of BBX32

I posited the existence of two domains within BBX32: A four beta sheet B-box1 domain (Figure 6.3.6 [Page 220]) and a novel cyclin core-like domain (Figure 6.3.2 [Page 210]; Figure 6.3.3 [Page 211]). This was drawn from the Phyre 2.0 (Figure 6.3.2 [Page 210]) and Alphafold structures which were nearly identical. The Alphafold structure contained more detail due to the Phyre 2.0 structure being comprised of other known protein structures (Kelley *et al*., 2015; Jumper *et al*., 2021). Dividing up these regions revealed very different theoretical isoelectric points with the core-like domain having the greatest pI of 10.00 (Figure 6.3.9 [Page 226]). This implies that these domains have different functionalities and have adapted to exist and function in different micro-environments. This could mean they have different sets of interaction partners. This is discussed further in section 7.1.2 [Page 264].

The B-box1 domain was previously known (Khanna *et al*., 2009). However, there are similarities between the sequence of the fourth beta sheet of BBX32 and the

beginning of the B-box2 domain of other BBX family members (Table 6.3.4 [Page 218]). Structurally, the fourth beta sheet of clade VI BBX proteins mimics the positioning of the seventh beta sheet of BBX proteins with B-box2 domains (Figure 6.3.6 [Page 220]). It is probable, due to the presence of conserved cysteines, that this region also assists in the coordination of zinc ions. No *BBX32* alleles were found that altered just these cysteines even though these were targeted with a CAS9 gRNA (gRNA A1; Figure 6.4.3 [Page 233]). Further *BBX32* alleles could be gathered from M_2 mutants to identify the functionality of these cysteines. However, the weak hypocotyl and HL acclimation phenotypes of *bbx32-1* and *bbx32-2* would make any novel *BBX32* mutant difficult to study. Other methodologies for testing the phenotype of *BBX32* mutants was explored in section 7.1 [Page 260].

The novel C-terminal domain of BBX32 is an interesting discovery for the implications on the function of BBX32. The domain most likely consists of 5 alpha helices in a tight structure with a degree of coordination with the B-box1 domain. This was drawn from the relatively low expected alignment error between the two domains (Figure 6.3.3 [Page 211]). This potentially leads to a degree of *in vivo* flexibility between the two domains. The core-like domain has a greater theoretical isoelectric point than any other region of BBX32 (Figure 6.3.9 [Page 226]). This was extremely useful for the identification of *BBX32* homologues in different plant species as they (in monocots and dicots) had far higher theoretical pIs than all other BBX family members in all species studied (Figure 6.3.8 [Page 225]). The conserved high theoretical pI could mean that this domain exists as a positively charged region and therefore likely to be drawn to negatively charged molecules such as DNA. Holtan *et*

al. (2011) stated that BBX32 did not bind DNA, although as previously noted, no methodology or evidence was provided for such a claim.

The core-like domain makes *BBX32* distinct from other Clade VI members of the BBX family of proteins (discussed further in section 7.1.3 [Page 267]). The *BBX32* gene lacking the core-like domain was seen in the single point insert mutants *bbx32-3* and *bbx32-4* (Figure 6.4.10 [Page 241]). These mutants exhibited a similar hypocotyl phenotype as *bbx32-1* and *bbx32-2* mutants which were considered to be *BBX32*-null (Figure 6.5.1 [Page 246]). However, *bbx32-3* and *bbx32-4* did not have a perturbed HL acclimation phenotype unlike *bbx32-1* and *bbx32-2*. This prompts the idea that the core-like domain of *BBX32* is crucial for normal functionality of *BBX32* but only for its impact on the hypocotyl in the dark phenotype and not the HL acclimation phenotype. This may be due to the bridged interaction with HY5 as posited by Holtan *et al*. (2011). The core-like domain may be crucial for this interaction or the general suppression of HY5 activity and not for HL acclimation. The expression of HL acclimation genes differed between *hy5-2* and BBX32-10 (Figure 3.3.2 [Page 71]) which led to the early hypothesis that *BBX32* and *HY5* impacted HL acclimation through different pathways. This was thought to be disproven by the RNA-seq data from section 3.4 [Page 73] as the *hy5-2* and BBX32-10 mutants strongly overlapped (Figure 3.4.2 [Page 78]). However, it may still be true that *hy5-2* and BBX32-10 have similar impacts on the transcriptome without *HY5* and *BBX32* altering HL acclimation through identical pathways.

7.1.2: Predicted functionality of BBX32

The evidence showing that *BBX32* is a transcription co-factor consists of: BBX32 interacting with certain transcription factors, such as EMF1 (Park *et al*., 2011). BBX4 (Tripathi *et al*., 2017) and BBX21 (Holtan *et al*., 2011) *in vitro*, and impacts of *BBX32* mutants on hypocotyl length (Holtan *et al*., 2011), flowering-time (Tripathi *et al*., 2017), HL acclimation (Alvarez-Fernandez *et al*., 2021), and phosphate starvation (Yeh *et al*., 2020). None of the interactions of *BBX32* have been shown *in vivo* to gather data on the occurrence of these interactions. The functionality of *BBX32* beyond transcription co-factor is difficult to elucidate.

The high-throughput yeast-two hybrid experiments performed by Trigg *et al*. (2017) discovered a large number of BBX intra-family interactions (Figure 6.3.10 [Page 229]). In a similar fashion to the B-box1 and core-like domains of BBX32, a low degree of coordination exists between the B-box domains and CCT domains of Clade I, II and III BBX family members (Figure S5 [Page 334]). The CCT domain is already a relatively dis-coordinated domain according to Alphafold predicted alignment errors (Figure S5 [Page 334]). Clades IV and VI bind to many of the Clade I, II, and III members, which most probably alters their conformations (Figure 6.3.10 [Page 229]). No Clade I, II or III BBX family members have been found to bind to each other (Trigg *et al*., 2017; Figure 6.3.10 [Page 229]). This may be more significant than can easily be identified by yeast-two hybrid. Tripathi *et al*. (2017) identified a significant role of the Clade I BBX4 (COL3) and BBX32 in regulating the expression of the significant flowering-time gene *FT*. BBX4 and BBX32 heterodimerise to bind the *FT* promoter and repress its expression. I posit that this

interaction could be used as a model for a family-wide method of action for the BBX proteins.

A BBX intra-family heterodimerisation model would hypothesise that members of Clade I, II and III (BBX1 - BBX17) readily bind to members of Clade IV (BBX18 - BBX25) and VI (BBX28 - BBX32). The heterodimer partner would influence their functionalities as transcription factors as shown previously in Tripathi *et al*. (2017). Not all of Clades I, II and III would have to be capable of any of Clades IV and VI as seen in the high-throughput Trigg *et al*. (2017) for this hypothesis to be true. The heterodimerisation may even be necessary for the function and regular *in vivo* folding of these Clade I, II and III members.

Tripathi *et al*. (2017) explored the negative regulator BBX32 binding to BBX4 however not all of these interactions would necessarily involve the repression of gene expression. The over-expression of the clade IV member *BBX21* decreased hypocotyl length under dark and red light (45 µmol m^{-2} s^{-1}) conditions (Holtan *et al*., 2011). The decrease in hypocotyl length is associated with the positive regulation of photomorphogenesis (Holtan *et al*., 2011). *BBX32* over-expression negatively regulates the photomorphogenesis pathway to increase hypocotyl length under the same dark and red light conditions (Holtan *et al*., 2011). BBX21 has only been shown to bind BBX32 within the BBX family however BBX21 does bind HY5, a positive regulator of photomorphogenesis (Holtan *et al*., 2011). *BBX32* over-expression had impacted the hypocotyl length of *BBX21* over-expressing seedlings (Holtan *et al*., 2011). Though HY5 is not a BBX family protein this may provide some

insight into the intra-family interactions of the BBX members. The positive Clade IV regulators may bind the same Clade I, II and III regulators to enhance transcription.

This may explain the functionality of *BBX32*. BBX32 binds the positive regulator BBX21 but also forms associations with negative regulators such as BBX4. The *BBX32* over-expressor produces an overabundance of BBX32 protein. Excess BBX32 could bind positive Clade IV regulators altering the transcriptional availability or conformation of their previous Clade I, II and III binding partners. Also, the BBX32 binds to newly freed Clade I, II and III proteins to form negative regulatory heterodimers completely shifting the transcriptional state of play from positive to negative. This could explain the dramatic impact of the BBX32-10 over-expressor, which significantly altered a comparable number of genes to those affected by exposure to HL and an order of magnitude more genes than *hy5-2* (Figure S6 [Page 335]). *BBX32* acts as a negative regulatory adaptor however the scope of this function has not yet been determined.

To explore this hypothesis further, full small-scale yeast-two hybrid or BiFC experiments could be performed on the BBX family to determine *in vitro* and *in vivo* binding patterns. From this data, two BBX family members that bind could be expressed as a hybrid protein. Promoter binding analysis could be performed with these hybrid proteins to identify positive and negative regulatory units. Mutant plants richer or poorer for certain BBX intra-family interactions could influence processes such as HL acclimation to enhance photosynthetic capacity and productivity.

7.1.3: Differentiation of *BBX32* from other Clade VI members

Evolution has produced a Clade VI of the BBX family that exists throughout all higher plant species studied (Table S7 [Page 338]). Clade VI split between the *Arabidopsis* genes *BBX28* and *BBX29* from *BBX30*, *BBX31*, and *BBX32* occurred prior to the divide between angiosperms and gymnosperm. All but one of the Clade VI genes *Picea abies* were more closely related to either *BBX28* and *BBX29* or *BBX30*, *BBX31* and *BBX32* than each other (Figure S3 [Page 332]). The remaining gene (labelled *PaBBX11*) appears to have diverged prior to the BBX28/29 and BBX30/31/32 split. The monocots *Zea mays* and *Oryza sativa s. japonica* did not contain homologues of *BBX30*/*31* but did have homologues of *BBX28/BBX29* and *BBX32*. *BBX30/31* and *BBX32* appear to have diverged after the appearance of eudicots as evidenced by species like *Glycine soja* (Figure S3 [Page 332]).

The very high intra-family connectivity of Clade VI appears to have been conserved throughout this evolutionary time period. BBX29 and BBX32 were found to have the most intraconnectivity of the BBX family (Trigg *et al*., 2017; Figure 6.3.10 [Page 229]). It is very possible that the entirety of Clade VI evolved from a gene containing the core-like domain of *BBX32* and that two separate evolutionary events resulting in its loss in both BBX28 and BBX29 and, BBX30 and BBX31. *Selaginella moellendorffii* contained two Clade VI *BBX* genes which when placed on a phylogenetic tree with the *Arabidopsis* BBX genes formed a clade with *BBX30* and *BBX31* (Figure S7 [Page 336]). However, when run through Phyre 2.0, *SmBBX17* was found to have a core-like domain similar to *BBX32* (Figure S8 [Page 337]). This places the genetic event that led to the Clade VI *BBX* family genes to have occurred prior to the divergence between land plants and the charophytes.

The *bbx32-2* mutant highlighted the potential for functional redundancy within the Clade VI members as the *bbx32-2* mutant had a relatively weak HL acclimation phenotype compared to the over-expressor BBX32-10 (Figure 1.3.2 [Page 25]; Figure 6.5.2 [Page 248]). This could be analysed through the use of a second CAS9 system. This new CAS9 system could be transformed into the *bbx32-2* too with 4 gRNAs targeting each of the remaining Clade VI members (*BBX28*, *BBX29*, *BBX30*, and *BBX31*). Analysis could be performed on the HL acclimation and hypocotyl phenotypes of the M_3 generation to identify the most severe perturbations. These plants can then be genotyped to identify which genes have been altered. It is possible that the quintuple knockout of all the Clade VI genes would be lethal.

7.1.4: Genetic and proteomic prospects with *BBX32*

The phenotype of *bbx32-2* was not able to elucidate more of the functionality of *BBX32*. Further developments with *BBX32* required both new genetic manipulations and testing protein functionality. The initial experiment I would conduct would be to test if BBX32 does bind DNA by itself. It is known that BBX4 and BBX32 heterodimerise and bind to the promoter of *FT* (Tripathi *et al*., 2017). Other BBX family members could also enable BBX32 to bind DNA which could be tested with *in vitro* binding to a promoter sequence. As discussed in section 7.1.2 [Page 264], hybrid proteins could be used to test promoter and protein binding while controlling the formation of the specific BBX heterodimers.

If BBX32 can heterodimerise with many of the BBX family members, BBX32 may also be capable of heterodimerising. BBX32 homodimerising in the BBX32-10

mutant may diminish the impact of its over-expression. Holtan *et al*. (2011) stated that BBX32 could not bind DNA without the presentation of evidence. If BBX32 readily homodimerizes it may occur *in vitro* during DNA binding experiments. Therefore, it would be likely that if BBX32 monomer doesn't bind DNA, then the homodimer is unlikely to as well. This implies that there are diminishing returns for the over-expression of *BBX32.* If there is more BBX32 protein, the likelihood of heterodimerisation, if possible, would increase. However, this would be an important feedback mechanism for limiting the negative transcriptional impacts of BBX32. This could be tested through a hybridisation of two BBX32 proteins and identifying the impacts on protein binding and the phenotype of *Arabidopsis*.

As discussed previously, further *BBX32* mutant alleles from the *CAS9* lines could be identified. However, the weak mutant allele phenotype makes these difficult to distinguish from the WT as seen in the HL acclimation phenotype of *bbx32-3* and *bbx32-4* (Figure 6.5.2 [Page 248]). These alleles could be PCR cloned from the *BBX32* mutants and transformed back into *bbx32-2* with a 35S promoter to be overexpressed. The phenotypic differentiation should therefore be clearer from BBX32-10, *bbx32-2* and WT controls.

The over-expression of mutant alleles of *BBX32* would be useful for reducing selection bias over which mutant allele is used. However, the creation of novel *in vitro BBX32* mutations is also possible. Over-expressing *BBX32* mutants with specific mutations would allow the analysis of those mutations. Targets for alterations include: zinc-coordinating cysteines and histidines, removal of the novel

domain; only the novel domain, removal of each of the beta sheets in the B-box1 domain and a potential sulphide bridges (C47 and C71).

7.2: Developments of HL acclimation

As discussed in Chapter 1 [Page 16], the dynamic acclimation and developmental acclimation split is very unclear. Developmental acclimation is the acclimation to HL undergone by immature and developing leaves whereas dynamic acclimation is acclimation to HL undergone by mature leaves (Oguchi *et al*., 2003; Athanasiou *et al*., 2010). Chloroplast physiological changes are seen to be more significant for the enhancement of photosynthetic capacity during dynamic acclimation compared to developmental acclimation (Oguchi *et al*., 2003). The other significant form of enhancing photosynthetic capacity, morphological changes, are possible within the mature leaves (Sims and Pearcy, 1992; Weston *et al*., 2000; Oguchi *et al*., 2003). The delineation between mature and immature leaves in reference to dynamic and developmental acclimation is unknown. It is not known if there is a true point of delineation between dynamic and developmental acclimation Therefore, HL acclimation was used as a neutral term as not to contribute to questions I did not seek to answer within this study.

I designed the methodology for measuring leaves explicit as to answer questions related to those conditions. Leaves were measured on day 1 if they exceeded 50 % of the petiole length of the next newest leaf. This size is arbitrary but was used as keeping track of leaves between the day 1 and day 5 measurements was quite difficult due to image quality of the chlorophyll fluorescence Fluoroimager (Technologica, Colchester, Essex). If a leaf exceeded the 50 % boundary on day 1, it

would be almost impossible to distinguish by size alone on day 5 due to its growth. Therefore, on day 5, only leaves that appeared to be fully grown were measured. These leaves were considered to be mature, and the HL acclimation could be considered to be analogous to dynamic acclimation. However, the comparisons to dynamic acclimation experiments should be taken on a study-by-study basis for the dissimilarity of other variables such as light conditions and day length.

7.2.1: Comparisons to previous acclimation studies

The HL acclimation conditions used in this study and the partially overlapping study Alvarez-Fernandez *et al*. (2021) involved 4-6-week-old plants grown under short day conditions (8 h/ 16h; day/ night) and 150 µmol m^{-2} s^{-1} PPFD. Athanasiou *et al*. (2010) did not find the ecotype, Columbia-0 (Col-0), to be able to acclimate to their HL conditions (100 µmol m^{-2} s^{-1}, growth; 400 µmol m^{-2} s^{-1}, HL). Col-0 was used as a WT control within this study and Alvarez-Fernandez *et al*. (2021) also found that Col-0 could acclimate to the 1000 µmol m^{-2} s^{-1} HL conditions over 5 days (150 µmol m^{-2} s^{-1}, growth; section 2.2.2 [Page 35]). The HL conditions being so different may completely account for the difference between the response of Col-0 between the experiments.

Weston *et al*. (2000) conducted some of the earliest HL acclimation experiments on *Arabidopsis* involving the transfer to new higher light conditions. However, Weston *et al*. (2000) did not perform any experiments on changes in photosynthetic capacity by these conditions and instead relied on an earlier study, Walters *et al*. (1999), which grew and maintained plants under LL or HL conditions (LL, 100 µmol m^{-2} s-1; HL, 400 µmol m^{-2} s^{-1}; 8 h/ 16 h; day/ night). The growing of plants under HL conditions

5067 does not easily parallel plants transferred to new HL conditions (Athanasiou *et al*.,
5068 2010).
5069
5070 Weston *et al*. (2000) transferred plants to LL and HL conditions (constant day) of 60
5071 µmol m^{-2} s^{-1} (LL) and 400 µmol m^{-2} s^{-1} (HL), respectively, at two-weeks-old (growth,
5072 150 µmol m^{-2} s^{-1}, constant light). Huang *et al*. (2019) used similar conditions with
5073 two-week-old plants (growth, 60 µmol m^{-2} s^{-1}, constant day) being transferred to HL
5074 conditions (1200 µmol m^{-2} s^{-1}, constant day). Weston *et al*. (2000) and Huang *et al*.
5075 (2019) chose the terms light acclimation and acclimation, respectively, for their
5076 studies. *Arabidopsis* plants at 2-weeks-old are very unlikely to have mature true
5077 leaves (not cotyledons). Images from Huang *et al*. (2019) show the first set of true
5078 leaves still developing. These findings therefore cannot easily be applied to HL
5079 acclimation.
5080
5081 The use of constant light conditions by Weston *et al*. (2000) and Huang *et al*. (2019)
5082 is completely baffling. The circadian rhythm regulates approximately a third of all
5083 genes in the *Arabidopsis* genome (Goodspeed *et al*., 2012). In the wild, there is a
5084 relationship between light, photosynthesis, and the time of day. Plants cannot entrain
5085 to constant light and temperature conditions (Kikis *et al*., 2005; Salomé and
5086 McClung, 2005). The disruption of the circadian rhythms alters the expression of
5087 photosynthesis associated genes (Salomé *et al*., 2008). Performing acclimation
5088 experiments in constant light conditions does not mimic common field conditions
5089 plants experience. A key task in designing HL acclimation experiments is providing
5090 conditions similar to field conditions to make the results as transferable to the field as

possible to increase plant productivity. The use of constant light conditions is antithetical to this goal.

7.2.2: HL RNA-seq studies

Huang *et al*. (2019) performed an RNA-seq upon 2-week-old whole plants following 0.5 h, 6 h, 12 h, 24 h, 48 h, 72 h of HL (1200 µmol m^{-2} s^{-1}) and a recovery 14 h of 60 µmol m^{-2} s^{-1} and 22 °C following 72 h of HL. Each time point also had a growth light control (60 µmol m^{-2} s^{-1}). The use of whole plants increases the amount of RNA in the sample but does mean that study is not tissue specific. Alvarez-Fernandez *et al*. (2021), for example, solely used mature leaves. This means that the whole plant samples from Huang *et al*. (2019) used roots, hypocotyl, and cotyledon in their sample for RNA-seq. If RNA quantity was at issue, the plants could have been allowed to grow for longer before extraction. Huang *et al*. (2019) also only used only two biological replicates per time point and treatment is statistically limiting. Costs are a factor for RNA-seq experiments however time point number could also be restricted to increase the number of biological replicates.

For the RNA-seq experiment, Huang *et al*. (2019) cooled plants to reduce the temperature of the adaxial leaf surface to comparable temperatures as the leaves under standard growth conditions. This required cooling the growth chamber to 11.5 °C which cooled the whole plant. This may not have been a great issue if only leaf samples were taken however whole plant samples were used as previously discussed. RNA-seq was performed on plants exposed to these and control conditions and GO analysis was performed. The ‘Response to Cold’ GO term was significant for the significantly upregulated genes at all time points other than 72 h.

‘Response to Cold’ was also significant for the significantly downregulated gene list following recovery conditions. These plants, compared to growth condition controls, increased the expression of cold-related genes in response to these HL conditions and when returned to growth conditions decreased the expression of cold-related genes. The RNA-seq data reveals how immaterial these experimental conditions were for proving or disproving the hypotheses. These plants were signalling that they were cold when placed into the colder HL conditions and signalled that they were no longer cold when they were taken out.

An increase in leaf surface temperature regularly accompanies an increase in PPFD in natural environments, such as by going from cloudy to sunny conditions (Vialet-Chabrand *et al*., 2017; Huang *et al*., 2019). These two phenomena (light and temperature) co-occur in nature and therefore parting them in laboratory conditions may not be the best for testing HL acclimation. However, if temperature changes were a strong concern, an increased temperature could have also been separately transcriptionally reviewed from the HL conditions such as was carried out in Alvarez-Fernandez *et al*. (2021).

BBX14 was identified as a HL-related gene within both the Huang *et al*. (2019) gene network and Alvarez-Fernandez *et al*. (2021) HL TF network. Considering the gulf in experimental conditions the discovery of a gene that is shared between the two HL networks is very interesting. Testing *BBX14* did not yield a strong HL acclimation phenotype, however there was no proof that *BBX14* over-expression was induced in the plants containing the *BBX14* construct. There is no SALK knockout that could have been used like for other HL TF network genes. This does make *BBX14* a

suitable target for a CAS9 system like that used for *BBX32*. The rest of Clade III (*BBX15*, *BBX16* and *BBX17*) have very similar theoretical structures and therefore the entire clade could be targeted by a singular CAS9 construct.

7.2.3: The use of *BBX32* crop lines

The further research of HL acclimation should involve determining the relevance of *Arabidopsis* HL acclimation to the HL acclimation of crop species. With this in mind, previous studies that involve *Arabidopsis* HL acclimation genes can be analysed. Preuss *et al*. (2012) studied *Glycine max* that over-expressed *Arabidopsis BBX32* (*AtBBX32*). These plants had an increased seed yield by up to 14 % in field conditions. However, the *Arabidopsis BBX32* over-expressors experimented upon had a decreased yield compared to the WT and *bbx32-1* (Figure 6.3.1 [Page 208]). Reconciling this incongruence may lead to a better understanding of HL acclimation and its impacts on plant productivity.

Preuss *et al*. (2012) quantified the expression of the circadian regulators *GmLCL2* (*CCA1/LHY* homologue) and *GmTOC1*. These are key morning and evening regulators, respectively (Singh and Mas, 2018). This experiment was performed on plants exposed to a standard day/ night cycle (14 h/ 10h) with 9 RNA-extraction time points. Two different *AtBBX32* lines were compared against the control and the circadian rhythm was determined to be perturbed due to significant differences in the expression of *GmLCL2* and *GmTOC1* at specific time points; ZT23, ZT8 and ZT20 for *GmLCL2* and ZT23, ZT1, ZT2 and ZT11 for *GmTOC1* (Preuss *et al*., 2012; Figure 7.2.1 [Page 277]). However, the amplitude of expression is only part of the circadian phenotype. Both rhythmicity and amplitude of expression of circadian clock genes

5164 are analysed from plants grown under day/night conditions and transferred to new
5165 constant light (or dark) conditions (Haydon *et al*., 2013; Jones *et al*., 2015; Zhang *et*
5166 *al*., 2019). The rhythmicity is measured through numerically determining the time
5167 which expression peaks, often using luciferase imaging, and statistically calculating
5168 the significance between different genotypes. The very minimal differences and
5169 optimal experimental conditions hamper the determination as to whether these
5170 *BBX32* mutants do have a perturbed circadian phenotype (Figure 7.2.1 [Page 277]).
5171

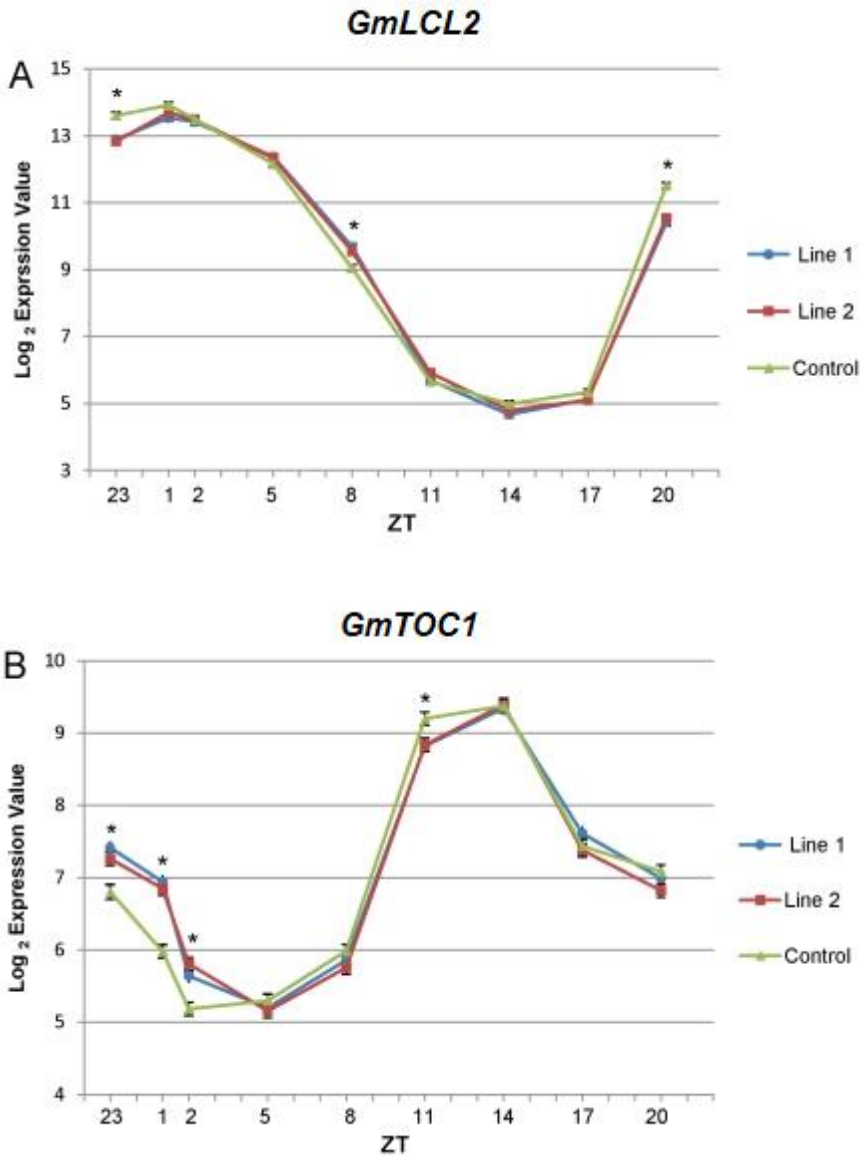

5172

Figure 7.2.1: Expression of *GmLCL2* (A) and *GmTOC1* (B) in *AtBBX32* over-expressing *Glycine max* (Line 1 and Line 2) and WT control. Modified from Preuss *et al*. (2012).

Leaf senescence regulators *ATAF1, NAC032*, and *GLK2* are a part of the HL TF network (Garapati *et al*., 2015; Mahmood *et al*., 2016; Alvarez-Fernandez *et al*., 2021). Preuss *et al*. (2012) discovered a difference in the rate of leaf senescence with the *AtBBX32* plants senescing later than the WT control. This may be a contributing factor to the increased field yield of the *AtBBX32* plants. However, leaf senescence parameters were not directly measured. A leaf greenness score of between 0 and 9 was used based on visual inspections. It would have been preferable if leaf senescence was measured using foliar chlorophyll content or the chlorophyll fluorescence parameter Fo.

A reduction of leaf number at flowering time in the *Arabidopsis BBX32* over-expressors was found which may also be true within *Glycine max* plants over-expressing *AtBBX32* (Figure 6.5.2 [Page 248]). If *BBX32* over-expression improves leaf longevity, as shown in Preuss *et al*. (2012), this may lead to a more efficient use of energy in the creation of biomass. However, the *BBX32* over-expressors in *Arabidopsis* had a reduced PSII operational efficiency. If the photosynthetic properties apply to the *Glycine max AtBBX32* over-expressors, it is difficult to parse the increased yield with a reduced PSII operational efficiency.

Glycine max plants, as row crops, are tightly packed in field conditions. Different senescence characteristics and number of leaves alter the canopy coverage within a

field. Individual leaves may have a reduced PSII operational efficiency as indicated by the lower Fq'/Fm' of BBX32-10. This may increase leaf longevity and increase the efficiency of the leaves over their lifetime. *Arabidopsis* is far flatter and closer to the ground which leads to a far different canopy. It would be very interesting to over-express *AtBBX32* in other eudicot plant species with similar higher dense canopies to *Glycine max* such as plants from the *Solanaceae* family.

7.3: Further understanding and exploiting HL acclimation

7.3.1: Reviewing the experimental conditions

The HL conditions (section 2.2.2 [Page 35]) used mimics an environment a plant may experience in the field or wild. A plant that originally grew in shaded or cloudy conditions may be exposed to new HL conditions through new growth or the removal of competitors for light. The top of the canopy may still be higher than the plant or there may be obstructions common in fields and greenhouses such as hedges, walls, or buildings. This would limit the amount of time during the day that a plant is exposed to direct sunlight. This was demonstrated by Varella *et al*. (2011) which recorded the PPFD under direct sunlight, under a cloth to mimic complete shade and under a wooden slat to emulate intermittent tree shade (Figure 7.3.1 [Page 279]).

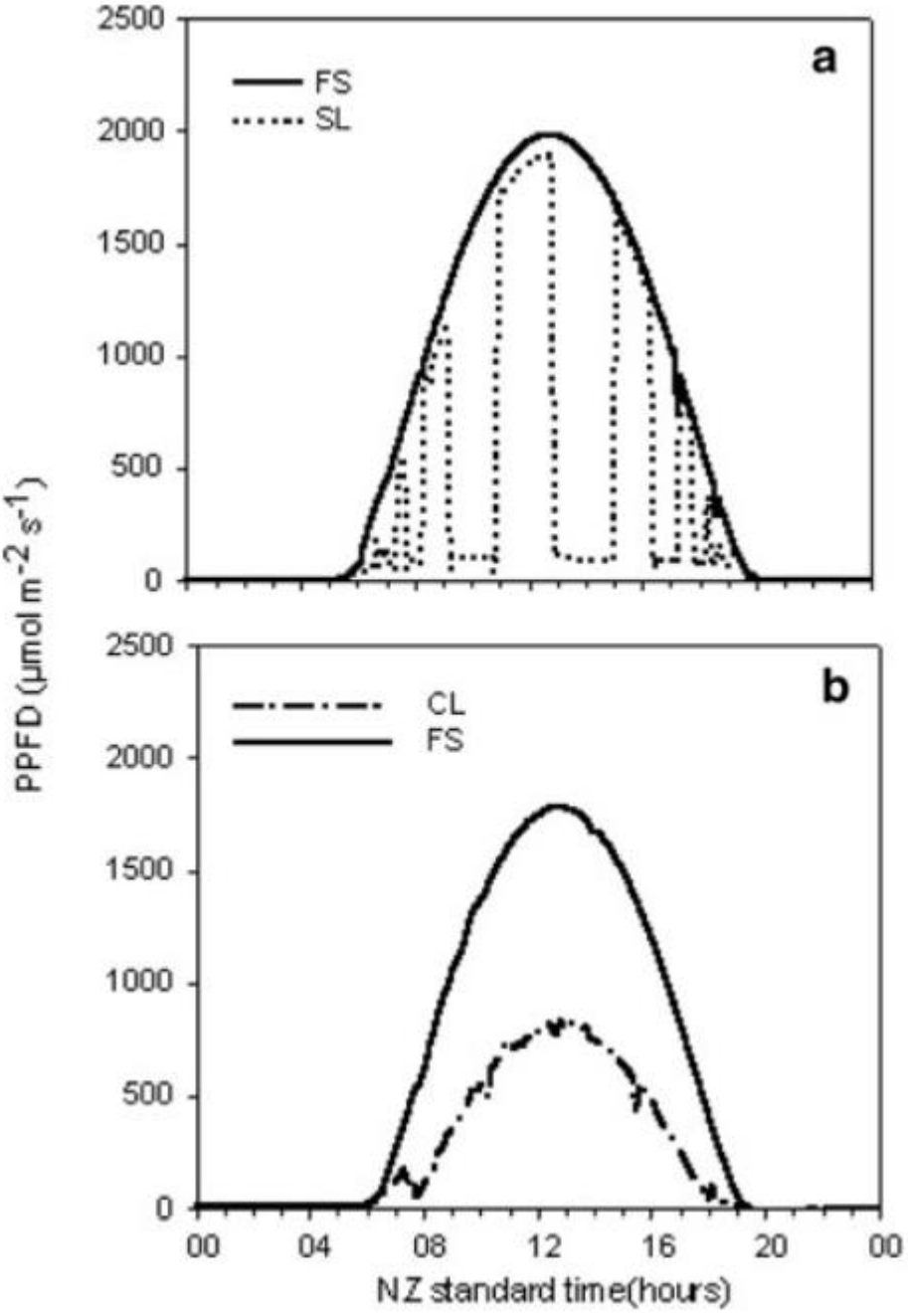

5215

5216 **Figure 7.3.1: The PPFD measured under direct sunlight (FS), under a slat (SL)**

5217 **and, shaded by cloth (CL) on a clearly sunny day in Canterbury, New Zealand.**

5218 Results from a and b were recorded on separate days. Modified from Varella *et al*.

5219 (2011).

5220

I exposed plants to 4 hours of HL in the middle of their 8 hour day (Figure 7.3.2 [Page 281]). This was to mimic the aforementioned intermittent exposure to direct sunlight experienced in many common natural, field and greenhouse conditions. The amount of photosynthesis a LL grown plant can achieve under HL conditions may not only be limited by photosynthesis but also sucrose and starch synthesis (Nguyen *et al*., 2016; Stein and Granot, 2019). Plants accumulate more sucrose under HL conditions (Dyson *et al*., 2015). Limits of *Arabidopsis* that have grown under LL conditions (150 µmol m^{-2} s^{-1}) may exist not just in photosynthesis but in primary metabolism as well. This is evidenced by primary metabolism mutants such as *gpt2* which had a reduced ability to dynamically acclimate (Athanasiou *et al*., 2010). Primary metabolism GO terms “Response to glucose”, “glucose metabolic processes” and “pentose-phosphate shunt” were significant within the significantly upregulated gene set between overlap of the BBX32-10 and *hy5-2* HL acclimation mutants (Figure 3.4.4 [Page 80]). The use of shorter HL periods may be necessary to avoid the overaccumulation of sucrose while the plants acclimate to the new HL conditions. This might be an interesting observation for the transfer of plants from controlled growth conditions to less controlled higher light conditions such as growth cabinets to greenhouses.

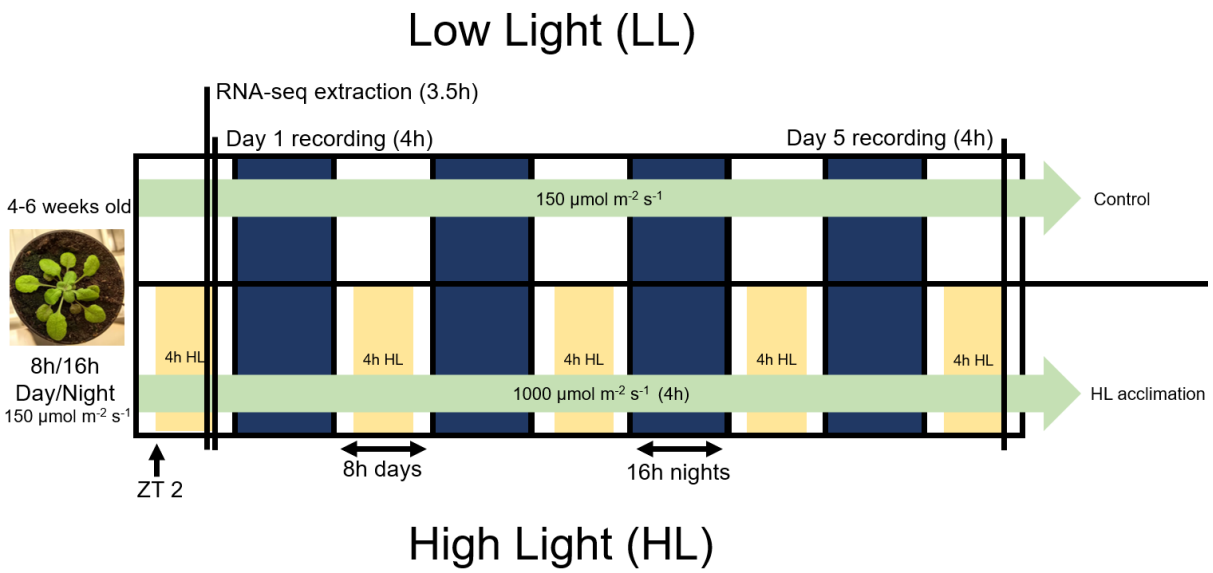

5240

5241 **Figure 7.3.2: A diagram of the light conditions used in the *BBX32-HY5* HL RNA-**

5242 **seq and HL acclimation experiments.** ZT2 indicates two hours after artificial dawn.

5243

5244 Plants in direct sunlight can be exposed to up to 2000 µmol m^{-2} s^{-1} during the sun's

5245 zenith (Valladares *et al*., 2004; Varella *et al*., 2011). The light of a shaded

5246 environment can be far more varied depending on the amount of shade. A lower light

5247 environment may be necessary for the low growing *Arabidopsis thaliana* which

5248 grows closer to the ground than many crop cultivars. Future experiments on crop

5249 cultivars should use a higher PPFD than 1000 µmol m^{-2} s^{-1} for the HL conditions to

5250 reflect the more typical field conditions. The difference between experimental and

5251 real world conditions is far more pronounced in studies such as Athanasiou *et al*.

5252 (2010) and Walters *et al*. (1999) which used 400 µmol m^{-2} s^{-1} as their HL PPFD. It

5253 could be argued that these conditions may more closely mimic conditions that exist

5254 under a dense canopy however these are not accurate for field and greenhouse

5255 conditions.

5256

Athanasiou *et al*. (2010) could not get Col-0 plants to enhance their photosynthetic capacity in response to a PPFD of 400 µmol m^{-2} s^{-1}. This may be due to laboratory inbreeding of the Col-0 plants that may have resulted in genotypic difference between the Col-0 plants used in Athanasiou *et al*. (2010) and Alvarez-Fernandez *et al*. (2021). The 400 µmol m^{-2} s^{-1} HL conditions may also not be enough to have produced significant differences in the plants exposed to HL and LL controls as several ecotypes failed to acclimate (Nossen, Cape Verdi Island and C24; Athanasiou *et al*., 2010). This reduced PPFD may also have impacted the rate of photosynthetic enhancement of the *gpt2-* mutant. It would have been interesting to have tested this mutant under HL acclimation conditions (section 2.2.2 [Page 35]).

7.3.2: C4 photosynthesis and HL acclimation

C4 photosynthetic plants actively concentrate CO_2 around Rubisco to increase its catalytic activity (Westhoff and Gowik, 2010). C4 plants are capable of using nitrogen and water more efficiently which has made the introduction of C4 photosynthesis into C3 plants an intriguing prospect for plant productivity and food security (Westhoff and Gowik, 2010). Within *Zea mays*, a C4 species, there exists, similarly to *Arabidopsis thaliana*, two *GLK* genes *GOLDEN2* (*ZmG2*) and *ZmGLK1*. Disruption of the *ZmG2* gene caused bundle sheath (BS) cells' chloroplasts to aberrantly develop and C4 photosynthetic products to not accumulate (Langdale and Kidner, 1994). Unlike *ZmG2*, *ZmGLK1* has barely detectable transcript levels within the bundle sheath but readily accumulated within the mesophyll (Rossini *et al*., 2001). Due to compartmentalisation, *ZmGLK1* may also be as necessary as *G2* for regulation of C4 cellular differentiation specifically of the C4 mesophyll cells (Hall *et al*., 1998). The differentiation of the HL acclimation phenotypes of *Arabidopsis GLK1* and *GLK2*

mutants may have implications on the regulation of photosynthesis, HL acclimation and the transgenic development of C4 plants.

The *GLKs* have been identified as part of a breeding strategy to convert plants from C3 to C4 (Westhoff and Gowik, 2010; Wang *et al*., 2017). Constitutive expression of *Zea mays GLK* genes *ZmG2* and Zm*GLK1* both induced the transition of *Oryza sativa* to being proto-Kranz like (an evolutionary stage between C3 and C4 photosynthetic plants) without impacting plant productivity (Wang *et al*., 2017). Further studies on these plants proposed by Wang *et al*. (2017) included the transcription factors *CGA1* and *GNC* which were both highlighted as transcription factors that were upregulated within both BBX32-10 LL and *hy5-2* LL compared to Col-0 LL (Table 3.4.1 [Page 84]). *CGA1* and *GNC* are close homologues which fit into the interaction map and are regulated by *PIF4*, a member of the HL TF network (Figure 3.4.5 [Page 83]; Alvarez-Fernandez *et al*., 2021). *GNC* and *CGA1* indirectly regulate the expression of *GLK2* (Zubo *et al*., 2018). There are strong parallels between the alterations of expression induced within HL acclimation mutants and those evidenced and proposed as methods of transitioning plants to C4 photosynthesis. These may be due to the alterations of photosynthetic capacity within both HL acclimation and C4 photosynthesis however the differentiation of *GLK1* and *GLK2* requires further exploratory analysis.

7.3.3: Advances in HL acclimation

As previously shown, many acclimation experiments have widely different experimental HL conditions (section 7.2.1 [Page 271]). The wide variety of

photosynthetic changes that occurred are difficult to reconcile. It would be very useful to have a wide physiological study looking into HL acclimation with many various conditions testing carbon fixation and chlorophyll fluorescence to develop a set of conditions that could be used in a wide variety of contexts. In particular the molecular studies could use a unifying set of conditions to make the experiments directly comparable. I used the same growth and HL conditions as Alvarez-Fernandez *et al*. (2021) however we couldn't be assured that the selected conditions were optimal.

HL acclimation has many alterable conditions that could be experimentally tested. Alvarez-Fernandez *et al*. (2021) identified that plants grown under 150 µmol m^{-2} s^{-1} exposed to HL conditions of 1000 µmol m^{-2} s^{-1} enhanced photosynthesis over 5 days. Athanasiou *et al*. (2010) found that plants grown at 100 µmol m^{-2} s^{-1} exposed to HL conditions of 400 µmol m^{-2} s^{-1} enhanced photosynthetic capacity over 9 days. These were different ecotype (Col-0 and Ws-2, respectively) however it is probable that the different growth and HL conditions contributed to the number of days to achieve an enhanced photosynthetic capacity. The HL and growth light conditions should ideally be optimised to fit a set of conditions that match a natural, field or greenhouse light conditions to make the transfer from model plant species to crop cultivars as seamless as possible. As identified in section 7.3.1 [Page 278], this involves HL conditions of between 1500 µmol m^{-2} s^{-1} and 1800 µmol m^{-2} s^{-1}. These conditions were unachievable with the equipment used in this study. These HL conditions would probably cause *Arabidopsis* plants grown at 150 µmol m^{-2} s^{-1} to experience photoinhibition (section 5.5.3 [Page 194]). Therefore, the growth light conditions should also be increased to avoid any long-term photoinhibition.

New lighting would allow us to more closely mimic sunlight conditions for both growth and HL conditions. The switch from growth light fluorescent tubing to HL LEDs did lead to a change in spectra as well as PPFD (Figure S1 [Page 328]). This may cause photoreceptors to become activated in different quantities. The HL conditions had very limited amounts of far-red light which may have impacted the role of *phyA*, the photoreceptor responsive to far-red light (Figure S1 [Page 328]). High intensity monochromatic lights could also be used to specifically target certain photoreceptors.

All these experiments should be with the goal of creating a set of experimental conditions that can easily be transferred over to crop species. If a particular species acclimates to HL slower or faster, that can be accounted for, and the experimental conditions can be altered. The HL acclimation genes being studied already add a degree of complexity due to interspecies differences that can't be controlled. Understanding HL acclimation better within *Arabidopsis* would provide a breadth of knowledge for overcoming issues encountered when studying other species.

References

Adams III, W.W., Cohu, C.M., Amiard, V. and Demmig-Adams, B. (2014) 'Associations between the acclimation of phloem-cell wall ingrowths in minor veins and maximal photosynthesis rate', *Frontiers in Plant Science*, 5, p. 24. doi:10.3389/fpls.2014.00024.

Alabadí, D., Gil, J., Blázquez, M.A. and García-Martínez, J.L. (2004) 'Gibberellins repress photomorphogenesis in darkness', *Plant Physiology*, 134(3), pp. 1050–1057. doi:10.1104/pp.103.035451.

Alabadí, D., Gallego-Bartolomé, J., Orlando, L., García-Cárcel, L., Rubio, V., Martínez, C., Frigerio, M., Iglesias-Pedraz, J.M., Espinosa, A., Deng, X.W. and Blázquez, M.A. (2008) 'Gibberellins modulate light signaling pathways to prevent Arabidopsis seedling de-etiolation in darkness', *The Plant Journal*, 53(2), pp. 324–335. doi:10.1111/j.1365-313X.2007.03346.x.

Albanese, P., Manfredi, M., Meneghesso, A., Marengo, E., Saracco, G., Barber, J., Morosinotto, T. and Pagliano, C. (2016) 'Dynamic reorganization of photosystem II supercomplexes in response to variations in light intensities', *Biochimica et Biophysica Acta (BBA) - Bioenergetics*, 1857(10), pp. 1651–1660. doi:10.1016/j.bbabio.2016.06.011.

Albanese, P., Tamara, S., Saracco, G., Scheltema, R.A. and Pagliano, C. (2020) 'How paired PSII–LHCII supercomplexes mediate the stacking of plant thylakoid membranes unveiled by structural mass-spectrometry', *Nature Communications*, 11(1), p. 1361. doi:10.1038/s41467-020-15184-1.

Albihlal, W.S., Obomighie, I., Blein, T., Persad, R., Chernukhin, I., Crespi, M., Bechtold, U. and Mullineaux, P.M. (2018) 'Arabidopsis HEAT SHOCK TRANSCRIPTION FACTORA1b regulates multiple developmental genes under benign and stress conditions', *Journal of Experimental Botany*, 69(11), pp. 2847–2862. doi:10.1093/jxb/ery142.

Albinsky, D., Kusano, M., Higuchi, M., Hayashi, N., Kobayashi, M., Fukushima, A., Mori, M., Ichikawa, T., Matsui, K., Kuroda, H., Horii, Y., Tsumoto, Y., Sakakibara, H., Hirochika, H., Matsui, M. and Saito, K. (2010) 'Metabolomic Screening Applied to Rice FOX Arabidopsis Lines Leads to the Identification of a Gene-Changing Nitrogen Metabolism', *Molecular Plant*, 3(1), pp. 125–142. doi:10.1093/mp/ssp069.

Ali, S., Ganai, B.A., Kamili, A.N., Bhat, A.A., Mir, Z.A., Bhat, J.A., Tyagi, A., Islam, S.T., Mushtaq, M., Yadav, P., Rawat, S. and Grover, A. (2018) 'Pathogenesis-related proteins and peptides as promising tools for engineering plants with multiple stress tolerance', *Microbiological Research*, 212–213, pp. 29–37. doi:10.1016/j.micres.2018.04.008.

Alonso, J.M., Stepanova, A.N., Leisse, T.J., Kim, C.J., Chen, H., Shinn, P., Stevenson, D.K., Zimmerman, J., Barajas, P., Cheuk, R., Gadrinab, C., Heller, C., Jeske, A., Koesema, E., Meyers, C.C., Parker, H., Prednis, L., Ansari, Y., Choy, N., Deen, H., Geralt, M., Hazari, N., Hom, E., Karnes, M., Mulholland, C., Ndubaku, R., Schmidt, I., Guzman, P., Aguilar-Henonin, L., Schmid, M., Weigel, D., Carter, D.E., Marchand, T., Risseeuw, E., Brogden, D., Zeko, A., Crosby, W.L., Berry, C.C. and Ecker, J.R. (2003) 'Genome-wide insertional mutagenesis of Arabidopsis thaliana', *Science (New York, N.Y.)*, 301(5633), pp. 653–657. doi:10.1126/science.1086391.

Altmann, M., Altmann, S., Rodriguez, P.A., Weller, B., Elorduy Vergara, L., Palme, J., Marín-de la Rosa, N., Sauer, M., Wenig, M., Villaécija-Aguilar, J.A., Sales, J., Lin, C.-W., Pandiarajan, R., Young, V., Strobel, A., Gross, L., Carbonnel, S., Kugler, K.G., Garcia-Molina, A., Bassel, G.W., Falter, C., Mayer, K.F.X., Gutjahr, C., Vlot, A.C., Grill, E. and Falter-Braun, P. (2020) 'Extensive signal integration by the phytohormone protein network', *Nature*, 583(7815), pp. 271–276. doi:10.1038/s41586-020-2460-0.

Altschul, S.F., Gish, W., Miller, W., Myers, E.W. and Lipman, D.J. (1990) 'Basic local alignment search tool', *Journal of Molecular Biology*, 215(3), pp. 403–410. doi:10.1016/S0022-2836(05)80360-2.

Alvarez-Buylla, E.R., Liljegren, S.J., Pelaz, S., Gold, S.E., Burgeff, C., Ditta, G.S., Vergara-Silva, F. and Yanofsky, M.F. (2000) 'MADS-box gene evolution beyond flowers: expression in pollen, endosperm, guard cells, roots and trichomes', *The Plant Journal*, 24(4), pp. 457–466. doi:10.1111/j.1365-313X.2000.00891.x.

Alvarez-Fernandez, R., Penfold, C.A., Galvez-Valdivieso, G., Exposito-Rodriguez, M., Stallard, E.J., Bowden, L., Moore, J.D., Mead, A., Davey, P.A., Matthews, J.S.A., Beynon, J., Buchanan-Wollaston, V., Wild, D.L., Lawson, T., Bechtold, U., Denby, K.J. and Mullineaux, P.M. (2021) 'Time-series transcriptomics reveals a BBX32-directed control of acclimation to high light in mature Arabidopsis leaves', *The Plant Journal*, 107(5), pp. 1363–1386. doi:10.1111/tpj.15384.

Anderson, J.M., Chow, W.S. and Park, Y.-I. (1995) 'The grand design of photosynthesis: Acclimation of the photosynthetic apparatus to environmental cues', *Photosynthesis Research*, 46(1), pp. 129–139. doi:10.1007/BF00020423.

Anderson, J.P., Badruzsaufari, E., Schenk, P.M., Manners, J.M., Desmond, O.J., Ehlert, C., Maclean, D.J., Ebert, P.R. and Kazan, K. (2004) 'Antagonistic Interaction between Abscisic Acid and Jasmonate-Ethylene Signaling Pathways Modulates Defense Gene Expression and Disease Resistance in Arabidopsis', *The Plant Cell*, 16(12), pp. 3460–3479. doi:10.1105/tpc.104.025833.

Ang, L.H. and Deng, X.W. (1994) 'Regulatory hierarchy of photomorphogenic loci: allele-specific and light-dependent interaction between the HY5 and COP1 loci.', *The Plant Cell*, 6(5), pp. 613–628. doi:10.1105/tpc.6.5.613.

Ang, L.H., Chattopadhyay, S., Wei, N., Oyama, T., Okada, K., Batschauer, A. and Deng, X.W. (1998) 'Molecular interaction between COP1 and HY5 defines a regulatory switch for light control of Arabidopsis development', *Molecular Cell*, 1(2), pp. 213–222. doi:10.1016/s1097-2765(00)80022-2.

Araguirang, G.E., Niemann, N., Kiontke, S., Eckel, M., Dionisio-Sese, M.L. and Batschauer, A. (2019) 'The Arabidopsis cryptochrome 2 I404F mutant is hypersensitive and shows flavin reduction even in the absence of light', *Planta*, 251(1), p. 33. doi:10.1007/s00425-019-03323-y.

5427 Arana, M.V., Sánchez-Lamas, M., Strasser, B., Ibarra, S.E., Cerdán, P.D., Botto, J.F. and
5428 Sánchez, R.A. (2014) 'Functional diversity of phytochrome family in the control of light
5429 and gibberellin-mediated germination in Arabidopsis: Diversity of phytochrome function in
5430 germination', *Plant, Cell & Environment*, 37(9), pp. 2014–2023. doi:10.1111/pce.12286.

5431 Athanasiou, K., Dyson, B.C., Webster, R.E. and Johnson, G.N. (2010) 'Dynamic Acclimation
5432 of Photosynthesis Increases Plant Fitness in Changing Environments', *Plant Physiology*,
5433 152(1), pp. 366–373. doi:10.1104/pp.109.149351.

5434 Bagnall, D.J., King, R.W. and Hangarter, R.P. (1996) 'Blue-light promotion of flowering is
5435 absent in hy4 mutants of Arabidopsis', *Planta*, 200(2), pp. 278–280.
5436 doi:10.1007/BF00208319.

5437 Bailey, S., Horton, P. and Walters, R.G. (2004) 'Acclimation of Arabidopsis thaliana to the
5438 light environment: the relationship between photosynthetic function and chloroplast
5439 composition', *Planta*, 218(5), pp. 793–802. doi:10.1007/s00425-003-1158-5.

5440 Baker, N.R. (2008) 'Chlorophyll fluorescence: a probe of photosynthesis in vivo', *Annual*
5441 *Review of Plant Biology*, 59, pp. 89–113. doi:10.1146/annurev.arplant.59.032607.092759.

5442 Beal, M.J., Falciani, F., Ghahramani, Z., Rangel, C. and Wild, D.L. (2005) 'A Bayesian
5443 approach to reconstructing genetic regulatory networks with hidden factors',
5444 *Bioinformatics*, 21(3), pp. 349–356. doi:10.1093/bioinformatics/bti014.

5445 Bhagat, P.K., Verma, D., Sharma, D. and Sinha, A.K. (2021) 'HY5 and ABI5 transcription
5446 factors physically interact to fine tune light and ABA signaling in Arabidopsis', *Plant*
5447 *Molecular Biology*, 107(1–2), pp. 117–127. doi:10.1007/s11103-021-01187-z.

5448 Blanco-Touriñán, N., Legris, M., Minguet, E.G., Costigliolo-Rojas, C., Nohales, M.A., Iniesto,
5449 E., García-León, M., Pacín, M., Heucken, N., Blomeier, T., Locascio, A., Černý, M.,
5450 Esteve-Bruna, D., Díez-Díaz, M., Brzobohatý, B., Frerigmann, H., Zurbriggen, M.D., Kay,

S.A., Rubio, V., Blázquez, M.A., Casal, J.J. and Alabadí, D. (2020) 'COP1 destabilizes DELLA proteins in Arabidopsis', *Proceedings of the National Academy of Sciences of the United States of America*, 117(24), pp. 13792–13799. doi:10.1073/pnas.1907969117.

Block, A., Schmelz, E., Jones, J.B. and Klee, H.J. (2005) 'Coronatine and salicylic acid: the battle between Arabidopsis and Pseudomonas for phytohormone control', *Molecular Plant Pathology*, 6(1), pp. 79–83. doi:10.1111/j.1364-3703.2004.00265.x.

Boccalandro, H.E., Rossi, M.C., Saijo, Y., Deng, X.-W. and Casal, J.J. (2004) 'Promotion of photomorphogenesis by COP1', *Plant Molecular Biology*, 56(6), pp. 905–915. doi:10.1007/s11103-004-5919-8.

Broekgaarden, C., Caarls, L., Vos, I.A., Pieterse, C.M.J. and Van Wees, S.C.M. (2015) 'Ethylene: Traffic Controller on Hormonal Crossroads to Defense', *Plant Physiology*, 169(4), pp. 2371–2379. doi:10.1104/pp.15.01020.

Bu, X., Wang, X., Yan, J., Zhang, Y., Zhou, S., Sun, X., Yang, Y., Ahammed, G.J., Liu, Y., Qi, M., Wang, F. and Li, T. (2021) 'Genome-Wide Characterization of B-Box Gene Family and Its Roles in Responses to Light Quality and Cold Stress in Tomato', *Frontiers in Plant Science*, 12, p. 698525. doi:10.3389/fpls.2021.698525.

Cameron, R.K., Paiva, N.L., Lamb, C.J. and Dixon, R.A. (1999) 'Accumulation of salicylic acid and PR-1 gene transcripts in relation to the systemic acquired resistance (SAR) response induced by Pseudomonas syringae pv. tomato in Arabidopsis', *Physiological and Molecular Plant Pathology*, 55(2), pp. 121–130. doi:10.1006/pmpp.1999.0214.

Cao, H., Glazebrook, J., Clarke, J.D., Volko, S. and Dong, X. (1997) 'The Arabidopsis NPR1 Gene That Controls Systemic Acquired Resistance Encodes a Novel Protein Containing Ankyrin Repeats', *Cell*, 88(1), pp. 57–63. doi:10.1016/S0092-8674(00)81858-9.

Cao, Y., Han, Y., Meng, D., Li, D., Jiao, C., Jin, Q., Lin, Y. and Cai, Y. (2017) 'B-BOX genes: genome-wide identification, evolution and their contribution to pollen growth in pear (Pyrus bretschneideri Rehd.)', *BMC Plant Biology*, 17(1), p. 156. doi:10.1186/s12870-017-1105-4.

Cao, Y., Meng, D., Han, Y., Chen, T., Jiao, C., Chen, Y., Jin, Q. and Cai, Y. (2019) 'Comparative analysis of B-BOX genes and their expression pattern analysis under various treatments in Dendrobium officinale', *BMC Plant Biology*, 19(1), p. 245. doi:10.1186/s12870-019-1851-6.

Ceasar, S.A., Rajan, V., Prykhozhij, S.V., Berman, J.N. and Ignacimuthu, S. (2016) 'Insert, remove or replace: A highly advanced genome editing system using CRISPR/Cas9', *Biochimica et Biophysica Acta (BBA) - Molecular Cell Research*, 1863(9), pp. 2333–2344. doi:10.1016/j.bbamcr.2016.06.009.

Chen, H., Shen, Y., Tang, X., Yu, L., Wang, J., Guo, L., Zhang, Y., Zhang, H., Feng, S., Strickland, E., Zheng, N. and Deng, X.W. (2006) 'Arabidopsis CULLIN4 Forms an E3 Ubiquitin Ligase with RBX1 and the CDD Complex in Mediating Light Control of Development', *The Plant Cell*, 18(8), pp. 1991–2004. doi:10.1105/tpc.106.043224.

Chen, D., Xu, G., Tang, W., Jing, Y., Ji, Q., Fei, Z. and Lin, R. (2013) 'Antagonistic Basic Helix-Loop-Helix/bZIP Transcription Factors Form Transcriptional Modules That Integrate Light and Reactive Oxygen Species Signaling in Arabidopsis[W]', *The Plant Cell*, 25(5), pp. 1657–1673. doi:10.1105/tpc.112.104869.

Chen, S., Wirthmueller, L., Stauber, J., Lory, N., Holtkotte, X., Leson, L., Schenkel, C., Ahmad, M. and Hoecker, U. (2016) 'The functional divergence between SPA1 and SPA2 in Arabidopsis photomorphogenesis maps primarily to the respective N-terminal kinase-like domain', *BMC Plant Biology*, 16, p. 165. doi:10.1186/s12870-016-0854-9.

5498 Chen, Y.-S., Chao, Y.-C., Tseng, T.-W., Huang, C.-K., Lo, P.-C. and Lu, C.-A. (2017) 'Two
5499 MYB-related transcription factors play opposite roles in sugar signaling in Arabidopsis',
5500 *Plant Molecular Biology*, 93. doi:10.1007/s11103-016-0562-8.

5501 Chory, J., Peto, C., Feinbaum, R., Pratt, L. and Ausubel, F. (1989) 'Arabidopsis thaliana
5502 mutant that develops as a light-grown plant in the absence of light', *Cell*, 58(5), pp. 991–
5503 999. doi:10.1016/0092-8674(89)90950-1.

5504 Chu, Z., Wang, X., Li, Y., Yu, H., Li, J., Lu, Y., Li, H. and Ouyang, B. (2016) 'Genomic
5505 Organization, Phylogenetic and Expression Analysis of the B-BOX Gene Family in
5506 Tomato', *Frontiers in Plant Science*, 7, p. 1552. doi:10.3389/fpls.2016.01552.

5507 Coego, A., Brizuela, E., Castillejo, P., Ruíz, S., Koncz, C., del Pozo, J.C., Piñeiro, M., Jarillo,
5508 J.A., Paz-Ares, J., León, J., and TRANSPLANTA Consortium (2014) 'The
5509 TRANSPLANTA collection of Arabidopsis lines: a resource for functional analysis of
5510 transcription factors based on their conditional overexpression', *The Plant Journal: For
5511 Cell and Molecular Biology*, 77(6), pp. 944–953. doi:10.1111/tpj.12443.

5512 Crocco, C.D. and Botto, J.F. (2013) 'BBX proteins in green plants: insights into their
5513 evolution, structure, feature and functional diversification', *Gene*, 531(1), pp. 44–52.
5514 doi:10.1016/j.gene.2013.08.037.

5515 Cui, H., Gobbato, E., Kracher, B., Qiu, J., Bautor, J. and Parker, J.E. (2017) 'A core function
5516 of EDS1 with PAD4 is to protect the salicylic acid defense sector in Arabidopsis
5517 immunity', *The New Phytologist*, 213(4), pp. 1802–1817. doi:10.1111/nph.14302.

5518 Delker, C., Sonntag, L., James, G.V., Janitza, P., Ibañez, C., Ziermann, H., Peterson, T.,
5519 Denk, K., Mull, S., Ziegler, J., Davis, S.J., Schneeberger, K. and Quint, M. (2014) 'The
5520 DET1-COP1-HY5 pathway constitutes a multipurpose signaling module regulating plant
5521 photomorphogenesis and thermomorphogenesis', *Cell Reports*, 9(6), pp. 1983–1989.
5522 doi:10.1016/j.celrep.2014.11.043.

5523 Deng, X.W., Caspar, T. and Quail, P.H. (1991) ‘cop1: a regulatory locus involved in light-
5524 controlled development and gene expression in Arabidopsis’, *Genes & Development*,
5525 5(7), pp. 1172–1182. doi:10.1101/gad.5.7.1172.

5526 Ding, Y., Sun, T., Ao, K., Peng, Y., Zhang, Yaxi, Li, X. and Zhang, Yuelin (2018) ‘Opposite
5527 Roles of Salicylic Acid Receptors NPR1 and NPR3/NPR4 in Transcriptional Regulation of
5528 Plant Immunity’, *Cell*, 173(6), pp. 1454-1467.e15. doi:10.1016/j.cell.2018.03.044.

5529 Doench, J.G., Fusi, N., Sullender, M., Hegde, M., Vaimberg, E.W., Donovan, K.F., Smith, I.,
5530 Tothova, Z., Wilen, C., Orchard, R., Virgin, H.W., Listgarten, J. and Root, D.E. (2016)
5531 ‘Optimized sgRNA design to maximize activity and minimize off-target effects of CRISPR-
5532 Cas9’, *Nature Biotechnology*, 34(2), pp. 184–191. doi:10.1038/nbt.3437.

5533 Doudna, J.A. and Charpentier, E. (2014) ‘The new frontier of genome engineering with
5534 CRISPR-Cas9’, *Science*, 346(6213), p. 1258096. doi:10.1126/science.1258096.

5535 Dyson, B.C., Allwood, J.W., Feil, R., Xu, Y., Miller, M., Bowsher, C.G., Goodacre, R., Lunn,
5536 J.E. and Johnson, G.N. (2015) ‘Acclimation of metabolism to light in Arabidopsis thaliana:
5537 the glucose 6-phosphate/phosphate translocator GPT2 directs metabolic acclimation’,
5538 *Plant, Cell & Environment*, 38(7), pp. 1404–1417. doi:10.1111/pce.12495.

5539 Eroglu, S., Meier, B., von Wirén, N. and Peiter, E. (2016) ‘The Vacuolar Manganese
5540 Transporter MTP8 Determines Tolerance to Iron Deficiency-Induced Chlorosis in
5541 Arabidopsis’, *Plant Physiology*, 170(2), pp. 1030–1045. doi:10.1104/pp.15.01194.

5542 Fatima, M., Zhang, X., Lin, J., Zhou, P., Zhou, D. and Ming, R. (2020) ‘Expression profiling of
5543 MADS-box gene family revealed its role in vegetative development and stem ripening in
5544 S. spontaneum’, *Scientific Reports*, 10(1), p. 20536. doi:10.1038/s41598-020-77375-6.

5545 Feng, Z., Li, M., Li, Y., Yang, X., Wei, H., Fu, X., Ma, L., Lu, J., Wang, H. and Yu, S. (2021)
5546 'Comprehensive identification and expression analysis of B-Box genes in cotton', *BMC*
5547 *Genomics*, 22(1), p. 439. doi:10.1186/s12864-021-07770-4.

5548 Ferguson, J.N., Meyer, R.C., Edwards, K.D., Humphry, M., Brendel, O. and Bechtold, U.
5549 (2019) 'Accelerated flowering time reduces lifetime water use without penalizing
5550 reproductive performance in Arabidopsis', *Plant, Cell & Environment*, 42(6), pp. 1847–
5551 1867. doi:10.1111/pce.13527.

5552 Fitter, D.W., Martin, D.J., Copley, M.J., Scotland, R.W. and Langdale, J.A. (2002) 'GLK gene
5553 pairs regulate chloroplast development in diverse plant species', *The Plant Journal: For*
5554 *Cell and Molecular Biology*, 31(6), pp. 713–727. doi:10.1046/j.1365-313x.2002.01390.x.

5555 Fittinghoff, K., Laubinger, S., Nixdorf, M., Fackendahl, P., Baumgardt, R.-L., Batschauer, A.
5556 and Hoecker, U. (2006) 'Functional and expression analysis of Arabidopsis SPA genes
5557 during seedling photomorphogenesis and adult growth', *The Plant Journal*, 47(4), pp.
5558 577–590. doi:10.1111/j.1365-313X.2006.02812.x.

5559 Flannery, S.E., Hepworth, C., Wood, W.H.J., Pastorelli, F., Hunter, C.N., Dickman, M.J.,
5560 Jackson, P.J. and Johnson, M.P. (2021) 'Developmental acclimation of the thylakoid
5561 proteome to light intensity in Arabidopsis', *The Plant Journal*, 105(1), pp. 223–244.
5562 doi:10.1111/tpj.15053.

5563 Foyer, C.H., Lelandais, M. and Kunert, K.J. (1994) 'Photooxidative stress in plants',
5564 *Physiologia Plantarum*, 92(4), pp. 696–717. doi:10.1111/j.1399-3054.1994.tb03042.x.

5565 Franco-Zorrilla, J.M., López-Vidriero, I., Carrasco, J.L., Godoy, M., Vera, P. and Solano, R.
5566 (2014) 'DNA-binding specificities of plant transcription factors and their potential to define
5567 target genes', *Proceedings of the National Academy of Sciences*, 111(6), pp. 2367–2372.
5568 doi:10.1073/pnas.1316278111.

5569 Franklin, K.A., Davis, S.J., Stoddart, W.M., Vierstra, R.D. and Whitelam, G.C. (2003) 'Mutant
5570 Analyses Define Multiple Roles for Phytochrome C in Arabidopsis Photomorphogenesis',
5571 *The Plant Cell*, 15(9), pp. 1981–1989. doi:10.1105/tpc.015164.

5572 Frerigmann, H., Hoecker, U. and Gigolashvili, T. (2021) 'New Insights on the Regulation of
5573 Glucosinolate Biosynthesis via COP1 and DELLA Proteins in Arabidopsis Thaliana',
5574 *Frontiers in Plant Science*, 12, p. 680255. doi:10.3389/fpls.2021.680255.

5575 Fu, Z.Q., Yan, S., Saleh, A., Wang, W., Ruble, J., Oka, N., Mohan, R., Spoel, S.H., Tada, Y.,
5576 Zheng, N. and Dong, X. (2012) 'NPR3 and NPR4 are receptors for the immune signal
5577 salicylic acid in plants', *Nature*, 486(7402), pp. 228–232. doi:10.1038/nature11162.

5578 Fu, M., Kang, H.K., Son, S.-H., Kim, S.-K. and Nam, K.H. (2014) 'A Subset of Arabidopsis
5579 RAV Transcription Factors Modulates Drought and Salt Stress Responses Independent of
5580 ABA', *Plant and Cell Physiology*, 55(11), pp. 1892–1904. doi:10.1093/pcp/pcu118.

5581 Gaille, C., Reimmann, C. and Haas, D. (2003) 'Isochorismate Synthase (PchA), the First and
5582 Rate-limiting Enzyme in Salicylate Biosynthesis of Pseudomonas aeruginosa*', *Journal of*
5583 *Biological Chemistry*, 278(19), pp. 16893–16898. doi:10.1074/jbc.M212324200.

5584 Gangappa, S.N. and Botto, J.F. (2014) 'The BBX family of plant transcription factors', *Trends*
5585 *in Plant Science*, 19(7), pp. 460–470. doi:10.1016/j.tplants.2014.01.010.

5586 Gangappa, S.N. and Botto, J.F. (2016) 'The Multifaceted Roles of HY5 in Plant Growth and
5587 Development', *Molecular Plant*, 9(10), pp. 1353–1365. doi:10.1016/j.molp.2016.07.002.

5588 Gao, J., Wang, X., Zhang, M., Bian, M., Deng, W., Zuo, Z., Yang, Z., Zhong, D. and Lin, C.
5589 (2015) 'Trp triad-dependent rapid photoreduction is not required for the function of
5590 Arabidopsis CRY1'. Available at: https://pubag.nal.usda.gov/catalog/3318547 (Accessed:
5591 23 June 2022).

5592 Garapati, P., Xue, G.-P., Munné-Bosch, S. and Balazadeh, S. (2015) ‘Transcription Factor
5593 ATAF1 in Arabidopsis Promotes Senescence by Direct Regulation of Key Chloroplast
5594 Maintenance and Senescence Transcriptional Cascades’, *Plant Physiology*, 168(3), pp.
5595 1122–1139. doi:10.1104/pp.15.00567.

5596 Garcion, C., Lohmann, A., Lamodière, E., Catinot, J., Buchala, A., Doermann, P. and
5597 Métraux, J.-P. (2008) ‘Characterization and Biological Function of the ISOCHORISMATE
5598 SYNTHASE2 Gene of Arabidopsis’, *Plant Physiology*, 147(3), pp. 1279–1287.
5599 doi:10.1104/pp.108.119420.

5600 Gerganova, M., Popova, A., Stanoeva, D. and Velitchkova, M. (2016) ‘Tomato plants
5601 acclimate better to elevated temperature and high light than to treatment with each factor
5602 separately’, *Plant Physiology and Biochemistry*, 104. doi:10.1016/j.plaphy.2016.03.030.

5603 Gerhardt, R., Stitt, M. and Heldt, H.W. (1987) ‘Subcellular Metabolite Levels in Spinach
5604 Leaves: Regulation of Sucrose Synthesis during Diurnal Alterations in Photosynthetic
5605 Partitioning’, *Plant Physiology*, 83(2), pp. 399–407. doi:10.1104/pp.83.2.399.

5606 Goodspeed, D., Chehab, E.W., Min-Venditti, A., Braam, J. and Covington, M.F. (2012)
5607 ‘Arabidopsis synchronizes jasmonate-mediated defense with insect circadian behavior’,
5608 *Proceedings of the National Academy of Sciences of the United States of America*,
5609 109(12), pp. 4674–4677. doi:10.1073/pnas.1116368109.

5610 Goto, N., Kumagai, T. and Koornneef, M. (1991) ‘Flowering responses to light-breaks in
5611 photomorphogenic mutants of Arabidopsis thaliana, a long-day plant’, *Physiologia*
5612 *Plantarum*, 83(2), pp. 209–215. doi:10.1111/j.1399-3054.1991.tb02144.x.

5613 Guan-Peng, M., Da-Qin, Z., Tian-Wen, W., Lin-Bi, Z. and Gui-Lian, L. (2019) ‘BBX32
5614 Interacts with AGL24 Involved in Flowering Time Control in Chinese Cabbage (Brassica
5615 rapa L. ssp. pekinensis)’, *Notulae Botanicae Horti Agrobotanici Cluj-Napoca*, 47(1), pp.
5616 34–45. doi:https://doi.org/10.15835/nbha47111205.

5617 Guo, Y. and Gan, S. (2006) ‘AtNAP, a NAC family transcription factor, has an important role
5618 in leaf senescence’, *The Plant Journal*, 46(4), pp. 601–612. doi:10.1111/j.1365-
5619 313X.2006.02723.x.

5620 Hall, L.N., Rossini, L., Cribb, L. and Langdale, J.A. (1998) ‘GOLDEN 2: a novel
5621 transcriptional regulator of cellular differentiation in the maize leaf’, *The Plant Cell*, 10(6),
5622 pp. 925–936. doi:10.1105/tpc.10.6.925.

5623 Hamamouch, N., Li, C., Seo, P.J., Park, C.-M. and Davis, E.L. (2011) ‘Expression of
5624 Arabidopsis pathogenesis-related genes during nematode infection’, *Molecular Plant*
5625 *Pathology*, 12(4), pp. 355–364. doi:10.1111/j.1364-3703.2010.00675.x.

5626 Harari-Steinberg, O., Ohad, I. and Chamovitz, D.A. (2001) ‘Dissection of the Light Signal
5627 Transduction Pathways Regulating the Two Early Light-Induced Protein Genes in
5628 Arabidopsis’, *Plant Physiology*, 127(3), pp. 986–997. doi:10.1104/pp.010270.

5629 Hauvermale, A.L., Ariizumi, T. and Steber, C.M. (2012) ‘Gibberellin Signaling: A Theme and
5630 Variations on DELLA Repression’, *Plant Physiology*, 160(1), pp. 83–92.
5631 doi:10.1104/pp.112.200956.

5632 Hayami, N., Sakai, Y., Kimura, M., Saito, T., Tokizawa, M., Iuchi, S., Kurihara, Y., Matsui,
5633 M., Nomoto, M., Tada, Y. and Yamamoto, Y.Y. (2015) ‘The Responses of Arabidopsis
5634 Early Light-Induced Protein2 to Ultraviolet B, High Light, and Cold Stress Are Regulated
5635 by a Transcriptional Regulatory Unit Composed of Two Elements’, *Plant Physiology*,
5636 169(1), pp. 840–855. doi:10.1104/pp.15.00398.

5637 Haydon, M.J., Mielczarek, O., Robertson, F.C., Hubbard, K.E. and Webb, A.A.R. (2013)
5638 ‘Photosynthetic entrainment of the Arabidopsis thaliana circadian clock’, *Nature*,
5639 502(7473), pp. 689–692. doi:10.1038/nature12603.

Holm, M., Ma, L.-G., Qu, L.-J. and Deng, X.-W. (2002) 'Two interacting bZIP proteins are direct targets of COP1-mediated control of light-dependent gene expression in Arabidopsis', *Genes & Development*, 16(10), pp. 1247–1259. doi:10.1101/gad.969702.

Holtan, H.E., Bandong, S., Marion, C.M., Adam, L., Tiwari, S., Shen, Y., Maloof, J.N., Maszle, D.R., Ohto, M., Preuss, S., Meister, R., Petracek, M., Repetti, P.P., Reuber, T.L., Ratcliffe, O.J. and Khanna, R. (2011) 'BBX32, an Arabidopsis B-Box Protein, Functions in Light Signaling by Suppressing HY5-Regulated Gene Expression and Interacting with STH2/BBX21', *Plant Physiology*, 156(4), pp. 2109–2123. doi:10.1104/pp.111.177139.

Holtkotte, X., Ponnu, J., Ahmad, M. and Hoecker, U. (2017) 'The blue light-induced interaction of cryptochrome 1 with COP1 requires SPA proteins during Arabidopsis light signaling', *PLOS Genetics*, 13(10), p. e1007044. doi:10.1371/journal.pgen.1007044.

Hoshino, R., Yoshida, Y. and Tsukaya, H. (2019) 'Multiple steps of leaf thickening during sun-leaf formation in Arabidopsis', *The Plant Journal*, 100(4), pp. 738–753. doi:10.1111/tpj.14467.

Hou, W., Ren, L., Zhang, Y., Sun, H., Shi, T., Gu, Y., Wang, A., Ma, D., Li, Z. and Zhang, L. (2021) 'Characterization of BBX family genes and their expression profiles under various stresses in the sweet potato wild ancestor Ipomoea trifida', *Scientia Horticulturae*, 288, p. 110374. doi:10.1016/j.scienta.2021.110374.

Hough, S.H., Ajetunmobi, A., Brody, L., Humphryes-Kirilov, N. and Perello, E. (2016) 'Desktop Genetics', *Personalized Medicine*, 13(6), pp. 517–521. doi:10.2217/pme-2016-0068.

Hsu, P.D., Scott, D.A., Weinstein, J.A., Ran, F.A., Konermann, S., Agarwala, V., Li, Y., Fine, E.J., Wu, X., Shalem, O., Cradick, T.J., Marraffini, L.A., Bao, G. and Zhang, F. (2013) 'DNA targeting specificity of RNA-guided Cas9 nucleases', *Nature Biotechnology*, 31(9), pp. 827–832. doi:10.1038/nbt.2647.

Hu, W., Su, Y.-S. and Lagarias, J.C. (2009) 'A Light-Independent Allele of Phytochrome B Faithfully Recapitulates Photomorphogenic Transcriptional Networks', *Molecular Plant*, 2(1), pp. 166–182. doi:10.1093/mp/ssn086.

Huang, J., Zhao, X., Weng, X., Wang, L. and Xie, W. (2012) 'The Rice B-Box Zinc Finger Gene Family: Genomic Identification, Characterization, Expression Profiling and Diurnal Analysis', *PLOS ONE*, 7(10), p. e48242. doi:10.1371/journal.pone.0048242.

Huang, P.-Y., Catinot, J. and Zimmerli, L. (2016) 'Ethylene response factors in Arabidopsis immunity', *Journal of Experimental Botany*, 67(5), pp. 1231–1241. doi:10.1093/jxb/erv518.

Huang, J., Zhao, X. and Chory, J. (2019) 'The Arabidopsis Transcriptome Responds Specifically and Dynamically to High Light Stress', *Cell Reports*, 29(12), pp. 4186-4199.e3. doi:10.1016/j.celrep.2019.11.051.

Hudson, D., Guevara, D., Yaish, M.W., Hannam, C., Long, N., Clarke, J.D., Bi, Y.-M. and Rothstein, S.J. (2011) 'GNC and CGA1 Modulate Chlorophyll Biosynthesis and Glutamate Synthase (GLU1/Fd-GOGAT) Expression in Arabidopsis', *PLOS ONE*, 6(11), p. e26765. doi:10.1371/journal.pone.0026765.

Hughes, R.M., Vrana, J.D., Song, J. and Tucker, C.L. (2012) 'Light-dependent, dark-promoted interaction between Arabidopsis cryptochrome 1 and phytochrome B proteins', *The Journal of Biological Chemistry*, 287(26), pp. 22165–22172. doi:10.1074/jbc.M112.360545.

Ishikawa, M., Kiba, T. and Chua, N.-H. (2006) 'The Arabidopsis SPA1 gene is required for circadian clock function and photoperiodic flowering', *The Plant Journal*, 46(5), pp. 736–746. doi:10.1111/j.1365-313X.2006.02737.x.

Jang, K., Gil Lee, H., Jung, S.-J., Paek, N.-C. and Joon Seo, P. (2015) 'The E3 Ubiquitin Ligase COP1 Regulates Thermosensory Flowering by Triggering GI Degradation in Arabidopsis', *Scientific Reports*, 5(1), p. 12071. doi:10.1038/srep12071.

Jinek, M., Chylinski, K., Fonfara, I., Hauer, M., Doudna, J.A. and Charpentier, E. (2012) 'A Programmable Dual-RNA–Guided DNA Endonuclease in Adaptive Bacterial Immunity', *Science*, 337(6096), pp. 816–821. doi:10.1126/science.1225829.

Jones, M.A., Hu, W., Litthauer, S., Lagarias, J.C. and Harmer, S.L. (2015) 'A Constitutively Active Allele of Phytochrome B Maintains Circadian Robustness in the Absence of Light', *Plant Physiology*, 169(1), pp. 814–825. doi:10.1104/pp.15.00782.

Jumper, J., Evans, R., Pritzel, A., Green, T., Figurnov, M., Ronneberger, O., Tunyasuvunakool, K., Bates, R., Žídek, A., Potapenko, A., Bridgland, A., Meyer, C., Kohl, S.A.A., Ballard, A.J., Cowie, A., Romera-Paredes, B., Nikolov, S., Jain, R., Adler, J., Back, T., Petersen, S., Reiman, D., Clancy, E., Zielinski, M., Steinegger, M., Pacholska, M., Berghammer, T., Bodenstein, S., Silver, D., Vinyals, O., Senior, A.W., Kavukcuoglu, K., Kohli, P. and Hassabis, D. (2021) 'Highly accurate protein structure prediction with AlphaFold', *Nature*, 596(7873), pp. 583–589. doi:10.1038/s41586-021-03819-2.

Karpiński, S., Szechyńska-Hebda, M., Wituszyńska, W. and Burdiak, P. (2013) 'Light acclimation, retrograde signalling, cell death and immune defences in plants', *Plant, Cell & Environment*, 36(4), pp. 736–744. doi:10.1111/pce.12018.

Kattge, J., Knorr, W., Raddatz, T. and Wirth, C. (2009) 'Quantifying photosynthetic capacity and its relationship to leaf nitrogen content for global-scale terrestrial biosphere models', *Global Change Biology*, 15(4), pp. 976–991. doi:10.1111/j.1365-2486.2008.01744.x.

Kelley, L.A., Mezulis, S., Yates, C.M., Wass, M.N. and Sternberg, M.J.E. (2015) 'The Phyre2 web portal for protein modeling, prediction and analysis', *Nature Protocols*, 10(6), pp. 845–858. doi:10.1038/nprot.2015.053.

Kesarwani, M., Yoo, J. and Dong, X. (2007) 'Genetic Interactions of TGA Transcription Factors in the Regulation of Pathogenesis-Related Genes and Disease Resistance in Arabidopsis', *Plant Physiology*, 144(1), pp. 336–346. doi:10.1104/pp.106.095299.

Khanna, R., Kronmiller, B., Maszle, D.R., Coupland, G., Holm, M., Mizuno, T. and Wu, S.-H. (2009) 'The Arabidopsis B-Box Zinc Finger Family', *The Plant Cell*, 21(11), pp. 3416–3420. doi:10.1105/tpc.109.069088.

Kikis, E.A., Khanna, R. and Quail, P.H. (2005) 'ELF4 is a phytochrome-regulated component of a negative-feedback loop involving the central oscillator components CCA1 and LHY', *The Plant Journal: For Cell and Molecular Biology*, 44(2), pp. 300–313. doi:10.1111/j.1365-313X.2005.02531.x.

Kim, W.-Y., Fujiwara, S., Suh, S.-S., Kim, J., Kim, Y., Han, L., David, K., Putterill, J., Nam, H.G. and Somers, D.E. (2007) 'ZEITLUPE is a circadian photoreceptor stabilized by GIGANTEA in blue light', *Nature*, 449(7160), pp. 356–360. doi:10.1038/nature06132.

Kim, D., Cho, Y., Ryu, H., Kim, Y., Kim, T.-H. and Hwang, I. (2013) 'BLH1 and KNAT3 modulate ABA responses during germination and early seedling development in Arabidopsis', *The Plant Journal*, 75(5), pp. 755–766. doi:10.1111/tpj.12236.

Kleine, T., Kindgren, P., Benedict, C., Hendrickson, L. and Strand, Å. (2007) 'Genome-Wide Gene Expression Analysis Reveals a Critical Role for CRYPTOCHROME1 in the Response of Arabidopsis to High Irradiance', *Plant Physiology*, 144(3), pp. 1391–1406. doi:10.1104/pp.107.098293.

Kliebenstein, D.J., Lim, J.E., Landry, L.G. and Last, R.L. (2002) 'Arabidopsis UVR8 Regulates Ultraviolet-B Signal Transduction and Tolerance and Contains Sequence Similarity to Human Regulator of Chromatin Condensation 1', *Plant Physiology*, 130(1), pp. 234–243. doi:10.1104/pp.005041.

5736 Kong, S.-G. and Okajima, K. (2016) ‘Diverse photoreceptors and light responses in plants’,
5737 *Journal of Plant Research*, 129(2), pp. 111–114. doi:10.1007/s10265-016-0792-5.

5738 Koorneef, M., Elgersma, A., Hanhart, C.J., van Loenen-Martinet, E.P., van Rijn, L. and
5739 Zeevaart, J. a. D. (1985) ‘A gibberellin insensitive mutant of Arabidopsis thaliana’,
5740 *Physiologia Plantarum*, 65(1), pp. 33–39. doi:10.1111/j.1399-3054.1985.tb02355.x.

5741 Kozomara, A. and Griffiths-Jones, S. (2011) ‘miRBase: integrating microRNA annotation and
5742 deep-sequencing data’, *Nucleic Acids Research*, 39(Database issue), pp. D152-157.
5743 doi:10.1093/nar/gkq1027.

5744 Kozomara, A., Birgaoanu, M. and Griffiths-Jones, S. (2019) ‘miRBase: from microRNA
5745 sequences to function’, *Nucleic Acids Research*, 47(D1), pp. D155–D162.
5746 doi:10.1093/nar/gky1141.

5747 Laloi, C., Stachowiak, M., Pers-Kamczyc, E., Warzych, E., Murgia, I. and Apel, K. (2007)
5748 ‘Cross-talk between singlet oxygen- and hydrogen peroxide-dependent signaling of stress
5749 responses in Arabidopsis thaliana’, *Proceedings of the National Academy of Sciences of*
5750 *the United States of America*, 104(2), pp. 672–677. doi:10.1073/pnas.0609063103.

5751 Langdale, J.A. and Kidner, C.A. (1994) ‘bundle sheath defective, a mutation that disrupts
5752 cellular differentiation in maize leaves’, *Development*, 120(3), pp. 673–681.
5753 doi:10.1242/dev.120.3.673.

5754 Lau, O.S. and Deng, X.W. (2012) ‘The photomorphogenic repressors COP1 and DET1: 20
5755 years later’, *Trends in Plant Science*, 17(10), pp. 584–593.
5756 doi:10.1016/j.tplants.2012.05.004.

5757 Lau, K., Podolec, R., Chappuis, R., Ulm, R. and Hothorn, M. (2019) ‘Plant photoreceptors
5758 and their signaling components compete for COP1 binding via VP peptide motifs’, *The*
5759 *EMBO journal*, 38(18), p. e102140. doi:10.15252/embj.2019102140.

Laubinger, S. and Hoecker, U. (2003) 'The SPA1-like proteins SPA3 and SPA4 repress photomorphogenesis in the light', *The Plant Journal*, 35(3), pp. 373–385. doi:10.1046/j.1365-313X.2003.01813.x.

Laubinger, S., Fittinghoff, K. and Hoecker, U. (2004) 'The SPA Quartet: A Family of WD-Repeat Proteins with a Central Role in Suppression of Photomorphogenesis in Arabidopsis', *The Plant Cell*, 16(9), pp. 2293–2306. doi:10.1105/tpc.104.024216.

Laubinger, S., Marchal, V., Le Gourrierec, J., Gentilhomme, J., Wenkel, S., Adrian, J., Jang, S., Kulajta, C., Braun, H., Coupland, G. and Hoecker, U. (2006) 'Arabidopsis SPA proteins regulate photoperiodic flowering and interact with the floral inducer CONSTANS to regulate its stability', *Development (Cambridge, England)*, 133(16), pp. 3213–3222. doi:10.1242/dev.02481.

Lawton, K.A., Potter, S.L., Uknes, S. and Ryals, J. (1994) 'Acquired Resistance Signal Transduction in Arabidopsis Is Ethylene Independent.', *The Plant Cell*, 6(5), pp. 581–588. doi:10.1105/tpc.6.5.581.

Lee, I., Michaels, S.D., Masshardt, A.S. and Amasino, R.M. (1994) 'The late-flowering phenotype of FRIGIDA and mutations in LUMINIDEPENDENS is suppressed in the Landsberg erecta strain of Arabidopsis', *The Plant Journal*, 6(6), pp. 903–909. doi:10.1046/j.1365-313X.1994.6060903.x.

Lee, S., Cheng, H., King, K.E., Wang, W., He, Y., Hussain, A., Lo, J., Harberd, N.P. and Peng, J. (2002) 'Gibberellin regulates Arabidopsis seed germination via RGL2, a GAI/RGA-like gene whose expression is up-regulated following imbibition', *Genes & Development*, 16(5), pp. 646–658. doi:10.1101/gad.969002.

Lee, J., He, K., Stolc, V., Lee, H., Figueroa, P., Gao, Y., Tongprasit, W., Zhao, H., Lee, I. and Deng, X.W. (2007) 'Analysis of transcription factor HY5 genomic binding sites

5784 revealed its hierarchical role in light regulation of development', *The Plant Cell*, 19(3), pp.
5785 731–749. doi:10.1105/tpc.106.047688.

5786 Lee, J., Kang, M.H., Kim, J.Y. and Lim, P.O. (2021) 'The Role of Light and Circadian Clock
5787 in Regulation of Leaf Senescence', *Frontiers in Plant Science*, 12, p. 669170.
5788 doi:10.3389/fpls.2021.669170.

5789 Legris, M., Nieto, C., Sellaro, R., Prat, S. and Casal, J.J. (2017) 'Perception and signalling of
5790 light and temperature cues in plants', *The Plant Journal*, 90(4), pp. 683–697.
5791 doi:10.1111/tpj.13467.

5792 Lei, W., Li, Y., Yao, X., Qiao, K., Wei, L., Liu, B., Zhang, D. and Lin, H. (2020) 'NAP is
5793 involved in GA-mediated chlorophyll degradation and leaf senescence by interacting with
5794 DELLAs in Arabidopsis', *Plant Cell Reports*, 39(1), pp. 75–87. doi:10.1007/s00299-019-
5795 02474-2.

5796 Leivar, P., Monte, E., Al-Sady, B., Carle, C., Storer, A., Alonso, J.M., Ecker, J.R. and Quail,
5797 P.H. (2008) 'The Arabidopsis phytochrome-interacting factor PIF7, together with PIF3 and
5798 PIF4, regulates responses to prolonged red light by modulating phyB levels', *The Plant*
5799 *Cell*, 20(2), pp. 337–352. doi:10.1105/tpc.107.052142.

5800 Li, J., Li, G., Wang, H. and Wang Deng, X. (2011) 'Phytochrome Signaling Mechanisms',
5801 *The Arabidopsis Book / American Society of Plant Biologists*, 9, p. e0148.
5802 doi:10.1199/tab.0148.

5803 Li, M., An, F., Li, W., Ma, M., Feng, Y., Zhang, X. and Guo, H. (2016) 'DELLA proteins
5804 interact with FLC to repress flowering transition: DELLAs-FLC interactions in regulating
5805 flower time', *Journal of Integrative Plant Biology*, 58(7), pp. 642–655.
5806 doi:10.1111/jipb.12451.

Li, M., Chen, H., Chen, J., Chang, M., Palmer, I.A., Gassmann, W., Liu, F. and Fu, Z.Q. (2018) 'TCP Transcription Factors Interact With NPR1 and Contribute Redundantly to Systemic Acquired Resistance', *Frontiers in Plant Science*, 9. Available at: https://www.frontiersin.org/article/10.3389/fpls.2018.01153 (Accessed: 22 June 2022).

Lian, H.-L., He, S.-B., Zhang, Y.-C., Zhu, D.-M., Zhang, J.-Y., Jia, K.-P., Sun, S.-X., Li, L. and Yang, H.-Q. (2011) 'Blue-light-dependent interaction of cryptochrome 1 with SPA1 defines a dynamic signaling mechanism', *Genes & Development*, 25(10), pp. 1023–1028. doi:10.1101/gad.2025111.

Liping, R., Jinbo, Z., Xiaohan, C., Wenyang, W., Dandan, Y. and Xiaohui, S. (2021) 'Transcriptome-wide identification and functional characterization of BBX transcription factor family in Toona sinensis', *Pakistan Journal of Botany*, 53(3). doi:10.30848/PJB2021-3(8).

Liu, B., Zuo, Z., Liu, H., Liu, X. and Lin, C. (2011) 'Arabidopsis cryptochrome 1 interacts with SPA1 to suppress COP1 activity in response to blue light', *Genes & Development*, 25(10), pp. 1029–1034. doi:10.1101/gad.2025011.

Liu, X., Sun, Y., Kørner, C.J., Du, X., Vollmer, M.E. and Pajerowska-Mukhtar, K.M. (2015) 'Bacterial Leaf Infiltration Assay for Fine Characterization of Plant Defense Responses using the Arabidopsis thaliana-Pseudomonas syringae Pathosystem', *JoVE (Journal of Visualized Experiments)*, (104), p. e53364. doi:10.3791/53364.

Liu, H., Ding, Y., Zhou, Y., Jin, W., Xie, K. and Chen, L.-L. (2017) 'CRISPR-P 2.0: An Improved CRISPR-Cas9 Tool for Genome Editing in Plants', *Molecular Plant*, 10(3), pp. 530–532. doi:10.1016/j.molp.2017.01.003.

Liu, X., Liu, R., Li, Y., Shen, X., Zhong, S. and Shi, H. (2017) 'EIN3 and PIF3 Form an Interdependent Module That Represses Chloroplast Development in Buried Seedlings', *The Plant Cell*, 29(12), pp. 3051–3067. doi:10.1105/tpc.17.00508.

5832 Liu, X., Li, R., Dai, Y., Chen, X. and Wang, X. (2018) ‘Genome-wide identification and
5833 expression analysis of the B-box gene family in the Apple (Malus domestica Borkh.)
5834 genome’, *Molecular Genetics and Genomics*, 293(2), pp. 303–315. doi:10.1007/s00438-
5835 017-1386-1.

5836 Livak, K.J. and Schmittgen, T.D. (2001) ‘Analysis of relative gene expression data using
5837 real-time quantitative PCR and the 2(-Delta Delta C(T)) Method’, *Methods (San Diego,
5838 Calif.)*, 25(4), pp. 402–408. doi:10.1006/meth.2001.1262.

5839 Long, S.P., Zhu, X.-G., Naidu, S.L. and Ort, D.R. (2006) ‘Can improvement in
5840 photosynthesis increase crop yields?’, *Plant, Cell & Environment*, 29(3), pp. 315–330.
5841 doi:10.1111/j.1365-3040.2005.01493.x.

5842 Love, M.I., Huber, W. and Anders, S. (2014) ‘Moderated estimation of fold change and
5843 dispersion for RNA-seq data with DESeq2’, *Genome Biology*, 15(12), p. 550.
5844 doi:10.1186/s13059-014-0550-8.

5845 Lund, B.A., Leiros, H.-K.S. and Bjerga, G.E.K. (2014) ‘A high-throughput, restriction-free
5846 cloning and screening strategy based on ccdB-gene replacement’, *Microbial Cell
5847 Factories*, 13, p. 38. doi:10.1186/1475-2859-13-38.

5848 Lv, R., Li, Z., Li, M., Dogra, V., Lv, S., Liu, R., Lee, K.P. and Kim, C. (2019) ‘Uncoupled
5849 Expression of Nuclear and Plastid Photosynthesis-Associated Genes Contributes to Cell
5850 Death in a Lesion Mimic Mutant’, *The Plant Cell*, 31(1), pp. 210–230.
5851 doi:10.1105/tpc.18.00813.

5852 Lyu, G., Li, D. and Li, S. (2020) ‘Bioinformatics analysis of BBX family genes and its
5853 response to UV-B in Arabidopsis thaliana’, *Plant Signaling & Behavior*, 15(9), p. 1782647.
5854 doi:10.1080/15592324.2020.1782647.

Ma, L., Zhao, H. and Deng, X.W. (2003) 'Analysis of the mutational effects of the *COP/DET/FUS* loci on genome expression profiles reveals their overlapping yet not identical roles in regulating *Arabidopsis* seedling development', *Development*, 130(5), pp. 969–981. doi:10.1242/dev.00281.

Ma, D., Li, X., Guo, Y., Chu, J., Fang, S., Yan, C., Noel, J.P. and Liu, H. (2016) 'Cryptochrome 1 interacts with PIF4 to regulate high temperature-mediated hypocotyl elongation in response to blue light', *Proceedings of the National Academy of Sciences of the United States of America*, 113(1), pp. 224–229. doi:10.1073/pnas.1511437113.

Ma, R., Chen, J., Huang, B., Huang, Z. and Zhang, Z. (2021) 'The BBX gene family in Moso bamboo (Phyllostachys edulis): identification, characterization and expression profiles', *BMC Genomics*, 22(1), p. 533. doi:10.1186/s12864-021-07821-w.

Mahmood, K., El-Kereamy, A., Kim, S.-H., Nambara, E. and Rothstein, S.J. (2016) 'ANAC032 Positively Regulates Age-Dependent and Stress-Induced Senescence in Arabidopsis thaliana', *Plant and Cell Physiology*, 57(10), pp. 2029–2046. doi:10.1093/pcp/pcw120.

Maki, H., Sakaoka, S., Itaya, T., Suzuki, T., Mabuchi, K., Amabe, T., Suzuki, N., Higashiyama, T., Tada, Y., Nakagawa, T., Morikami, A. and Tsukagoshi, H. (2019) 'ANAC032 regulates root growth through the MYB30 gene regulatory network', *Scientific Reports*, 9(1), p. 11358. doi:10.1038/s41598-019-47822-0.

Mateo, A., Funck, D., Mühlenbock, P., Kular, B., Mullineaux, P.M. and Karpinski, S. (2006) 'Controlled levels of salicylic acid are required for optimal photosynthesis and redox homeostasis', *Journal of Experimental Botany*, 57(8), pp. 1795–1807. doi:10.1093/jxb/erj196.

McNellis, T W, von Arnim, A.G., Araki, T., Komeda, Y., Miséra, S. and Deng, X.W. (1994) 'Genetic and molecular analysis of an allelic series of cop1 mutants suggests functional

roles for the multiple protein domains.', *The Plant Cell*, 6(4), pp. 487–500. doi:10.1105/tpc.6.4.487.

Mi, H., Ebert, D., Muruganujan, A., Mills, C., Albou, L.-P., Mushayamaha, T. and Thomas, P.D. (2021) 'PANTHER version 16: a revised family classification, tree-based classification tool, enhancer regions and extensive API', *Nucleic Acids Research*, 49(D1), pp. D394–D403. doi:10.1093/nar/gkaa1106.

Michaels, S.D., Ditta, G., Gustafson-Brown, C., Pelaz, S., Yanofsky, M. and Amasino, R.M. (2003) 'AGL24 acts as a promoter of flowering in Arabidopsis and is positively regulated by vernalization', *The Plant Journal: For Cell and Molecular Biology*, 33(5), pp. 867–874. doi:10.1046/j.1365-313x.2003.01671.x.

Miller, M.A.E., O'Cualain, R., Selley, J., Knight, D., Karim, M.F., Hubbard, S.J. and Johnson, G.N. (2017) 'Dynamic Acclimation to High Light in Arabidopsis thaliana Involves Widespread Reengineering of the Leaf Proteome', *Frontiers in Plant Science*, 8. Available at: https://www.frontiersin.org/article/10.3389/fpls.2017.01239 (Accessed: 22 June 2022).

Morris, J.L., Puttick, M.N., Clark, J.W., Edwards, D., Kenrick, P., Pressel, S., Wellman, C.H., Yang, Z., Schneider, H. and Donoghue, P.C.J. (2018) 'The timescale of early land plant evolution', *Proceedings of the National Academy of Sciences of the United States of America*, 115(10), pp. E2274–E2283. doi:10.1073/pnas.1719588115.

Mühlenbock, P., Szechyńska-Hebda, M., Płaszczyca, M., Baudo, M., Mateo, A., Mullineaux, P.M., Parker, J.E., Karpińska, B. and Karpiński, S. (2008) 'Chloroplast Signaling and LESION SIMULATING DISEASE1 Regulate Crosstalk between Light Acclimation and Immunity in Arabidopsis', *The Plant Cell*, 20(9), pp. 2339–2356. doi:10.1105/tpc.108.059618.

Müller, M. and Munné-Bosch, S. (2021) ‘Hormonal impact on photosynthesis and photoprotection in plants’, *Plant Physiology*, 185(4), pp. 1500–1522. doi:10.1093/plphys/kiaa119.

Mullineaux, P.M. and Baker, N.R. (2010) ‘Oxidative Stress: Antagonistic Signaling for Acclimation or Cell Death?’, *Plant Physiology*, 154(2), pp. 521–525. doi:10.1104/pp.110.161406.

Muñoz, P. and Munné-Bosch, S. (2018) ‘Photo-Oxidative Stress during Leaf, Flower and Fruit Development’, *Plant Physiology*, 176(2), pp. 1004–1014. doi:10.1104/pp.17.01127.

Murchie, E.H. and Horton, P. (1997) ‘Acclimation of photosynthesis to irradiance and spectral quality in British plant species: chlorophyll content, photosynthetic capacity and habitat preference’, *Plant, Cell & Environment*, 20(4), pp. 438–448. doi:10.1046/j.1365-3040.1997.d01-95.x.

Murchie, E.H., Hubbart, S., Peng, S. and Horton, P. (2005) ‘Acclimation of photosynthesis to high irradiance in rice: gene expression and interactions with leaf development’, *Journal of Experimental Botany*, 56(411), pp. 449–460. doi:10.1093/jxb/eri100.

Murmu, J., Wilton, M., Allard, G., Pandeya, R., Desveaux, D., Singh, J. and Subramaniam, R. (2013) ‘Arabidopsis GOLDEN2-LIKE (GLK) transcription factors activate jasmonic acid (JA)-dependent disease susceptibility to the biotrophic pathogen Hyaloperonospora arabidopsidis, as well as JA-independent plant immunity against the necrotrophic pathogen Botrytis cinerea’, *Molecular Plant Pathology*, 15(2), pp. 174–184. doi:10.1111/mpp.12077.

Narusaka, M., Shiraishi, T., Iwabuchi, M. and Narusaka, Y. (2010) ‘The floral inoculating protocol: a simplified *Arabidopsis thaliana* transformation method modified from floral dipping’, *Plant Biotechnology*, 27(4), pp. 349–351. doi:10.5511/plantbiotechnology.27.349.

5928 Nguyen, N.H., Jeong, C.Y., Kang, G.-H., Yoo, S.-D., Hong, S.-W. and Lee, H. (2015) 'MYBD
5929 employed by HY5 increases anthocyanin accumulation via repression of MYBL2 in
5930 Arabidopsis', *The Plant Journal*, 84(6), pp. 1192–1205. doi:10.1111/tpj.13077.

5931 Nguyen, Q.A., Luan, S., Wi, S.G., Bae, H., Lee, D.-S. and Bae, H.-J. (2016) 'Pronounced
5932 Phenotypic Changes in Transgenic Tobacco Plants Overexpressing Sucrose Synthase
5933 May Reveal a Novel Sugar Signaling Pathway', *Frontiers in Plant Science*, 6. Available at:
5934 https://www.frontiersin.org/article/10.3389/fpls.2015.01216 (Accessed: 22 June 2022).

5935 Nikolov, D.B., Chen, H., Halay, E.D., Usheva, A.A., Hisatake, K., Lee, D.K., Roeder, R.G.
5936 and Burley, S.K. (1995) 'Crystal structure of a TFIIB–TBP–TATA-element ternary
5937 complex', *Nature*, 377(6545), pp. 119–128. doi:10.1038/377119a0.

5938 Ochsenbein, C., Przybyla, D., Danon, A., Landgraf, F., Göbel, C., Imboden, A., Feussner, I.
5939 and Apel, K. (2006) 'The role of EDS1 (enhanced disease susceptibility) during singlet
5940 oxygen-mediated stress responses of Arabidopsis', *The Plant Journal*, 47(3), pp. 445–
5941 456. doi:10.1111/j.1365-313X.2006.02793.x.

5942 Oguchi, R., Hikosaka, K. and Hirose, T. (2003) 'Does the photosynthetic light-acclimation
5943 need change in leaf anatomy?', *Plant, Cell & Environment*, 26(4), pp. 505–512.
5944 doi:10.1046/j.1365-3040.2003.00981.x.

5945 Ohgishi, M., Saji, K., Okada, K. and Sakai, T. (2004) 'Functional analysis of each blue light
5946 receptor, cry1, cry2, phot1, and phot2, by using combinatorial multiple mutants in
5947 Arabidopsis', *Proceedings of the National Academy of Sciences of the United States of
5948 America*, 101(8), pp. 2223–2228. doi:10.1073/pnas.0305984101.

5949 Okushima, Y., Mitina, I., Quach, H.L. and Theologis, A. (2005) 'AUXIN RESPONSE
5950 FACTOR 2 (ARF2): a pleiotropic developmental regulator', *The Plant Journal*, 43(1), pp.
5951 29–46. doi:10.1111/j.1365-313X.2005.02426.x.

Ordon, J., Bressan, M., Kretschmer, C., Dall'Osto, L., Marillonnet, S., Bassi, R. and Stuttmann, J. (2020) 'Optimized Cas9 expression systems for highly efficient Arabidopsis genome editing facilitate isolation of complex alleles in a single generation', *Functional & Integrative Genomics*, 20(1), pp. 151–162. doi:10.1007/s10142-019-00665-4.

Orphanides, G., Lagrange, T. and Reinberg, D. (1996) 'The general transcription factors of RNA polymerase II.', *Genes & Development*, 10(21), pp. 2657–2683. doi:10.1101/gad.10.21.2657.

Osborn, R.W., De Samblanx, G.W., Thevissen, K., Goderis, I., Torrekens, S., Van Leuven, F., Attenborough, S., Rees, S.B. and Broekaert, W.F. (1995) 'Isolation and characterisation of plant defensins from seeds of Asteraceae, Fabaceae, Hippocastanaceae and Saxifragaceae', *FEBS Letters*, 368(2), pp. 257–262. doi:10.1016/0014-5793(95)00666-W.

Osterlund, M.T., Hardtke, C.S., Wei, N. and Deng, X.W. (2000) 'Targeted destabilization of HY5 during light-regulated development of Arabidopsis', *Nature*, 405(6785), pp. 462–466. doi:10.1038/35013076.

Oughtred, R., Stark, C., Breitkreutz, B.-J., Rust, J., Boucher, L., Chang, C., Kolas, N., O'Donnell, L., Leung, G., McAdam, R., Zhang, F., Dolma, S., Willems, A., Coulombe-Huntington, J., Chatr-Aryamontri, A., Dolinski, K. and Tyers, M. (2019) 'The BioGRID interaction database: 2019 update', *Nucleic Acids Research*, 47(D1), pp. D529–D541. doi:10.1093/nar/gky1079.

Pagnussat, G.C., Yu, H.-J. and Sundaresan, V. (2007) 'Cell-Fate Switch of Synergid to Egg Cell in Arabidopsis eostre Mutant Embryo Sacs Arises from Misexpression of the BEL1-Like Homeodomain Gene BLH1', *The Plant Cell*, 19(11), pp. 3578–3592. doi:10.1105/tpc.107.054890.

5976 Paik, I., Chen, F., Ngoc Pham, V., Zhu, L., Kim, J.-I. and Huq, E. (2019) 'A phyB-PIF1-SPA1
5977 kinase regulatory complex promotes photomorphogenesis in Arabidopsis', *Nature*
5978 *Communications*, 10(1), p. 4216. doi:10.1038/s41467-019-12110-y.

5979 Park, H.-Y., Lee, S.-Y., Seok, H.-Y., Kim, S.-H., Sung, Z.R. and Moon, Y.-H. (2011) 'EMF1
5980 interacts with EIP1, EIP6 or EIP9 involved in the regulation of flowering time in
5981 Arabidopsis', *Plant & Cell Physiology*, 52(8), pp. 1376–1388. doi:10.1093/pcp/pcr084.

5982 Pepper, A., Delaney, T., Washburn, T., Poole, D. and Chory, J. (1994) 'DET1, a negative
5983 regulator of light-mediated development and gene expression in arabidopsis, encodes a
5984 novel nuclear-localized protein', *Cell*, 78(1), pp. 109–116. doi:10.1016/0092-
5985 8674(94)90577-0.

5986 Ponnu, J., Riedel, T., Penner, E., Schrader, A. and Hoecker, U. (2019) 'Cryptochrome 2
5987 competes with COP1 substrates to repress COP1 ubiquitin ligase activity during
5988 Arabidopsis photomorphogenesis', *Proceedings of the National Academy of Sciences*,
5989 116(52), pp. 27133–27141. doi:10.1073/pnas.1909181116.

5990 Ponnu, J. and Hoecker, U. (2021) 'Illuminating the COP1/SPA Ubiquitin Ligase: Fresh
5991 Insights Into Its Structure and Functions During Plant Photomorphogenesis', *Frontiers in*
5992 *Plant Science*, 12. Available at:
5993 https://www.frontiersin.org/article/10.3389/fpls.2021.662793 (Accessed: 22 June 2022).

5994 Ponnu, J. and Hoecker, U. (2022) 'Signaling Mechanisms by Arabidopsis Cryptochromes',
5995 *Frontiers in Plant Science*, 13. Available at:
5996 https://www.frontiersin.org/article/10.3389/fpls.2022.844714 (Accessed: 22 June 2022).

5997 Preuss, S.B., Meister, R., Xu, Q., Urwin, C.P., Tripodi, F.A., Screen, S.E., Anil, V.S., Zhu, S.,
5998 Morrell, J.A., Liu, G., Ratcliffe, O.J., Reuber, T.L., Khanna, R., Goldman, B.S., Bell, E.,
5999 Ziegler, T.E., McClerren, A.L., Ruff, T.G. and Petracek, M.E. (2012) 'Expression of the

6000 Arabidopsis thaliana BBX32 Gene in Soybean Increases Grain Yield', *PLoS ONE*, 7(2), p.
6001 e30717. doi:10.1371/journal.pone.0030717.

6002 Qin, M., Zhang, B., Gu, G., Yuan, J., Yang, X., Yang, J. and Xie, X. (2021) 'Genome-Wide
6003 Analysis of the G2-Like Transcription Factor Genes and Their Expression in Different
6004 Senescence Stages of Tobacco (Nicotiana tabacum L.)', *Frontiers in Genetics*, 12, p.
6005 626352. doi:10.3389/fgene.2021.626352.

6006 Quail, P.H. (1991) 'Phytochrome: a light-activated molecular switch that regulates plant gene
6007 expression', *Annual Review of Genetics*, 25, pp. 389–409.
6008 doi:10.1146/annurev.ge.25.120191.002133.

6009 Rauf, M., Arif, M., Dortay, H., Matallana-Ramírez, L.P., Waters, M.T., Gil Nam, H., Lim, P.-
6010 O., Mueller-Roeber, B. and Balazadeh, S. (2013) 'ORE1 balances leaf senescence
6011 against maintenance by antagonizing G2-like-mediated transcription', *EMBO Reports*,
6012 14(4), pp. 382–388. doi:10.1038/embor.2013.24.

6013 Richter, R., Behringer, C., Müller, I.K. and Schwechheimer, C. (2010) 'The GATA-type
6014 transcription factors GNC and GNL/CGA1 repress gibberellin signaling downstream from
6015 DELLA proteins and PHYTOCHROME-INTERACTING FACTORS', *Genes &*
6016 *Development*, 24(18), pp. 2093–2104. doi:10.1101/gad.594910.

6017 Richter, R., Bastakis, E. and Schwechheimer, C. (2013) 'Cross-Repressive Interactions
6018 between SOC1 and the GATAs GNC and GNL/CGA1 in the Control of Greening, Cold
6019 Tolerance, and Flowering Time in Arabidopsis', *Plant Physiology*, 162(4), pp. 1992–2004.
6020 doi:10.1104/pp.113.219238.

6021 Roach, T. and Krieger-Liszkay, A. (2012) 'The role of the PsbS protein in the protection of
6022 photosystems I and II against high light in Arabidopsis thaliana', *Biochimica et Biophysica*
6023 *Acta (BBA) - Bioenergetics*, 1817(12), pp. 2158–2165. doi:10.1016/j.bbabio.2012.09.011.

6024 Robb, G.B. (2019) ‘Genome Editing with CRISPR-Cas: An Overview’, *Current Protocols*
6025 *Essential Laboratory Techniques*, 19(1), p. e36. doi:10.1002/cpet.36.

6026 Rossini, L., Cribb, L., Martin, D.J. and Langdale, J.A. (2001) ‘The Maize Golden2 Gene
6027 Defines a Novel Class of Transcriptional Regulators in Plants’, *The Plant Cell*, 13(5), pp.
6028 1231–1244.

6029 Rosso, M.G., Li, Y., Strizhov, N., Reiss, B., Dekker, K. and Weisshaar, B. (2003) ‘An
6030 Arabidopsis thaliana T-DNA mutagenized population (GABI-Kat) for flanking sequence
6031 tag-based reverse genetics’, *Plant Molecular Biology*, 53(1), pp. 247–259.
6032 doi:10.1023/B:PLAN.0000009297.37235.4a.

6033 Rozen, S. and Skaletsky, H. (2000) ‘Primer3 on the WWW for general users and for biologist
6034 programmers’, *Methods in Molecular Biology (Clifton, N.J.)*, 132, pp. 365–386.
6035 doi:10.1385/1-59259-192-2:365.

6036 Ruban, A.V. and Murchie, E.H. (2012) ‘Assessing the photoprotective effectiveness of non-
6037 photochemical chlorophyll fluorescence quenching: a new approach’, *Biochimica Et*
6038 *Biophysica Acta*, 1817(7), pp. 977–982. doi:10.1016/j.bbabio.2012.03.026.

6039 Ruban, A.V. and Belgio, E. (2014) ‘The relationship between maximum tolerated light
6040 intensity and photoprotective energy dissipation in the photosynthetic antenna:
6041 chloroplast gains and losses’, *Philosophical Transactions of the Royal Society of London.*
6042 *Series B, Biological Sciences*, 369(1640), p. 20130222. doi:10.1098/rstb.2013.0222.

6043 Saijo, Y., Sullivan, J.A., Wang, H., Yang, J., Shen, Y., Rubio, V., Ma, L., Hoecker, U. and
6044 Deng, X.W. (2003) ‘The COP1-SPA1 interaction defines a critical step in phytochrome A-
6045 mediated regulation of HY5 activity’, *Genes & Development*, 17(21), pp. 2642–2647.
6046 doi:10.1101/gad.1122903.

6047 Salomé, P.A. and McClung, C.R. (2005) 'PSEUDO-RESPONSE REGULATOR 7 and 9 are
6048 partially redundant genes essential for the temperature responsiveness of the Arabidopsis
6049 circadian clock', *The Plant Cell*, 17(3), pp. 791–803. doi:10.1105/tpc.104.029504.

6050 Salomé, P.A., Xie, Q. and McClung, C.R. (2008) 'Circadian Timekeeping during Early
6051 Arabidopsis Development', *Plant Physiology*, 147(3), pp. 1110–1125.
6052 doi:10.1104/pp.108.117622.

6053 Sanda, S.L. and Amasino, R.M. (1996) 'Ecotype-Specific Expression of a Flowering Mutant
6054 Phenotype in Arabidopsis thaliana.', *Plant Physiology*, 111(2), pp. 641–644.

6055 Sessions, A., Burke, E., Presting, G., Aux, G., McElver, J., Patton, D., Dietrich, B., Ho, P.,
6056 Bacwaden, J., Ko, C., Clarke, J.D., Cotton, D., Bullis, D., Snell, J., Miguel, T., Hutchison,
6057 D., Kimmerly, B., Mitzel, T., Katagiri, F., Glazebrook, J., Law, M. and Goff, S.A. (2002) 'A
6058 High-Throughput Arabidopsis Reverse Genetics System', *The Plant Cell*, 14(12), pp.
6059 2985–2994. doi:10.1105/tpc.004630.

6060 Shalmani, A., Fan, S., Jia, P., Li, G., Muhammad, I., Li, Y., Sharif, R., Dong, F., Zuo, X., Li,
6061 K., Chen, K.-M. and Han, M. (2018) 'Genome Identification of B-BOX Gene Family
6062 Members in Seven Rosaceae Species and Their Expression Analysis in Response to
6063 Flower Induction in Malus domestica', *Molecules*, 23(7), p. 1763.
6064 doi:10.3390/molecules23071763.

6065 Shalmani, A., Jing, X.-Q., Shi, Y., Muhammad, I., Zhou, M.-R., Wei, X.-Y., Chen, Q.-Q., Li,
6066 W.-Q., Liu, W.-T. and Chen, K.-M. (2019) 'Characterization of B-BOX gene family and
6067 their expression profiles under hormonal, abiotic and metal stresses in Poaceae plants',
6068 *BMC genomics*, 20(1), p. 27. doi:10.1186/s12864-018-5336-z.

6069 Sharrock, R.A. and Clack, T. (2002) 'Patterns of expression and normalized levels of the five
6070 Arabidopsis phytochromes', *Plant Physiology*, 130(1), pp. 442–456.
6071 doi:10.1104/pp.005389.

6072 Sher Khan, R., Iqbal, A., Malak, R., Shehryar, K., Attia, S., Ahmed, T., Ali Khan, M., Arif, M.
6073 and Mii, M. (2019) 'Plant defensins: types, mechanism of action and prospects of genetic
6074 engineering for enhanced disease resistance in plants', *3 Biotech*, 9(5), p. 192.
6075 doi:10.1007/s13205-019-1725-5.

6076 Shimada, T.L., Shimada, T. and Hara-Nishimura, I. (2010) 'A rapid and non-destructive
6077 screenable marker, FAST, for identifying transformed seeds of Arabidopsis thaliana', *The*
6078 *Plant Journal: For Cell and Molecular Biology*, 61(3), pp. 519–528. doi:10.1111/j.1365-
6079 313X.2009.04060.x.

6080 Sims, D.A. and Pearcy, R.W. (1992) 'Response of Leaf Anatomy and Photosynthetic
6081 Capacity in Alocasia Macrorrhiza (araceae) to a Transfer from Low to High Light',
6082 *American Journal of Botany*, 79(4), pp. 449–455. doi:10.1002/j.1537-
6083 2197.1992.tb14573.x.

6084 Singh, S., Chhapekar, S.S., Ma, Y., Rameneni, J.J., Oh, S.H., Kim, J., Lim, Y.P. and Choi,
6085 S.R. (2021) 'Genome-Wide Identification, Evolution, and Comparative Analysis of B-Box
6086 Genes in Brassica rapa, B. oleracea, and B. napus and Their Expression Profiling in B.
6087 rapa in Response to Multiple Hormones and Abiotic Stresses', *International Journal of*
6088 *Molecular Sciences*, 22(19), p. 10367. doi:10.3390/ijms221910367.

6089 Singh, M. and Mas, P. (2018) 'A Functional Connection between the Circadian Clock and
6090 Hormonal Timing in Arabidopsis', *Genes*, 9(12), p. 567. doi:10.3390/genes9120567.

6091 Song, Y., Yang, C., Gao, S., Zhang, W., Li, L. and Kuai, B. (2014) 'Age-Triggered and Dark-
6092 Induced Leaf Senescence Require the bHLH Transcription Factors PIF3, 4, and 5',
6093 *Molecular Plant*, 7(12), pp. 1776–1787. doi:10.1093/mp/ssu109.

6094 Srivastava, A.K., Senapati, D., Srivastava, A., Chakraborty, M., Gangappa, S.N. and
6095 Chattopadhyay, S. (2015) 'Short Hypocotyl in White Light1 Interacts with Elongated
6096 Hypocotyl5 (HY5) and Constitutive Photomorphogenic1 (COP1) and Promotes COP1-

6097 Mediated Degradation of HY5 during Arabidopsis Seedling Development', *Plant*
6098 *Physiology*, 169(4), pp. 2922–2934. doi:10.1104/pp.15.01184.

6099 Stacey, M.G., Kopp, O.R., Kim, T.-H. and von Arnim, A.G. (2000) 'Modular Domain Structure
6100 of Arabidopsis COP1. Reconstitution of Activity by Fragment Complementation and
6101 Mutational Analysis of a Nuclear Localization Signal in Planta', *Plant Physiology*, 124(3),
6102 pp. 979–990.

6103 Stein, O. and Granot, D. (2019) 'An Overview of Sucrose Synthases in Plants', *Frontiers in*
6104 *Plant Science*, 10. Available at:
6105 https://www.frontiersin.org/article/10.3389/fpls.2019.00095 (Accessed: 22 June 2022).

6106 Stewart, J.J., Polutchko, S.K., Adams, W.W. and Demmig-Adams, B. (2017) 'Acclimation of
6107 Swedish and Italian ecotypes of Arabidopsis thaliana to light intensity', *Photosynthesis*
6108 *Research*, 134(2), pp. 215–229. doi:10.1007/s11120-017-0436-1.

6109 Stotz, H.U., Thomson, J. and Wang, Y. (2009) 'Plant defensins: Defense, development and
6110 application', *Plant Signaling & Behavior*, 4(11), pp. 1010–1012.
6111 doi:10.4161/psb.4.11.9755.

6112 Straus, M.R., Rietz, S., Ver Loren van Themaat, E., Bartsch, M. and Parker, J.E. (2010)
6113 'Salicylic acid antagonism of EDS1-driven cell death is important for immune and
6114 oxidative stress responses in Arabidopsis', *The Plant Journal: For Cell and Molecular*
6115 *Biology*, 62(4), pp. 628–640. doi:10.1111/j.1365-313X.2010.04178.x.

6116 Su, Y. and Lagarias, J.C. (2007) 'Light-Independent Phytochrome Signaling Mediated by
6117 Dominant GAF Domain Tyrosine Mutants of Arabidopsis Phytochromes in Transgenic
6118 Plants', *The Plant Cell*, 19(7), pp. 2124–2139. doi:10.1105/tpc.107.051516.

6119 Su, L., Hou, P., Song, M., Zheng, X., Guo, L., Xiao, Y., Yan, L., Li, W. and Yang, J. (2015)
6120 'Synergistic and Antagonistic Action of Phytochrome (Phy) A and PhyB during Seedling

De-Etiolation in Arabidopsis thaliana', *International Journal of Molecular Sciences*, 16(6), pp. 12199–12212. doi:10.3390/ijms160612199.

Takeuchi, T., Newton, L., Burkhardt, A., Mason, S. and Farré, E.M. (2014) 'Light and the circadian clock mediate time-specific changes in sensitivity to UV-B stress under light/dark cycles', *Journal of Experimental Botany*, 65(20), pp. 6003–6012. doi:10.1093/jxb/eru339.

Talar, U. and Kiełbowicz-Matuk, A. (2021) 'Beyond Arabidopsis: BBX Regulators in Crop Plants', *International Journal of Molecular Sciences*, 22(6), p. 2906. doi:10.3390/ijms22062906.

Talbott, L.D., Shmayevich, I.J., Chung, Y., Hammad, J.W. and Zeiger, E. (2003) 'Blue Light and Phytochrome-Mediated Stomatal Opening in the npq1 and phot1 phot2 Mutants of Arabidopsis', *Plant Physiology*, 133(4), pp. 1522–1529. doi:10.1104/pp.103.029587.

Talhouët, A.-C., Meyer, S., Baudin, X. and Streb, P. (2020) 'Dynamic acclimation to sunlight in an alpine plant, Soldanella alpina L', *Physiologia Plantarum*, 168(3), pp. 563–575. doi:10.1111/ppl.12982.

Tamura, K., Stecher, G. and Kumar, S. (2021) 'MEGA11: Molecular Evolutionary Genetics Analysis Version 11', *Molecular Biology and Evolution*, 38(7), pp. 3022–3027. doi:10.1093/molbev/msab120.

Tanaka, K., Tozawa, Y., Mochizuki, N., Shinozaki, K., Nagatani, A., Wakasa, K. and Takahashi, H. (1997) 'Characterization of three cDNA species encoding plastid RNA polymerase sigma factors in Arabidopsis thaliana: evidence for the sigma factor heterogeneity in higher plant plastids', *FEBS Letters*, 413(2), pp. 309–313. doi:10.1016/S0014-5793(97)00906-X.

Thompson, J.D., Higgins, D.G. and Gibson, T.J. (1994) 'CLUSTAL W: improving the sensitivity of progressive multiple sequence alignment through sequence weighting, position-specific gap penalties and weight matrix choice', *Nucleic Acids Research*, 22(22), pp. 4673–4680. doi:10.1093/nar/22.22.4673.

Tilbrook, K., Arongaus, A.B., Binkert, M., Heijde, M., Yin, R. and Ulm, R. (2013) 'The UVR8 UV-B Photoreceptor: Perception, Signaling and Response', *The Arabidopsis Book*, 11, p. e0164. doi:10.1199/tab.0164.

Tokumaru, M., Adachi, F., Toda, M., Ito-Inaba, Y., Yazu, F., Hirosawa, Y., Sakakibara, Y., Suiko, M., Kakizaki, T. and Inaba, T. (2017) 'Ubiquitin-Proteasome Dependent Regulation of the GOLDEN2-LIKE 1 Transcription Factor in Response to Plastid Signals', *Plant Physiology*, 173(1), pp. 524–535. doi:10.1104/pp.16.01546.

Triantaphylidès, C., Krischke, M., Hoeberichts, F.A., Ksas, B., Gresser, G., Havaux, M., Van Breusegem, F. and Mueller, M.J. (2008) 'Singlet oxygen is the major reactive oxygen species involved in photooxidative damage to plants', *Plant Physiology*, 148(2), pp. 960–968. doi:10.1104/pp.108.125690.

Trigg, S.A., Garza, R.M., MacWilliams, A., Nery, J.R., Bartlett, A., Castanon, R., Goubil, A., Feeney, J., O'Malley, R., Huang, S.-S.C., Zhang, Z.Z., Galli, M. and Ecker, J.R. (2017) 'CrY2H-seq: a massively multiplexed assay for deep-coverage interactome mapping', *Nature Methods*, 14(8), pp. 819–825. doi:10.1038/nmeth.4343.

Tripathi, P., Carvallo, M., Hamilton, E.E., Preuss, S. and Kay, S.A. (2017) 'Arabidopsis B-BOX32 interacts with CONSTANS-LIKE3 to regulate flowering', *Proceedings of the National Academy of Sciences of the United States of America*, 114(1), pp. 172–177. doi:10.1073/pnas.1616459114.

6167 Valladares, F. (2004) ‘Photoinhibition and drought in Mediterranean woody saplings: scaling
6168 effects and interactions in sun and shade phenotypes’, *Journal of Experimental Botany*,
6169 56(411), pp. 483–494. doi:10.1093/jxb/eri037.

6170 Vandenbussche, F., Habricot, Y., Condiff, A.S., Maldiney, R., Straeten, D.V.D. and Ahmad,
6171 M. (2007) ‘HY5 is a point of convergence between cryptochrome and cytokinin signalling
6172 pathways in Arabidopsis thaliana’, *The Plant Journal*, 49(3), pp. 428–441.
6173 doi:10.1111/j.1365-313X.2006.02973.x.

6174 Varella, A.C., Moot, D.J., Pollock, K.M., Peri, P.L. and Lucas, R.J. (2011) ‘Do light and alfalfa
6175 responses to cloth and slatted shade represent those measured under an agroforestry
6176 system?’, *Agroforestry Systems*, 81(2), pp. 157–173. doi:10.1007/s10457-010-9319-6.

6177 Veciana, N., Martín, G., Leivar, P. and Monte, E. (2022) ‘BBX16 mediates the repression of
6178 seedling photomorphogenesis downstream of the GUN1/GLK1 module during retrograde
6179 signalling’, *New Phytologist*, 234(1), pp. 93–106. doi:10.1111/nph.17975.

6180 Vialet-Chabrand, S., Matthews, J.S.A., Simkin, A.J., Raines, C.A. and Lawson, T. (2017)
6181 ‘Importance of Fluctuations in Light on Plant Photosynthetic Acclimation’, *Plant*
6182 *Physiology*, 173(4), pp. 2163–2179. doi:10.1104/pp.16.01767.

6183 Wagner, S., Stuttmann, J., Rietz, S., Guerois, R., Brunstein, E., Bautor, J., Niefind, K. and
6184 Parker, J.E. (2013) ‘Structural basis for signaling by exclusive EDS1 heteromeric
6185 complexes with SAG101 or PAD4 in plant innate immunity’, *Cell Host & Microbe*, 14(6),
6186 pp. 619–630. doi:10.1016/j.chom.2013.11.006.

6187 Walper, E., Weiste, C., Mueller, M.J., Hamberg, M. and Dröge-Laser, W. (2016) ‘Screen
6188 Identifying Arabidopsis Transcription Factors Involved in the Response to 9-
6189 Lipoxygenase-Derived Oxylipins’, *PLOS ONE*, 11(4), p. e0153216.
6190 doi:10.1371/journal.pone.0153216.

6191 Walters, R.G. and Horton, P. (1994) ‘Acclimation of Arabidopsis thaliana to the light
6192 environment: Changes in composition of the photosynthetic apparatus’, *Planta*, 195(2),
6193 pp. 248–256. doi:10.1007/BF00199685.

6194 Walters, R.G., Rogers, J.J.M., Shephard, F. and Horton, P. (1999) ‘Acclimation of
6195 Arabidopsis thaliana to the light environment: the role of photoreceptors’, *Planta*, 209(4),
6196 pp. 517–527. doi:10.1007/s004250050756.

6197 Walters, R.G., Ibrahim, D.G., Horton, P. and Kruger, N.J. (2004) ‘A Mutant of Arabidopsis
6198 Lacking the Triose-Phosphate/Phosphate Translocator Reveals Metabolic Regulation of
6199 Starch Breakdown in the Light’, *Plant Physiology*, 135(2), pp. 891–906.
6200 doi:10.1104/pp.104.040469.

6201 Walters, R.G. (2005) ‘Towards an understanding of photosynthetic acclimation’, *Journal of*
6202 *Experimental Botany*, 56(411), pp. 435–447. doi:10.1093/jxb/eri060.

6203 Wang, C.-Q., Sarmast, M.K., Jiang, J. and Dehesh, K. (2015) ‘The Transcriptional Regulator
6204 BBX19 Promotes Hypocotyl Growth by Facilitating COP1-Mediated EARLY
6205 FLOWERING3 Degradation in Arabidopsis’, *The Plant Cell*, 27(4), pp. 1128–1139.
6206 doi:10.1105/tpc.15.00044.

6207 Wang, P., Khoshravesh, R., Karki, S., Tapia, R., Balahadia, C.P., Bandyopadhyay, A.,
6208 Quick, W.P., Furbank, R., Sage, T.L. and Langdale, J.A. (2017) ‘Re-creation of a Key
6209 Step in the Evolutionary Switch from C3 to C4 Leaf Anatomy’, *Current Biology*, 27(21),
6210 pp. 3278-3287.e6. doi:10.1016/j.cub.2017.09.040.

6211 Wang, Q. and Lin, C. (2019) ‘Photoreceptor signaling: when COP1 meets VPs’, *The EMBO*
6212 *Journal*, 38(18), p. e102962. doi:10.15252/embj.2019102962.

6213 Wang, Y., Zhang, Y., Liu, Q., Zhang, T., Chong, X. and Yuan, H. (2021) ‘Genome-Wide
6214 Identification and Expression Analysis of BBX Transcription Factors in Iris germanica L.’,
6215 *International Journal of Molecular Sciences*, 22(16), p. 8793. doi:10.3390/ijms22168793.

6216 Waters, M.T., Wang, P., Korkaric, M., Capper, R.G., Saunders, N.J. and Langdale, J.A.
6217 (2009) ‘GLK Transcription Factors Coordinate Expression of the Photosynthetic
6218 Apparatus in Arabidopsis’, *The Plant Cell*, 21(4), pp. 1109–1128.
6219 doi:10.1105/tpc.108.065250.

6220 Wei, H., Wang, P., Chen, J., Li, C., Wang, Y., Yuan, Y., Fang, J. and Leng, X. (2020)
6221 ‘Genome-wide identification and analysis of B-BOX gene family in grapevine reveal its
6222 potential functions in berry development’, BMC Plant Biology, 20(1), p. 72.
6223 doi:10.1186/s12870-020-2239-3.

6224 Wen, C.-K. and Chang, C. (2002) ‘Arabidopsis RGL1 Encodes a Negative Regulator of
6225 Gibberellin Responses’, *The Plant Cell*, 14(1), pp. 87–100. doi:10.1105/tpc.010325.

6226 Wen, S., Zhang, Y., Deng, Y., Chen, G., Yu, Y. and Wei, Q. (2020) ‘Genomic identification
6227 and expression analysis of the BBX transcription factor gene family in Petunia hybrida’,
6228 *Molecular Biology Reports*, 47(8), pp. 6027–6041. doi:10.1007/s11033-020-05678-y.

6229 Wester, L., Somers, D.E., Clack, T. and Sharrock, R.A. (1994) ‘Transgenic complementation
6230 of the hy3 phytochrome B mutation and response to PHYB gene copy number in
6231 Arabidopsis’, *The Plant Journal*, 5(2), pp. 261–272. doi:10.1046/j.1365-
6232 313X.1994.05020261.x.

6233 Westhoff, P. and Gowik, U. (2010) ‘Evolution of C4 Photosynthesis—Looking for the Master
6234 Switch1’, *Plant Physiology*, 154(2), pp. 598–601. doi:10.1104/pp.110.161729.

6235 Weston, E., Thorogood, K., Vinti, G. and López-Juez, E. (2000) ‘Light quantity controls leaf-
6236 cell and chloroplast development in Arabidopsis thaliana wild type and blue-light-
6237 perception mutants’, *Planta*, 211(6), pp. 807–815. doi:10.1007/s004250000392.

6238 Whippo, C.W. and Hangarter, R.P. (2004) ‘Phytochrome modulation of blue-light-induced
6239 phototropism’, *Plant, Cell & Environment*, 27(10), pp. 1223–1228. doi:10.1111/j.1365-
6240 3040.2004.01227.x.

6241 Wildermuth, M.C., Dewdney, J., Wu, G. and Ausubel, F.M. (2001) ‘Isochorismate synthase is
6242 required to synthesize salicylic acid for plant defence’, *Nature*, 414(6863), pp. 562–565.
6243 doi:10.1038/35107108.

6244 Wolosiuk, R.A., Ballicora, M.A. and Hagelin, K. (1993) ‘The reductive pentose phosphate
6245 cycle for photosynthetic CO2 assimilation: enzyme modulation’, *The FASEB Journal*, 7(8),
6246 pp. 622–637. doi:10.1096/fasebj.7.8.8500687.

6247 Wu, G. and Spalding, E.P. (2007) ‘Separate functions for nuclear and cytoplasmic
6248 cryptochrome 1 during photomorphogenesis of Arabidopsis seedlings’, *Proceedings of*
6249 *the National Academy of Sciences of the United States of America*, 104(47), pp. 18813–
6250 18818. doi:10.1073/pnas.0705082104.

6251 Wu, Y., Zhang, D., Chu, J.Y., Boyle, P., Wang, Y., Brindle, I.D., De Luca, V. and Després, C.
6252 (2012) ‘The Arabidopsis NPR1 Protein Is a Receptor for the Plant Defense Hormone
6253 Salicylic Acid’, *Cell Reports*, 1(6), pp. 639–647. doi:10.1016/j.celrep.2012.05.008.

6254 Xu, D. (2020) ‘COP1 and BBXs-HY5-mediated light signal transduction in plants’, *New*
6255 *Phytologist*, 228(6), pp. 1748–1753. doi:10.1111/nph.16296.

6256 Yalpani, N., Silverman, P., Wilson, T.M., Kleier, D.A. and Raskin, I. (1991) ‘Salicylic acid is a
6257 systemic signal and an inducer of pathogenesis-related proteins in virus-infected
6258 tobacco’, *The Plant Cell*, 3(8), pp. 809–818. doi:10.1105/tpc.3.8.809.

Yang, J., Lin, R., Hoecker, U., Liu, B., Xu, L. and Wang, H. (2005) 'Repression of light signaling by Arabidopsis SPA1 involves post-translational regulation of HFR1 protein accumulation: Arabidopsis SPA1 regulates degradation of HFR1', *The Plant Journal*, 43(1), pp. 131–141. doi:10.1111/j.1365-313X.2005.02433.x.

Yang, D.-L., Yao, J., Mei, C.-S., Tong, X.-H., Zeng, L.-J., Li, Q., Xiao, L.-T., Sun, T., Li, J., Deng, X.-W., Lee, C.M., Thomashow, M.F., Yang, Y., He, Z. and He, S.Y. (2012) 'Plant hormone jasmonate prioritizes defense over growth by interfering with gibberellin signaling cascade', *Proceedings of the National Academy of Sciences of the United States of America*, 109(19), pp. E1192-1200. doi:10.1073/pnas.1201616109.

Yasumura, Y., Moylan, E.C. and Langdale, J.A. (2005) 'A conserved transcription factor mediates nuclear control of organelle biogenesis in anciently diverged land plants', *The Plant Cell*, 17(7), pp. 1894–1907. doi:10.1105/tpc.105.033191.

Ye, J., Coulouris, G., Zaretskaya, I., Cutcutache, I., Rozen, S. and Madden, T.L. (2012) 'Primer-BLAST: a tool to design target-specific primers for polymerase chain reaction', *BMC bioinformatics*, 13, p. 134. doi:10.1186/1471-2105-13-134.

Ye, Y., Liu, Y., Li, X., Wang, G., Zhou, Q., Chen, Q., Li, J., Wang, X. and Tang, H. (2021) 'An Evolutionary Analysis of B-Box Transcription Factors in Strawberry Reveals the Role of FaBBx28c1 in the Regulation of Flowering Time', *International Journal of Molecular Sciences*, 22(21), p. 11766. doi:10.3390/ijms222111766.

Yeh, C.-M., Kobayashi, K., Fujii, S., Fukaki, H., Mitsuda, N. and Ohme-Takagi, M. (2020) 'Blue Light Regulates Phosphate Deficiency-Dependent Primary Root Growth Inhibition in Arabidopsis', *Frontiers in Plant Science*, 10, p. 1803. doi:10.3389/fpls.2019.01803.

Yoshida, Y., Sarmiento-Mañús, R., Yamori, W., Ponce, M.R., Micol, J.L. and Tsukaya, H. (2018) 'The Arabidopsis phyB-9 Mutant Has a Second-Site Mutation in the VENOSA4

6283 Gene That Alters Chloroplast Size, Photosynthetic Traits, and Leaf Growth1', *Plant*
6284 *Physiology*, 178(1), pp. 3–6. doi:10.1104/pp.18.00764.

6285 Yu, L., Lyu, Z., Liu, H., Zhang, G., He, C. and Zhang, J. (2022) 'Insights into the evolutionary
6286 origin and expansion of the BBX gene family', *Plant Biotechnology Reports*, 16(2), pp.
6287 205–214. doi:10.1007/s11816-022-00745-1.

6288 Zhang, Y., Cheng, Y.T., Qu, N., Zhao, Q., Bi, D. and Li, X. (2006) 'Negative regulation of
6289 defense responses in Arabidopsis by two NPR1 paralogs', *The Plant Journal*, 48(5), pp.
6290 647–656. doi:10.1111/j.1365-313X.2006.02903.x.

6291 Zhang, Y., Li, C., Zhang, J., Wang, J., Yang, J., Lv, Y., Yang, N., Liu, J., Wang, X., Palfalvi,
6292 G., Wang, G. and Zheng, L. (2017) 'Dissection of HY5/HYH expression in Arabidopsis
6293 reveals a root-autonomous HY5-mediated photomorphogenic pathway', *PLOS ONE*,
6294 12(7), p. e0180449. doi:10.1371/journal.pone.0180449.

6295 Zhang, N., Wang, Z., Bao, Z., Yang, L., Wu, D., Shu, X. and Hua, J. (2018) 'MOS1 functions
6296 closely with TCP transcription factors to modulate immunity and cell cycle in Arabidopsis',
6297 *The Plant Journal*, 93(1), pp. 66–78. doi:10.1111/tpj.13757.

6298 Zhang, N., Meng, Y., Li, X., Zhou, Y., Ma, L., Fu, L., Schwarzländer, M., Liu, H. and Xiong,
6299 Y. (2019) 'Metabolite-mediated TOR signaling regulates the circadian clock in
6300 Arabidopsis', *Proceedings of the National Academy of Sciences of the United States of*
6301 *America*, 116(51), pp. 25395–25397. doi:10.1073/pnas.1913095116.

6302 Zhang, D., Tan, W., Yang, F., Han, Q., Deng, X., Guo, H., Liu, B., Yin, Y. and Lin, H. (2021)
6303 'A BIN2-GLK1 Signaling Module Integrates Brassinosteroid and Light Signaling to
6304 Repress Chloroplast Development in the Dark', *Developmental Cell*, 56(3), pp. 310-
6305 324.e7. doi:10.1016/j.devcel.2020.12.001.

6306 Zhang, X., Zhang, L., Ji, M., Wu, Y., Zhang, S., Zhu, Y., Yao, J., Li, Z., Gao, H. and Wang,
6307 X. (2021) 'Genome-wide identification and expression analysis of the B-box transcription
6308 factor gene family in grapevine (Vitis vinifera L.)', *BMC Genomics*, 22(1), p. 221.
6309 doi:10.1186/s12864-021-07479-4.

6310 Zhao, D., Zheng, Y., Yang, lingjun, Yao, Z., Cheng, J., Zhang, F., Jiang, H. and Liu, D.
6311 (2021) 'The transcription factor AtGLK1 acts upstream of MYBL2 to genetically regulate
6312 sucrose-induced anthocyanin biosynthesis in Arabidopsis', *BMC Plant Biology*, 21(1), p.
6313 242. doi:10.1186/s12870-021-03033-2.

6314 Zhao, J., Li, H., Huang, J., Shi, T., Meng, Z., Chen, Q. and Deng, J. (2021) 'Genome-wide
6315 analysis of BBX gene family in Tartary buckwheat (Fagopyrum tataricum)', *PeerJ*, 9, p.
6316 e11939. doi:10.7717/peerj.11939.

6317 Zheng, L., Ma, S., Zhou, T., Yue, C., Hua, Y. and Huang, J. (2021) 'Genome-wide
6318 identification of Brassicaceae B-BOX genes and molecular characterization of their
6319 transcriptional responses to various nutrient stresses in allotetraploid rapeseed', *BMC*
6320 *Plant Biology*, 21(1), p. 288. doi:10.1186/s12870-021-03043-0.

6321 Zhu, D., Maier, A., Lee, J.-H., Laubinger, S., Saijo, Y., Wang, H., Qu, L.-J., Hoecker, U. and
6322 Deng, X.W. (2008) 'Biochemical Characterization of Arabidopsis Complexes Containing
6323 CONSTITUTIVELY PHOTOMORPHOGENIC1 and SUPPRESSOR OF PHYA Proteins in
6324 Light Control of Plant Development', *The Plant Cell*, 20(9), pp. 2307–2323.
6325 doi:10.1105/tpc.107.056580.

6326 Zou, Z., Wang, Rihong, Wang, Ran, Yang, S. and Yang, Y. (2018) 'Genome-wide
6327 identification, phylogenetic analysis, and expression profiling of the BBX family genes in
6328 pear', *The Journal of Horticultural Science and Biotechnology*, 93(1), pp. 37–50.
6329 doi:10.1080/14620316.2017.1338927.

Zubo, Y.O., Blakley, I.C., Franco-Zorrilla, J.M., Yamburenko, M.V., Solano, R., Kieber, J.J., Loraine, A.E. and Schaller, G.E. (2018) ‘Coordination of Chloroplast Development through the Action of the GNC and GLK Transcription Factor Families’, *Plant Physiology*, 178(1), pp. 130–147. doi:10.1104/pp.18.00414.

Appendices

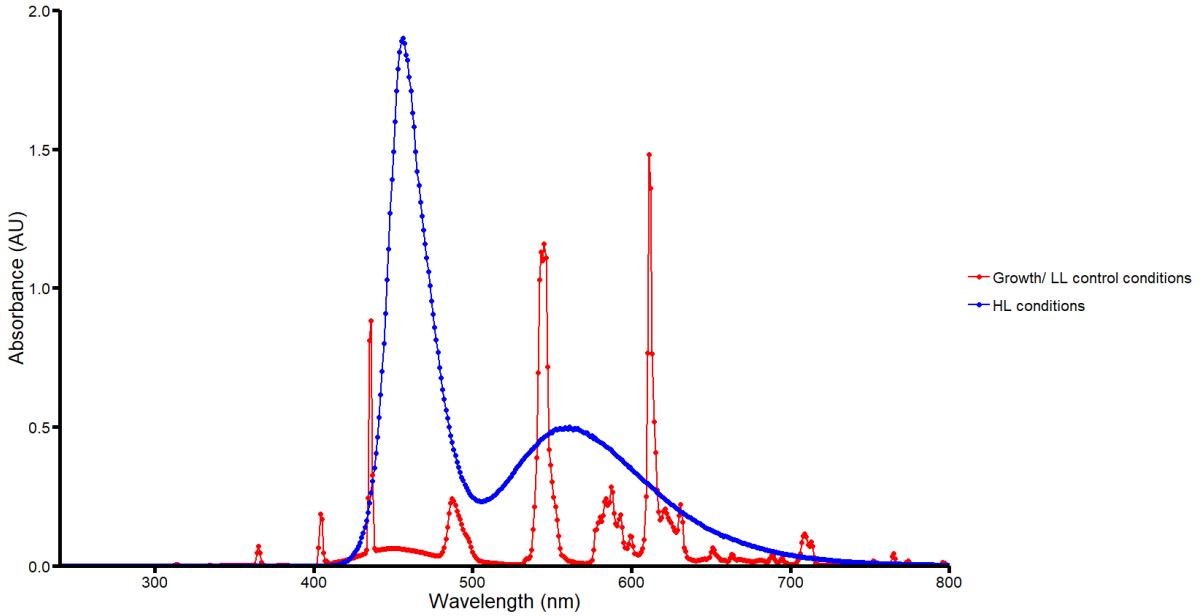

Figure S1: The spectra of the light conditions used throughout this study. The spectra was measured between 240 and 800 nm.

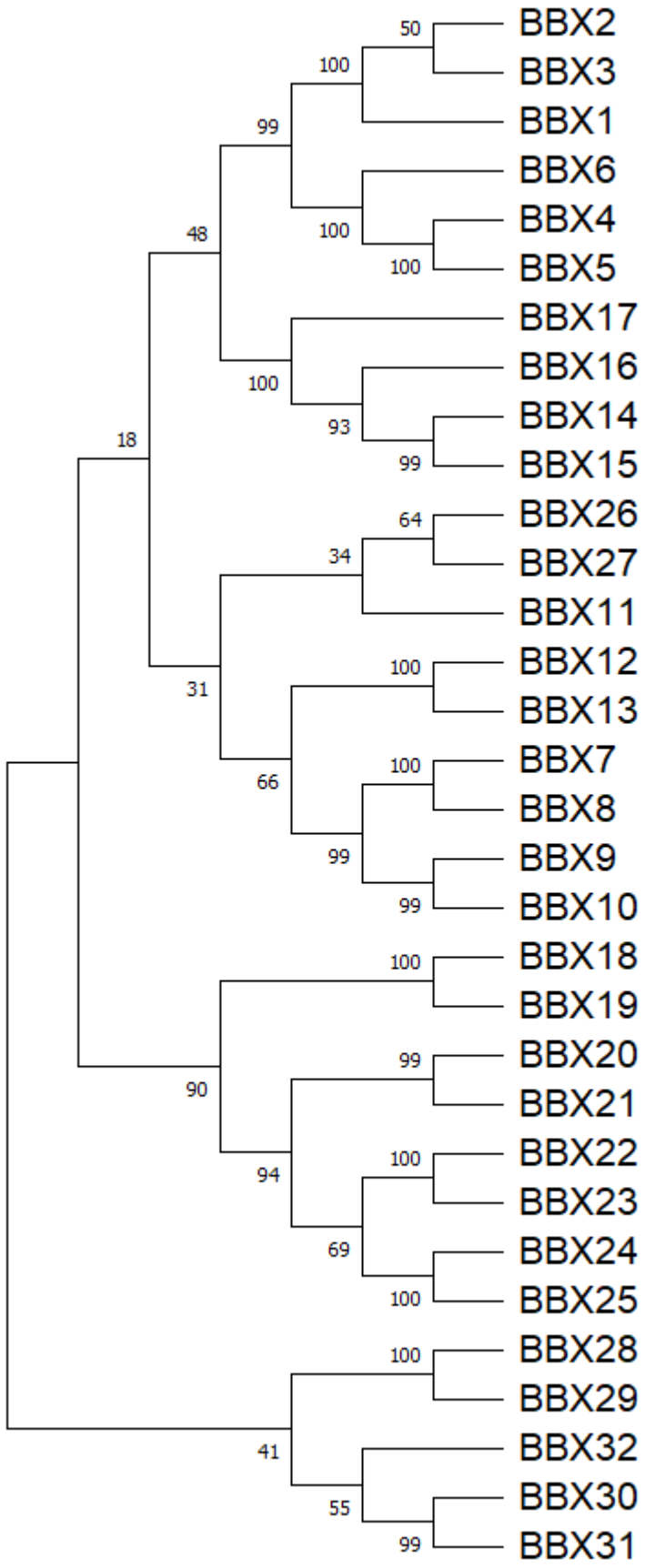
BBX2
BBX3
BBX1
BBX6
BBX4
BBX5
BBX17
BBX16
BBX14
BBX15
BBX26
BBX27
BBX11
BBX12
BBX13
BBX7
BBX8
BBX9
BBX10
BBX18
BBX19
BBX20
BBX21
BBX22
BBX23
BBX24
BBX25
BBX28
BBX29
BBX32
BBX30
BBX31
50
100
99
48
100
100
100
93
99
18
64
34
31
100
66
100
99
99
100
99
90
94
100
69
100
100
41
55
99

6355

Figure S2: Phylogenetic tree of the *Arabidopsis thaliana* BBX family of proteins. Protein sequences were aligned using Clustal W in Mega X (section 2.4.8 [Page 53]). A maximum likelihood phylogenetic tree was built using the JTT model with 100 bootstrap replicates (section 2.4.9 [Page 53]).

6360

Figure S3: Phylogenetic tree of the BBX family proteins of *Arabidopsis thaliana*, *Brassica oleracea*, *Glycine soja*, *Solanum chilense*, *Zea mays*, *Picea abies*, *Selaginella moellendorffii*, *Physcomitrella patens* and *Klebsormidium nitens*. Protein sequences were aligned using Clustal W in Mega X (section 2.4.8 [Page 53]). A maximum likelihood phylogenetic tree was built using the JTT model with 100 bootstrap replicates (section 2.4.9 [Page 53]). List of the genes used can be found in Table S9 [Page 338].

Arabidopsis thaliana B-box 32 (BBX32), mRNA

Sequence ID: NM_113009.3 Length: 1283 Number of Matches: 1

Range 1: 244 to 1019 GenBank Graphics ▼ Next Match ▲ Previous Match

Score	Expect	Identities	Gaps	Strand
1434 bits(776)	0.0	776/776(100%)	0/776(0%)	Plus/Plus

```
Query  1    CATTTACATCTCTTCCTTAAATCTCTCTTCCCACCATCATCATTCCAAACCAATTCTCTC  60
            ||||||||||||||||||||||||||||||||||||||||||||||||||||||||||||
Sbjct  244  CATTTACATCTCTTCCTTAAATCTCTCTTCCCACCATCATCATTCCAAACCAATTCTCTC  303

Query  61   TCACTTCTTTCTGGTGATCAGAGAGATCGACTCAATGGTGAGCTTTTGCGAGCTTTGTGG  120
            ||||||||||||||||||||||||||||||||||||||||||||||||||||||||||||
Sbjct  304  TCACTTCTTTCTGGTGATCAGAGAGATCGACTCAATGGTGAGCTTTTGCGAGCTTTGTGG  363

Query  121  TGCCGAAGCTGATCTCCATTGTGCCGCGGACTCTGCCTTCCTCTGCCGTTCTTGTGACGC  180
            ||||||||||||||||||||||||||||||||||||||||||||||||||||||||||||
Sbjct  364  TGCCGAAGCTGATCTCCATTGTGCCGCGGACTCTGCCTTCCTCTGCCGTTCTTGTGACGC  423

Query  181  TAAGTTCCATGCCTCAAATTTTCTCTTCGCTCGTCATTTCCGGCGTGTCATCTGCCCAAA  240
            ||||||||||||||||||||||||||||||||||||||||||||||||||||||||||||
Sbjct  424  TAAGTTCCATGCCTCAAATTTTCTCTTCGCTCGTCATTTCCGGCGTGTCATCTGCCCAAA  483

Query  241  TTGCAAATCTCTTACTCAAAATTTCGTTTCTGGTCCTCTTCTTCCTTGGCCTCCACGAAC  300
            ||||||||||||||||||||||||||||||||||||||||||||||||||||||||||||
Sbjct  484  TTGCAAATCTCTTACTCAAAATTTCGTTTCTGGTCCTCTTCTTCCTTGGCCTCCACGAAC  543

Query  301  AACATGTTGTTCAGAATCGTCGTCTTCTTCTTGCTGCTCGTCTCTTGACTGTGTCTCAAG  360
            ||||||||||||||||||||||||||||||||||||||||||||||||||||||||||||
Sbjct  544  AACATGTTGTTCAGAATCGTCGTCTTCTTCTTGCTGCTCGTCTCTTGACTGTGTCTCAAG  603

Query  361  CTCCGAGCTATCGTCAACGACGCGTGACGTAAACAGAGCGCGAGGGAGGGAAAACAGAGT  420
            ||||||||||||||||||||||||||||||||||||||||||||||||||||||||||||
Sbjct  604  CTCCGAGCTATCGTCAACGACGCGTGACGTAAACAGAGCGCGAGGGAGGGAAAACAGAGT  663

Query  421  GAATGCCAAGGCCGTTGCGGTTACGGTGGCGGATGGCATTTTTGTAAATTGGTGTGGTAA  480
            ||||||||||||||||||||||||||||||||||||||||||||||||||||||||||||
Sbjct  664  GAATGCCAAGGCCGTTGCGGTTACGGTGGCGGATGGCATTTTTGTAAATTGGTGTGGTAA  723

Query  481  GTTAGGACTAAACAGGGATTTAACAAACGCTGTCGTTTCATATGCGTCTTTGGCTTTGGC  540
            ||||||||||||||||||||||||||||||||||||||||||||||||||||||||||||
Sbjct  724  GTTAGGACTAAACAGGGATTTAACAAACGCTGTCGTTTCATATGCGTCTTTGGCTTTGGC  783

Query  541  TGTGGAGACGAGGCCAAGAGCGACGAAGAGAGTGTTCTTAGCGGCGGCGTTTTGGTTCGG  600
            ||||||||||||||||||||||||||||||||||||||||||||||||||||||||||||
Sbjct  784  TGTGGAGACGAGGCCAAGAGCGACGAAGAGAGTGTTCTTAGCGGCGGCGTTTTGGTTCGG  843

Query  601  CGTTAAGAACACGACGACGTGGCAGAATTTAAAGAAAGTAGAAGATGTGACTGGAGTTTC  660
            ||||||||||||||||||||||||||||||||||||||||||||||||||||||||||||
Sbjct  844  CGTTAAGAACACGACGACGTGGCAGAATTTAAAGAAAGTAGAAGATGTGACTGGAGTTTC  903

Query  661  AGCTGGGATGATTCGAGCGGTTGAAAGCAAATTGGCGCGTGCAATGACGCAGCAGCTTAG  720
            ||||||||||||||||||||||||||||||||||||||||||||||||||||||||||||
Sbjct  904  AGCTGGGATGATTCGAGCGGTTGAAAGCAAATTGGCGCGTGCAATGACGCAGCAGCTTAG  963

Query  721  ACGGTGGCGCGTGGATTCGGAGGAAGGATGGGCTGAAAACGACAACGTTTGAGAAA  776
            ||||||||||||||||||||||||||||||||||||||||||||||||||||||||
Sbjct  964  ACGGTGGCGCGTGGATTCGGAGGAAGGATGGGCTGAAAACGACAACGTTTGAGAAA  1019
```

Figure S4: The alignment of the Col-0 *BBX32* allele with the allele on the NCBI database.

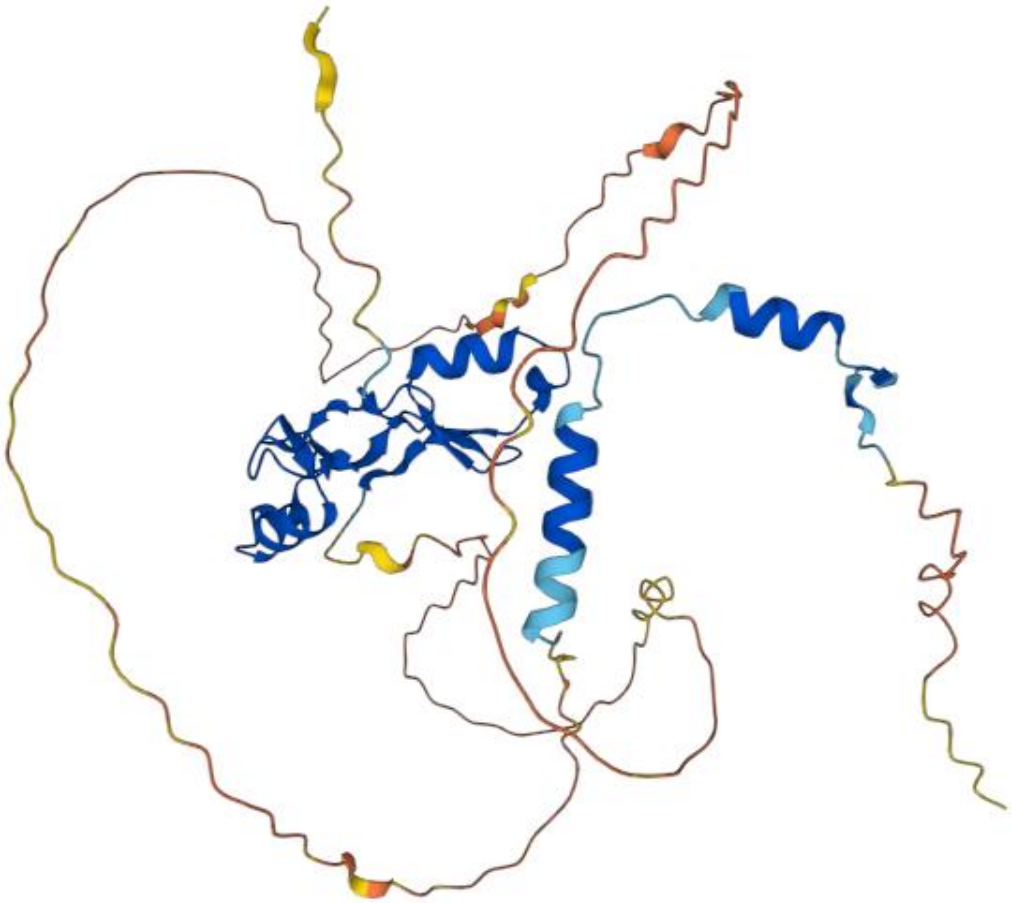

Figure S5: The Alphafold 3D structure of BBX1 (CO; Jumper *et al*., 2021). At the centre is the B-box1 domain and the CCT domain is on the right.

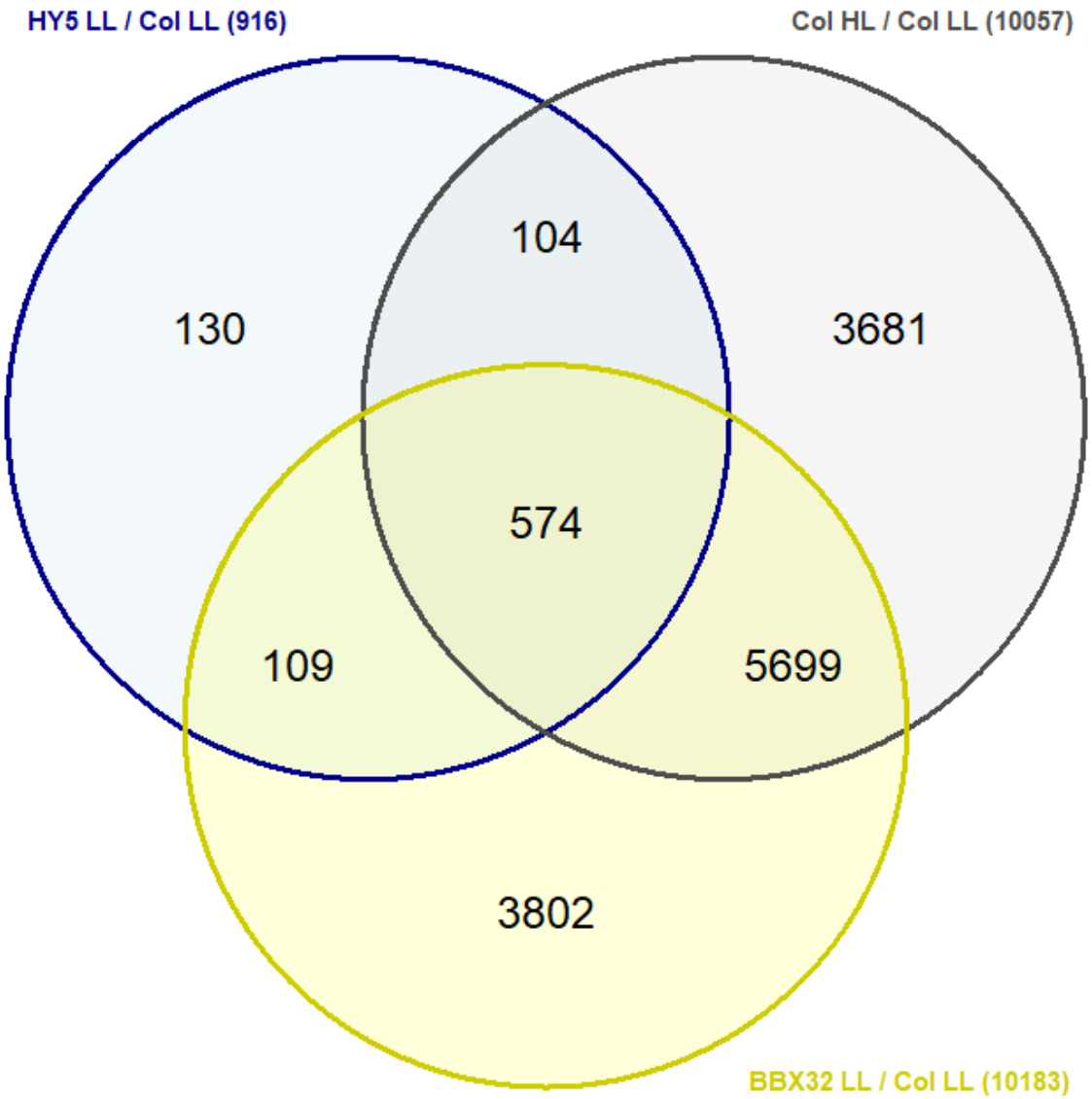

Figure S6: Venn diagram of the gene lists of significant DEGs between Col-0 HL and Col-0 LL, *BBX32* LL and Col-0 LL and *HY5* LL and Col-0 LL.

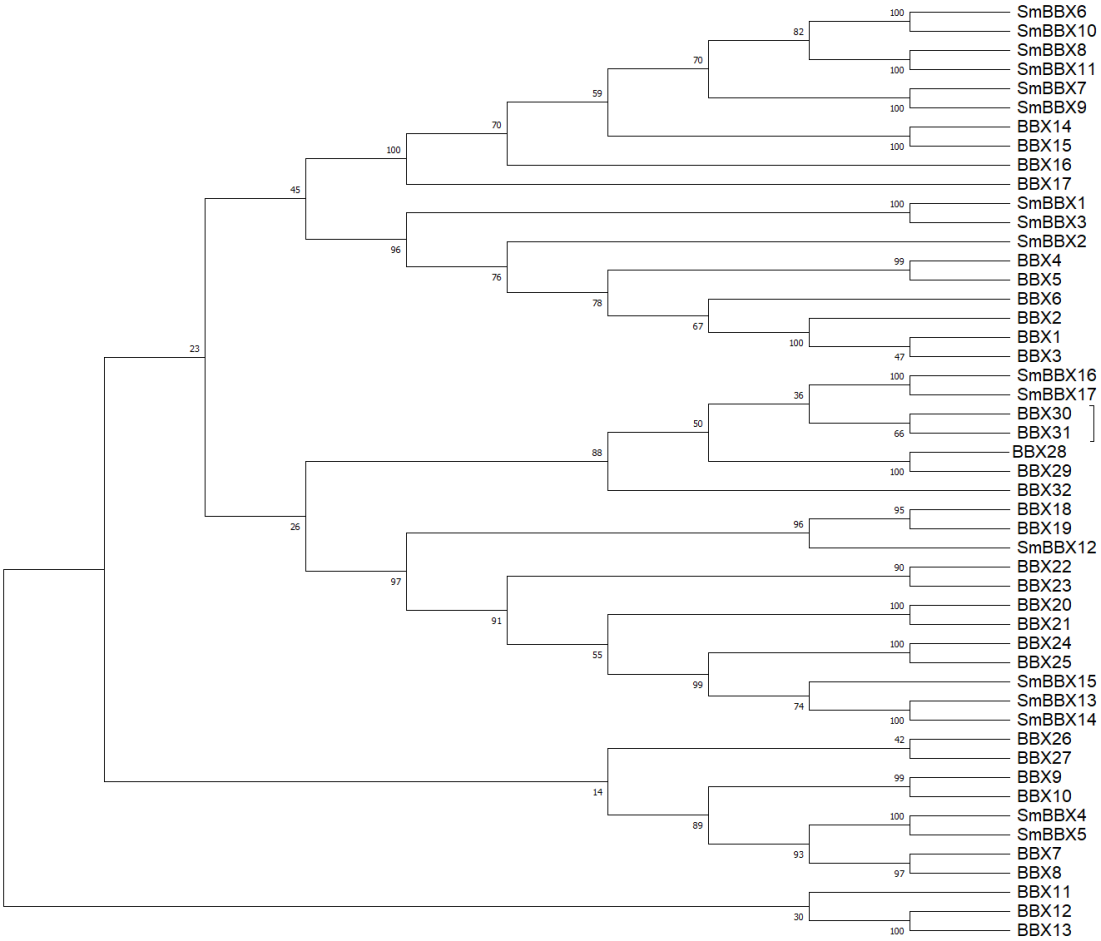

6380

6381 **Figure S7: Phylogenetic tree of the *Arabidopsis thaliana* and *Selaginella***

6382 ***moellendorffii* BBX family of proteins.** Protein sequences were aligned using

6383 Clustal W in Mega X (section 2.4.8 [Page 53]). A maximum likelihood phylogenetic

6384 tree was built using the JTT model with 100 bootstrap replicates (section 2.4.9 [Page

6385 53]).

6386

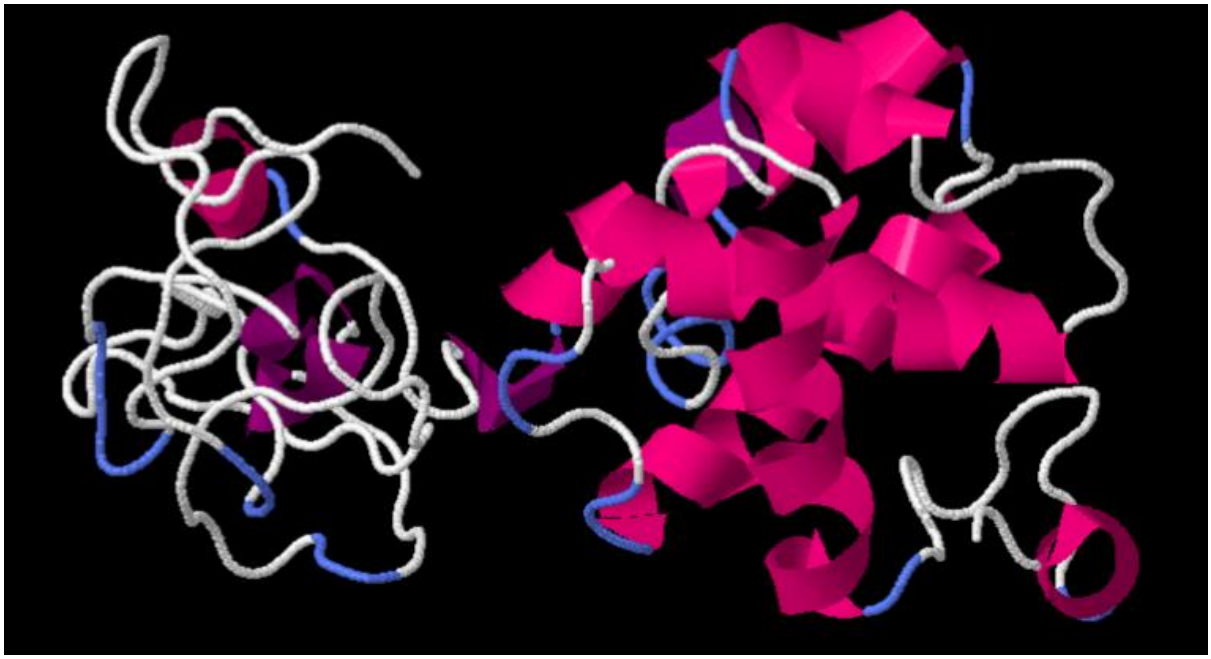

Figure S8: The Phyre 2.0 structure of SmBBX17, the *Selaginella moellendorffii BBX32* homologue (Kelley *et al*., 2015). The B-box1 domain is on the left and the cyclin core-like domain is on the right of the image.

Table S1: The 'Response to' phytohormone gene groups of Arabidopsis thaliana. Lists of genes were downloaded from http://www.arabidopsis.org.

Table S2: A list of Arabidopsis thaliana transcription factor genes. Lists of genes were downloaded from http://planttfdb.gao-lab.org/

Table S3: List of the mutant Arabidopsis thaliana mutants obtained from the Nottingham Arabidopsis Stock Centre.

Table S4: A list of HL acclimation-related genes from Figure 3.3.2 and Figure 3.4.6.

Table S5: A list of papers that studied BBX proteins and the species studied.

Table S6: A list of primers used by this study.

Table S7: A list of BBX32-homologues across 46 plant species. If a plant contained multiple BBX32 homologues, the one with the greatest sequence similarity is given.

Table S8: The specificity and efficiency scores of the BBX32 gRNAs. Determined using https://benchling.com (section 2.5.3 [Page 58]).

Table S9: A list of the BBX proteins used in Figure S3 [Page 332]. Proteins are from *Arabidopsis thaliana*, *Brassica oleracea*, *Glycine soja*, *Solanum chilense*, *Zea mays*, *Picea abies*, *Selaginella moellendorffii*, *Physcomitrella patens* and *Klebsormidium nitens*.